



UNIVERSITY OF NAPLES FEDERICO II

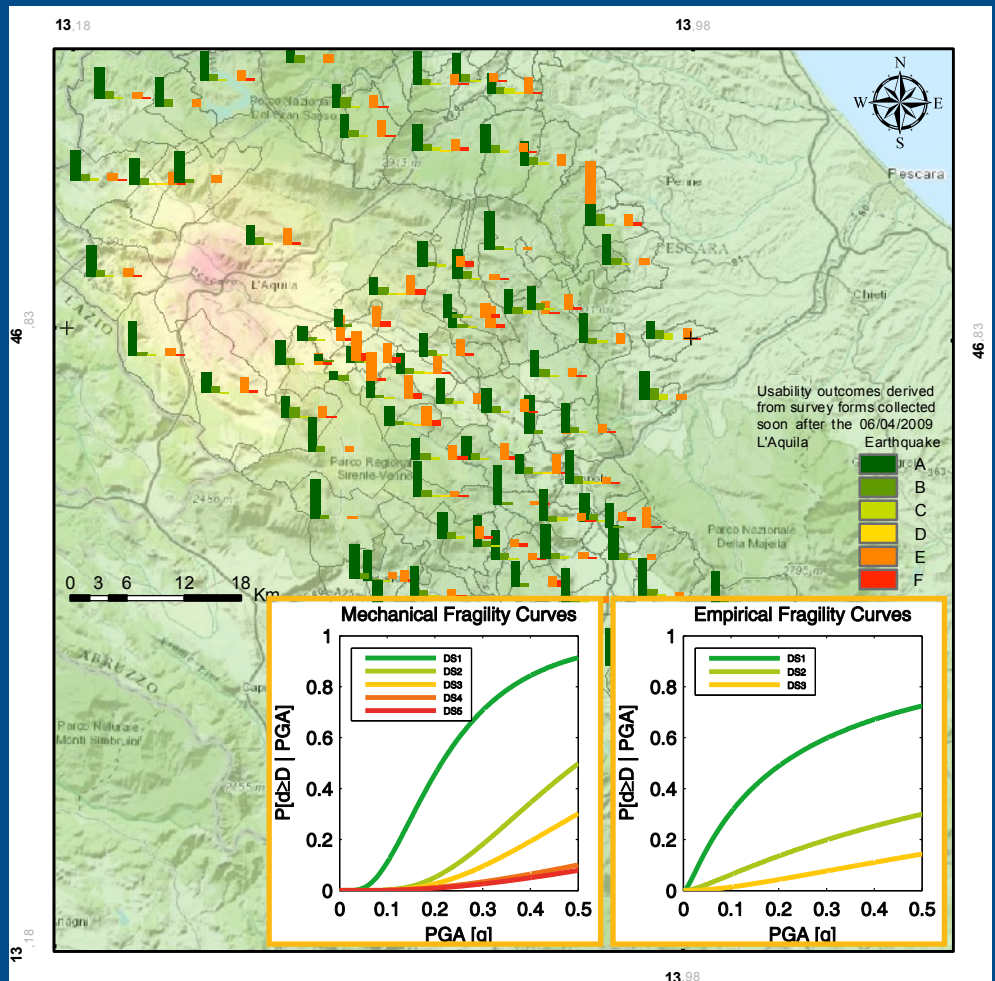
PH.D. PROGRAMME IN

SEISMIC RISK

XXVII CYCLE

Carlo Del Gaudio

SEISMIC FRAGILITY ASSESSMENT OF RC BUILDINGS AT LARGE SCALE



UNIVERSITY OF NAPLES FEDERICO II

*Department of Structures
for Engineering and Architecture*

PH.D. PROGRAMME IN
SEISMIC RISK
COORDINATOR PROF. ALDO ZOLLO
XXVII CYCLE



CARLO DEL GAUDIO

PH.D. THESIS

**SEISMIC FRAGILITY ASSESSMENT OF RC
BUILDINGS AT LARGE SCALE**

TUTOR PROF. ING. GERARDO M. VERDERAME
CO-TUTOR DR. ING. PAOLO RICCI

2015

Index

Chapter 1	1
Introduction.....	1
1.1 Motivation	1
1.2 Objectives	2
1.3 Organization of the thesis	4
1.4 References.....	1
Chapter 2.....	5
Simplified methods for seismic vulnerability assessment of RC buildings at large scale	5
2.1 Introduction.....	5
2.2 Empirical Methods	8
2.3 Analytical Methods.....	18
2.4 Hybrid Methods	43
2.5 Expert Judgement-Based Methods	45
2.6 References.....	46
Chapter 3	53
Simplified approach to the seismic vulnerability assessment of existing RC buildings	53

3.1	Introduction.....	53
3.2	Methods for Seismic Vulnerability Assessment of RC Buildings..	55
3.3	A Simplified Procedure For Seismic Vulnerability Assessment Of Rc Buildings	58
3.4	Senitivity analysis	96
3.5	Summary of results	115
3.6	References.....	117
Chapter 4	125
	Avellino Municipality: a high detail level damage prediction.....	125
4.1	Field survey on building stock of Avellino city.....	126
4.2	Analysis of building stock data.....	127
4.3	Input Data	143
4.4	Evaluation of seismic hazard	150
4.5	Seismic vulnerability assessment	154
4.6	Comparison with fragility curves from literature	166
4.7	Summary of remarks.....	172
4.8	References.....	173
Chapter 5	181
	Pettino area: a single-building comparison with observed post-earthquake damage	181
5.1	Introduction.....	181
5.2	Derivation of Building database from Survey form data.....	183
5.3	Seismic vulnerability methods at large scale	198
5.4	Simplified methodology for seismic vulnerability of existing RC buildings: PushOver on Shear Type models (POST).....	208

5.5	Analysis of results.....	223
5.6	Summary of remarks.....	232
5.7	References.....	234
Chapter 6	239
L'Aquila Province: a class-oriented large scale comparison with post-earthquake damage		239
6.1	Introduction.....	239
6.2	Derivation of Building database from Survey form data.....	240
6.3	Residential RC buildings Database	264
6.4	Observed damage scenario	270
6.5	Predicted damage scenario.....	280
6.6	Comparison and Analysis of Results	297
6.7	Summary of remarks.....	314
6.8	References.....	316
Chapter 7	321
Seismic vulnerability assessment at urban scale based on field survey, remote sensing and census data		321
7.1	Introduction.....	322
7.2	Seismic Hazard	323
7.3	Field Survey Data	323
7.4	Remote Sensing Data.....	327
7.5	Census Data	330
7.6	Seismic Vulnerability Assessment Procedure	332
7.7	Methodology.....	336
7.8	Analysis of results.....	341

7.9	Summary of remarks.....	355
7.10	References.....	358
Chapter 8.....		361
Experimental Tests on GLD RC Frames with and without Infills		361
8.1	Introduction.....	361
8.2	Experimental Program	363
8.3	Infilled Frame: Analysis of Experimental Results.....	370
8.4	Bare Frames: Analysis of Experimental Results	382
8.5	Summary of remarks.....	402
8.6	References.....	403

List of figures

Figure 2-1: Damage Probability Matrix proposed by Whitman et al. (1973) (from (Calvi et al., 2006))	9
Figure 2-2: Vulnerability classes adopted in (Di Pasquale et al., 2005)	10
Figure 2-3: Vulnerability classes according to EMS-98 scale (Grünthal, 1998)	12
Figure 2-4: Definition of quantities “few”, “many” and “most” according to EMS-98 scale (Grünthal, 1998)	12
Figure 2-5: Definition of damage grades to RC buildings according to EMS-98 scale (Grünthal, 1998)	13
Figure 2-6: Vulnerability functions to relate damage ratio and PGA for different values of vulnerability index (adapted from Guagenti and Petrini (1989)) (from (Calvi et al., 2006))	16
Figure 2-7: General framework of the methodology adopted in (Singhal and Kiremidjian, 1996)	19
Figure 2-8: Probability distribution of Park and Ang’s damage index at $S_a=3g$ (Singhal and Kiremidjian, 1996)	20
Figure 2-9: Ranges of Park and Ang's damage index for different damage states (Singhal and Kiremidjian, 1996)	20
Figure 2-10: Vulnerability curves for Mid-Rise frames (Singhal and Kiremidjian, 1996)	21
Figure 2-11: Correlation between MMI intensity and spectral acceleration over period range 0.5-0.9 s (Singhal and Kiremidjian, 1996)	22

Figure 2-12: Damage Probability Matrix for Mid-Rise frames (Singhal and Kiremidjian, 1996)	22
Figure 2-13: Predefined collapse mechanisms (Cosenza et al., 2005).....	24
Figure 2-14: Capacity parameters (Iervolino et al., 2007)	26
Figure 2-15: Building-related modules of HAZUS methodology (FEMA, 2001)	27
Figure 2-16: Example building capacity curve and control points (FEMA, 2001)	28
Figure 2-17: “Elastic” period values and average inter-story drift ratios of capacity curve control points and structural damage state thresholds (fragility medians) for C1M ¹ building class (FEMA, 2001)	29
Figure 2-18: Capacity curves and structural damage-state thresholds (fragility medians) for five seismic design levels (Special High, High, Moderate, Low and Pre-Code) for C1M building class (FEMA, 2001)	29
Figure 2-19: Example demand spectrum construction and calculation of peak response displacement (D) and acceleration (A) (FEMA, 2001)	30
Figure 2-20: Example fragility curves for Slight, Moderate, Extensive and Complete damage (FEMA, 2001)	32
Figure 2-21: An example of the intersection of capacity areas and demand spectrum (Calvi, 1999)	37
Figure 2-22: Deformation based seismic vulnerability assessment procedure (Glaister and Pinho, 2003)	38
Figure 2-23: Joint Probability Density Function (JPDF) of displacement capacity and period (Crowley et al., 2004).....	39
Figure 3-1: Italian seismic classification according to RDL n. 193 18/04/190961	
Figure 3-2: Italian seismic classification according to RDL n. 431 13/03/192762	
Figure 3-3: Italian seismic classification according to DM 26/06/1981	63
Figure 3-4: Italian seismic classification according to OPCM n. 3274 20/03/2003.....	64
Figure 3-5: Evolution of seismic classification for the Municipality of Napoli through ECSit software based on MATLAB® code (http://www.reluis.it/)	68

Figure 3-6. Moment-rotation relationship for RC columns, lateral force-displacement relationship for infill panels	71
Figure 3-7. Lateral force-displacement relationship for infill panels.....	74
Figure 3-8: Lateral force-displacement relationship for infill panels with opening	77
Figure 3-9: Lateral force-displacement relationship for internal infill panels ..	80
Figure 3-10. Example interstorey shear displacement relationships (black line) obtained as the sum of shear-displacement contributions of RC columns and infill panels (grey lines with dots indicating displacement thresholds)	81
Figure 3-11: Static Pushover curve and IDA-curves for 4-storeys building.	83
Figure 3-12. Displacement thresholds assumed on the backbone of the lateral response of infill panels (a) and RC columns (b), and corresponding Damage State displacement ranges adopted.....	88
Figure 3-13.Capacity curve and IDA-curves for 4-storeys building	89
Figure 3-14. Example fragility curves for a 5-storey building.....	91
Figure 3-15: Evolution of seismic classification for the Municipality of L'Aquila through ECSit software based on MATLAB® code (http://www.reluis.it/).....	98
Figure 3-16: Results of sensitivity analysis for NC LS 2-Storeys Case-study Building.....	104
Figure 3-17: Simplified IDA-curves for 2-Storeys Case-study buildings in longitudinal direction (Lower, median and Upper value for G_w).....	106
Figure 3-18: Simplified IDA-curves for 2-Storeys Case-study buildings in transversal direction (Lower, median and Upper value for G_w).....	107
Figure 3-19: Simplified IDA-curves for 2-Storeys Case-study buildings in longitudinal direction (Plan ratio equal to 1, 2 and 3).....	108
Figure 3-20: Simplified IDA-curves for 2-Storeys Case-study buildings in transversal direction (Plan ratio equal to 1, 2 and 3).....	108
Figure 3-21: Results of sensitivity analysis for NC LS 4-Storeys Case-study Building.....	113
Figure 3-22: Results of sensitivity analysis for NC LS 6-Storeys Case-study	

Building.....	114
Figure 4-1. Piazza del Popolo (Avellino), (a) 24 novembre 1980, (b), 2014..	126
Figure 4-2: Distribution of building typologies.	128
Figure 4-3: Distribution of plan morphologies.	128
Figure 4-4: Distribution of number of storeys.	128
Figure 4-5. Distribution of: age of construction.....	129
Figure 4-6. Percentages of RC buildings complying with EC8 prescriptions about in plan-regularity	129
Figure 4-7: Spatial distribution at level of building of building typologies....	130
Figure 4-8: Spatial distribution at level of census cell of the building typologies	131
Figure 4-9: Spatial distribution at level of building of number of storeys.....	132
Figure 4-10: Spatial distribution at level of census cell of number of storeys	133
Figure 4-11: Spatial distribution at level of building of age of construction ..	134
Figure 4-12: Spatial distribution at level of census cell of age of construction	135
Figure 4-13: Distribution of inter-storey height at first storey.....	138
Figure 4-14: Distribution of inter-storey height at upper storeys.....	139
Figure 4-15: Distribution of average plan area.	139
Figure 4-16: Distribution of plan ratio.....	139
Figure 4-17: Distribution of bay length.	140
Figure 4-18. Distribution of opening percentage in infill panels at the bottom storey	140
Figure 4-19. Comparison between the statistics obtained from the field survey carried out in the framework of the SIMURAI project and from the 14th general census (ISTAT): (a) building typology, (b) number of storeys, (c) age of construction.....	142
Figure 4-20. Comparison between the statistics obtained from the field survey carried out in the framework of the SIMURAI project and from LSU: (a) age of construction, (b) number of storeys	143
Figure 4-21: Evolution of seismic classification for the Municipality of	

Avellino through ECS-it software based on MATLAB® code (http://www.reluis.it/).....	144
Figure 4-22.10% probability of exceedance in 50 years (return period of 475 years) PGA[g] in Italy and in Campania region	152
Figure 4-23.Stratigraphic and topographic soil conditions in Avellino city ...	153
Figure 4-24.Median and lognormal standard deviation values of PGA Distribution (Fragility Curves) and Failure probabilities of surveyed RC buildings at each DS, as a function of the number of storeys	156
Figure 4-25. Median and lognormal standard deviation values of PGA Distribution (Fragility Curves) and Failure probabilities of surveyed RC buildings at each DS, as a function of the number of storeys, evaluated on horizontal stiff soil	158
Figure 4-26. Median and lognormal standard deviation values of PGA Distribution (Fragility Curves) and Failure probabilities of surveyed RC buildings at each DS, as a function of the age of construction.....	160
Figure 4-27: Failure probabilities of surveyed RC buildings at DS1	162
Figure 4-28: Failure probabilities of surveyed RC buildings at DS2.....	163
Figure 4-29: Failure probabilities of surveyed RC buildings at DS3.....	164
Figure 4-30: Failure probabilities of surveyed RC buildings at DS4.....	165
Figure 4-31: Failure probabilities of surveyed RC buildings at DS5.....	166
Figure 4-32: Comparison between mean fragility curves evaluated with POST and fragility curves provided by (Lagomarsino and Giovinazzi, 2006) for pre-1981 buildings with $4 \leq N_{storeys} \leq 7$	169
Figure 4-33. Comparison between mean fragility curves evaluated with POST and fragility curves provided by (Lagomarsino and Giovinazzi, 2006) for post-1981 buildings with $4 \leq N_{storeys} \leq 7$	170
Figure 4-34. Comparison between mean fragility curves evaluated with POST and fragility curves provided by (Rota et al., 2008) for pre-1981 buildings with $4 \leq N_{storeys} \leq 7$	171
Figure 5-1: Damage classification according to (Baggio 2007).....	186
Figure 5-2: Map of Pettino area with indication of building plan area	188

Figure 5-3: Map of Pettino area with indication of building plan area and shake map data according to (http://shakemap.rm.ingv.it/shake/index.html).	189
Figure 5-4: Distribution of number of floors for the 131 buildings of database located in Pettino area.	190
Figure 5-5: Distribution of age of construction for the 131 buildings of database located in Pettino area.	191
Figure 5-6: Distribution of Plan area for the 131 buildings of database located in Pettino area.	191
Figure 5-7: Distribution of Building Plan ratio (d) for the 131 buildings of database located in Pettino area.	192
Figure 5-8: Damage distribution to vertical structures (a) and to infill panels (b) for the 131 buildings of the database deduced from survey (Baggio et al., 2007) with the indication of the damage extension.	193
Figure 5-9: Usability outcomes for the 131 buildings of the database deduced from survey form AEDES (Baggio et al., 2007)	195
Figure 5-10: Damage State outcomes for the 131 buildings of the database..	198
Figure 5-11: Fragility curves provided by (Rota et al., 2008) for low-rise Reinforced Concrete buildings with seismic design.	202
Figure 5-12: Fragility curves provided by (Rota et al., 2008) for low-rise Reinforced Concrete buildings without seismic design.	203
Figure 5-13: Fragility curves provided by (Rota et al., 2008) for high-rise Reinforced Concrete buildings without seismic design.	203
Figure 5-14: Fragility curves provided by (Borzi et al., 2008b) for RC Regularly distributed infill panels buildings non-seismically designed with a lateral force $c=10\%$	205
Figure 5-15: Fragility curves provided by (Borzi et al., 2008b) for RC Regularly distributed infill panels buildings seismically designed with a lateral force $c=10\%$	206
Figure 5-16: Fragility curves provided by (Lagomarsino and Giovinazzi, 2006) for Low-Rise Concrete Moment Frames with ERD in second seismic category with Low Ductility.	207

Figure 5-17: Fragility curves provided by (Lagomarsino and Giovinazzi, 2006) for Medium-Rise Concrete Moment Frames with ERD in second seismic category with Low Ductility.....	208
Figure 5-18: Evolution of seismic classification for the Municipality of L'Aquila through ECS-it software based on MATLAB® code (http://www.reluis.it/).....	210
Figure 5-19: Comparison of the damage predicted by POST methodology, obtained by adopting these displacement thresholds to define the damage to non-structural elements, and observed damage.....	217
Figure 5-20: Results of parametric analysis on lateral force-displacement relationship for infill panels	219
Figure 5-21: Mean fragility curves according to POST Methodology for Low-Rise class for the 131 Buildings of Pettino area.....	222
Figure 5-22: Mean fragility curves according to POST Methodology for Medium-Rise class for the 131 Buildings of Pettino area.....	223
Figure 5-23: Comparison of the cumulative distribution of damage predicted by POST methodology and observed damage.....	225
Figure 5-24: Comparison of the cumulative distribution of damage predicted by POST methodology and observed damage.....	225
Figure 5-25: Comparison of the distribution of damage predicted by (Rota et al., 2008) methodology and observed damage.	227
Figure 5-26: Comparison of the cumulative distribution of damage predicted by (Rota et al., 2008) methodology and observed damage.	227
Figure 5-27: Comparison of the distribution of damage predicted by (Lagomarsino and Giovinazzi, 2006) methodology and observed damage.	228
Figure 5-28: Comparison of the cumulative distribution of damage predicted by (Lagomarsino and Giovinazzi, 2006) methodology and observed damage.	229
Figure 5-29: Comparison of the damage predicted by (Borzi et al., 2008b) methodology and observed damage.	232

Figure 6-1: Map of L'Aquila area with indication of surveyed buildings after the 6/4/2009 earthquake	243
Figure 6-2: Structural Typology Distribution for each Municipality	245
Figure 6-3: Number of Storeys Distribution for the whole building database	247
Figure 6-4: Number of storeys Distribution for each Municipality	248
Figure 6-5: Number of Basement Distribution for the whole building database	249
Figure 6-6: Average storeys surface Distribution for the whole building database	250
Figure 6-7: Age of construction Distribution for the whole building database	251
Figure 6-8: Age of renovation Distribution for the whole building database .	252
Figure 6-9: Age of construction Distribution for each Municipality	253
Figure 6-10: Use Distribution for the whole building database	254
Figure 6-11: Masonry building classification	255
Figure 6-12: Masonry building classification (A = most vulnerable, C = less vulnerable) from (Dolce et al, 2015).	256
Figure 6-13: Damage classification according to (Baggio 2007).	257
Figure 6-14: Usability outcomes Distribution for the whole building database	261
Figure 6-15: Usability outcomes Distribution for each Municipality	263
Figure 6-16: Number of Storeys Distribution for the RC residential buildings	265
Figure 6-17: Number of Basements Distribution for the RC residential buildings	265
Figure 6-18: Age of construction Distribution for the RC residential buildings	266
Figure 6-19: Age of renovation Distribution for the RC residential buildings	267
Figure 6-20: Average storey surface Distribution for the RC residential buildings	268
Figure 6-21: Usability outcomes Distribution for the RC residential buildings	

.....	269
Figure 6-22: Damage grades Distribution for the Residential RC buildings ..	273
Figure 6-23: Map of L'Aquila area and shake map data according to (http://shakemap.rm.ingv.it/shake/index.html)	274
Figure 6-24: Linear regression parameters for the evaluation of lognormal distributions for DS1-DS4 according to (Porter et al., 2007) for RC-LH-NS building class.....	275
Figure 6-25: Observational fragility curves for pre-1981 buildings with $3 \leq N_{storeys}$ (RC-LH-NS)	277
Figure 6-26: Observational fragility curves for post-1981 buildings with $3 \leq N_{storeys}$ (RC-LH-S)	278
Figure 6-27: Observational fragility curves for pre-1981 buildings with $N_{storeys} > 3$ (RC-MH-NS)	278
Figure 6-28: Observational fragility curves for post-1981 buildings with $N_{storeys} > 3$ (RC-MH-S)	279
Figure 6-29: Distribution of plan area depending on number of storeys for residential RC Building of L'Aquila area	286
Figure 6-30: Percentage distribution of plan area depending on number of storeys for residential RC Building of L'Aquila area.....	286
Figure 6-31: Correlation between Number of storeys and age of construction for residential RC Building of L'Aquila area	287
Figure 6-32: Correlation between Number of storeys and age of construction for residential RC Building of L'Aquila area	288
Figure 6-33: Correlation between age of construction and average storey surface for residential RC Building of L'Aquila area.....	289
Figure 6-34: Correlation between age of construction and average storey surface for residential RC Building of L'Aquila area.....	289
Figure 6-35: Correlation between plan ratio and average storey surface for 131 Building of Pettino area.....	292
Figure 6-36: Distribution of predicted damage according to POST methodology and observed damage	298

Figure 6-37: Cumulative distribution of predicted damage according to POST methodology and observed damage.	299
Figure 6-38: Distribution of predicted damage according to (Lagomarsino and Giovinazzi, 2006) methodology and observed damage	300
Figure 6-39: Cumulative distribution of predicted damage according to (Lagomarsino and Giovinazzi, 2006) methodology and observed damage methodology and observed damage.	300
Figure 6-40: Distribution of predicted damage according to (Rota et al., 2008) methodology and observed damage methodology and observed damage..	302
Figure 6-41: Cumulative distribution of predicted damage according to (Rota et al., 2008) methodology and observed damage methodology and observed damage.	302
Figure 6-42: Damage Scenario from POST methodology subdivided into PGA bins	304
Figure 6-43: Damage Scenario derived from AEDES inspection forms subdivided into PGA bins	304
Figure 6-44: Comparison of the damage predicted by POST methodology and observed damage subdivided into PGA for DS0.....	305
Figure 6-45: Comparison of the damage predicted by POST methodology and observed damage subdivided into PGA for DS1.....	306
Figure 6-46: Comparison of the damage predicted by POST methodology and observed damage subdivided into PGA for DS2.....	307
Figure 6-47: Comparison of the damage predicted by POST methodology and observed damage subdivided into PGA for DS3.....	308
Figure 6-48: Comparison of the damage predicted by POST methodology and observed damage subdivided into PGA for DS4.....	308
Figure 6-49: Damage Scenario derived from POST methodology subdivided for building classes	310
Figure 6-50: Damage Scenario derived from AEDES inspection forms subdivided for building classes	310
Figure 6-51: Comparison of the damage predicted by POST methodology and	

observed damage for RC-LH-NS class	311
Figure 6-52: Comparison of the damage predicted by POST methodology and observed damage for RC-LH-S class	312
Figure 6-53: Comparison of the damage predicted by POST methodology and observed damage for RC-MH-NS class	312
Figure 6-54: Comparison of the damage predicted by POST methodology and observed damage for RC-MH-S class	313
Figure 6-55: Distribution of PGA from ShakeMap for RC-MH-NS class	314
Figure 7-1: Structural typology (a), Number of storeys (b), and Age of Construction (c) of surveyed buildings.	324
Figure 7-2: Spatial distribution at level of census cell of the building typologies.	326
Figure 7-3: Spatial distribution at level of census cell of age of construction.	327
Figure 7-4: Spatial distribution at level of census cell of the Number of Storeys.	327
Figure 7-5: Spatial distribution at level of census cell of Number of Storeys according to LIDAR data.	330
Figure 7-6: Comparison between the statistics obtained from the field survey carried out in the framework of the SIMURAI project and from the 14th general census (ISTAT): (a) building typology, (b) number of storeys, (c) age of construction.....	332
Figure 7-7: Vulnerability curves for different age of construction.	335
Figure 7-8: Vulnerability curves for different class of height.....	336
Figure 7-9: Expected mean damage based on FIELD SURVEY data as a function of the Number of storeys (a) and of the Age of Construction (b).	342
Figure 7-10: Error in the estimate of expected mean damage depending on the error in the determination of Structural Typology and Age of Construction derived from the disaggregation of census data (a) and on the error in the Class of height (b).	344
Figure 7-11: Error in the estimate of expected mean damage depending on the error in the determination of Class of height integrated by data on Structural	

Typology provided by FIELD SURVEY hypothesis “c”	345
Figure 7-12: Error in the estimate of expected mean damage depending on the error in the determination of Class of Height based on hypothesis “a” (a), on hypothesis “c” (b) and . hypothesis “d” (c).	349
Figure 7-13: Error in the estimate of expected mean damage depending on the error in the determination of Age of Construction.	351
Figure 7-14: Error in the estimate of expected mean damage depending on the error in the determination of Structural Typology.....	352
Figure 7-15: Spatial distribution of expected mean damage based on FIELD SURVEY data.	354
Figure 7-16: Spatial distribution of relative error in expected mean damage based on “pure” LIDAR.	354
Figure 7-17: Spatial distribution of error in the determination of Age of Construction.	355
Figure 7-18: Spatial distribution of error in the determination of Structural Typology.....	355
Figure 8-1: Geometry and reinforcement details of specimens	365
Figure 8-2: Compressionn tests on three-course masonry wallette specimens perpendicular (a) and parallel (b) to the holes, and diagonal shear test on five-course masonry wallette specimen (c)	368
Figure 8-3: Test setup	369
Figure 8-4: Instrumentation layout.....	370
Figure 8-5: Lateral load-drift response of Infilled specimen GI-80	370
Figure 8-6: Damage to specimen GI-80.....	372
Figure 8-7: Axial strain of infill diagonal strut (elongation is taken as positive)	374
Figure 8-8: Lateral load-drift response of specimen GI-80. Load Cycles are marked by means of vertical dashed lines. Initiation of significant sliding along diagonal shear cracks and widening of these cracks is highlighted by means of a black and a grey circle for left and right column, respectively.	374
Figure 8-9: Lateral drift history (a), displacement of LVDTs across diagonal	

crack (b) in left joint, and vertical displacement of left (c) column of specimen GI-80. Load Cycles are marked by means of vertical dashed lines. Initiation of significant sliding along diagonal shear cracks and widening of these cracks is highlighted by means of a black and a grey circle for left and right column, respectively.	376
Figure 8-10: Lateral drift history (a), displacement of LVDTs across diagonal crack (b) in right joint, and vertical displacement of right (c) column of specimen GI-80. Load Cycles are marked by means of vertical dashed lines. Initiation of significant sliding along diagonal shear cracks and widening of these cracks is highlighted by means of a black and a grey circle for left and right column, respectively.	377
Figure 8-11: Lateral drift-base rotation relationship for left column of Specimen GI-80.	378
Figure 8-12: Global lateral load-drift (a) and global lateral load-base rotation for left column (b) relationships of Specimen GI-80.	379
Figure 8-13: Instrumentation layout and derivation of displacement measures for left joint.....	380
Figure 8-14: Left column displacement (a) and horizontal crack width (b) versus global lateral displacement for Specimen GI-80.....	381
Figure 8-15: Right column displacement (a) and horizontal crack width (b) versus global lateral displacement for Specimen GI-80.....	382
Figure 8-16: Damage to beam-column joint regions in specimens GB	384
Figure 8-17: Damage to beam-column joint regions in specimens GB2	385
Figure 8-18: Lateral load-drift response of Bare specimens GB (a) and GB2 (b)	385
Figure 8-19: Envelopes of lateral load-drift responses	386
Figure 8-20: Lateral load-drift response of specimen GB. Load Cycles are marked by means of vertical dashed lines. Initiation of significant sliding along diagonal shear crack and widening of this crack for left joint is highlighted by means of a black circle	387
Figure 8-21: Lateral drift history (a), displacement of LVDTs across major	

diagonal crack (b) in left joint, and vertical displacement (c) of left column of specimen GB. Load Cycles are marked by means of vertical dashed lines. Initiation of significant sliding along diagonal shear crack and widening of this crack for left joint is highlighted by means of a black circle.....	388
Figure 8-22: Lateral drift history (a), displacement of LVDTs across major diagonal crack (b) in right joint, and vertical displacement (c) of right column of specimen GB. Load Cycles are marked by means of vertical dashed lines. Initiation of significant sliding along diagonal shear crack and widening of this crack for left joint is highlighted by means of a black circle	389
Figure 8-23: Shear strain of left (a) and right (b) joint in specimen GB.....	390
Figure 8-24: Major crack opening and corresponding equivalent shear deformation of joint panel for left (a) and right (b) joint	391
Figure 8-25: End rotation at the base of left column (a), end rotation at the top of left column (b) versus global lateral drift for Specimen GB.....	392
Figure 8-26: End rotation at the left end of beam (a), and shear strain of left joint (b) versus global lateral drift for Specimen GB.....	393
Figure 8-27: Schematic macroscopic representation of deformation mechanisms under positive imposed lateral displacement	394
Figure 8-28: Schematic macroscopic representation of deformation mechanisms under negative imposed lateral displacement.....	394
Figure 8-29: Photographic images of back view of left joint for closing (a,c) and opening (b,d) moments during cycle VI (drift= $\pm 4.20\%$) (a,b) and cycle VII (drift= $\pm 5.10\%$) (c,d)	395
Figure 8-30: Lateral load-drift response of specimen GB2. Load Cycles are marked by means of vertical dashed lines.....	396
Figure 8-31: Lateral drift history (a), displacement of LVDTs across major diagonal crack in left (b) joint, and vertical displacement of left (c) column of specimen GB2. Load Cycles are marked by means of vertical dashed lines	397
Figure 8-32: Lateral drift history (a), displacement of LVDTs across major	

diagonal crack in right (b) joint, and vertical displacement of right (c) column of specimen GB2. Load Cycles are marked by means of vertical dashed lines	398
Figure 8-33: Shear strain of left (a) and right (b) joint in specimen GB2.....	399
Figure 8-34: Yielding in longitudinal reinforcement according to strain gauges in left column of specimen GB2 in lateral load-drift response (a) and lateral drift history (b); yielding at left column base, left column top and beam left end are highlighted by means of a circle, a square and a triangle, respectively	400

List of tables

Table 3-1. Displacement thresholds at the assumed Damage States, based on the mechanical interpretation of the damage grades described by EMS-98.	85
Table 3-2: Median and logarithmic standard deviation values of predicted to observed data for RC capacity model (Haselton et al, 2008)	100
Table 3-3: Parameters selected as Random Variables for sensitivity analysis	103
Table 4-1.Type of design and material properties as a function of the age of construction	148
Table 4-2.Median and logarithmic standard deviation values of predicted to observed data for RC capacity model (Haselton et al, 2008)	149
Table 4-3.Building classes used for seismic fragility comparison.....	171
Table 5-1: Italian building classification for post-earthquake usability [from Goretti and Di Pasquale (2006)].....	194
Table 5-2.Type of design and material properties as a function of the age of construction	213
Table 5-3: Median and logarithmic standard deviation values of predicted to observed data for RC capacity model (Haselton et al, 2008)	215
Table 5-4. Displacement thresholds at the assumed Damage States, based on the mechanical interpretation of the damage grades described by EMS-98.	216
Table 5-5: Definition of infills Drift thresholds.....	220
Table 5-6. Definition of infills Drift thresholds [%] from (Colangelo, 2013).	220
Table 5-7: The equivalence in the association of Damage States between	

EMS98 and investigated methodologies (POST; Rota et al., 2008; Lagomarsino and Giovinazzi, 2006; Borzi et al., 2008b)	231
Table 6-1: indication of the sections that compose the survey form (Baggio et al. 2007).....	241
Table 6-2: Structural Typology Distribution for the whole building database	244
Table 6-3: Number of Storeys Distribution for the whole building database .	246
Table 6-4: Average storey surface Distribution for the whole building database	250
Table 6-5: Age of construction Distribution for the whole building database	251
Table 6-6: Possible usability outcomes from (Baggio 2007).....	260
Table 6-7: Usability outcomes Distribution for the whole building database	262
Table 6-8: Parameters of observational lognormal fragility curves for the class of building	276
Table 6-9: Definition of Building Class.....	283
Table 6-10: Parameters of lognormal fragility curves for the class of building	296
Table 7-1: Differences in terms of vulnerability and ductility indexes ΔQ e ΔV for low-rise and high-rise buildings on respect to medium-rise ones (from (Giovanazzi,2005)).....	336
Table 8-1: Properties of concrete	366
Table 8-2: Properties of reinforcing steel.....	366
Table 8-3: Properties of infill materials	367
Table 8-4: Evolution of damage in Infilled specimen GI-80	373
Table 8-5: Evolution of damage in Bare specimens GB and GB2.....	384
Table 8-6: Expected moment at first yielding and at maximum strength in beam and column (kNm)	401

Chapter 1

Introduction

1.1 Motivation

Among natural disasters, earthquakes represent one of the most unpredictable phenomena even lethal and devastating from the economic and social standpoint. Actually, earthquakes are able to produce effects in spread geographical areas far away from the epicentral areas in which the phenomenon triggers. Obviously the consequences in terms of casualties and in terms of damage to the structures and infrastructures are function of the degree of urbanization and the demographic level of the affected areas, as well as the quality and type of housing, which is connected substantially to the presence or absence of seismic codes for constructions. Hence, earthquakes frequently hits uninhabited areas, causing negligible losses, however, if the affected area is densely inhabited its consequences are devastating.

Moreover, rapid population growth and urbanization have made RC buildings the predominant type of construction in densely populated urban areas. In particular, in Italy in early after World War II, RC buildings became one of the most popular structural systems for multi-storey buildings.

Actually, between the methods for seismic vulnerability assessment of RC Buildings at large scale, most of them are essentially based on

the derivation of empirical fragility curves derived from observation of damage suffered during past seismic events (Braga et al., 1982, Di Pasquale et al., 2005, Rota et al., 2008) or such in (Lagomarsino and Giovinazzi, 2006), where fragility curves are derived from the damage probability matrix implicitly defined by European Macroseismic Scale (EMS98) (Grünthal, 1998). Conversely, very few mechanical methods for seismic vulnerability assessment of RC Buildings at large scale have been derived in last years, namely (Cosenza et al., 2005, Iervolino et al., 2007; Calvi, 1999; Crowley and Pinho, 2004, Borzi et al., 2008a), and even less methods accounting for the presence of infill panels (Borzi et al., 2008b).

Thus, a simplified method for seismic vulnerability assessment of infilled RC building is presented to respond to the need of supporting the decision process involved in policies of disaster prevention and emergency management.

Nevertheless, seismic vulnerability models not necessarily have to be used just after an earthquake in order to estimate losses in the affected area, but they can be used to manage the decision process involved in policies of disaster prevention, detecting the areas most prone at risk. Thus they can be used in cost/benefit studies for the evaluation of retrofitting solutions by comparing the costs for improving the seismic structural response with the potential losses subsequently avoided, thus guiding prioritization of financial intervention.

Moreover, earthquake loss models are used as basis for the decision-making process with respect to insurance policy. Hence, in order to mitigate the impact on government derived from the statutory obligation to cover the full costs of rebuilding, earthquake loss models are used to design insurance schemes allowing to privatise the risk.

1.2 Objectives

In this study, a simplified method for seismic vulnerability assessment of infilled RC building is presented. The methodology is essentially based on a simulated design procedure to evaluate the

geometrical and structural model of the building based on few data such as number of storeys, global dimensions and type of design (Verderame et al. 2010). Building non-linear static response is evaluated through a closed-form procedure starting from non-linear behavior of structural (RC columns) and non-structural components (infill panels), considering acting in parallel, thanks to the simplified assumption of a Shear Type behavior.

The assessment of the seismic capacity is based on the mechanical interpretation of the damage states described by the European Macroseismic Scale (EMS-98) (Grünthal, 1998) through the simplified IDA curves derived from (Vamvatsikos and Cornell, 2006). Hence the methodology allows to take into account the influence of infill panel both in the definition of the non-linear static response of building and seismic capacity, relating displacement thresholds on the non-linear behavior of infill sub-assemblages, selected on mechanical basis and experimentally validated, to the description of damage reported in EMS98.

A simulation technique is introduced to take into account uncertainties, and a probabilistic seismic capacity assessment is carried out, leading to the construction of fragility curves and, finally, to the evaluation of the failure probability in given time windows for the assumed damage states.

Hence, the procedure is applied, considering data with different level of detail as input parameters, namely from data provided by the field survey carried out within the framework of the SIMURAI Research Project (2010), and data derived from post-earthquake inspection form collected after 2009 L'Aquila earthquake (Dolce et al, 2015a; Dolce et al, 2015b).

Therefore, the influence of the detail level of input data on seismic vulnerability assessment at urban scale is investigated within a multilevel approach. To this aim, data from field survey are assumed as a reference, and when using census or Remote Sensing data, due to the lack of information affecting such data sources, some of the input

parameters to the seismic vulnerability assessment procedure are assumed as random variables.

Finally, a comparison between predicted and observed damage scenario, the latter derived from the damage grades reported for vertical structures and infill panels in the inspection form, is shown. The comparison between the results is used to test the reliability of numerical results and to allow validation and calibration of the analytical methodology. To this aim, proper analytical displacement thresholds corresponding to the damage to structural and non-structural elements described by EMS-98, based on the mechanical interpretation of the reported description of damage, have been set.

Afterwards, in order to investigate the influence of infill panels on global and local behaviour of the frame preliminary results of an experimental campaign on non-seismically designed infilled frames are presented. Experimental results show the importance in considering the local interaction between infill panel and surrounding RC frame. Hence, the post-elastic behavior of specimens was controlled by brittle failure mechanisms. In particular, failure of infilled specimen was due to shear failure at the top of the columns due to local interaction with infill panel.

1.3 Organization of the thesis

Chapter II presents an overview of literature methods, illustrating main empirical and analytical approaches to large scale vulnerability assessment.

Chapter III describes extensively the simplified method for seismic vulnerability assessment of infilled RC building, which has been implemented in POST (PushOver on Shear Type models), a software based on MATLAB® code ([Ricci, 2010](#), [Del Gaudio et al, 2015](#)).

Chapter IV exhibit the application of present methodology at single building level to the whole RC building stock of the city of Avellino, which has been the object of a field survey in the framework of SIMURAI Project (2010) that allowed to collect a database of

geometrical and morphological parameters of the whole building stock, such as number of storeys, structural typology and age of construction. Results of the procedure application are illustrated and discussed, showing the influence of key parameters in determining seismic fragility and the spatial distribution of the mean annual frequency of exceedance of the assumed damage states within the Municipality, thus identifying areas most prone to seismic risk.

Chapter V shows the application of present methodology at single building level for a sample of 131 buildings located in L'Aquila Municipality. As a matter of fact a database of 131 reinforced concrete (RC) buildings collected after 2009 L'Aquila earthquake, in the neighborhood of Pettino, has been derived. For each building the outcomes of official usability and damage inspections collected by Italian National Civil Protection right after the event are available. The comparison between predicted and observed damage scenario had allowed the validation and calibration of the analytical methodology. To this aim, proper analytical displacement thresholds corresponding to the damage to structural and non-structural elements described by EMS-98, based on the mechanical interpretation of the reported description of damage, have been set.

Chapter VI analyses the outcomes of about (78,062) official usability and damage inspections collected after 2009 L'Aquila earthquake by Italian National Civil Protection ([Dolce et al, 2015a](#); [Dolce et al, 2015b](#)). The data collected in a GIS database are analyzed in detail, showing the distribution of main parameters at the level of each municipality. Hence, they have allowed the derivation of empirical fragility curves for RC buildings for different assumed building typologies. Therefore, observed damage scenario is compared with analytical damage scenario, obtained from mechanical fragility curves for building classes derived from present methodology. The comparison shows a good agreement between the results, proving the reliability of present methodology.

Chapter VII presents a seismic vulnerability assessment at urban scale in a high-seismic city in Southern Italy using building stock data from different sources, namely (in a growing order of accuracy): census data providing information on buildings aggregate for relatively large spatial units (census cells); data from an airborne Remote Sensing mission carried out over the municipality, providing a detailed estimate of 3D geometric parameters of buildings; data from a field survey, provided detailed information on geometrical and structural characteristics of each single building. Such data are used, within a multilevel approach, in order to evaluate the influence of the detail level of input data on seismic vulnerability assessment at urban scale.

Chapter VIII shows preliminary results of an experimental campaign on one-storey one-bay frames (scale 1:2) representative of the existing Italian building stock. Frames are designed for gravity loads only according to code provisions and with material properties representative of 1970s-90s. Frames are tested both with and without the presence of infills, in order to investigate the influence of such (non-structural) elements on global and local behavior of the frame. Experimental results show that the post-elastic behavior of specimens was controlled by brittle failure mechanisms.

1.4 References

- Del Gaudio C., Ricci P., Verderame G.M., Manfredi G., 2015. Development and urban-scale application of a simplified method for seismic fragility assessment of RC buildings. *Engineering Structures*. Vol. 91, pp. 40-57. doi:10.1016/j.engstruct.2015.01.031
- Ricci P., 2010. Seismic vulnerability of existing RC buildings. PhD thesis, University of Naples Federico II, Naples, Italy.
- Dolce M., and Goretti A., 2015a. "Building damage assessment after the 2009 Abruzzi earthquake." *Bulletin of Earthquake Engineering* (2015): 1-24.
- Dolce M., Manfredi G., 2015b. Libro bianco sulla ricostruzione privata fuori dai centri storici nei comuni colpiti dal sisma dell'Abruzzo del 6 aprile 2009, ISBN 978-88-89972-50-2, Doppiavoce, Napoli, 2015. In press. (in italian)
- Grünthal G., 1998. *Cahiers du Centre Européen de Géodynamique et de Séismologie: Volume 15 – European Macroseismic Scale 1998*. European Center for Geodynamics and Seismology, Luxembourg.
- Vamvatsikos D., Cornell C.A., 2006. Direct estimation of the seismic demand and capacity of oscillators with multi-linear static pushovers through IDA. *Earthquake Engineering and Structural Dynamics*, 35(9), 1097-1117.
- Verderame G.M., Polese M., Mariniello C., Manfredi G., 2010. A simulated design procedure for the assessment of seismic capacity of existing reinforced concrete buildings. *Advances in Engineering Software*, 41(2), 323-335.
- Borzi B., Pinho R., Crowley H., 2008a. Simplified pushover-based vulnerability analysis for large scale assessment of RC buildings. *Engineering Structures*, 30(3), 804-820.
- Borzi B., Crowley H., Pinho R., 2008b, The influence of infill panels on vulnerability curves for RC buildings. *Proceedings of*

- the 14th World Conference on Earthquake Engineering, Beijing, China, October 12-17. Paper 09-01-0111.
- Braga F., Dolce M., Liberatore D., 1982. A statistical study on damaged buildings and an ensuing review of the MSK-76 scale. Proceedings of the 7th European Conference on Earthquake Engineering, Athens, Greece. Pp. 431-450.
 - Di Pasquale G., Orsini G., Romero R.W., 2005. New developments in seismic risk assessment in Italy. Bulletin of Earthquake Engineering, 3(1), 101-128.
 - Lagomarsino, S., Giovinazzi, S. (2006). "Macroseismic and mechanical models for the vulnerability assessment of current buildings." Bulletin of Earthquake Engineering, 4(4), 415-443.
 - Rota, M., A. Penna, and C. L. Strobbia. "Processing Italian damage data to derive typological fragility curves." Soil Dynamics and Earthquake Engineering 28.10 (2008): 933-947.
 - Cosenza E., Manfredi G., Polese M., Verderame G.M., 2005. A multi-level approach to the capacity assessment of existing RC buildings. Journal of Earthquake Engineering, 9(1), 1-22.
 - Iervolino I., Manfredi G., Polese M., Verderame G.M., Fabbrocino G., 2007. Seismic risk of R.C. building classes. Engineering Structures, 29(5), 813-820.
 - Calvi G.M., 1999. A displacement-based approach for vulnerability evaluation of classes of buildings. Journal of Earthquake Engineering, 3(3), 411-438.
 - Crowley H., Pinho R., Bommer J.J., 2004. A probabilistic displacement-based vulnerability assessment procedure for earthquake loss estimation. Bulletin of Earthquake Engineering, 2(2), 173-219.

Chapter 2

Simplified methods for seismic vulnerability assessment of RC buildings at large scale

2.1 Introduction

Earthquakes are one of the highest sources of natural risk, leading to heavy human and economic losses worldwide, also due to the presence of very large and populated cities – where structural quality of constructions often is not on a level with modern prescriptions of earthquake engineering – in areas of high seismic hazard. The impact of these losses on national economy can be really heavy, particularly in less developed countries. Hence, assessment and mitigation of seismic risk is of a fundamental importance.

In order to support the decision process involved in policies of disaster prevention and emergency management, complete and reliable instruments for seismic risk analysis are needed, such as loss models. These models do not only support the disaster emergency planning, but can also be used in cost/benefit studies for the evaluation of retrofitting solutions by comparing the costs for improving the seismic structural response with the potential losses subsequently avoided, thus guiding prioritization of financial intervention. Moreover, loss models are needed to design insurance schemes allowing to privatise the risk, thus

mitigating the impact on the national economy by avoiding the economic burden to fall entirely on the government.

Loss models provide the expected losses at a given site of interest and in a given time window by convolving the seismic hazard, the vulnerability of the structures and infrastructures composing the built environment and the exposed value (accounting for costs of repair or replacement of structures, contents losses and interruption of activities due to the loss of functionality).

In this framework, structural vulnerability is given by methodologies which provide the probability of a given level of damage as a function of a parameter representing the seismic intensity (e.g., macroseismic intensity, Peak Ground Acceleration (PGA)). A method for the assessment of seismic vulnerability of a building stock has to represent the best compromise between reliability and reasonable demand of computational effort, depending on the availability of data (that is, the availability of time and money necessary to gather them) and on the required level of detail.

A fundamental distinction has to be made between empirical and analytical vulnerability methods: in empirical methods the assessment of expected damage for a given building typology is based on the observation of damage suffered during past seismic events; in analytical methods the relationship between seismic intensity and expected damage is provided by a model with direct physical meaning.

Reliability and significance of observed data allow empirical methods to give a realistic indication about expected damage, provided they are applied to a building stock with similar characteristic compared with the one used for their construction. However, different disadvantages come from the use of empirical methods. These methods do not allow to account for the vibration characteristics of the buildings. They do not explicitly model the different sources of uncertainty, thus not allowing to remove the uncertainty in the seismic demand from the vulnerability assessment. A macroseismic measure is often used to define the

seismic intensity, but macroseismic intensity is, in turn, obtained from observed damage, thus seismic intensity and damage are not independent (Crowley et al., 2009). The collection of data about building damage after a seismic event, required for the derivation of any empirical relationship between seismic intensity and expected damage, is affected by different shortcomings such as a not homogeneous availability of data, resulting in a higher statistical reliability for the low damage/ground motion range compared with the high damage/ground motion range, or the errors due to inadequate compilation of the post-earthquake assessment forms (Colombi et al., 2008). Also, empirical methods do not allow to model the influence of retrofit solutions on vulnerability, given by the improvement in structural response.

On the contrary, the use of an algorithm to evaluate the structural vulnerability allows to take into account directly and transparently, in a detailed way, the various characteristics of building stock, and also to explicitly account for the uncertainties involved in the assessment procedure. An analytical approach allows to include in the vulnerability assessment structures characterized by different (or new) construction practices, as well as to consider the influence of retrofitting on the response of existing structures. Furthermore, analytical methods can take advantage of advances in seismic hazard assessment, such as the derivation of seismic hazard maps in terms of spectral ordinates (e.g., INGV-DPC S1, 2007), different from macroseismic intensity or PGA. However, generally speaking analytical methods need a larger amount of detailed data and a higher computational effort, compared with empirical methods. Therefore, the effective increase in accuracy of vulnerability assessment, when analytical methods are adopted, should be checked by means of a comparison with observed damage data. Further critical issues in the application of analytical methods have to be carefully considered: first of all, the degree of confidence in the capability of a numerical model to accurately predict the response of real structures and, in particular, the confidence in the correlation

between the assumed analytical damage index (such as the interstorey drift or a cyclic damage index) and the actual structural damage. Also, many of the collapses observed after seismic events are due to constructive errors and deficiencies, which normally are not considered in an analytical model (e.g., Verderame et al., 2010).

Empirical and analytical methods can be used complementing each other, as happens in so-called “hybrid” methods. Moreover, relationships between seismic intensity and expected damage for different structural typologies can also be based on expert-judgement.

A very comprehensive and detailed review of seismic vulnerability assessment methodologies can be found in (Calvi et al., 2006). In the following, main vulnerability assessment procedures are illustrated, referring to Reinforced Concrete (RC) buildings.

2.2 Empirical Methods

First developments of seismic vulnerability assessment of building stocks took place in 1970s, through empirical methods based on macroseismic intensity; at the time, the major part of hazard maps adopted this kind of measure for the seismic intensity.

Different types of empirical methods for the seismic vulnerability assessment of buildings can be distinguished:

- Damage Probability Matrices (DPMs), expressing in a discrete form the conditional probability of reaching a damage level $D = j$ due to a ground motion of intensity $I = i$, $P_{ij} = P [D = j \mid I = i]$;
- vulnerability functions, expressing in a continuous form the probability $P_{ij} = P [D \geq j \mid I = i]$;
- methods based on a so-called “Vulnerability Index”;
- screening methods.

2.2.1 Damage Probability Matrices

First DPMs have been proposed in (Whitman et al., 1973), see Figure 2-1 for a given structural typology, the probability of being in a given state of structural and non-structural damage is provided. For each damage state, the damage ratio is provided too, representing the ratio between the cost of repair and the cost of replacement. These DPMs are compiled for different structural typologies based on the damage observed in over 1600 buildings after the 1971 San Fernando earthquake.

Damage State	Structural Damage	Non-structural Damage	Damage Ratio (%)	Intensity of Earthquake				
				V	VI	VII	VIII	IX
0	None	None	0-0.05	10.4	-	-	-	-
1	None	Minor	0.05-0.3	16.4	0.5	-	-	-
2	None	Localised	0.3-1.25	40.0	22.5	-	-	-
3	Not noticeable	Widespread	1.25-3.5	20.0	30.0	2.7	-	-
4	Minor	Substantial	3.5-4.5	13.2	47.1	92.3	58.8	14.7
5	Substantial	Extensive	7.5-20	-	0.2	5.0	41.2	83.0
6	Major	Nearly total	20-65	-	-	-	-	2.3
7	Building condemned		100	-	-	-	-	-
8	Collapse		100	-	-	-	-	-

Figure 2-1: Damage Probability Matrix proposed by Whitman et al. (1973) (from (Calvi et al., 2006))

Braga et al. (1982) propose the first European version of DPMs based on the damage observed after the 1980 Irpinia earthquake. Three vulnerability classes (A, B and C) corresponding to different building typologies are defined, and the seismic intensity measure is based on the Medvedev-Sponheuer-Karnik (MSK) scale.

DPMs proposed by Braga et al. (1982) are improved by Di Pasquale et al. (2005) changing the seismic intensity measure from the MSK to the Mercalli-Cancani-Sieberg (MCS) scale and dividing class C into two sub-classes to differentiate between good masonry (C1) and RC

buildings (C2) (see Figure 2-2), as described in (Di Pasquale and Orsini, 1997). Furthermore, the number of buildings is replaced by the number of dwellings in order to use the original inventory from the 1991 census of the Italian National Institute of Statistics (Istituto Nazionale di Statistica, ISTAT).

The DPMs from (Braga et al., 1982) are also adapted for the town of Potenza by Dolce et al. (2003), adding the vulnerability class D, which represents the buildings constructed since 1980, and expressing the seismic intensity according to the European Macroseismic Scale (EMS-98) (Grünthal, 1998).

Table I. Vulnerability classes vs. horizontal and vertical structural elements.

Horizontal structure	Vertical structure			
	Masonry walls			R.C.
	Field stone	Hewn stone	Bricks	
Vaults	<i>A</i>	<i>A</i>	<i>A</i>	\
Wood	<i>A</i>	<i>A</i>	<i>B</i>	\
Steel & vaults	<i>B</i>	<i>B</i>	<i>C1</i>	\
R.C.	<i>B</i>	<i>C1</i>	<i>C1</i>	<i>C2</i>

Table II. Vulnerability classes vs. age for masonry buildings.

Age	Vulnerability class		
	<i>A</i>	<i>B</i>	<i>C1</i>
< 1919	0.74	0.23	0.03
'19-'45	0.52	0.40	0.08
'46-'60	0.25	0.47	0.28
'61-'71	0.04	0.31	0.65
'72-'91	0.02	0.19	0.79

Figure 2-2: Vulnerability classes adopted in (Di Pasquale et al., 2005)

According to EMS-98 scale six vulnerability building classes (A to F, see Figure 2-3) are defined, then for each class a qualitative description

(“few”, “many” and “most”, see Figure 2-4) of the proportion of buildings suffering a given level of damage (1 to 5, see Figure 2-5) is provided as a function of the seismic intensity level, ranging from V to XII. Hence, DPMs are implicitly defined in EMS-98 scale. Nevertheless, they are incomplete (the proportion of buildings suffering a given damage level for a given seismic intensity is not provided for all possible combinations of damage levels and seismic intensities) and vague (proportion of buildings is described only qualitatively)

Type of Structure		Vulnerability Class					
		A	B	C	D	E	F
MASONRY	rubble stone, fieldstone	○					
	adobe (earth brick)	○	—				
	simple stone	—	○				
	massive stone		—	○	—		
	unreinforced, with manufactured stone units	—	○	—			
	unreinforced, with RC floors		—	○	—		
	reinforced or confined			—	○	—	
REINFORCED CONCRETE (RC)	frame without earthquake-resistant design (ERD)	—	—	○	—		
	frame with moderate level of ERD		—	—	○	—	
	frame with high level of ERD			—	—	○	—
	walls without ERD		—	○	—		
	walls with moderate level of ERD			—	○	—	
	walls with high level of ERD				—	○	—
STEEL	steel structures			—	—	○	—
WOOD	timber structures		—	—	○	—	

○ most likely vulnerability class; — probable range;
range of less probable, exceptional cases

Figure 2-3: Vulnerability classes according to EMS-98 scale (Grünthal, 1998)

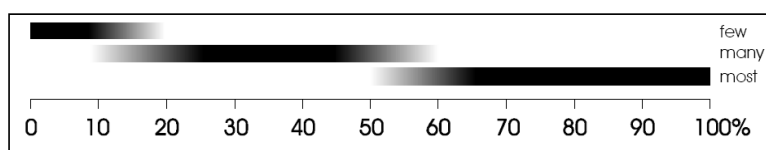


Figure 2-4: Definition of quantities “few”, “many” and “most” according to EMS-98 scale (Grünthal, 1998)

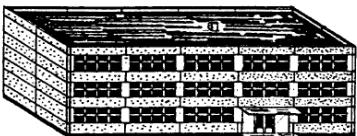
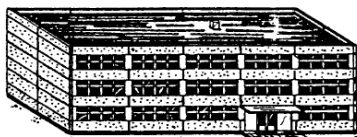
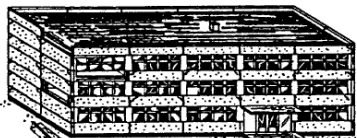
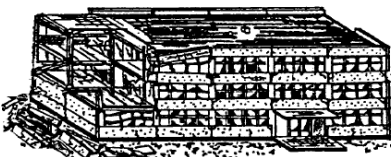

Classification of damage to buildings of reinforced concrete	
	<p>Grade 1: Negligible to slight damage (no structural damage, slight non-structural damage)</p> <p>Fine cracks in plaster over frame members or in walls at the base.</p> <p>Fine cracks in partitions and infills.</p>
	<p>Grade 2: Moderate damage (slight structural damage, moderate non-structural damage)</p> <p>Cracks in columns and beams of frames and in structural walls.</p> <p>Cracks in partition and infill walls; fall of brittle cladding and plaster. Falling mortar from the joints of wall panels.</p>
	<p>Grade 3: Substantial to heavy damage (moderate structural damage, heavy non-structural damage)</p> <p>Cracks in columns and beam column joints of frames at the base and at joints of coupled walls. Spalling of concrete cover, buckling of reinforced rods.</p> <p>Large cracks in partition and infill walls, failure of individual infill panels.</p>
	<p>Grade 4: Very heavy damage (heavy structural damage, very heavy non-structural damage)</p> <p>Large cracks in structural elements with compression failure of concrete and fracture of rebars; bond failure of beam reinforced bars; tilting of columns.</p> <p>Collapse of a few columns or of a single upper floor.</p>
	<p>Grade 5: Destruction (very heavy structural damage)</p> <p>Collapse of ground floor or parts (e. g. wings) of buildings.</p>

Figure 2-5: Definition of damage grades to RC buildings according to EMS-98 scale (Grünthal, 1998)

Giovinazzi and Lagomarsino (2004) start from these matrices and overcome their limits of incompleteness and vagueness, then relate the obtained DPMs to the building stock through a vulnerability index.

2.2.2 Continuous vulnerability curves

Relationships between seismic intensity and expected damage based on empirical data can also be derived in a continuous form.

Orsini (1999) elaborates the data of the damage survey carried out after the 1980 Irpinia earthquake in order to evaluate, for each municipality, a value of seismic intensity according to the Parameterless Scale of Intensity (PSI) proposed by Spence et al. (1991). The main hypothesis at the basis of the PSI model is that the intensity at which the structures belonging to a single vulnerability class overcome a given damage threshold is continuously distributed according to a Gaussian model. The use of PSI allows the definition of continuous vulnerability functions depending on a macroseismic intensity parameter, tackling the problem that macroseismic intensity is not a continuous variable. After determining PSI values for each municipality, Orsini (1999) proposes vulnerability curves for apartment units as a function of this continuous parameter.

Sabetta et al. (1998) derive vulnerability curves depending on PGA, Arias Intensity and effective peak acceleration based on the elaboration of about 50000 building damage surveys from past Italian earthquakes, by calculating for each municipality a mean damage index as the weighted average of the frequencies of each damage level for each structural class.

Rota et al. (2008) select more than 91000 damage survey forms from past Italian earthquakes out of a total amount of 164000 ones, (i) disregarding the data affected by important information missing and (ii) including only data related to municipalities surveyed for at least 60%, thus avoiding a biased sample. The authors subdivide these data into 23 different building

typologies and 10 ground motion intervals. Both PGA and Housner intensity are considered as ground motion parameters; their values are estimated for each municipality using the attenuation law of Sabetta and Pugliese (1987, 1996) for rock conditions, with the parameters (magnitude and epicentral coordinates) of the earthquake of interest. The adopted damage scale is similar to the EMS-98 scale, consisting of five levels of damage plus the case of no damage. DPMs are extracted from the data for all of the 23 considered vulnerability classes, according to the defined damage scale and seismic intensity scale. Hence, continuous vulnerability curves are obtained by fitting with lognormal distributions the data evaluated in form of DPMs; also, when carrying out this fitting, for each sample (given a building class, a seismic intensity and a damage level) the inverse of the estimated standard deviation is used as a weight expressing the reliability of the single sample.

It is to be noted that when the seismic intensity is measured by means of a parameter related to the spectral acceleration or spectral displacement at the fundamental period of vibration (e.g., Rossetto and Elnashai, 2003), different from macroseismic intensity or PGA, the vulnerability curves show a better prediction capacity, because taking into consideration the relationship between the frequency content of the ground motion and the dynamic characteristics of the building stock.

2.2.3 Vulnerability Index method

The “Vulnerability Index” method is first proposed in (Benedetti and Petrini, 1984; GNDT, 1993). The index I_v is evaluated by means of a field survey form where “scores” K_i (from A to D) are assigned to eleven parameters having a high influence on building vulnerability (e.g., plan and elevation configuration, type of foundation, structural and non-structural elements); then, the index is defined as the weighted sum

$$I_v = \sum_{i=1}^{11} K_i W_i \quad \text{Eq 2-1}$$

according to the importance assigned to each parameter.

Based on observed damage data from past earthquakes, for different values of this vulnerability index a relationship can be calibrated between seismic intensity and damage ratio (see Figure 2-6).

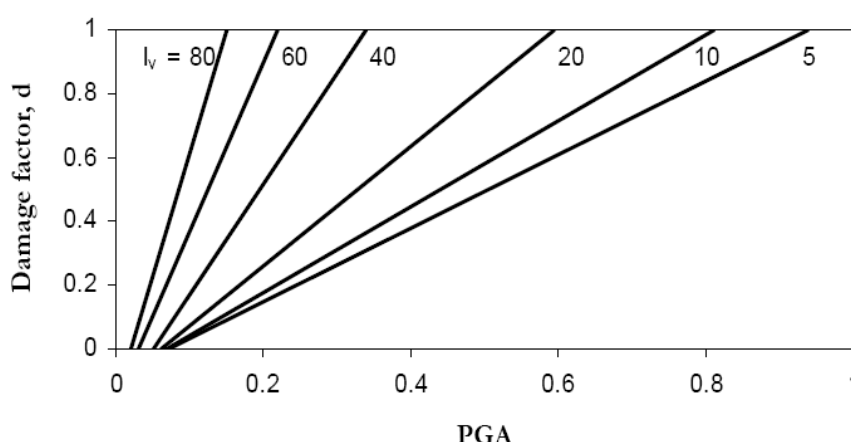


Figure 2-6: Vulnerability functions to relate damage ratio and PGA for different values of vulnerability index (adapted from Guagenti and Petrini (1989)) (from (Calvi et al., 2006))

The use of Vulnerability Index Method was quite widespread; it was also adopted in different projects such as RISK-UE (Mouroux and Le Brun, 2006) and “Progetto Catania” (Faccioli et al., 1999; Faccioli and Pessina, 2000).

2.2.4 Screening methods

According to the Japanese Seismic Index Method (JBDPA, 1990), the seismic performance of the building is represented by a seismic

performance index, I_s , evaluated by means of a screening procedure. The procedure can be carried out according to three different levels of detail. I_s is calculated for each storey in every frame direction according to the following expression:

$$I_s = E_0 S_D T \quad \text{Eq 2-2}$$

where E_0 , S_D and T correspond to the basic structural performance, to the structural design and to the time-dependent deterioration of the building, respectively. E_0 is given by the product between C and F , respectively representing the ultimate strength and the ductility of the building, depending on the failure mode, the total number of storeys and the position of the considered storey. S_D accounts for irregularity in stiffness and/or mass distribution. A field survey is needed to define T . The calculated seismic performance index I_s is compared with the seismic judgement index I_{s0} to determine the degree of safety of the building. I_{s0} represents a storey shear force and is given by

$$I_{s0} = E_s Z G U \quad \text{Eq 2-3}$$

where E_s conservatively increases with the decreasing accuracy of the screening procedure, Z is a zone index modifying the ground motion intensity assumed at the site of the building, G accounts for local effects such as ground-building interaction or stratigraphic and topographic amplification and U is a kind of importance factor depending on the function of the building. In the 1998 revised version of the Japanese Building Standard Law the index I_{s0} is taken as the spectral acceleration (in terms of g) at the period of the considered building, and it should be distributed along the height of the structure according to a triangular distribution.

Preliminary assessment methods based on screening procedures have been proposed in Turkey, too, during last years. Some methods require the dimensions of the lateral load resisting elements to be defined: the “Priority Index” proposed by Hassan and Sozen (1997) is a function of a wall index (area of walls and infill panels divided by total floor area) and a column index (area of columns divided by total floor area); the “Capacity Index” proposed by Yakut (2004) depends on orientation, size and material properties of the lateral load-resisting structural system as well as the quality of workmanship and materials and other features such as short columns and plan irregularities. The Seismic Safety Screening Method (SSSM) by Ozdemir et al. (2005) derives from the Japanese Seismic Index Method (JBDPA, 1990): in this method, too, the seismic capacity of a building is represented by a seismic index value which is a function of structural strength and ductility; this index value has to be compared with a seismic demand index value – representing the seismic hazard of the zone where the building is located – for assessing the degree of safety of the building.

2.3 Analytical Methods

Singhal and Kiremidjian (1996) estimate vulnerability curves and DPMs for different RC frames (from Low-Rise, Mid-Rise and High-Rise classes, respectively) through nonlinear dynamic analyses and using the Monte Carlo simulation technique (see Figure 2-7).

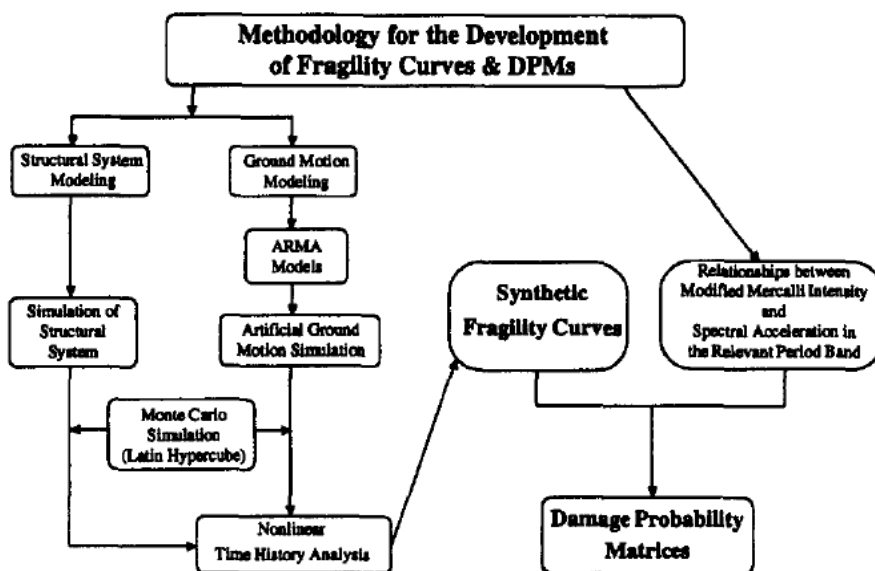


Figure 2-7: General framework of the methodology adopted in (Singhal and Kiremidjian, 1996)

The uncertainties associated with structural capacities and demands are modelled. Uncertainty in capacity is simulated assuming as random variables the compressive strength of concrete and the yield strength of steel. Uncertainty in seismic demands is accounted for by simulating 100 artificial time histories. Then, the conditional probability of reaching or exceeding a damage state given a ground motion intensity is determined by the Monte Carlo simulation method. 100 Latin hypercube samples are used for the nonlinear dynamic analyses at each ground motion level (expressed in terms of spectral acceleration value). After performing nonlinear dynamic analyses, for each level of ground motion the statistics of the Park and Ang (1985) damage index are used to obtain the parameters of a lognormal probability distribution function at that ground motion level (see Figure 2-8).

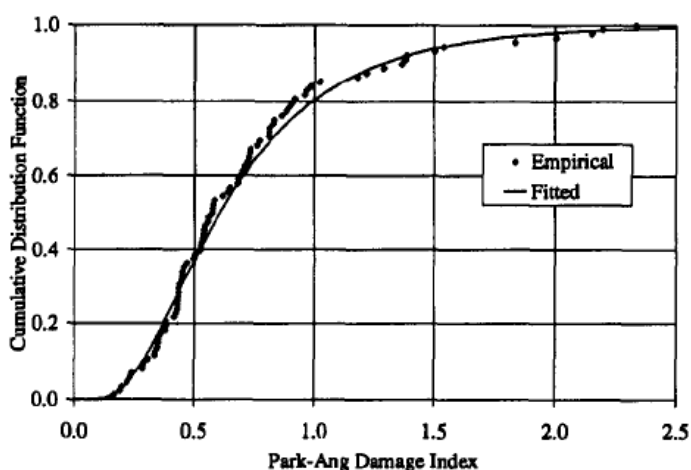


Figure 2-8: Probability distribution of Park and Ang's damage index at $S_a=3g$ (Singhal and Kiremidjian, 1996)

The lognormal probability functions at each level of ground motion are then used to obtain the probabilities of reaching or exceeding a damage state, adopting given threshold values for the different damage states (see Figure 2-9).

Damage state (1)	Range of the Park and Ang index (2)
Minor	0.1–0.2
Moderate	0.2–0.5
Severe	0.5–1.0
Collapse	>1.0

Figure 2-9: Ranges of Park and Ang's damage index for different damage states (Singhal and Kiremidjian, 1996)

Discrete points representing the probabilities of different damage states for a given spectral acceleration value are evaluated from the probability distributions of the damage measure. Hence, smooth

vulnerability curves are obtained fitting lognormal distribution functions to these points (see Figure 2-10).

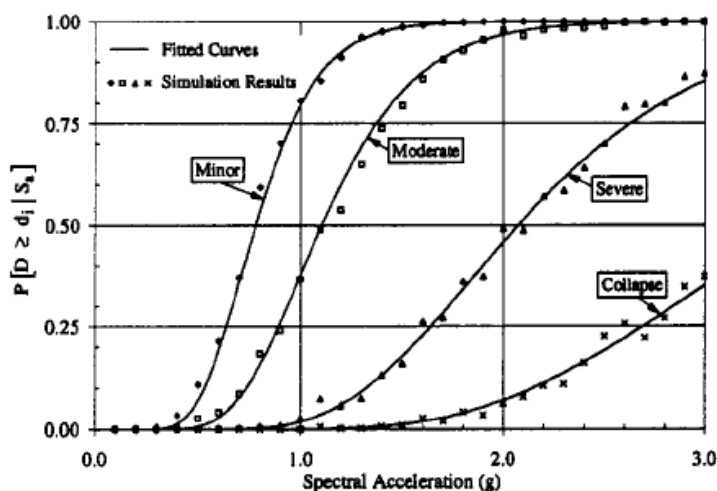


Figure 2-10: Vulnerability curves for Mid-Rise frames (Singhal and Kiremidjian, 1996)

The relationship between the Modified Mercalli Intensity (MMI) and the average spectral acceleration (that is, the conditional probability of a spectral acceleration at a specified MMI value) in each period band, which is assumed to be lognormal, is developed in the paper based on average spectral acceleration values of the ground motions recorded on firm sites and the MMI values from these earthquakes at the respective recording stations (see Figure 2-11).

Finally, DPMs are evaluated from the fragility curves by calculating the probability of reaching or exceeding a given damage state for a given MMI intensity (see Figure 2-12). This probability is obtained by convolving (i) the probability of reaching or exceeding the given damage state for a specified MMI and spectral acceleration and (ii) the conditional probability of a spectral acceleration at specified MMI.

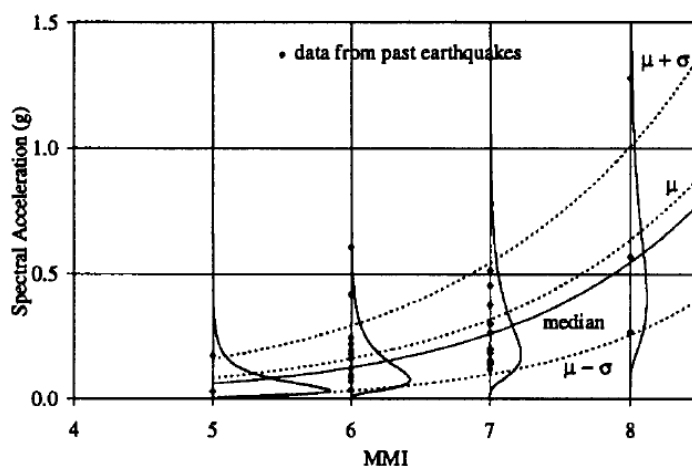


Figure 2-11: Correlation between MMI intensity and spectral acceleration over period range 0.5-0.9 s (Singhal and Kiremidjian, 1996)

Damage state (1)	Modified Mercalli Intensity						
	VI (2)	VII (3)	VIII (4)	IX (5)	X (6)	XI (7)	XII (8)
None	99.0	93.5	70.0	24.5	1.6	—	—
Minor	0.7	4.2	15.8	23.0	6.1	0.1	—
Moderate	0.3	2.1	12.0	36.6	33.7	4.9	0.2
Severe	—	0.2	1.9	12.5	34.6	22.3	1.8
Collapse	—	—	0.3	3.4	24.0	72.7	98.0

Figure 2-12: Damage Probability Matrix for Mid-Rise frames (Singhal and Kiremidjian, 1996)

A similar approach is adopted in (Masi, 2003), where three main structural typologies are examined: bare frames, regularly infilled frames and pilotis frames, designed for gravity loads only. Structural models are generated through a simulated design procedure considering current practice and codes in force at the age of construction. Nonlinear dynamic analyses with ground motions of various levels of intensity are carried out. Based on the obtained

results, each type of building can be assigned to a different vulnerability class of EMS-98 scale.

Rossetto and Elnashai (2005) derive vulnerability curves for a low-rise infilled RC frame with inadequate seismic provisions according to the following methodology: a population of 25 buildings is generated from a single building through consideration of material parameter uncertainty; uncertainty in demand is accounted for through the use of 30 different accelerograms; for each of the generated buildings, an adaptive pushover analysis is carried out, and the performance point is found following the Capacity Spectrum framework of assessment, for all the accelerograms; a damage scale experimentally calibrated to maximum inter-storey drift is adopted. Hence, the results of the population assessment are used to generate second-order response surfaces, one for each damage state. Vulnerability curves are generated from response surfaces through re-sampling. The derived curves show good correlation with observational post-earthquake damage statistics.

In (Cosenza et al., 2005) a procedure to evaluate the seismic capacity of a building class is proposed that enables to reduce dispersion of results depending on the level of knowledge. A building class is defined in terms of age of construction and number of storeys. The level of knowledge of the building stock is accounted for through a “specification” of building classes in different orders depending on the level of knowledge of the parameters. RC rectangular shaped frame buildings are considered.

For each class, a number of building models is generated by means of a simulated design procedure, based on the probabilistic distribution of the structural (geometrical and mechanical) parameters. Seismic capacity is determined in terms of base shear coefficient and global drift for each of the generated buildings of the building class, through a

mechanics-based approach: $3n_z$ predefined mechanisms, where n_z is the number of storeys, are considered (see Figure 2-13) and the corresponding base shear, V_{bi} , is calculated for each mechanism assuming a linear distribution of horizontal seismic forces.

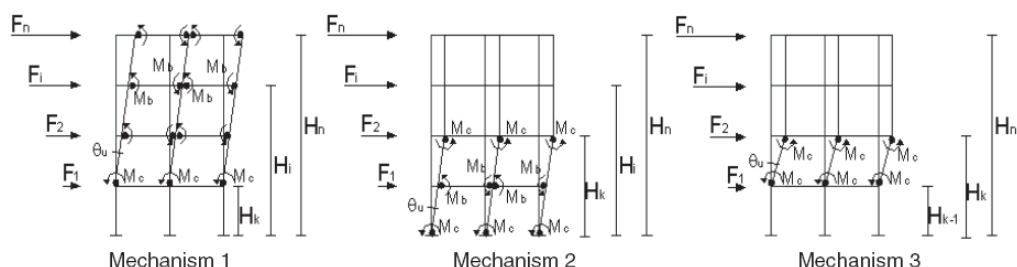


Figure 2-13: Predefined collapse mechanisms (Cosenza et al., 2005)

The ultimate roof displacement Δ_{ui} is determined as a function of the ultimate rotation θ_u of the structural elements:

$$\Delta_{u,1} = \theta_u \cdot (H_n - H_k) \quad \text{Eq 2-4}$$

$$\Delta_{u,2} = \theta_u \cdot H_k \quad \text{Eq 2-5}$$

$$\Delta_{u,3} = \theta_u \cdot (H_k - H_{k-1}) \quad \text{Eq 2-6}$$

The collapse mechanism is identified by the lowest value of V_{bi} . Then, the capacity of the building is finally evaluated in terms of base shear coefficient $C_{b,i}$ (= ratio between the base shear $V_{b,i}$ and the seismic weight W) and corresponding lateral (drift) $_i$ (= ratio between the ultimate roof displacement $\Delta_{u,i}$ and the building height H_n) for the determined collapse mechanism:

$$C_{b,i} = \frac{V_{b,i}}{W} \quad \text{Eq 2-7}$$

$$(\text{drift}_u)_i = \frac{\Delta_{u,i}}{H_n} \quad \text{Eq 2-8}$$

Starting from the capacity of the analyzed buildings, the response surface method is adopted and the influence of each parameter is investigated. Capacity curves expressing the probability of having a capacity lower than the assigned value are obtained through a Monte Carlo simulation technique. The influence of the knowledge level on the probability of reaching a fixed capacity threshold is shown, too.

However, this study only provides cumulative frequency distributions of capacity parameters (base shear coefficient and ultimate roof drift) within a building class. No vulnerability curve, relating a seismic demand measure to the probability of reaching or exceeding a given damage state, is provided.

In (Iervolino et al., 2007) a complete seismic risk assessment framework is presented, where the mechanisms-based approach is overcome.

In order to investigate the building class capacity, n geometrical and mechanical characteristics of the buildings are identified as random variables. Then, a possible range of variation and a corresponding “scanning step” are assumed for each one of this variables. A simulated design procedure, a nonlinear FE modelling of the structure and a Static PushOver (SPO) analysis are carried out for all of the resulting combinations of values. Hence, response surfaces are obtained for the capacity parameters T (period), C_s (strength) and C_d (displacement capacity) of the equivalent SDOF system (see Figure 2-14), expressed as function of the assumed random variables.

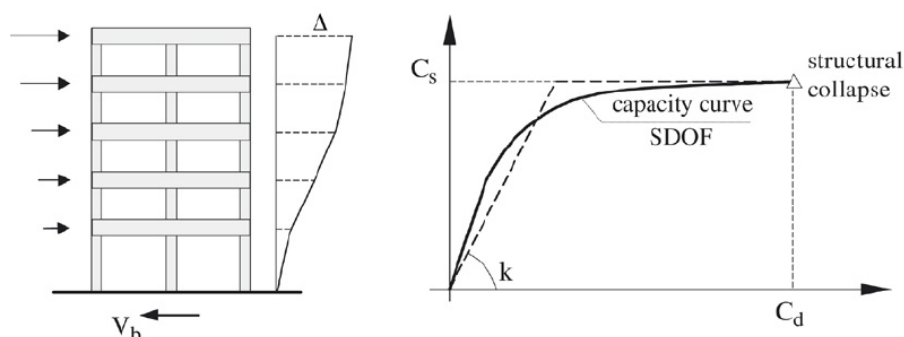


Figure 2-14: Capacity parameters (Iervolino et al., 2007)

Seismic demand is provided by Probabilistic Seismic Hazard Analysis (PSHA).

Hence, a calculation of seismic risk can be carried out through a Monte Carlo simulation technique, according to the following steps:

- sampling of N values of the n input random variables describing different geometrical and mechanical building characteristics according to the Probability Density Functions (PDFs) respectively assigned;
- evaluation of N arrays of capacity parameters $\{T, C_s, C_d\}$ as a function of the sampled random variables by linearly interpolating between the points obtained from the SPO analyses;
- sampling of N values of elastic spectral displacement demand $S_{d,e}$ according to the probability distribution given by the PSHA;
- evaluation of the corresponding N values of *median* inelastic displacement demand $S_{d,i} = S_{d,e} \cdot C_R$ according to the Capacity Spectrum Method assessment procedure (Fajfar, 1999);
- sampling of N values of the random variable ε_{C_R} representing the variability of the inelastic displacement demand, according to

the assigned PDF, thus giving the N final values of the displacement demand $D = S_{d,i} \cdot \varepsilon_{CR}$;

-comparison between the N values of displacement capacity C_d and the corresponding N values of displacement demand D , thus leading to the number N_f of buildings for which the capacity is exceeded by the demand;

-estimation of the failure probability as $P_f = \frac{N_f}{N}$.

HAZUS (HAZard in United States) is an earthquake loss estimation methodology including many components. It was developed by the Federal Emergency Management Agency (FEMA) under agreements with the National Institute of Building Sciences (NIBS) (FEMA, 2001; Kircher et al., 1997a; Kircher et al., 1997b; Whitman et al., 1997).

Estimates of building damage are used as inputs to other damage modules. Most importantly, building damage is used as an input to a number of loss modules (see Figure 2-15).

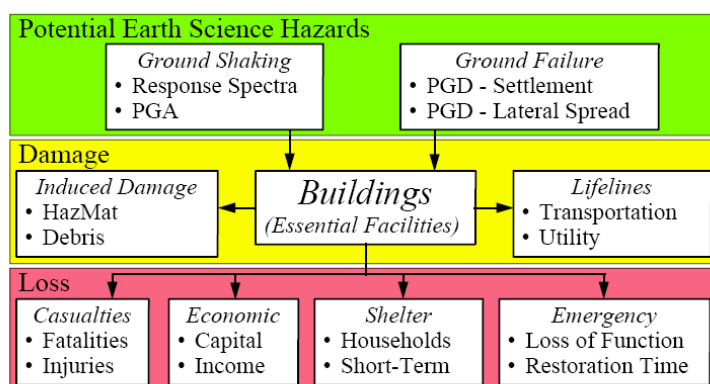


Figure 2-15: Building-related modules of HAZUS methodology (FEMA, 2001)

HAZUS damage functions for ground shaking have two basic components: capacity curves and fragility curves.

Capacity curves are defined by two control points: the yield capacity and the ultimate capacity. The yield capacity accounts for design strength, redundancies in design, conservatism in code requirements and expected (rather than nominal) strength of materials. Design strengths of model building types are based on the requirements of US seismic code provisions or on an estimate of lateral strength for buildings not designed for earthquake loads. The ultimate capacity represents the maximum strength of the building when the global structural system has reached a full mechanism. Up to yield, the building capacity curve is assumed to be linear with stiffness based on an estimate of the expected “elastic” period of the building. From yield to the ultimate point, the capacity curve transitions in slope from an essentially elastic state to a fully plastic state. The capacity curve is assumed to remain plastic past the ultimate point (see Figure 2-16).

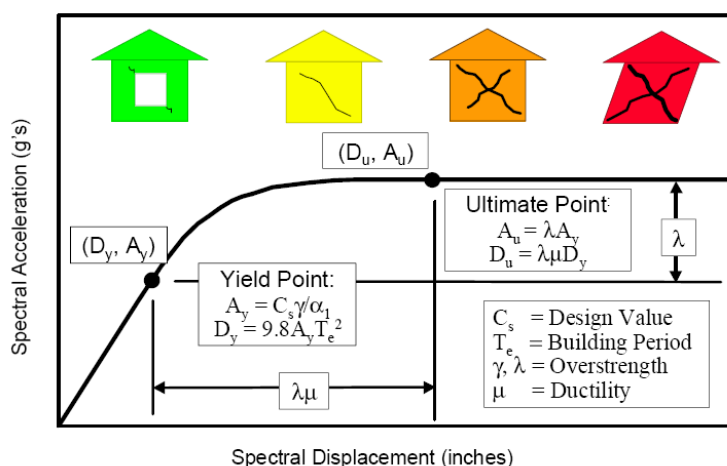


Figure 2-16: Example building capacity curve and control points (FEMA, 2001)

36 different building structural typologies are considered. For each typology, values of the parameters defining the capacity curves are

provided. As an example, see Figure 2-17 and Figure 2-18 for C1M building class (Mid-Rise Concrete Moment Frame).

Seismic Design Level	Elastic Period (sec.)	Average Inter-Story Drift Ratio					
		Capacity Curve Control Points		Structural Damage State Thresholds (Fragility Medians)			
		Yield	Plastic	Slight	Moderate	Extensive	Complete
Special High-Code	0.75	0.0038	0.0614	0.0042	0.0083	0.0250	0.0667
High-Code	0.75	0.0026	0.0410	0.0033	0.0067	0.0200	0.0533
Moderate-Code	0.76	0.0013	0.0154	0.0033	0.0058	0.0156	0.0400
Low Code	0.76	0.0006	0.0064	0.0033	0.0053	0.0133	0.0333
Pre-Code	0.76	0.0006	0.0077	0.0027	0.0043	0.0107	0.0267

1. A typical C1M building is 5-stories (i.e., 50 feet) in height. Spectral displacement is equal to 0.75 x roof displacement and base shear is equal to 0.80W x spectral acceleration.

Figure 2-17: “Elastic” period values and average inter-story drift ratios of capacity curve control points and structural damage state thresholds (fragility medians) for C1M¹ building class (FEMA, 2001)

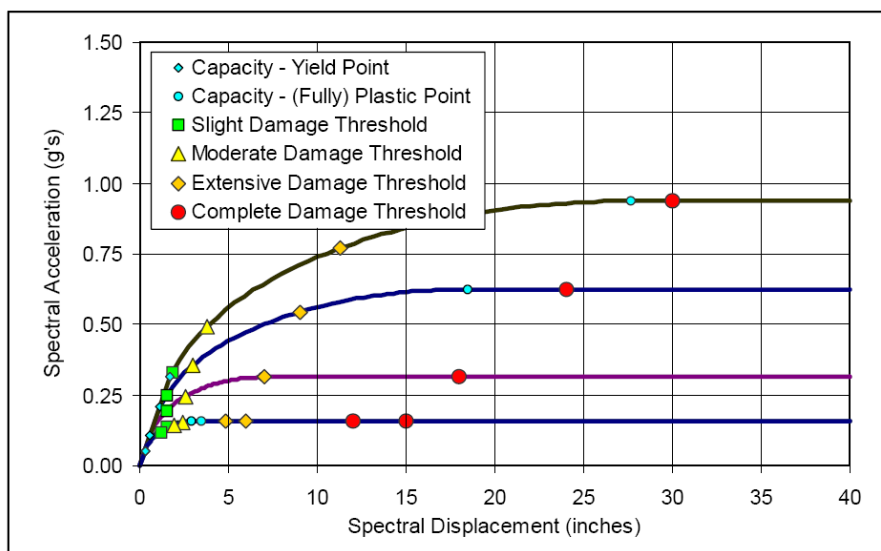


Figure 2-18: Capacity curves and structural damage-state thresholds (fragility medians)

for five seismic design levels (Special High, High, Moderate, Low and Pre-Code) for C1M building class (FEMA, 2001)

Capacity Spectrum Method is adopted in HAZUS to evaluate the demand corresponding to a given seismic intensity. To this end, the inelastic demand spectrum is obtained reducing the 5%-damped elastic response spectrum by means of an effective damping value which is defined as the total energy dissipated by the building during peak earthquake response and is the sum of an elastic damping term, β_E , and a hysteretic damping term, β_H , associated with post-yield, inelastic response and influenced by ground motion duration. Then, peak response displacement and acceleration are determined from the intersection between the demand spectrum and the building's capacity curve (see Figure 2-19).

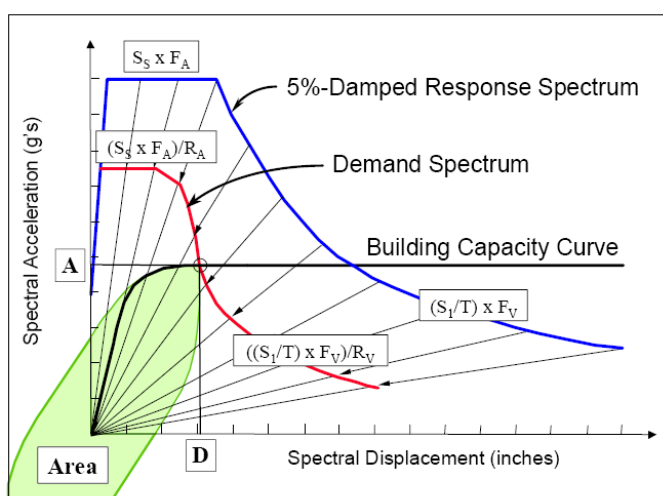


Figure 2-19: Example demand spectrum construction and calculation of peak response displacement (D) and acceleration (A) (FEMA, 2001)

HAZUS provides fragility curves for damage to structural system, non-structural components sensitive to drift and non-structural components (and contents) sensitive to acceleration. Fragility curves are lognormal functions defined by a median value of the demand parameter, which corresponds to the *threshold* of that damage state, and by the variability associated with that damage state. For example, the spectral displacement S_d that defines the threshold of a particular damage state ds is given by

$$S_d = \bar{S}_{d,ds} \cdot \varepsilon_{ds} \quad \text{Eq 2-9}$$

where $\bar{S}_{d,ds}$ is the median value of spectral displacement of damage state ds and ε_{ds} is a lognormal random variable with a unit median value and a logarithmic standard deviation β_{ds} , which controls the slope of the fragility curve and accounts for the variability and uncertainty associated with capacity curve properties, damage states and ground shaking.

Four damage states are defined: Slight, Moderate, Extensive and Complete (see Figure 2-20). Median values of spectral displacement associated with each damage state are evaluated calculating the average interstorey drift ratio (i.e., roof displacement divided by building height) corresponding to the step of pushover analysis at which a certain fraction of structural elements reaches a certain deformation limit. The value of this fraction is defined as the repair or replacement cost of components at limit divided by the total replacement value of the structural system.

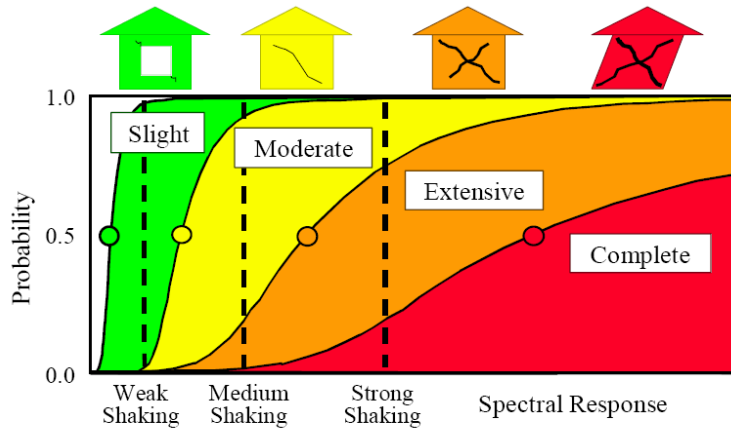


Figure 2-20: Example fragility curves for Slight, Moderate, Extensive and Complete damage (FEMA, 2001)

The lognormal standard deviation β_{ds} , which describes the total variability of fragility-curve damage state ds , is given by three contributions:

$$\beta_{ds} = \sqrt{(\text{CONV}[\beta_C, \beta_D])^2 + (\beta_{T,ds})^2} \quad \text{Eq 2-10}$$

where β_C is the lognormal standard deviation parameter that describes the variability of the capacity curve, β_D is the lognormal standard deviation parameter that describes the variability of the demand spectrum and $\beta_{T,ds}$ is the lognormal standard deviation parameter that describes the variability of the threshold of damage state ds . Since the demand spectrum is dependent on building capacity, a convolution process is required to combine their respective contributions to total variability, while the third contribution to total variability, $\beta_{T,ds}$, is assumed mutually independent of the first two and is combined with the results of the convolution process using the square-root-sum-of-the squares (SRSS) method. The convolution process

involves a complex numerical calculation that would be very difficult for most users to perform. To avoid this difficulty, sets of pre-calculated values of damage state Beta's are proposed.

These Beta values are given as a function of building height group, post-yield degradation of the structural system, damage state threshold variability and capacity curve variability.

Estimation of β_C and $\beta_{T,ds}$ must be made by users on a judgmental basis, based on the consideration that these variability values are influenced by uncertainty in capacity curve properties and thresholds of damage states and by building population (i.e., individual building or group of buildings): relatively low variability of damage states would be expected for an individual building with well known properties (e.g., complete set of as-built drawings, material test data, etc.) and whose performance and failure modes are known with confidence. Relatively high variability of damage states would be expected for a group of buildings whose properties are not well known and for which the user has low confidence in the results (of pushover analysis) that represent performance and failure modes of all buildings of the group.

Giovinazzi (2005) proposes a method for seismic risk assessment based on the assumption that, dealing with a territorial vulnerability assessment, building seismic response can be represented by simplified bilinear capacity curves defined by three parameters: the yield acceleration, the yield period of vibration and the structural ductility capacity.

The yield acceleration can be derived as a function of the seismic code design lateral force, multiplied by another factor in order to consider median values of material strength instead of nominal ones. The period can be evaluated through simplified expressions proposed by code. The ductility capacity can be derived from the behaviour factor adopted in design, if any; otherwise, for buildings non-specifically

designed to have dissipation capacity, a value of 2.5 is arbitrary assumed.

For non designed structures, the author states that bilinear capacity curve can be derived taking into account the geometrical and the technological features characterizing on the average the typology (number of floors, code level, material strength, drift capacity, age, etc.) and hypothesizing a certain collapse mode.

Displacement demand assessment for a given seismic intensity is carried out according to the Capacity Spectrum Method.

Four damage states are considered. Mean values of the corresponding displacement threshold are proposed as a function of the yielding and ultimate displacements, based on *expert judgement*, and are verified on the basis of the results of pushover analyses performed on prototype buildings.

In order to define fragility curves for the considered damage states, uncertainty in the estimate has to be evaluated. To this end, a different approach from HAZUS is proposed: the overall uncertainty in the damage estimation is evaluated in order to represent the same dispersion of observed damage data that are well fitted by binomial distributions. Repeating this procedure for different buildings typologies a lognormal standard deviation is found, depending on the ductility corresponding the mean damage values.

Grant et al. (2006) also adopt a code-based approach to the evaluation of building seismic vulnerability. In order to carry out a first, rapid and very simplified step of a multi-level screening procedure aimed at defining priorities and timescales for seismic intervention in school buildings, authors evaluate the PGA capacity from the code-prescribed seismic input at the age of construction, based on the assumption of a “perfect” code compliance. To this aim, starting from the design inelastic acceleration capacity prescribed by the seismic code in force at the age of construction, a sort of “back-analysis” is

applied, thus calculating the corresponding PGA, also accounting for modern seismic code requirements including adjustments for ductility capacity (i.e., the behaviour factor) and building importance. In a very conservative (but unrealistic) way the authors also assume that buildings designed for Gravity Loads only have a null seismic capacity. Following this procedure, the seismic vulnerability can be evaluated in terms of a “PGA deficit” obtained as the difference between the evaluated PGA capacity and the PGA demand, which is derived from modern seismic hazard studies.

However, a quite critical shortcoming can affect a procedure that evaluate seismic capacity based on the assumption of a perfect code compliance with seismic codes in force at the age of construction, since the actual seismic capacity of a building stock can differ greatly from the prediction of such a code prescription-based model. At least, factors accounting for material overstrength should be accounted for (e.g., Giovinazzi, 2005). Moreover, design conservatism approximations usually should lead to a higher capacity, compared with code prescriptions. Hence, a code-based procedure may systematically underestimate seismic capacity. This approach may be justified as *conservative*, but actually a seismic vulnerability assessment for a large scale earthquake loss model should not be *conservative*; it should rather provide a seismic capacity estimation as reliable as possible.

Ordaz et al. (2000) adopt a vulnerability analysis procedure where the damage level is expressed as a function of the maximum interstorey drift, which is evaluated as a function of the spectral acceleration. The relationship between the maximum expected interstorey drift and the spectral acceleration demand is evaluated through a simplified model based on the analogy with equivalent cantilever beams subjected to shear and flexural deformations. In this model, coefficients are used to account, among others, for the structural type, for the height of the

structure and for the ratio between inelastic and elastic demand. Moreover, further coefficients are used to account for the increase in seismic vulnerability due to some factors including, for instance, irregularities in elevation and/or in plan or the presence of short columns.

Calvi (1999) first proposes an approach for the evaluation of the vulnerability of building classes based on the Displacement-Based method (e.g., Priestley, 1997).

For each limit state, a displacement shape is assumed and a corresponding displacement capacity is evaluated, depending on the attainment of a local deformation limit [material strain capacity -> section curvature capacity -> element drift capacity -> building displacement capacity (on the equivalent SDOF model)]. A possible range of variation for the evaluated capacity is defined. At the same time, a possible range of variation for the period of vibration (secant to the displacement capacity) is defined, too. Hence, for each limit state, rectangles representing the possible “positions” of the points representing the building capacity in a period-displacement plane are obtained. A uniform probability density function over the rectangles is assumed, describing the variability of the capacity.

Seismic demand is represented by displacement response spectra adjusted to include the nonlinear response, wherein a reduction of the spectral ordinates is applied to account for the energy dissipation capacity of the structure as a function of the target displacement and the structural response.

Capacity and demand can be directly compared to each other as a function of the period: the rectangle area below the demand spectrum represents the expected proportion of buildings reaching (or exceeding) the limit state capacity (see Figure 2-21).

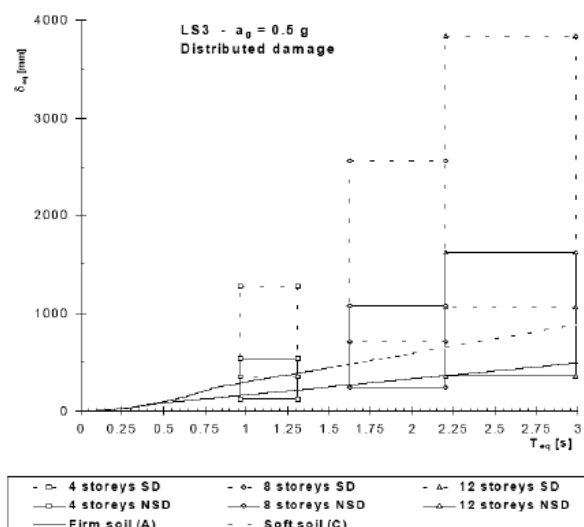


Figure 2-21: An example of the intersection of capacity areas and demand spectrum (Calvi, 1999)

The methodology proposed by Calvi (1999) is subsequently developed (Pinho et al., 2002; Glaister and Pinho, 2003; Crowley et al., 2004; Crowley et al., 2006) leading to the Displacement-Based Earthquake Loss Assessment (DBELA) procedure.

The main improvements to the original procedure by Calvi (1999) may be summarized in (i) the theoretical improvement of structural and non-structural displacement capacity equations, (ii) the derivation of an equation between yield period and height for European buildings both with and without infill panels (Crowley and Pinho, 2004, 2006) and (iii) the development of a fully probabilistic framework accounting for uncertainties in geometrical and mechanical properties, in capacity models and in demand spectrum.

In DBELA the displacement capacity can be expressed as a function of the building height; this relationship can be transformed into a direct relationship between displacement capacity and period, through the substitution of an equation relating the height of a building to its limit

state period. Hence, a direct comparison is possible at any period between the displacement capacity of a building class and the displacement demand predicted from a response spectrum (see Figure 2-22).

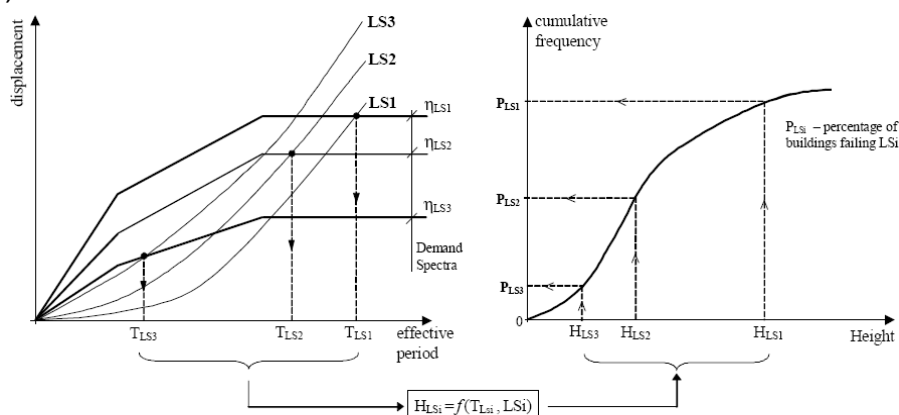


Figure 2-22: Deformation based seismic vulnerability assessment procedure (Glaister and Pinho, 2003)

The probabilistic treatment of the uncertainties involved in the assessment procedure leads to the definition of a Joint Probability Density Function (JPDF) of displacement capacity and period (see Figure 2-23), which was originally assumed to be uniform (Calvi, 1999).

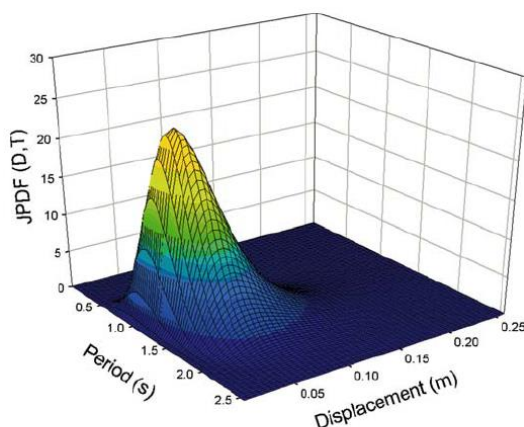


Figure 2-23: Joint Probability Density Function (JPDF) of displacement capacity and period (Crowley et al., 2004)

The Simplified Pushover-Based Earthquake Loss Assessment (SP-BELA) by Borzi et al. (2008a) combines the definition of a pushover curve using a simplified mechanics-based procedure – similar to (Cosenza et al., 2005) – to define the base shear capacity of the building stock with a displacement-based framework similar to that in DBELA, such that the vulnerability of building classes at different limit states can be obtained.

Simplified pushover curves are derived according to the following procedure: a prototype structure representing the building class is defined first, for which the collapse mechanism and, therefore, the collapse multiplier under a linear distribution of lateral forces is determined. Based on limit conditions given in terms of element chord rotations, the building displacement capacity (in terms of the equivalent SDOF) is evaluated for different Limit States. Then, the period of vibration for each Limit State is calculated, corresponding to the secant stiffness to the displacement capacity.

In order to derive vulnerability curves using this type of analytical procedure, a set of random variables is defined – together with the

corresponding probability distributions – including geometrical dimensions, material properties and design loads.

Seismic demand is defined in terms of inelastic displacement demand spectra, and the uncertainty in this demand is taken into account assuming the corner periods of the spectrum and the spectral amplification coefficient as random variables.

A Monte Carlo simulation approach is adopted, and random variables are generated through a Latin Hypercube Sampling procedure. Hence, vulnerability curves can be derived for a class of buildings and for different Limit States, carrying out the following steps:

- definition of a number of building samples through the generation of assumed random variables;
- definition of building capacity through a pushover curve for each generated building;
- definition of the displacement demand;
- comparison between demand and capacity to define the number of buildings – out of the generated population – exceeding the given Limit State conditions.

SP-BELA has been further developed in order to approximately account for the presence of infill panels in (Borzi et al., 2008b). Two possible distributions of the infill panels are considered: a uniform distribution along the height of the building or a “pilotis” distribution. It is assumed that the panels have an influence on the lateral resistance of the building up to the yield limit state. When the frames evolve into the nonlinear range, the panels are considered to collapse and, therefore, they no longer contribute to the base shear resistance. The behaviour of the single strut representing the infill panel is assumed to be linear up to failure. The influence of the panels is not considered in defining the displacement capacity on the pushover curve as the panels are often not perfectly in contact with the frames and they are assumed to play a role on the overall building performance only after the frames have

already been deformed beyond their elastic limit. On the other hand, the panels are assumed to collapse before the frames reach the significant damage limit condition.

Hence, the only way the influence of infill panels is accounted for is that they are assumed to increase the lateral strength of the building up to the yielding of the RC structure. In other terms, the presence of infill panels leads to a lower value of the secant period to the yielding Limit State by increasing the yield strength, thus decreasing the corresponding failure probability within the adopted Displacement-Based assessment framework. No influence at all is considered on other Limit States.

However, authors do not clarify how the presence of elements characterized by a brittle behaviour (such as infill trusses) can be accounted for in a mechanisms-based approach, where all the structural elements should have an elastic-perfectly plastic behaviour.

VC (*Vulnerabilità Calcestruzzo armato, reinforced concrete vulnerability*), by Dolce and Moroni (2005), is a simplified procedure – implemented in a spreadsheet software – for the vulnerability assessment of RC buildings. Two Limit States are considered: Slight Damage and Collapse. The vulnerability is expressed as the PGA values leading the attainment of these Limit States. The procedure is based on the evaluation of the storey strength at each storey and on the application of a ductility coefficient accounting for the inelastic displacement capacity.

Soft-storey (concentration of the inelastic demand only in columns in one storey) is the only collapse mechanism considered. In authors' opinion, this is the most probable collapse mechanism for existing RC buildings, due to frequent weak column/strong beam conditions.

Infill elements can be taken into account, both in terms of stiffness and strength.

For the definition of Slight Damage Limit State an interstorey drift limit, based on Italian code prescriptions, is assumed. An elastic behaviour is assumed up to this limit. Hence, interstorey shear stiffness has to be evaluated. To this end, the sum of column stiffness values is calculated, also considering the influence of the restrain condition given by the beams; a cracked stiffness is considered, too. If infill panels are present, their contribution is taken into account assuming the stiffness model provided by Italian code. Hence, a value of interstorey shear leading to the attainment of Slight Damage Limit State (V_{OPER}) is evaluated at each storey, corresponding to the prescribed interstorey drift limit.

For Collapse Limit State the ultimate value of interstorey shear strength (V_{COLL}) at each storey is evaluated. The ultimate interstorey shear strength is calculated as the sum of the ultimate shear strength of each column, given by the flexural capacity of the column section, also considering the influence of the restrain condition given by the beams on the moment distribution along the element and, therefore, on the corresponding shear value. Possible shear failures are considered, too. If infill panels are present, their contribution to the ultimate shear strength is taken into account considering different possible collapse mechanisms of the panels. Subsequently, this value is multiplied by a coefficient accounting for the inelastic displacement capacity in order to evaluate the interstorey shear value leading to Collapse in a spectral elastic approach, thus implicitly applying the equal rule between overstrength and ductility ($R=\mu$).

The procedure can be summarized in the following steps (each step is carried out in both building directions):

- at each storey, interstorey shear leading to Slight Damage drift limit (V_{OPER}) and ultimate interstorey shear strength (V_{COLL}) are evaluated, as above described;

- the interstorey shear demand distribution is evaluated, assuming a base shear demand equal to the weight of the structure (that is, a

pseudo-acceleration equal to 1g) and a linear distribution of lateral displacements;

at each storey, the ratios between V_{OPER} and V_{COLL} and the interstorey shear demand are evaluated, representing the pseudo-acceleration values $S_{D(OP)}$ and $S_{D(COLL)}$ (expressed in g) leading to the attainment of a shear demand equal to V_{OPER} and V_{COLL} , respectively;

at each storey, the PGA values corresponding to $S_{D(OP)}$ and $S_{D(COLL)}$ are evaluated by means of different coefficients: α_{PM} (accounting for the participating mass ratio of the first mode), α_{AD} (aimed at evaluating the PGA from the spectral pseudo-acceleration depending on the period of vibration and the shape of the demand spectrum), α_{DS} (accounting for the structural dissipation capacity) and α_{DUT} (accounting for the inelastic displacement capacity). Obviously, α_{DUT} is equal to 1 for Slight Damage Limit State. For Collapse Limit State, a coefficient $\alpha_{DUT,pil}$ is evaluated for each column as a function of the axial load ratio; it is assumed equal to 1 if the column behaviour is controlled by shear. Then, α_{DUT} is given by a weighted average of $\alpha_{DUT,pil}$ extended to all the columns in the storey. α_{DUT} can be reduced by means of coefficients accounting for the presence of a soft storey or for irregularities in strength/stiffness/mass distribution. If the presence of infill panels is taken into account α_{DUT} is assumed equal to 1.5 since in this case in authors' opinion the failure mechanism is controlled by brittle interaction mechanisms between structural and non-structural elements;

for both Limit States, the minimum PGA value between all the values calculated at each storey and in each direction is evaluated, representing the PGA capacity of the building.

2.4 Hybrid Methods

Hybrid methods allow to produce DPMs and vulnerability curves as a combination of analytical data from mechanical models and empirical data from observed damage, thus allowing, for example, to calibrate

analytical models or to provide for the lack of empirical damage data at certain intensity levels for the geographical area under consideration.

In (Kappos et al., 1995; Kappos et al., 1998) DPMs are provided which are partially derived from observed damage data from past earthquakes, through the vulnerability index procedure, and partially obtained from nonlinear dynamic analyses carried out on building models representing different building classes.

In order to include such analytical results into the DPMs, an empirical correlation between intensity and PGA values at which the accelerograms were scaled is used, and a correlation is also established between an analytical global damage index obtained from the analyses and the damage expressed as the cost of repair. 6 structural models representing existing Greek buildings, 10 accelerograms and 2 intensities are considered, thus leading to a total number of 120 nonlinear dynamic analyses. The damage results are then combined with the observed damage from the 1978 earthquake in Thessaloniki.

In (Singhal and Kiremidjian, 1998) the analytical vulnerability curves proposed in (Singhal and Kiremidjian, 1996) for Low-Rise RC frames are updated based on the observational data obtained on 84 buildings damaged during the 1994 Northridge earthquake, by means of a Bayesian updating technique accounting for the reliability of different data sources.

Nevertheless, special attention should be addressed to the treatment of uncertainties when using hybrid methods since analytical and empirical vulnerability data include different sources of uncertainty and are thus not directly comparable. Hence, in order to improve an analytical model through a comparison with an empirical model, it probably would be better to calibrate the former in order to obtain only median values equal to the ones provided by the latter. In this way, each source of uncertainty can be properly taken into account through a specific and explicit modelling (Calvi et al., 2006).

2.5 Expert Judgement-Based Methods

An example of Damage Probability Matrices derived from expert judgement can be found in ATC-13 (ATC, 1985), where DPMs are provided which were derived from the judgement of more than 50 senior earthquake engineering experts. Each expert provided, according to his engineering judgement and experience, an estimate of low, best and high values of the damage ratio for each of 36 different building classes, as a function of the seismic intensity expressed according to the MMI scale. These values were assumed as corresponding to 5th, 50th and 95th percentiles, respectively, of a lognormal distribution representing the estimated damage factor for a given seismic intensity. The estimates provided by the experts were also weighted according to the experience and confidence level of each expert for the considered building class.

2.6 References

- ATC, 1985. Earthquake damage evaluation data for California. Report ATC-13, Applied Technology Council, Redwood City, California, USA.
- Benedetti D., Petrini V., 1984. Sulla vulnerabilità di edifici in muratura: proposta di un metodo di valutazione. *L'industria delle Costruzioni*, 149(1), 66-74. (in Italian)
- Borzi B., Pinho R., Crowley H., 2008a. Simplified pushover-based vulnerability analysis for large scale assessment of RC buildings. *Engineering Structures*, 30(3), 804-820.
- Borzi B., Crowley H., Pinho R., 2008b, The influence of infill panels on vulnerability curves for RC buildings. *Proceedings of the 14th World Conference on Earthquake Engineering*, Beijing, China, October 12-17. Paper 09-01-0111.
- Braga F., Dolce M., Liberatore D., 1982. A statistical study on damaged buildings and an ensuing review of the MSK-76 scale. *Proceedings of the 7th European Conference on Earthquake Engineering*, Athens, Greece. Pp. 431-450.
- Calvi G.M., 1999. A displacement-based approach for vulnerability evaluation of classes of buildings. *Journal of Earthquake Engineering*, 3(3), 411-438.
- Calvi G.M., Pinho R., Magenes G., Bommer J.J., Restrepo-Veléz L.F., Crowley H., 2006. The development of seismic vulnerability assessment methodologies for variable geographical scales over the past 30 years. *ISSET Journal of Earthquake Technology*, 43(3), 75-104.
- Colombi M., Borzi B., Crowley H., Onida M., Meroni F., Pinho R., 2008. Deriving vulnerability curves using Italian earthquake damage data. *Bulletin of Earthquake Engineering*, 6(3), 485-504.

- Cosenza E., Manfredi G., Polese M., Verderame G.M., 2005. A multi-level approach to the capacity assessment of existing RC buildings. *Journal of Earthquake Engineering*, 9(1), 1-22.
- Crowley H., Colombi M., Borzi B., Faravelli M., Onida M., Lopez M., Polli D., Meroni F., Pinho R., 2009. A comparison of seismic risk maps for Italy. *Bulletin of Earthquake Engineering*, 7(1), 149-190.
- Crowley H., Pinho R., 2004. Period-height relationship for existing european reinforced concrete buildings. *Journal of Earthquake Engineering*, 8(1), 93-119.
- Crowley H., Pinho R., 2006. Simplified equations for estimating the period of vibration of existing buildings. *Proceedings of the 1st European Conference on Earthquake Engineering and Seismology*, Geneva, Switzerland, September 3-8. Paper No. 1122.
- Crowley H., Pinho R., Bommer J.J., 2004. A probabilistic displacement-based vulnerability assessment procedure for earthquake loss estimation. *Bulletin of Earthquake Engineering*, 2(2), 173-219.
- Crowley H., Pinho R., Bommer J.J., Bird, J.F., 2006. Development of a displacement-based method for earthquake loss assessment. ROSE Research Report No. 2006/01, IUSS Press, Pavia, Italy.
- Di Pasquale G., Orsini G., 1997. Proposta per la valutazione di scenari di danno conseguenti ad un evento sismico a partire dai dati ISTAT. *Atti dell'VIII convegno ANIDIS "L'ingegneria sismica in Italia"*, Taormina, Italy, September 21-24. Vol. 1, pp. 477–486. (in Italian)
- Di Pasquale G., Orsini G., Romero R.W., 2005. New developments in seismic risk assessment in Italy. *Bulletin of Earthquake Engineering*, 3(1), 101-128.

- Dolce M., Masi A., Marino M., Vona M., 2003. Earthquake damage scenarios of the building stock of Potenza (southern Italy) including site effects. *Bulletin of Earthquake Engineering*, 1(1), 115-140.
- Dolce M., Moroni C., 2005. La valutazione della vulnerabilità e del rischio sismico degli edifici pubblici mediante le procedure VC (vulnerabilità c.a.) e VM (vulnerabilità muratura), *Atti del Dipartimento di Strutture, Geotecnica, Geologia applicata all'ingegneria*, N. 4/2005. (in Italian)
- Faccioli E., Pessina V. (editors), 2000. The Catania project: earthquake damage scenarios for a high risk area in the Mediterranean. CNR-Gruppo Nazionale per la Difesa dai Terremoti, Rome, Italy.
- Faccioli E., Pessina V., Calvi G.M., Borzi B., 1999. A study on damage scenarios for residential buildings in Catania city. *Journal of Seismology*, 3(3), 327-343.
- Fajfar P., 1999. Capacity spectrum method based on inelastic demand spectra. *Earthquake Engineering and Structural Dynamics*, 28(9), 979-993.
- FEMA, 2001. HAZUS99 Technical Manual. Service Release 2. Federal Emergency Management Agency, Washington, D.C., USA.
- Giovinazzi S., 2005. The vulnerability assessment and the damage scenario in seismic risk analysis. PhD Thesis, Technical University Carolo-Wilhelmina at Braunschweig, Braunschweig, Germany and University of Florence, Florence, Italy.
- Giovinazzi S., Lagomarsino S., 2004. A macroseismic method for the vulnerability assessment of buildings. *Proceedings of the 13th World Conference on Earthquake Engineering*, Vancouver, Canada, August 1-6. Paper No. 896.

- Glaister S., Pinho R., 2003. Development of a simplified deformation-based method for seismic vulnerability assessment. *Journal of Earthquake Engineering*, 7(S11), 107-140.
- GNDT, 1993. Rischio sismico di edifici pubblici. Parte I: aspetti metodologici. CNR-Gruppo Nazionale per la Difesa dai Terremoti, Rome, Italy.
- Grant D., Bommer J.J., Pinho R., Calvi G.M., 2006. Defining priorities and timescales for seismic intervention in school buildings in Italy. ROSE Research Report No. 2006/03, IUSS Press, Pavia, Italy.
- Grünthal G., 1998. Cahiers du Centre Européen de Géodynamique et de Séismologie: Volume 15 – European Macroseismic Scale 1998. European Center for Geodynamics and Seismology, Luxembourg.
- Hassan A.F., Sozen M.A., 1997. Seismic vulnerability assessment of low-rise buildings in regions with infrequent earthquakes. *ACI Structural Journal*, 94(1), 31-39.
- Iervolino I., Manfredi G., Polese M., Verderame G.M., Fabbrocino G., 2007. Seismic risk of R.C. building classes. *Engineering Structures*, 29(5), 813-820.
- INGV-DPC S1, 2007. Progetto S1. Proseguimento della assistenza al DPC per il completamento e la gestione della mappa di pericolosità sismica prevista dall'Ordinanza PCM 3274 e progettazione di ulteriori sviluppi. Istituto Nazionale di Geofisica e Vulcanologia – Dipartimento della Protezione Civile, <http://esse1.mi.ingv.it> (in Italian)
- JBDPA, 1990. Standard for seismic capacity assessment of existing reinforced concrete buildings. Japanese Building Disaster Prevention Association, Ministry of Construction, Tokyo, Japan.

- Kappos A.J., Ptilakis K., Stylianidis K.C., 1995. Cost-benefit analysis for the seismic rehabilitation of buildings in Thessaloniki, based on a hybrid method of vulnerability assessment. Proceedings of the 5th International Conference on Seismic Zonation, Nice, France, October 17-19. Vol. 1, pp. 406-413.
- Kappos A.J., Stylianidis K.C., Ptilakis K., 1998. Development of seismic risk scenarios based on a hybrid method of vulnerability assessment. *Natural Hazards*, 17(2), 177-192
- Kircher C.A., Nassar A.A., Kustu O., Holmes W.T., 1997. Development of building damage functions for earthquake loss estimation. *Earthquake Spectra*, 13(4), 663-682.
- Kircher C.A., Reitherman R.K., Whitman R.V., Arnold C., 1997. Estimation of earthquake losses to buildings. *Earthquake Spectra*, 13(4), 703-720.
- Masi A., 2003. Seismic vulnerability assessment of Gravity Load Designed R/C frames. *Bulletin of Earthquake Engineering*, 1(3), 371-395.
- Mouroux P., Le Brun B., 2006. Presentation of RISK-UE project. *Bulletin of Earthquake Engineering*, 4(4), 323-339.
- Ordaz M., Miranda E., Reinoso E., Pérez-Rocha L.E., 2000. Seismic Loss estimation model for Mexico City. Proceedings of the 12th World Conference on Earthquake Engineering, Auckland, New Zealand, January 30-February 4. Paper No. 1902.
- Orsini G., 1999. A model for buildings' vulnerability assessment using the Parameterless Scale of Seismic Intensity (PSI). *Earthquake Spectra*, 15(3), 463-483.
- Ozdemir P., Boduroglu M.H., Ilki A., 2005. Seismic safety screening method. Proceedings of the International Workshop on Seismic Performance Assessment and Rehabilitation of

Existing Buildings (SPEAR), Ispra, Italy, April 4-5. Paper No. 23.

- Park Y.J., Ang A.H.S., 1985. Mechanistic seismic damage model for reinforced concrete. *ASCE Journal of Structural Engineering*, 111(4), 722-739.
- Pinho R., Bomber J.J., Glaister S., 2002. A simplified approach to displacement-based earthquake loss estimation analysis. *Proceedings of the 12th European Conference on Earthquake Engineering*, London, UK, September 9-13. Paper No. 738.
- Priestley M.J.N., 1997. Displacement-based seismic assessment of reinforced concrete buildings. *Journal of Earthquake Engineering*, 1(1), 157-192.
- Rossetto T., Elnashai A., 2003. Derivation of vulnerability functions for European-type RC structures based on observational data. *Engineering Structures*, 25(10), 1241-1263.
- Rossetto T., Elnashai A., 2005. A new analytical procedure for the derivation of displacement-based vulnerability curves for populations of RC structures. *Engineering Structures*, 7(3), 397-409.
- Rota M., Penna A., Strobbia C., Magenes G., 2008. Direct derivation of fragility curves from Italian post-earthquake survey data. *Proceedings of the 14th World Conference on Earthquake Engineering*, Beijing, China, October 12-17. Paper 09-01-0148.
- Sabetta F., Goretti A., Lucantoni A., 1998. Empirical fragility curves from damage surveys and estimated strong ground motion. *Proceedings of the 11th European Conference on Earthquake Engineering*, Paris, France, September 6-11.
- Sabetta F., Pugliese A., 1987. Attenuation of peak horizontal acceleration and velocity from Italian strong-motion records.

- Bulletin of the Seismological Society of America, 77(5), 1491-1513.
- Sabetta F., Pugliese A., 1996. Estimation of response spectra and simulation of nonstationary earthquake ground motions. Bulletin of the Seismological Society of America, 86(2), 337-352.
 - Singhal A., Kiremidjian A.S., 1996. Method for probabilistic evaluation of seismic structural damage. ASCE Journal of Structural Engineering, 122(12), 1459-1467.
 - Singhal A., Kiremidjian A.S., 1998. Bayesian updating of fragilities with application to RC frames. ASCE Journal of Structural Engineering, 124(8), 922-929.
 - Spence R.J.S., Coburn A.W., Sakai S., Pomonis A., 1991. A parameterless scale of seismic intensity for use in the seismic risk analysis and vulnerability assessment. International Conference on Earthquake, Blast and Impact, Manchester, UK, September 19-20. Pp. 19-30.
 - Verderame G.M., De Luca F., Ricci P., Manfredi G., 2010. Preliminary analysis of a soft storey mechanism after the 2009 L'Aquila earthquake. Earthquake Engineering and Structural Dynamics. DOI: 10.1002/eqe.1069
 - Whitman R.V., Anagnos T., Kircher C.A., Lagorio H.J., Lawson R.S., Schneider P., 1997. Development of a national earthquake loss estimation methodology. Earthquake Spectra, 13(4), 643-661.
 - Whitman R.V., Reed J.W., Hong S.T., 1973. Earthquake Damage Probability Matrices. Proceedings of the 5th World Conference on Earthquake Engineering, Rome, Italy, June 25-29. Vol. 2, pp. 2531-2540.
 - Yakut A., 2004. Preliminary seismic performance assessment procedure for existing RC buildings. Engineering Structures, 26(10), 1447-1461.

Chapter 3

Simplified approach to the seismic vulnerability assessment of existing RC buildings

3.1 Introduction

A seismic vulnerability analysis aims to estimate the damage to a single building or a building stock given a ground motion intensity. To this aim, empirical and mechanical methods can be used, the former providing the assessment of the expected damage based on the observation of damage suffered during past seismic events, the latter based on a mechanical model reflecting structural characteristics including the effect of design specifications and professional practice in force at the time of construction.

In this section an analytical methodology for the vulnerability assessment of infilled Reinforced Concrete (RC) buildings at large scale is presented, employing a simulated design procedure to evaluate the building structural characteristics based on few data such as number of storeys, global dimensions and type of design, and on the assumption of a Shear Type behaviour to evaluate in closed form the non-linear static response. Displacement capacity corresponding to different Damage States (DSs) is defined according to European Macroseismic Scale EMS-98 (Grünthal, 1998), based on damage models for RC and infill elements that allow to translate the damage description provided

by EMS-98 into numerical interstorey drift values through mechanical interpretation. A macroseismic damage scale is adopted in order to allow future comparison and validation of predicted seismic fragility based on observational-based damage data. Seismic capacity is evaluated through simplified Incremental Dynamic Analysis (IDA) curves are derived from (Vamvatsikos and Cornell, 2006). A simulation technique is introduced to take into account uncertainties (e.g., in material properties or in seismic demand estimation), and a probabilistic seismic capacity assessment is carried out, leading to the construction of fragility curves and, finally, to the evaluation of the failure probability in given time windows for the assumed DSs.

The procedure can be applied to data with different levels of detail, depending on the available data source. If one or more input parameters are unknown (or they cannot be considered as deterministically known) they can be assumed as random variables, characterized by defined statistical distributions. In this study, the described procedure is applied at single building level to the whole RC building stock of the city of Avellino, which has been the object of a field survey in the framework of SIMURAI Project (2010) that allowed to collect a database of geometrical and morphological parameters of the whole building stock, such as number of storeys, structural typology and age of construction. The results of the survey are illustrated and compared with statistical data about the characteristics of building stock provided by other sources. Results of the procedure application are illustrated and discussed, showing the influence of key parameters in determining seismic fragility and the spatial distribution of the mean annual frequency of exceedance of the assumed DSs within the Municipality, thus identifying areas most prone to seismic risk. A comparison with empirical-based fragility curves from literature is also illustrated.

3.2 Methods for Seismic Vulnerability Assessment of RC Buildings

Methods for seismic vulnerability assessment can be divided into two main categories: empirical methods, in which the assessment of expected damage for a given building typology is based on the observation of damage suffered during past seismic events; and analytical methods, where the relationship between seismic intensity and expected damage is provided by a model with direct physical meaning.

Reliability and significance of observed data allow empirical methods to give a realistic indication about expected damage, but these methods are affected by different disadvantages, such as the interdependency between macroseismic intensity (which is usually used as input ground motion intensity measure) and predicted damage, or the limited/not homogeneous availability that often affects the observational data used for their calibration. In the following, main features of most relevant observational-based vulnerability assessment methodologies for RC buildings are briefly reviewed.

In (Rossetto and Elnashai, 2003) observational-based vulnerability curves for European RC structures are derived from a large database of post-earthquake damage distributions. In the following, “homogeneous” vulnerability curves are obtained, which are applicable to different RC structural systems, thus allowing to combine data from such different systems in order to cover a range of ground motion intensities as wide as possible. Rota et al. (2008) collect damage survey forms from the main recent Italian earthquakes, and they subdivide these data into 23 different building typologies according to RISK-UE (Milutinovic and Trendafiloski, 2003) and 10 ground motion intervals. Then, Damage Probability Matrices (DPMs) are extracted from these data, providing points of estimate of probability of occurrence of the different DSs for each Peak Ground Acceleration (PGA) value and vulnerability class. In (Lagomarsino and Giovinazzi, 2006) two approaches are proposed, a “macroseismic” and a “mechanical” method. In both cases, the adopted

building typological classification essentially corresponds to the EMS-98 proposal (Grünthal, 1998). Following the macroseismic approach, vulnerability and fragility curves, respectively providing the expected (mean) damage grade for each building class and the probability of having each discrete damage grade as a function of macroseismic intensity, are derived from the DPMs implicitly defined by EMS-98. The mechanical approach is based on Capacity Spectrum Method (CSM), employing bilinear single degree of freedom (SDOF) capacity curves representative of each building class, which are derived from seismic design code lateral-force design requirements, factors like redundancies and conservatism, and the true strength of materials rather than the nominal ones, leading to the definition of fragility curves expressed as a function of PGA.

Analytical methods use a model to evaluate the structural vulnerability and they are able to take into account the various characteristics of building stock in a direct, transparent, and detailed way, and also to explicitly account for the uncertainties involved in the assessment procedure. However, analytical methods need a larger amount of detailed input data and a higher computational effort, compared with empirical methods. In the following main mechanical approaches to evaluate the vulnerability of RC buildings are presented.

The approach proposed by Calvi (1999), based on the Displacement-Based method (e.g., Priestley, 1997), provides the expected proportion of buildings reaching (or exceeding) the limit state capacity under a given seismic intensity represented by a displacement response spectra by assuming a possible range of variation for the evaluated displacement capacity and for the corresponding secant period of vibration. Such methodology is subsequently developed (Pinho et al., 2002; Glaister and Pinho, 2003; Crowley et al., 2004; Crowley et al., 2006) leading to the Displacement-Based Earthquake Loss Assessment (DBELA) procedure.

A complete earthquake loss estimation methodology is presented in HAZUS (FEMA, 2001; Kircher et al., 1997a; Kircher et al., 1997b; Whitman et al., 1997). Building response is characterized by building capacity curves, and CSM is adopted. Fragility curves are provided as lognormal functions defined by a median value of the demand parameter, which corresponds to the threshold of that DS, and by the associated variability. The latter is given by the contribution of the variability of the capacity curve, the variability of the demand spectrum and the variability of the threshold of DS.

In (Cosenza et al., 2005) a mechanics-based approach to evaluate the seismic capacity of a building class is proposed, defining the latter in terms of age of construction and number of storeys. For each class, a number of building models is generated by means of a simulated design procedure, based on the probabilistic distribution of the structural (geometrical and mechanical) parameters. Seismic capacity is determined in terms of base shear coefficient and global drift for the determined collapse mechanism. However, in this study no fragility curve is provided. In (Iervolino et al., 2007) a complete seismic risk assessment framework is presented. In order to investigate the building class capacity, geometrical and mechanical characteristics of the buildings are identified as random variables, and corresponding intervals are assumed. A simulated design procedure and a static pushover analysis are carried out for the generated buildings. Using a Response Surface Method, seismic risk is finally computed considering the number of buildings for which the displacement capacity is exceeded by the displacement demand.

The Simplified Pushover-Based Earthquake Loss Assessment (SP-BELA) by Borzi et al. (2008a) combines the definition of a pushover curve using a simplified mechanics-based procedure – similar to (Cosenza et al., 2005) – with a displacement-based approach similar to that in DBELA. A set of random variables is defined, including geometrical dimensions, material properties and design loads.

Uncertainty in seismic demand is taken into account, too. SP-BELA has been further developed in order to approximately account for the presence of infill panels in (Borzi et al., 2008b). In this work it is assumed that the panels have an influence on the lateral resistance of the building up to the yield limit state. Hence, the only way the influence of infill panels is accounted for is that they are assumed to increase the lateral strength of the building up to the yielding of the RC structure.

An hybrid approach for deriving vulnerability curves is presented in (Kappos et al, 1998), where damage data used in their generation derives from a combination of analytical simulation and observed post-earthquake surveys. As a matter of fact nonlinear dynamic and static analysis for RC structures for all typologies present in Greece has been performed to extrapolate statistical data to PGAs and/or spectral displacement for the cases in which no data sets are available.

3.3 A Simplified Procedure For Seismic Vulnerability Assessment Of Rc Buildings

Simplified methodologies for seismic vulnerability assessment of building stocks are of fundamental importance for the development of earthquake loss models. These models are needed to support the decision process in disaster prevention and emergency management, as far as seismic risk is concerned.

A simplified method is presented for RC buildings, employing:

- a simulated design procedure to evaluate the building structural characteristics based on few data such as number of storeys, global dimensions and type of design (Verderame et al. 2010).;
- the assumption of a Shear Type behaviour to evaluate in closed form the non-linear static response (Ricci, 2010).

The assessment of the seismic capacity is evaluated through the derivation of a simplified IDA-curve (Vamvatsikos and Cornell, 2006),

leading to the construction of fragility curves and, finally, to the evaluation of the failure probability in given time windows and for given DSs, that are based on the mechanical interpretation of the DSs described by the European Macroseismic Scale (EMS-98) (Grünthal, 1998).

In the following this procedure – which has been implemented in POST (PushOver on Shear Type models), a software based on MATLAB® code (Ricci, 2010, Del Gaudio et al, 2015) – is described.

3.3.1 Definition of building model

The reference unit of the procedure is the building. The procedure is based on few geometrical data that allow to define a geometrical-structural model of the building, based on design code prescriptions, professional practice and seismic classification of the area of interest at the time of construction, according to (Verderame et al. 2010).

A *simulated design* of the structural model is carried out in compliance with building codes and design practice in force at the time of construction. The design can be defined as *gravitational* or *seismic*.

First, design loads are defined. Dead loads are evaluated from a load analysis, whereas live loads are evaluated from past code prescriptions for ordinary structures.

If the design is seismic, firstly is necessary to identify the seismic category at the time of construction of the building and in the locality where is located. Secondly, it has to be determined the extent of the seismic forces that the codes have imposed to the designers for buildings located in localities classified as seismic.

The first seismic classification of the Italian territory dates back to 1909, with the (RDL n193/1909) which established a list of locations in which it was imposed the respect of "*technical and hygiene standards mandatory for repairs, reconstruction and new construction of public and private buildings*". (RDL n193/1909) ruled to the designers to

consider in the calculations of stability and resistance of buildings to “*dynamic actions due to seismic motion, represented with acceleration proportional to the masses of the building*”.

During the years followed a series of regulations (including the (RDL n573/1915); (RDL n431/1927) which instituted seismic categories I and II, in relation to the seismicity of the area; (Law n1684/1962)) which update the lists of locations after a seismic events.

(Law n64/1974) recognized the function to issue technical standards for the construction and upgrade the seismic classification through proper ministerial decrees (including the (DM n515/1981) issued following the Irpinia earthquake of 23 November 1980, with which it was introduced the seismic category III) to the Ministry of Public Works.

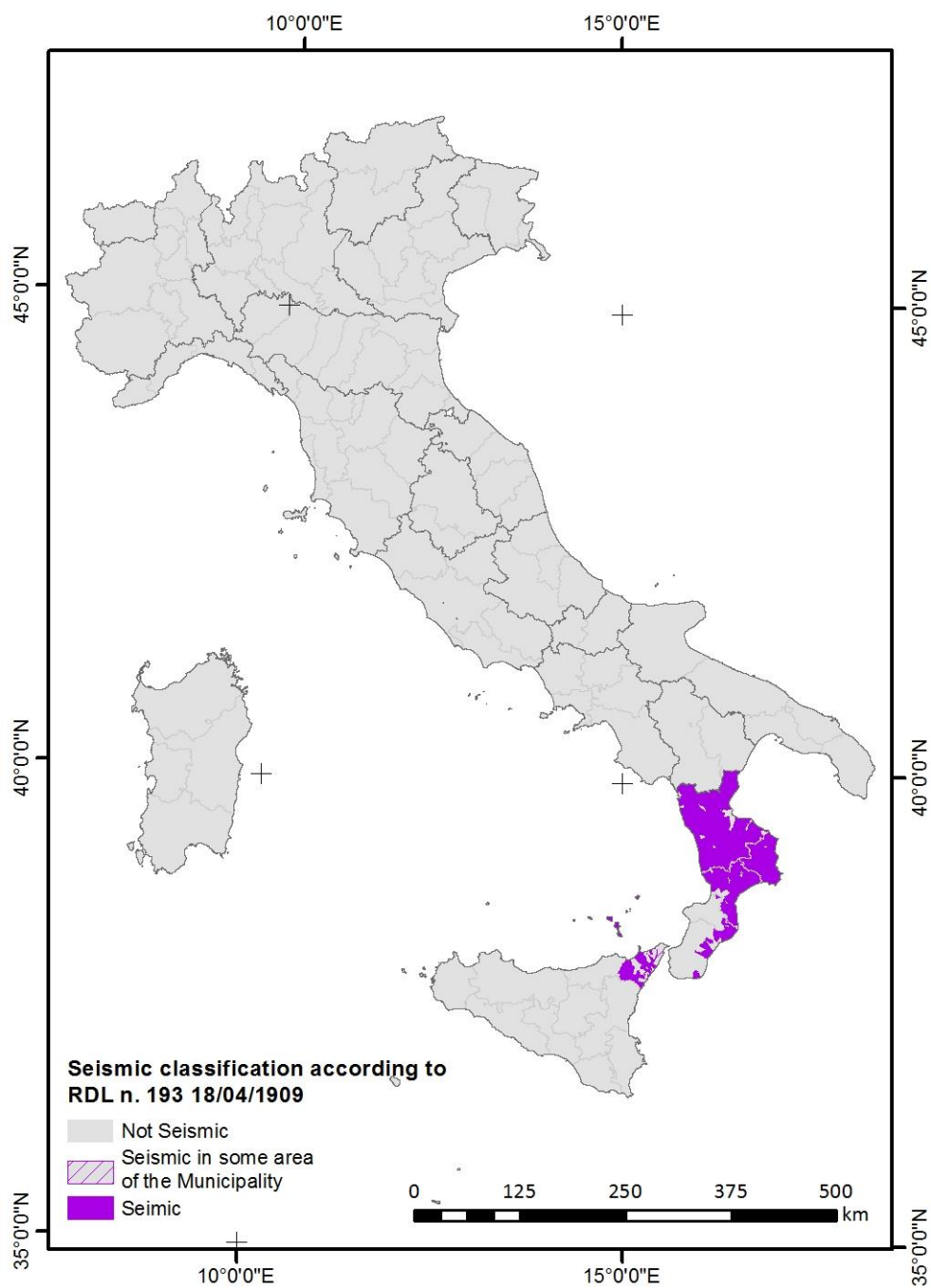


Figure 3-1: Italian seismic classification according to RDL n. 193 18/04/1909

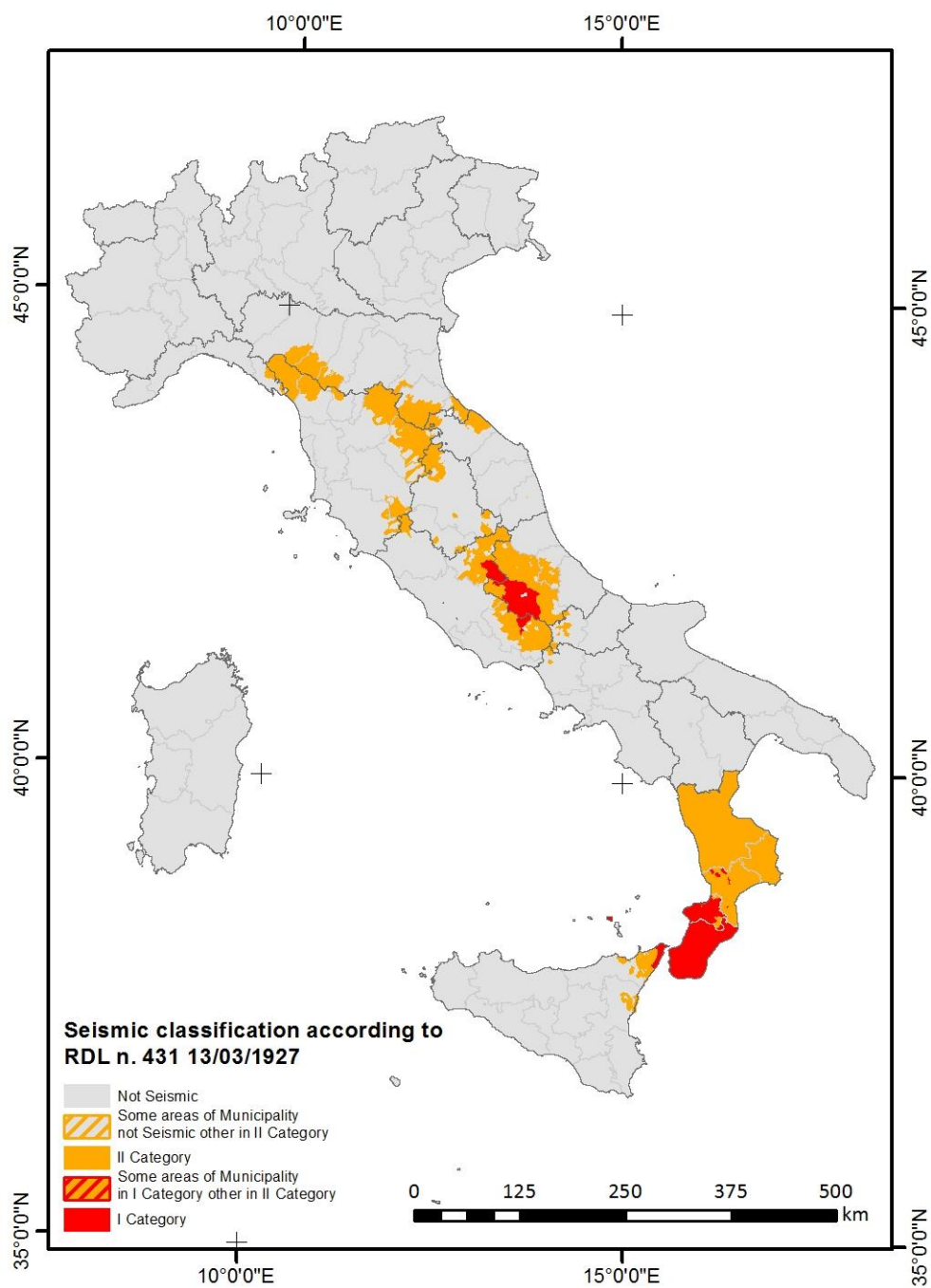


Figure 3-2: Italian seismic classification according to RDL n. 431 13/03/1927

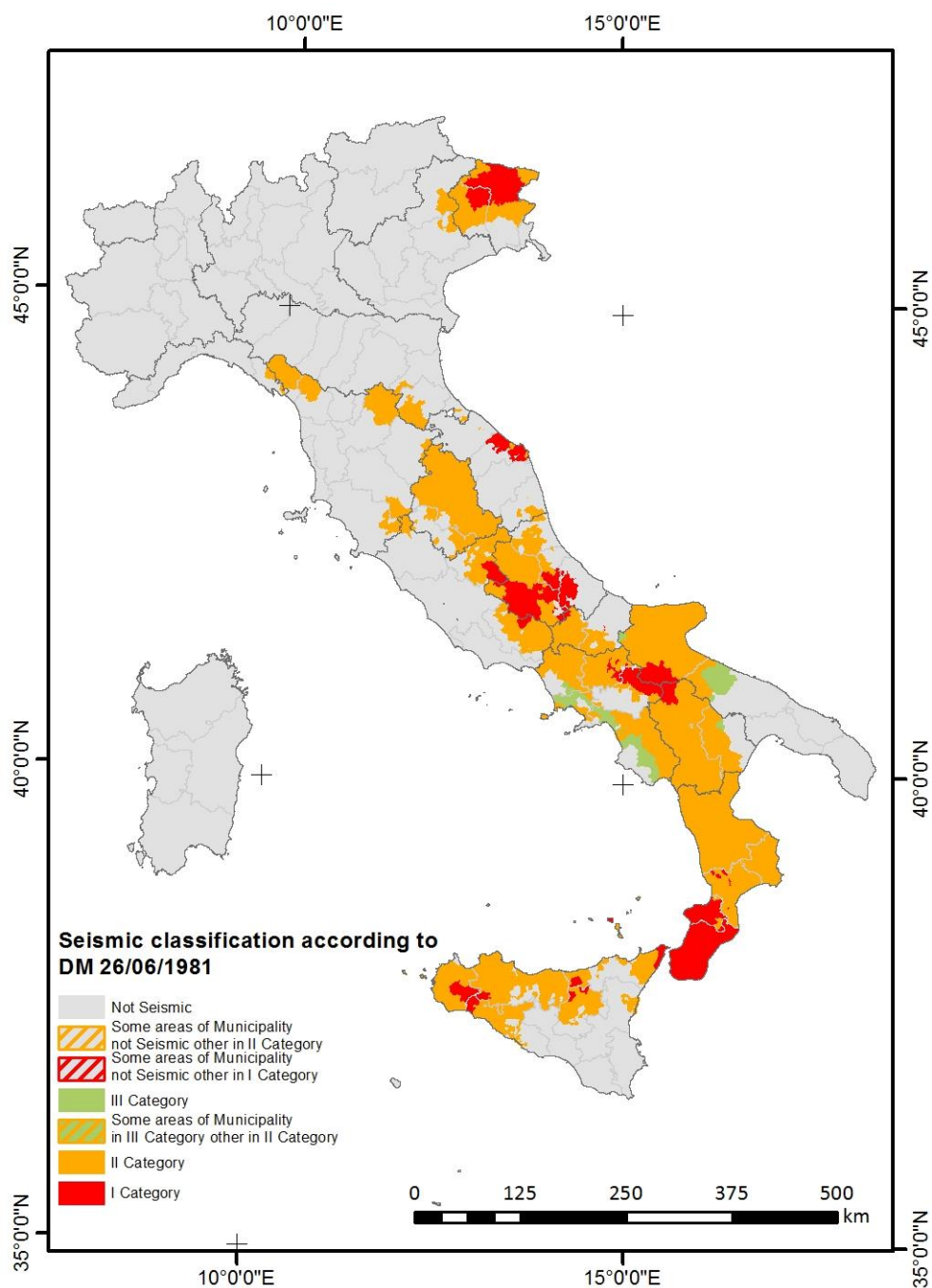


Figure 3-3: Italian seismic classification according to DM 26/06/1981

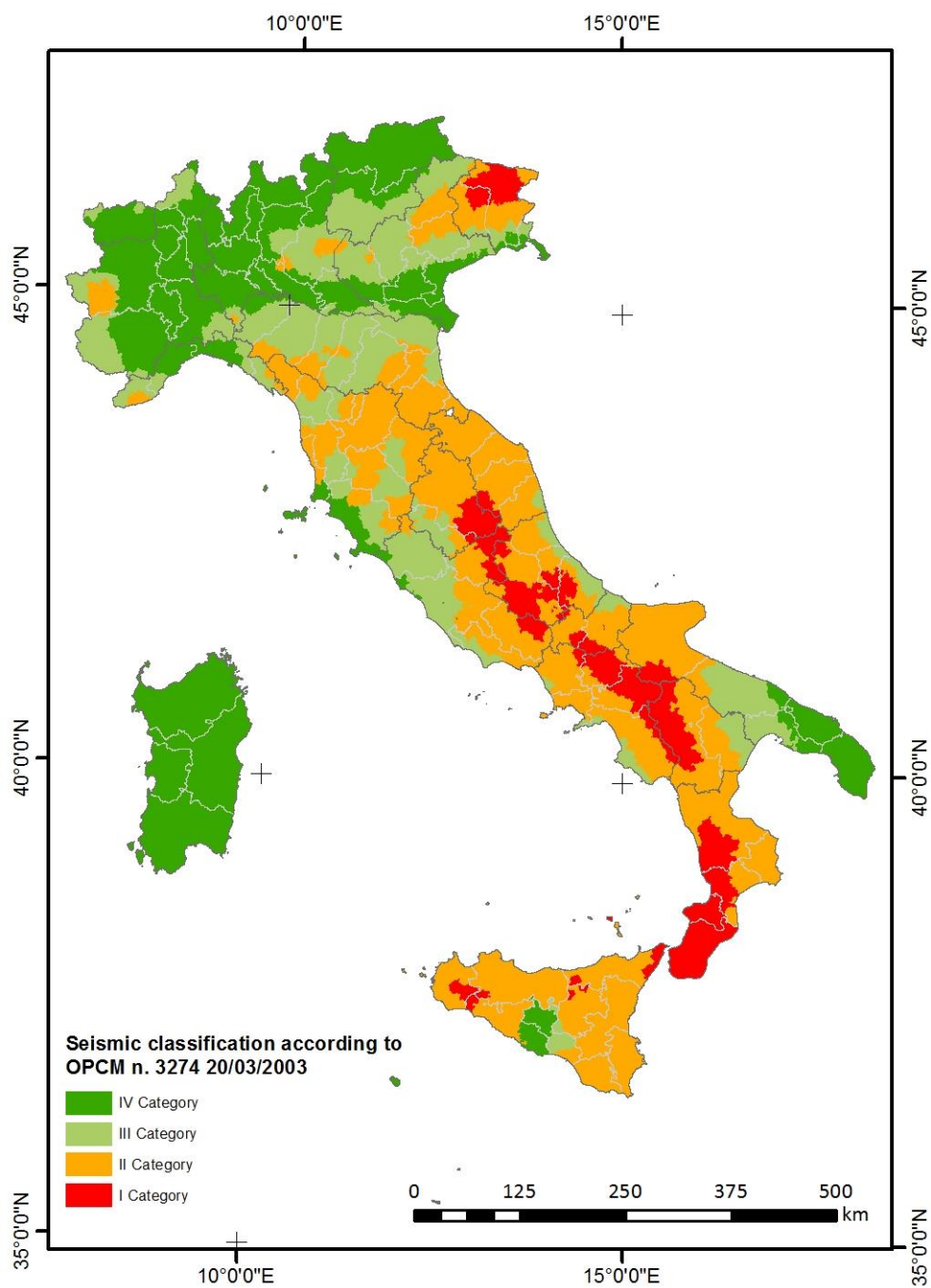


Figure 3-4: Italian seismic classification according to OPCM n. 3274 20/03/2003

A fundamental step for the update of seismic classification was the establishment of a working group, constituting by the National Seismic Service, the National Group for Defense against Earthquakes and the National Institute of Geophysics and Volcanology, for the drafting of a proposal for reclassification of the Italian territory. Later, the Italian Civil Protection issued by with the ([OPCM n3274/2003](#)) the current seismic classification. The document has classified the whole country as seismic into 4 areas, characterized by descending seismic hazard. Each areas is identified by a different value of pick ground acceleration (PGA) with probability of occurrence of 10% in 50 years: (i) Seismic category I: high seismicity, $PGA > 0.25g$; (ii) Seismic category II: medium seismicity, $0.25g < PGA < 0.15 g$; (iii) Seismic category III: low seismicity, $0.15 g < PGA < 0.05g$; (iv) Seismic category IV: very low seismicity, $PGA < 0.05g$.

Once the seismic category has been identified, it is necessary to assess the corresponding extent and distribution of lateral forces acting on the structure. The latter are established by technical codes as a function of the weight forces acting at each building storeys. ([RDL 1526/1916](#)), issued after the disastrous 1915 earthquake of Avezzano, ruled that seismic design of building were carried out considering a distribution of horizontal forces equal to 1/8 of the first storey weight force and 1/6 of the weight force of the remaining storeys. Hence, the ratio between the design base shear and the weight of the structure, later defined base shear coefficient, is equal respectively to 0.125, 0.145 and 0.152 for one- two- and three-storeys building.

Later, in ([RDL 431/1927](#)) the national territory classified as seismic was divided into two categories. The horizontal forces to be applied in structural analysis were equal for the buildings located in seismic category I respectively to 1/8 and 1/6 of the weight forces of the first and second storey of the building. On the other hand, for buildings located in seismic category II the horizontal forces to consider were

equal to 1/10 of the corresponding weight for heights up to 15 meters, or equal to 1/8 for higher heights.

([RDL 640/1935](#)) ruled a base shear coefficient equal to 0.1 and 0.07 for buildings located in Municipality classified respectively in I and II category, whatever the height of the building and the number of floors.

These values were confirmed by Law n.1684 / 1962.

([DM 40/1975](#)) introduced fundamental innovations seismic analysis that, for the first time, takes into account the dynamic characteristics of the buildings. Up to this date, in fact, seismic horizontal forces were determined simply as a fraction of storey weight through a code-coefficient related to the seismicity of the area considered.

The principal innovations introduced by ([DM 40/1975](#)) were the (i) the introduction of three seismic categories for the national territory; (ii) the introduction of a coefficient as a function of building fundamental period for the definition of horizontal forces and (iii) the introduction of a linear force distribution proportional the sum of weight force acting from the basement to considered storey. For ordinary buildings of normal importance (non-compressible soil, buildings without seismic walls) the base shear coefficient was equal respectively to 0.05, 0.07 to 0.10 for buildings located on seismic category I, II and III.

Then, element dimensions are evaluated. To this aim, according to past design practices, column area is determined as the ratio between the axial load (evaluated referring to the area of influence of each column) and the allowable stress of concrete. In seismic design, the latter was typically multiplied by a coefficient γ lower than 1, roughly accounting for combined axial load and bending action acting on the column due to lateral loads ([Pecce et al., 2004](#)). Hence, γ was typically assumed equal to 1 in gravity load design. The column section is then determined from the calculated area, assuming a square cross section. The beam width is given equal to 30 cm and the corresponding height is calculated based on the maximum bending moment acting on the beam for gravity loads from slabs; this moment is calculated with a formulation

accounting in a simplified way for the element constraint scheme. Finally, column dimensions are checked to avoid cross-section variation higher than 10 cm between two adjacent storeys.

Once column and beam dimensions have been calculated, reinforcement in columns is designed. Beam reinforcement is not designed since in the assumed Shear Type model the behaviour of beam elements has not to be modelled.

As far as gravitational design is concerned, the design of column reinforcement is based on the minimum amount of longitudinal reinforcement geometric ratio prescribed by code (e.g., 0.8% of the minimum concrete area according to (RDL 2229/1939), or 0.6% according to (DM 3/3/1975)). Once the minimum area of reinforcement has been determined, a set of possible values of bar diameter is considered and the combination of (even) number and diameter of bars providing the best upper approximation is chosen. Hence, bars are distributed along the periphery of the section as uniformly as possible.

In seismic design, storey shear forces are evaluated from lateral forces, which are calculated as a fraction of the weight of the structure, based on the assigned base shear coefficient.

The latter, defining the extent of horizontal forces to be applied to the structure simulating seismic forces, and the corresponding distribution at each storey of the building is identified through the technical code in force at the time of construction for the seismic category where the building is located. For these purpose the software ECS-it is used (see Figure 3-5), which is a Geographic Information System (GIS) based on MATLAB® code that allows the visualization and the identification of the evolution of the seismic classification of the Italian territory from 1909 to 2003.

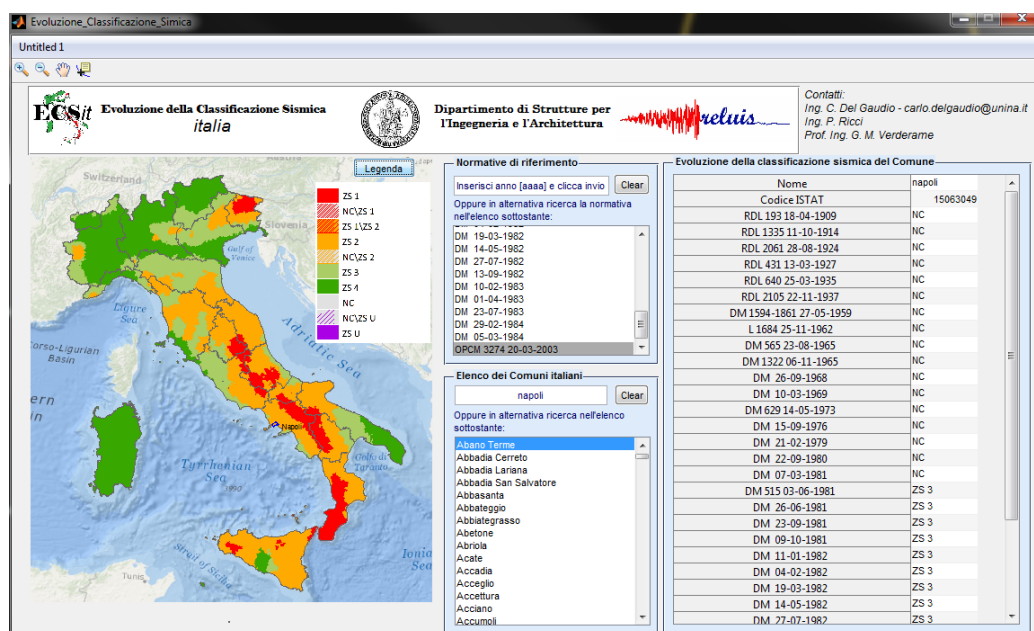


Figure 3-5: Evolution of seismic classification for the Municipality of Napoli through ECSit software based on MATLAB® code (<http://www.reluis.it/>)

Hence, the distribution of the storey shear among the columns of the storey is based on the ratio of inertia of the single column versus the sum of inertia of all the columns at the considered storey (Shear Type element model). The bending moment acting at the ends of each column is obtained multiplying the corresponding shear force by half of the column height, according to the assumed Shear Type model; the axial load is calculated from gravity loads, given by the sum of gravity loads and of a fraction of live loads (30%), always based on the area of influence of the column. Then, based on the assigned values of allowable stress for steel and concrete, the reinforcement area is designed to provide a flexural strength (according to the allowable stresses method) not lower than the bending moment from design. Again, the combination of number and diameter of bars providing the best upper approximation is chosen, provided at least two bars per layer. The described procedure is carried out in both directions. Hence,

the total amount of longitudinal reinforcement is compared with the minimum amount prescribed by the considered code; the maximum between these values is assumed.

Transverse reinforcement in columns is designed too. In gravitational design, a minimum amount of transverse reinforcement is provided, based on code prescriptions. For instance, according to (RDL 2229/1939) stirrup spacing in columns had to be determined as the minimum value between (i) half of the minimum section dimension and (ii) ten times the diameter of longitudinal reinforcement, whereas according to (DM 40/1975) it was determined as the minimum value between (i) 25 cm and (ii) fifteen times the minimum diameter of longitudinal reinforcement. In seismic design, transverse reinforcement is designed to resist the shear force due to lateral forces, calculated as previously illustrated. It is to be noted that in several old technical codes a so-called “*threshold-based*” design method for transverse reinforcement was proposed (see Section 2.3): a value of allowable tangential stress was assumed (e.g., τ_{c0}) and, if the design stress did not exceed this value, only a minimum amount of transverse reinforcement was prescribed. Hence, in the simulated design procedure τ_{c0} is evaluated, depending on the allowable concrete stress, and is compared with the shear stress demand τ . Then, if $\tau > \tau_{c0}$, the stirrup spacing is evaluated as

$$s = \frac{A_{sw} \cdot \sigma_{s,adm} \cdot 0.9d}{V} \quad \text{Eq 3-1}$$

where A_{sw} is the unit transverse reinforcement area, $\sigma_{s,adm}$ is the allowable steel stress, d is the column effective depth and V is the shear force. Stirrup diameter is given as an input.

Finally, the presence of infill panels can be defined according to three different options: (i) Uniformly infilled building, (ii) Pilotis building , (iii)

Bare building. The opening percentage can also be defined, both in bottom infill panels (case *i*) and in upper infill panels (cases *i* and *ii*). If present, infill panels are regularly distributed in plan in all the external frames in X and Y directions.

3.3.2 Characterization of nonlinear response

The evaluation of the non-linear static response of the building is performed through a simplified model. It is assumed that the ends of the columns are restrained against rotation (Shear Type model). Despite the simplification, the hypothesis of Shear Type model is still able to reproduce the typical seismic response of existing RC moment resisting frame buildings with a reasonable degree of approximation, both in presence and in absence of infill panels. It is to be noted that the hypothesis of Shear Type model has already been adopted by other authors (Dolce and Moroni, 2005; Mollaioli et al., 2009, Ricci, 2010, Verderame et al, 2012) for the simplified evaluation of the response of existing RC buildings, as it is considered a valid compromise between reliability of the results and computational effort.

Based on the assumed Shear Type model, the lateral response of the structure under a given distribution of lateral forces can be completely determined based on the interstorey shear-displacement relationships at each storey.

Hence, the nonlinear response of RC columns and infill elements has to be determined. The non-linear behaviour of each RC column is characterized by a shear-displacement relationship, $V-\Delta$, evaluated from the corresponding moment-rotation relationship, $M-\theta$, consistent with the Shear Type assumption, assuming a shear span equal to half of the column height ($L_v=h/2$).

A tri-linear envelope is assumed for the moment-rotation model, with cracking and yielding as characteristic points. Behaviour is linear elastic up to cracking and perfectly-plastic after yielding (see Figure 3-6).

Moment and rotation at cracking are evaluated as:

$$M_{cr} = \left(-f_{ct} + \frac{N}{B \cdot H} \right) \cdot \frac{B \cdot H^2}{6} \quad \text{Eq 3-2}$$

$$\theta_{cr} = \frac{M_{cr}}{EI} \cdot \frac{h}{6} \quad \text{Eq 3-3}$$

where f_{ct} is the concrete strength in tension, N is the axial load acting on the column, B and H are width and height of the column section (in the considered direction), EI is the gross flexural inertia of the section and h is the column height.

Moment at yielding (M_y) is calculated in closed form by means of the first principles-based simplified formulations proposed in proposed in (Fardis, 2007 – Section 3.2.2.2, Eqs. 3.33 to 3.37). Rotation at yielding (θ_y) is univocally identified by M_y and the secant stiffness to yield provided by (Haselton et al., 2007– Section 3.2.4.1, Eq. 3.1).

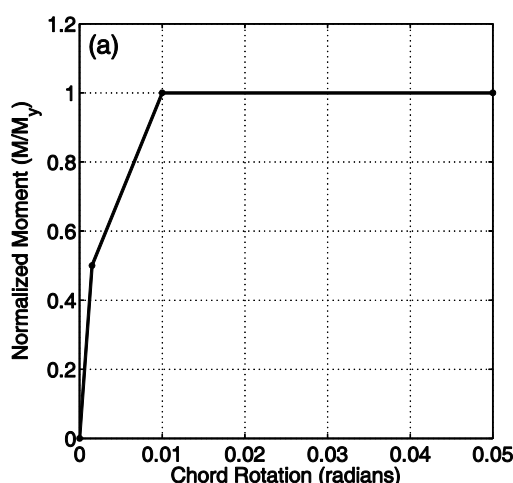


Figure 3-6. Moment-rotation relationship for RC columns, lateral force-displacement relationship for infill panels

Lateral force-displacement relationships for infill panels (see Figure 3-7) are evaluated according to the model proposed by (Panagiotakos

and Fardis, 1996), which supplies a multilinear envelope given by four branches:

- the first branch corresponds to the linear elastic behaviour up to the first cracking, and the stiffness is given by

$$K_{el} = \frac{G_w A_w}{h_w} \quad \text{Eq 3-4}$$

where A_w is the cross-sectional area of the infill panel, G_w is the elastic shear modulus of the infill material and h_w is the clear height of the infill panel. According to the authors, this assumption gives the best agreement with experimental initial stiffness values reported by (Stylianidis, 1985) and (Pires, 1990). The shear cracking strength is given by

$$F_{cr} = \tau_{cr} A_w \quad \text{Eq 3-5}$$

where τ_{cr} is the shear cracking stress;

- the second branch follows the first cracking, up to the point of maximum strength. The maximum strength is given by

$$F_{max} = 1.30 \cdot F_{cr} \quad \text{Eq 3-6}$$

and the corresponding displacement is evaluated assuming that the secant stiffness up to this point is given by Mainstone's formula (Mainstone, 1971), that is, assuming an equivalent strut width given by:

$$b_w = 0.175 (\lambda_h h_w)^{-0.4} d_w \quad \text{Eq 3-7}$$

where d_w is the clear diagonal length of the infill panel and λ_h is the well-known coefficient accounting for the ratio between stiffness of masonry panel and RC frame (Stafford Smith, 1966; Stafford Smith and Carter, 1969), given by:

$$\lambda_h = \sqrt[4]{\frac{E_w t_w \sin 2\theta}{4E_c I_p h_w}} \quad \text{Eq 3-8}$$

where E_w is the Young's elastic modulus of the infill material, t_w is the thickness infill panel, $E_w \sin 2\theta$ is the slope of diagonal of infill to horizontal and $E_c I_p$ is the flexural stiffness of RC columns adjacent to the infill panel.

Similar to initial elastic stiffness, this assumption is based on the comparison with experimental secant-to-maximum stiffness values reported in (Stylianidis, 1985) and (Pires, 1990).

The authors also say that a representative value for the post-cracking tangent stiffness could be $K_{\text{post-cracking}} = 0.03 \cdot K_{\text{el}}$ (Panagiotakos and Fardis, 1996);

- the third branch is the post-capping degrading branch, up to the residual strength. Its stiffness depends on the elastic stiffness through the parameter α :

$$K_{\text{soft}} = -\alpha K_{\text{el}} \quad \text{Eq 3-9}$$

the value of this parameter has to be arbitrarily assumed. However, the authors give some indication (Panagiotakos and Fardis, 1996): the range of values for α should be between 0.005 and 0.1, although a value of 0.1 is unrealistically high (very brittle

infill), while a value of 0.01 may be more realistic yet still conservative (well constructed infill);

- the fourth branch is the horizontal branch corresponding to the residual strength. This strength is given by

$$F_{\text{res}} = \beta F_{\text{max}} \quad \text{Eq 3-10}$$

with β between 0.05 and 0.1.

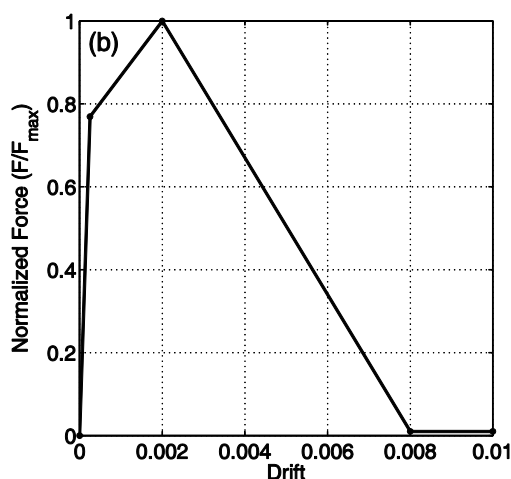


Figure 3-7. Lateral force-displacement relationship for infill panels

The infill panel in RC buildings mainly represent a vertical closure element from the external environment. The infill panels have the unique static function to bring their own weight. Therefore, the bearing function is ensured by the RC frame and separation function between the inner and the outer space is ensured by the infill panels that fill up the surrounding RC frames. In addition, infill panels ensure acoustic and thermo-hygrometric comfort.

Typically, such perimetral infill panels have openings to ensure adequate natural light and to guarantee health conditions related to air circulation.

As a matter of fact, Health Ministerial Decree 5/7/1975 requires that for each residential room, the window size should be proportionate in order to ensure a value of average daylight factor of at least 2%, and the opening windows surface shall not be less than 1/8 of the floor surface.

The opening windows are varyingly arranged along the outer perimeter of the building, sometimes following architectural or functional criteria. They can also be different for size, type (windows or balconies) or position along the outer perimeter.

The effects of windows openings in the behavior of infill panel is mainly a reduction of strength and stiffness compared to the solid panel (e.g., Mosalam, 1996; Asteris, 2003) and experimental (e.g., Mosalam et al., 1997; Kakaletsis and Karayannis, 2009). Moreover, it can produce a change in the stress fields that can potentially develop within the infill ([ASCE-SEI 41](#), [Combescure 2006](#), [Hamburger, 1993](#)).

In the present work opening in infill panels are explicitly considered. For this reason, non-linear behavior of the infills is modified according to model presented in ([Kakaletsis and Karayannis, 2009](#)). The Authors investigated the influence of opening shape and the opening size from the results of eight single-story, one-bay, 1/3-scale specimens of infilled RC frames. Hence, control parameters as a function of opening sizes and opening type are introduced in order to derive the corresponding monotonic force-displacement behaviour:

- The secant stiffness to peak resistance K_1 normalized to the that of the solid infill K_{1S} , ($K_{max}/K_{max,Solid}$), evaluated according to Mainstone's formula:

$$k_{max,solid} = \frac{s_w b_w E_w}{d_w} \cos^2 \theta \quad \text{Eq 3-11}$$

- The degrading stiffness normalized to secant stiffness to peak resistance, (K_{soft}/K_{max});
- The ultimate strength F_{max} normalized to the ultimate strength of the solid infill $F_{max,Solid}$, ($F_{max}/F_{max,Solid}$);

Hence, for each infill panel, once defined the opening shape, namely concentric window or door, and the corresponding size, the corresponding control parameters are defined. Hence, the full non-linear behavior of the infills with openings can be defined as follow:

- the first branch is evaluated considering the same elastic stiffness as the that of solid panel (Eq 3-4), regardless the opening shape and opening size. Moreover, the shear cracking strength is given by

$$F_{cr} = \frac{F_{max}}{1.3} \quad \text{Eq 3-12}$$

whereas F_{max} is evaluated according to Eq 3-13.

- the second branch is evaluated multiplying the ultimate strength and secant stiffness of solid infill panel by the corresponding control parameters, ($F_{max}/F_{max,Solid}$) and ($K_{max}/K_{max,Solid}$) relative to the proper opening size and opening type.
- the third branch is individuated by the residual strength evaluated as:

$$F_{res} = \beta F_{max} \quad \text{Eq 3-13}$$

with β assuming the same value of corresponding solid panel, ranging between 0.05 and 0.1, and by the corresponding degrading stiffness, evaluated as a function of the control

parameter (K_{soft}/K_{max}) relative to the proper opening size and opening type;

- The fourth branch is the horizontal branch corresponding to the residual strength.

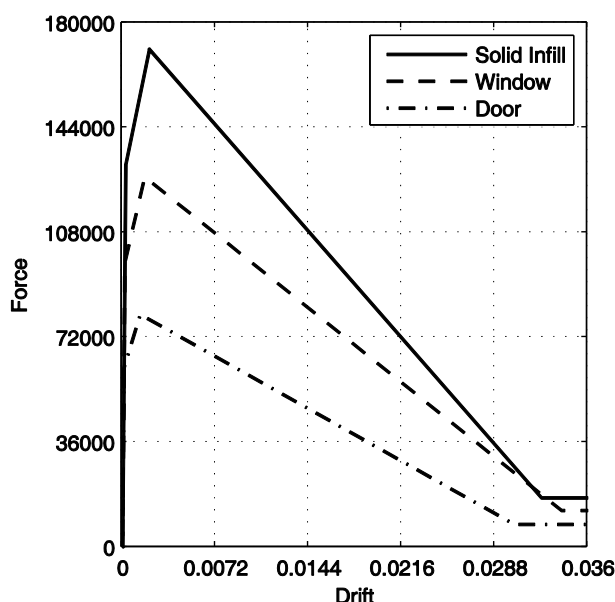


Figure 3-8: Lateral force-displacement relationship for infill panels with opening

Figure 3-8 reports the lateral force-displacement relationship varying the opening type (solid panel, window and door) for a 4700mmx2500mm infill panel ($l_w \times h_w$), with G_w and τ_{cr} equal respectively to 1350MPa and 0.35MPa, considering a concentric opening size equal to 25% of the corresponding length of the infill panel (l_w).

It is to be noted that the presence of opening produces a reduction of strength and stiffness in the behavior of infill panel compared to the solid panel. As a matter of fact the reduction of peak resistance is equal to 53.2% and 25.6% for infill panel with door and window opening, respectively. Analogously, the reduction of the secant stiffness up to

peak resistance is equal to 28.2% and 9.5% for infill panel with door and window opening.

Nevertheless, it can be observed that the presence of opening does not produce substantial differences in the values of displacement among the lateral force-displacement relationship varying the opening type.

The opening shape is an input parameter for the methodology, whereas the opening type is a parameter extremely difficult to identify and characterize. As a matter of fact, it is assumed that for each building facade the presence of the three types panel (solid, panel with window and balcony) is equally probable. In such a way, considering a facade consisting of three bays, each of them will be characterized by a different opening type, namely solid panel, window opening and door opening.

Moreover, in addition to the external infill panels residential buildings have different layers of infill panels along internal bays to define inner spaces. As well as the external infill panels, the internal infill panels could also affect the building response, leading to an increase of the overall resistance and stiffness.

However it appears difficult to quantify and locate internal infill panels in the structural mesh of the building. Renouncing to a refined, even though realistic, modelling, it is assumed in the following that the internal infills represent a rate of external ones. Typically, for the infill panel thickness, it can be roughly stated that the thickness of outer walls is 20-25cm, constructed with 15-20cm thick bricks plus plaster and insulation material, if any, on either side. Internal walls mainly have a thickness of around 12-15 cm with a 8-10 cm thick brick (Bal et al, 2007). Firstly, the external infill percentage, ρ_w , as the ratio between the external infill area, A_w , evaluated along one of the principal directions of the building and the building area A_b , has to be defined. Hence, the thickness of internal infill panels is evaluated assuming an internal infill percentage for that direction, $\rho_{w,int}$ equal to 50% of the corresponding

external one, and dividing the total amount by the number of internal frames.

Then, once thickness of internal infill panels is determined, assuming the same mechanical characteristic of external panels, the lateral force-displacement relationship is evaluated similarly to what reported from Eq 3-4 to Eq 3-10. Nevertheless, considering that the alignment of the internal infills not necessarily corresponds to that of the internal frames, namely that the internal infill panel is not always confined to a RC frame, the lateral force-displacement relationship of Figure 3-7 has to be modified. In fact, in RC infilled frames the initial response is given by a monolithic behaviour of the whole composite system, ensured by bond capacities at the interface between the panel and the frame. Secondly, after the separation at the interface between the two materials has occurred, a reduction in the stiffness in the force-displacement response can be observed. At this stage, a diagonal cracking together with an increase in the stress state narrowed in the opposite compression angles and along the diagonal of the panel takes place, up to the attainment of the maximum lateral strength of the infilled frame. The latter phenomenon can develop if the panel is adequately confined by the surrounding frame.

Then, considering that often the internal panel is not confined by an RC frame, it is assumed that the diagonal strut cannot fully develop, leading to a zero value of the stiffness of the second branch of the lateral force-displacement relationship, see Figure 3-9.

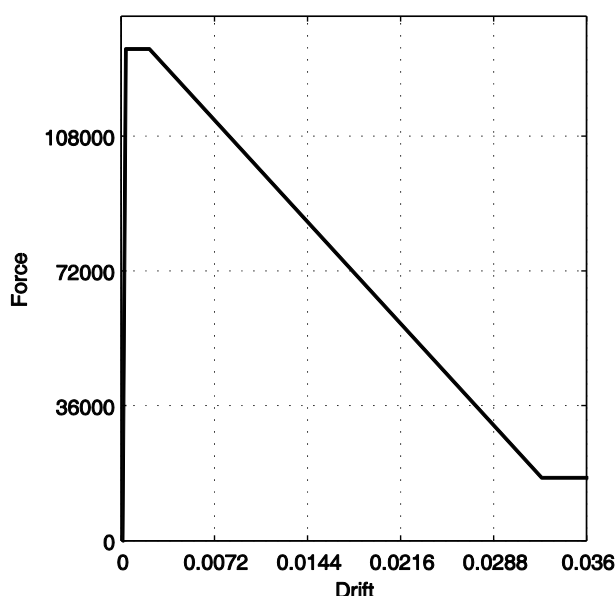


Figure 3-9: Lateral force-displacement relationship for internal infill panels

At each storey, the relationship between the interstorey displacement and the corresponding interstorey shear is evaluated considering all the RC columns and the internal and external (if present) infill elements acting in parallel. To this aim, displacement values corresponding to characteristic points of lateral force-displacement envelopes of RC columns and infill elements are sorted in a vector; then, for each of these displacement values the corresponding shear forces provided by each element are evaluated and summed. In this way, a multi-linear interstorey shear-displacement relationship is obtained at each storey by adding up the lateral shear-displacement relationships of all the RC columns and infill panels along longitudinal and transverse direction, respectively. An example interstorey shear-displacement relationship is shown in Figure 3-10.

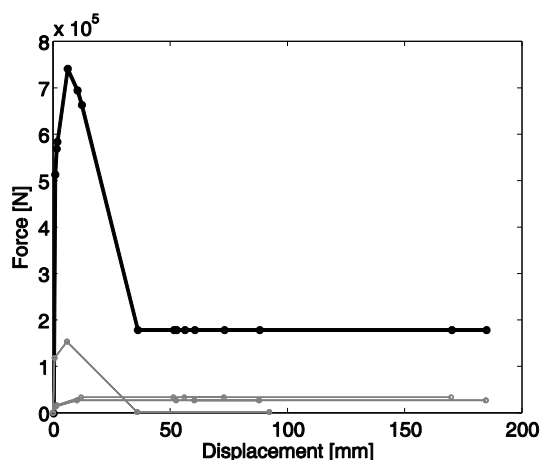


Figure 3-10. Example interstorey shear displacement relationships (black line) obtained as the sum of shear-displacement contributions of RC columns and infill panels (grey lines with dots indicating displacement thresholds)

3.3.3 Calculation of pushover curve

Once the interstorey shear-displacement relationship at each storey has been defined, the base shear-top displacement relationship representing the lateral response of the Shear Type building model – under a given distribution of lateral forces – can be evaluated through a closed-form procedure.

Hence, a linear, uniform or 1st mode lateral displacement shape is chosen and the corresponding lateral load shape is determined.

Once the shape of the applied distribution of *lateral forces* is given, the shape of the corresponding distribution of *interstorey shear demand* can be determined, too.

A normalized distribution of interstorey shear demand is assumed and the ratios between such demand forces and the corresponding interstorey shear strengths (i.e., maximum force values of the interstorey shear-displacement relationships) are calculated. Hence, the storey characterized by the maximum value of this ratio will be the first

(and only) to reach its maximum resistance (with increasing lateral displacement). Hence, if infill elements are present at that storey, leading to a degrading post-peak behaviour of the interstorey shear-displacement relationship, that storey will also be the first (and only) to start to degrade, thus controlling the softening behaviour of the structural response.

Therefore, the pushover curve can be evaluated by means of a force-controlled procedure up to the peak, and by means of a displacement-controlled procedure after the peak. In the latter phase, the evaluation of the response is based on the interstorey shear-displacement relationship of the storey where the collapse mechanism has taken place. At each step, the top displacement is calculated as the sum of the interstorey displacement at each storey, evaluated as a function of the corresponding interstorey shear demand, whereas the base shear is given by the sum of lateral applied forces. If the storey where the collapse mechanism takes place is characterized by a softening post-peak behaviour, during the post-peak phase in the remaining $N-1$ storeys (where N is the number of storeys) the interstorey shear will decrease starting from a pre-peak point of the interstorey shear-displacement relationship; hence, the corresponding displacement will decrease, too, following an unloading branch. An unloading stiffness equal to the elastic stiffness is assumed.

Following this procedure, the pushover curve can be completely determined in both directions.

3.3.4 Seismic capacity assessment

Once the pushover curve has been determined, a multi- or bi-linearization is carried out. When the lateral response is characterized by a strength degradation due to infill failure, a multi-linearization of the pushover curve is carried out by applying the equal energy rule, whereas an elastic-plastic bi-linearization is carried out when the lateral

response is not characterized by a strength degradation (because infill elements are not present or not involved in the collapse mechanism).

Hence, characteristic parameters of the equivalent SDOF system are determined and the displacement capacity is evaluated for different DSs.

Then, simplified Incremental Dynamic Analysis (IDA) curves are derived from (Vamvatsikos and Cornell, 2006), which allow to obtain a relationship between a seismic intensity measure (spectral ordinate) and an Engineering Demand Parameter (ductility) and to assess the variability of the intensity (R/R_y) given the value of ductility, as it will be seen in the following.

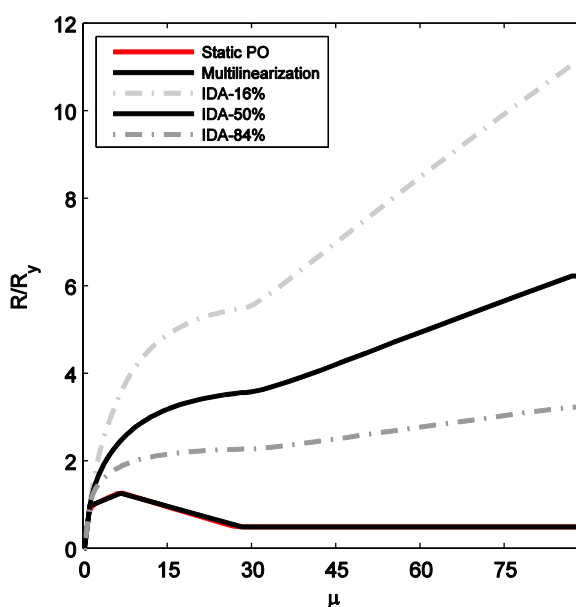


Figure 3-11: Static Pushover curve and IDA-curves for 4-storeys building.

Given the elastic spectral acceleration at a certain period, the corresponding PGA (capacity) is univocally determined based on the shape of the acceleration response spectrum.

In the next paragraph we describe the procedure to identify the considered DSs and the corresponding displacement capacity. Then, based on such displacement capacity, the values of seismic intensity expected to lead to the achievement of the assumed DSs are obtained through the simplified IDA curves.

3.3.5 Definition of Damage States

Damage States adopted in the proposed analytical methodology are defined according to the damage scale proposed by European Macroseismic Scale (EMS-98) (Grünthal, 1998).

To this aim, in this Section we define analytical displacement thresholds corresponding to the damage to structural and non-structural elements described by EMS-98, based on the mechanical interpretation of the reported description of damage.

Table 3-1 reports, for each one of the five EMS-98 damage grades, key sentences describing the damage to infills and RC members, respectively, and the corresponding assumed analytical displacement threshold. Note that, due to the assumed Shear-Type behaviour, the interstorey displacement leading to the attainment of each Damage State is the minimum between the values reported in Table 1 for infill panels and RC columns.

In the following, it is illustrated and discussed in detail how the qualitative description of damage provided by EMS-98 (e.g., with terms as “fine cracks”, “cracks” and “large cracks”) has been translated in analytical displacement thresholds through engineering judgment. Such discussion is reported separately for infill panels and RC columns, respectively. The resulting displacement thresholds at each Damage State are summarized in Table 3-1.

Damage States		Infill panels		RC columns	
		EMS 98 description	Displacement threshold	EMS 98 description	Displacement threshold
DS1	GRADE 1: Negligible to slight damage	<i>Fine cracks in partitions and infills</i>	Δ_{cr}^{inf}	<i>Fine cracks in plaster over frame members</i>	Δ_{cr}^{RC}
DS2	GRADE 2: Moderate damage	<i>Cracks in partition and infill walls.</i>	Δ_{max}^{inf}	<i>Cracks in columns</i>	Δ_y^{RC}
DS3	GRADE 3: Substantial to heavy damage	<i>Large cracks in partition and infill walls, failure of individual infill panels</i>	Δ_{ult}^{inf}	<i>Spalling of concrete cover, buckling of reinforced rods</i>	$\Delta_{spalling}^{RC}$ $\Delta_{buckling}^{RC}$
DS4	GRADE 4: Very heavy damage	-	-	<i>Large cracks in structural elements with compression failure of concrete and fracture of rebars</i>	Δ_{ult}^{RC}
DS5	GRADE 5: Destruction	-	-	<i>Collapse of ground floor or parts of buildings</i>	$\Delta_{collapse}^{RC}$

Table 3-1. Displacement thresholds at the assumed Damage States, based on the mechanical interpretation of the damage grades described by EMS-98.

Infills panels:

DS1 – “Fine cracks in partitions and infills”: this condition is associated with first visible cracks in infill panels, leading to a first stiffness decrease in the force-displacement response. Hence, displacement at this DS can be assumed to correspond to the end of the initial elastic branch of the lateral force-displacement response (Δ_{cr}^{inf}).

DS2 – “Cracks in partition and infill walls”: after first cracking, an increase in the stress state narrowed in the opposite compression angles and along the diagonal of the panel takes place. During this phase, cracking and damage in the panel gradually increase up to the attainment of the maximum lateral strength of the infilled frame. Hence, displacement at this DS can be assumed to correspond to the maximum resistance point on the backbone of the lateral force-displacement response (Δ_{max}^{inf}).

DS3 – “Large cracks in partition and infill walls, failure of individual infill panels”: after the peak, damage develops in the panel up to the attainment of the residual resistance condition. Hence, displacement at this DS can be identified with the point at the end of the post-peak degrading branch in the lateral force-displacement response (Δ_{ult}^{inf}).

RC columns:

DS1 – “Fine cracks in plaster over frame members”: this condition can be regarded as the onset of first visible cracks, hence it is assumed to correspond to the attainment of cracking moment at the end section of the RC columns (Δ_{cr}^{RC}).

DS2 – “Cracks in columns”: this condition can be associated with the widening of flexural cracks that takes place when longitudinal reinforcement yields. Hence, it is assumed to correspond to the

attainment of yielding moment at the end section of the RC columns (Δ_y^{RC}).

DS3 – “Spalling of concrete cover, buckling of reinforced rods”: the displacements corresponding to such conditions are evaluated from the study by Berry and Eberhard (2003), which reports empirical-based capacity models explicitly providing the values of lateral displacement at concrete cover spalling and longitudinal reinforcement buckling as a function of geometry, reinforcement and axial load of RC columns($\min(\Delta_{spalling}^{RC}; \Delta_{buckling}^{RC})$).

DS4 – “Large cracks in structural elements with compression failure of concrete and fracture of rebars”: this damage description is consistent with the typical assumption of “ultimate” condition for RC elements, usually assumed as corresponding to 20% strength degradation in the lateral force-displacement response (e.g., Panagiotakos and Fardis, 2001). Hence, according to this definition, displacement at this DS is identified for each column as the displacement corresponding to 80% of maximum strength on the degrading branch of the backbone curve provided by the model by Haselton et al. (2007) (Δ_{ult}^{RC}).

DS5 – “Collapse of ground floor or parts of buildings”: the heaviest damage grade, corresponding to this description, can be assumed as the loss of lateral load carrying capacity. Hence, displacement at this DS is identified for each column as the displacement corresponding to the zero resistance point of the backbone curve provided by the model by Haselton et al. (2007) ($\Delta_{collapse}^{RC}$).

Figure 3-12 reports a graphical representation of displacement thresholds assumed on the backbone of the lateral response of infill panels and RC columns, together with the corresponding Damage State displacement ranges adopted.

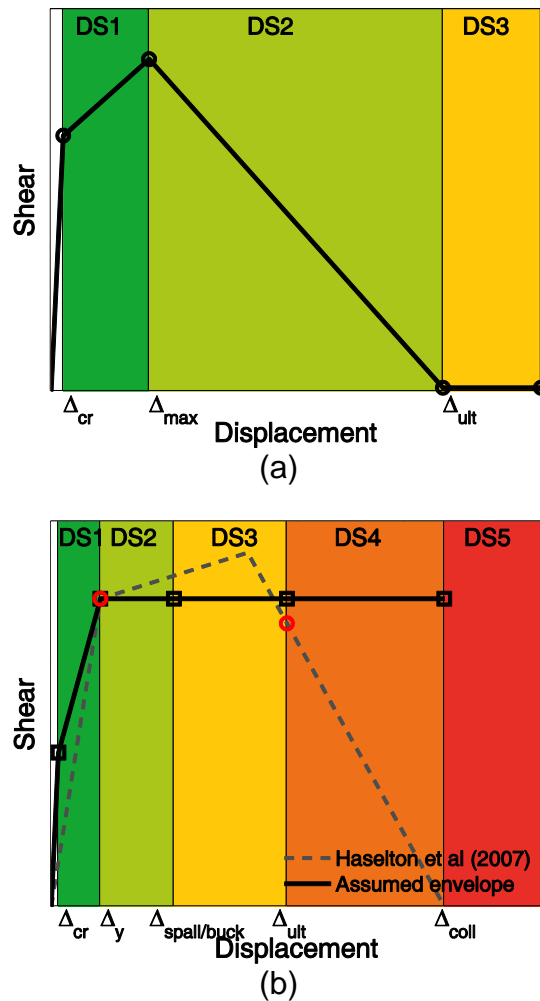


Figure 3-12. Displacement thresholds assumed on the backbone of the lateral response of infill panels (a) and RC columns (b), and corresponding Damage State displacement ranges adopted

An example representation of capacity curve with global displacements at the defined Damage States (corresponding to the attainment of the local interstorey displacement thresholds defined

above) is reported in Figure 3-13, together with the corresponding IDA-curves, evaluated according to (Vamvatsikos and Cornell, 2006).

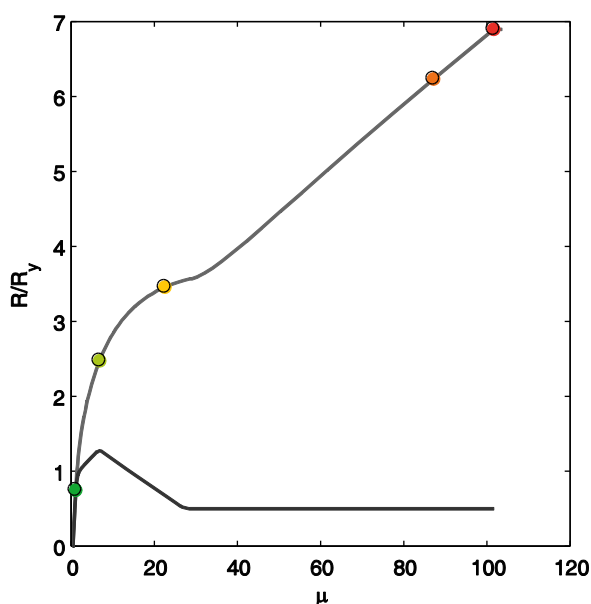


Figure 3-13.Capacity curve and IDA-curves for 4-storeys building

3.3.6 Evaluation of fragility curves

In this paragraph, the methodology used for the evaluation of fragility curves for the case study structure is illustrated.

A fragility curve represents a relationship between a seismic intensity parameter and the corresponding probability of exceedance of a given damage threshold (typically represented by a displacement capacity).

The PGA capacity – for a certain Limit State – is defined as the PGA corresponding to the demand spectrum under which the displacement demand is equal to the displacement capacity for that Damage State (see **Errore. L'origine riferimento non è stata trovata.**). Hence, the relative spectral ordinate is evaluated from IDA curve (see Figure 3-13) and finally Peak Ground Acceleration, given a spectrum shape.

Hence, if the seismic intensity is given by a PGA higher than the PGA capacity, the threshold displacement capacity for that Limit State is exceeded, and vice versa.

If PGA capacity is “observed” in a population of buildings, according to a frequentistic approach the cumulative frequency distribution of these observations provides the fragility curve (based on PGA seismic intensity measure) for that population of buildings and for that Damage State, based on the definitions themselves of fragility curve and PGA capacity.

Given a defined building, some variables – which are input parameters for the determination of the PGA capacity – can be defined as Random Variables, in order to investigate the influence of the uncertainty in the determination of such Variables on the seismic capacity of the structure.

Hence, Probability Density Functions describing the expected values and the corresponding variability for each one of these Variables can be defined. According to a simulation technique, for instance, a number of samplings for these Variables can be carried out. In this way, a population of buildings is generated, each one corresponding to a different set of values of the defined Random Variables. If PGA capacity, at a given Damage State, is calculated for all the generated buildings, the cumulative frequency distribution of the obtained values provides the fragility curve for the building at that Limit State.

In this study, the Monte Carlo simulation technique is used, and sampling of Random Variables is carried out through the efficient stratified Latin Hypercube Sampling (LHS) technique ([McKay et al., 1979](#)), adopting the “median” sampling scheme ([Vorechovsky and Novak, 2009](#)).

Hence, following the Monte Carlo simulation technique procedure the methodology is iteratively repeated. In any single run, a realization of random variable is sampled according to the marginal distributions chosen to define its variability. Accordingly, in any single run the

building non-linear static response (Static pushover analysis) is derived and seismic capacity is evaluated. Therefore, at the end of the simulation, once PGA capacity at a given damage state is calculated for all the runs, the corresponding cumulative frequency distributions provide the fragility curves in X and Y directions at each damage state.

In the same way fragility curves independent of the direction can be obtained, through the evaluation of the cumulative frequency distribution of the minimum PGA capacities between longitudinal and transversal direction for each sampling. In Figure 3-14 an example of fragility curves at each different DS for a 5-storey building is shown. In Figure 3-14 the empirical cumulative distribution functions and the corresponding fitted lognormal distribution functions are reported.

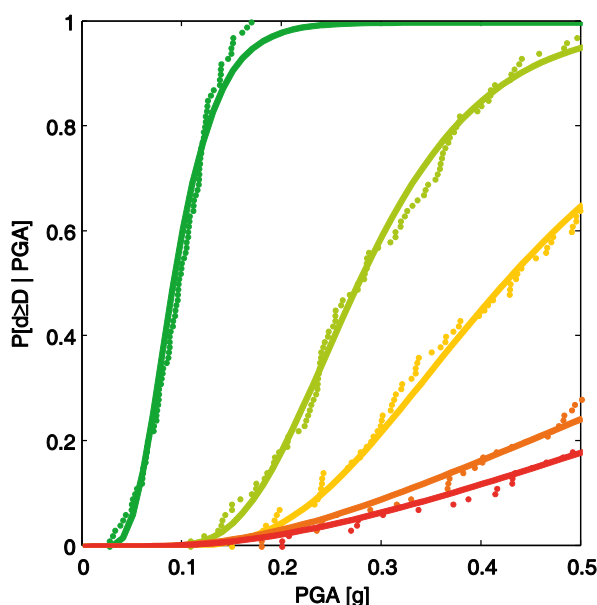


Figure 3-14. Example fragility curves for a 5-storey building

Furthermore, given a single defined building, some variables can be assumed as Random Variables because their values cannot be known in a deterministic manner, for lack of knowledge or because their

definition may require an excessive cost or it can not be easily and quickly determined.

Actually, within an engineering analysis model the lack of knowledge part of the uncertainty can be represented in the model by introducing auxiliary non-physical variables (Der Kiureghian and Ditlevsen, 2009). In such a way, homogeneous classes of buildings are defined, identified by the parameters that greatly influence their seismic fragility.

Obviously, the choice of the parameters defining the class, is necessarily conditioned by the available level of information.

The variability within a class takes into account the variability between the fragility of different buildings in the same class (intra-variability), apart from the variability between the fragility of different classes of building.

It can be stated that the fragility of a building should coincide with the fragility of the class to which it belongs, unless of some deviations between the fragility of buildings belonging to the same class, which in theory should be as limited as possible. Such deviations are greater the higher is the heterogeneity within the class of the parameters that greatly influence the seismic fragility. This heterogeneity is in turn necessarily conditioned by the available level of information.

In this regard, it is worth highlighting that does not exist a clear distinction between fragility of building and fragility of class of building. This distinction is greatly ascribable to the nature and the extent of the involved uncertainties, and is in turn mainly attributable to the available level of information.

In this way, for defining fragility curves for single building some input parameters have to be assigned, namely global geometrical parameters, including number of storeys, surface area and plan ratio, and the age of construction. The latter is a key parameter as it allows to determine firstly the structural model in compliance with building codes and design practice in force at that time and secondly the statistics on

mechanical characteristics of steel and concrete in addition to the type of reinforcement (plain or ribbed bars).

In particular the parameters needed to completely define the global building geometry include: number of storeys, plan dimensions in longitudinal (X) and transversal (Y) directions, number of bays in X and Y, height of the bottom storey, height of upper storeys. Hence, a possible irregularity in interstorey height (often due to architectonic or functional reasons) is considered.

The presence of infill panels can be defined according to three different options: (i) Uniformly infilled building, (ii) Pilotis building or (iii) Bare building. The opening percentage can also be defined, both in bottom infill panels (case i) and in upper infill panels (cases i and ii). If present, infill panels are regularly distributed in plan in all the external frames in X and Y directions.

The design can be defined as “gravitational” or “seismic”. If the design is seismic, the base shear coefficient prescribed by code (to be employed in the simulated design procedure) is evaluated as a function of the building codes in force at the time of construction.

Material characteristics are defined, namely the concrete compressive strength, the steel yield strength and the infill characteristics (if infill panels are present). The latter include the thickness of infill panels, the infill mechanical characteristics (shear cracking strength, shear elastic modulus and Young’s elastic modulus) and parameters α and β , respectively representing the ratio between post-capping degrading stiffness and elastic stiffness and the ratio between residual strength and maximum strength. Hence, the envelope of the lateral force displacement relationship of infill panels can be completely defined, according to the adopted model.

Finally, the data for the definition of seismic hazard are defined. The probabilistic seismic hazard assessment carried out for Italy ([INGV-DPC S1, 2007](#)) is adopted. Hence, the location of the building is needed, defined by its Longitude and Latitude. Stratigraphic (A to E) and

topographic (T1 to T4) conditions are defined, according to the Italian code (DM 14/1/2008). Moreover, V_N , C_U and P_{VR} are defined (representing the nominal life, the importance coefficient (providing the reference period V_R as $V_N \cdot C_U$) and the probability of exceedance in the reference period, respectively) to obtain the elastic spectrum used for a single assessment of seismic demand.

Nevertheless, in this study there is the need to extend elastic demand spectra above and below the extreme values, as in (Crowley et al., 2009). To this aim, the formulations proposed for the interpolation procedure are also used to extrapolate the above mentioned parameters out of the given range of values.

Alternatively it can be used the Uniform Hazard Newmark-Hall elastic spectrum defined in (Eurocode 8 Part1), regardless the location of the building and varying as a function of stratigraphic (A to E) conditions.

Hence, the remaining parameters (see **Errore. L'origine riferimento non è stata trovata.**) are assumed as random variable, defined through their Probability Density Functions describing the expected values and the corresponding variability for each of them.

In the present study, for defining fragility curves for single building Random Variables, regarding (i) Material properties, (ii) Capacity models and (iii) displacement threshold for infill panels are assumed.

Finally record to record variability can be estimated directly through the dispersion of IM given EDP (Vamvatsikos and Cornell, 2006). Thus, the effect of aleatory randomness can be estimated through SPO2IDA, which reports the lognormal standard deviation, β_R , as a function of spectral ordinates evaluated for IDA-curve-84% and IDA-curve-16% (see Figure 3-11) for the corresponding ductility capacity value, μ :

$$\beta_R \approx \frac{1}{2} \left(\ln R^{84\%} - \ln R^{16\%} \right) \quad \text{Eq 3-14}$$

3.3.7 Calculation of failure probability

The failure probability (P_f) is evaluated as

$$P_f = \int_0^{+\infty} f_s(S) F_R(S) dS \quad \text{Eq 3-15}$$

where $f_s(S)$ is the Probability Density Function (PDF) of the seismic intensity parameter and $F_R(S)$ is the probability that the resistance R is lower than a level S of seismic intensity. Hence, $F_R(S)$ is represented by a fragility curve, whereas the PDF of the seismic intensity S – in a given time window – is obtained from seismic hazard studies.

In particular, based on the seismic hazard data provided in (INGV-DPC S1, 2007) for the Italian territory, if the coordinates of the site of interest are given, PGA values corresponding to different return periods (T_R) can be determined. Hence, given a PGA value, the corresponding $T_R(\text{PGA})$ can be calculated. Finally, given a time window (V_R), the exceeding probability of the same PGA is given by the Poisson process:

$$P_{V_R}(\text{PGA}) = 1 - e^{-\frac{V_R}{T_R(\text{PGA})}} \quad \text{Eq 3-16}$$

In the procedure described herein, PGA is assumed as seismic intensity parameter S , $F_R(S)$ is represented by the calculated fragility curves and $f_s(S)$ is evaluated as the derivative of Cumulative Density Function (CDF) of the seismic intensity parameter:

$$\begin{aligned}
 PDF &= \frac{d}{dPGA} CDF = \frac{d}{dPGA} (1 - CCDF) = \\
 &= \frac{d}{dPGA} (1 - P_{V_R}) = \frac{d}{dPGA} \left(1 - \left(1 - e^{-\frac{V_R}{T_R}} \right) \right)
 \end{aligned}
 \tag{Eq 3-17}$$

Hence, P_f is calculated through Eq 3-15, by means of a numerical integration based on Simpson quadrature, for a time window assumed equal to 1 year.

3.4 Senitivity analysis

Based on the assumed Random Variables, a sensitivity analysis is carried out, in this section, in order to investigate the influence of each variable on the seismic capacity of the case study structure. To this aim, two models are generated for each random variable assuming median-minus-standard-deviation and median-plus-standard-deviation values for the considered variable, and median values for the remaining variables.

In addition to these analyses, another one is carried out assuming median values for all of the variables (Model #1).

It is to be noted that the influence of each single variable, which will be illustrated through the sensitivity analysis, not only depends on the influence of the variable on the seismic response, but also depends on the assumed dispersion for that variable. As a matter of fact, the amount of dispersion considered for the variable (through the assigned Coefficient of Variation) leads to consider – as Lower and Upper limits – values more or less distant from the central (median) value. A variable characterized by a lower uncertainty (i.e., a lower CoV) will have median-minus-1.7-standard-deviation and median-plus-1.7-standard-deviation values closer to the median value, and vice versa. Hence, the amount of the change in PGA capacity due to the change in each variable, compared with the model where median values are assigned

to all variables (Model #1), should be interpreted taking into account also the CoV value assigned to each variable.

3.4.1 Case study Buildings

In this Section, the results of a sensitivity analysis evaluating the influence of main material and capacity parameters on the seismic response of the building are presented.

Seismic response is evaluated through Static Push-Over analyses. Seismic demand is assessed by means of the simplified IDA-curve ([Vamvatsikos and Cornell, 2006](#)).

The case study structure is a Seismic Designed building, located in the Municipality of L'Aquila (42°21'14.43"N 13°23'31.17"E), defined by means of a simulated design procedure according to code prescriptions and design practices in force in Italy between 1970s and 1980s ([RDL 640/1935](#); [Verderame et al., 2010](#)). ([RDL n431/1927](#)) classifies firstly the territory of the Municipality of L'Aquila in II Seismic Category. The classification of the municipality of L'Aquila has remained unchanged over the years, until 2003 when the ([OPCM 3274/2003](#)) confirmed the seismic classification in II category. Moreover, in 1970 ruled ([RDL 640/1935](#)), which prescribes a uniform distribution of horizontal forces whatever the height of the building and the number of floors, equal to 0.07 of the storey weight force for buildings II seismic category, with a corresponding base shear coefficient equal to 0.07.

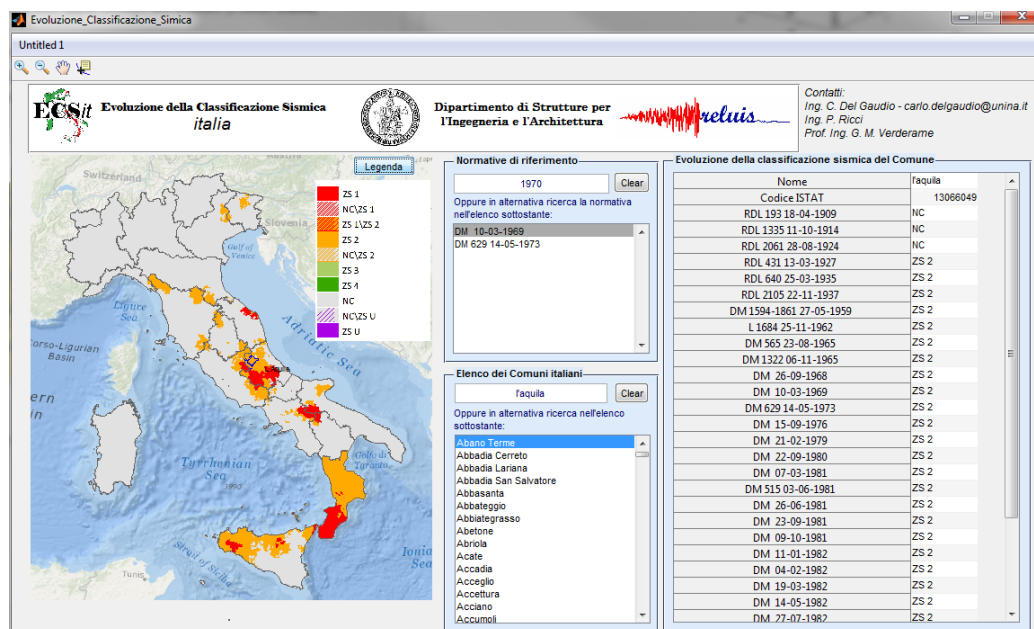


Figure 3-15: Evolution of seismic classification for the Municipality of L'Aquila through ECSit software based on MATLAB® code (<http://www.reluis.it/>)

The building is symmetric in plan, both in longitudinal (X) and in transversal (Y) direction. The number of storeys is one of the investigated parameters, assumed in the interval [2 4 6]. The surface area is assumed equal to 150m², whereas the building plan ratio, is assumed in the interval [1 2 3].

Hence, the number of bays in longitudinal and transversal direction is evaluated in correspondence with the value that minimizes the deviation from a target value of the bay length equal to 5 m. Interstorey height is equal to 3.0 m. The structural configuration follows the parallel plane frames system: gravity loads from slabs are carried only by frames in longitudinal direction. Beams in transversal direction are present only in the external frames. Element dimensions are calculated according to the allowable stresses method.

Values of allowable stresses for steel and concrete employed in the simulated design procedure were determined according to the age of

construction. As far as concrete is concerned, the allowable concrete stress for bending is assumed equal to

$$\sigma_c = 60 + \frac{R_{ck} - 150}{4} \quad \text{Eq 3-18}$$

Where R_{ck} is the cubic strength of concrete assumed equal to 25MPa in all cases. Hence, allowable compressive stress for axial load combined with bending is assumed equal to $0.7\sigma_c$. Moreover, the concrete allowable stress used to determine column dimensions in the simulated design procedure was multiplied by a coefficient equal to 0.7 in the case of seismic design ([Pecce et al., 2004](#)).

Maximum steel compressive stress is assumed equal to 208 MPa according to STIL software ([Verderame et al., 2012](#)).

Column dimensions are calculated according only to the axial load, beam dimensions and reinforcement are determined from bending due to loads from slabs.

Moreover, the design of column reinforcement is based on the assumed distribution of horizontal force, based on the assigned base shear coefficient, which in the present case study is assumed equal to 0.07.

Then, based on the assigned values of allowable stress for steel and concrete, the reinforcement area is designed to provide a flexural strength (according to the allowable stresses method) not lower than the bending moment from design.

Afterwards, a tri-linear envelope is assumed for the moment-rotation model, with cracking and yielding as characteristic points. Behaviour is linear elastic up to cracking and perfectly-plastic after yielding (see Figure 3-6).

Moment at yielding (M_y) is calculated in closed form by means of the first principles-based simplified formulations proposed in proposed in

(Fardis, 2007 – Section 3.2.2.2, Eqs. 3.33 to 3.37). Rotation at yielding (θ_y) is univocally identified by M_y and the secant stiffness to yield provided by (Haselton et al., 2007– Section 3.2.4.1, Eq. 3.1).

The Authors also investigate uncertainty associated with each prediction identified by the logarithmic standard deviation and by the average of the ratio between the observed and predicted values, reported in Table 3-2, assuming that the model parameters follow a lognormal distribution.

Table 3-2: Median and logarithmic standard deviation values of predicted to observed data for RC capacity model (Haselton et al, 2008)

Variable	$\mu_{pred/obs}$	$\beta_{pred/obs}$
EI_y / EI_g	0.95	0.28
M_c / M_y	0.97	0.10
θ_{cap}	1.02	0.54
θ_{pc}	1.00	0.72

Infill panels are modelled by means of equivalent struts. The adopted model for the envelope curve of the force-displacement relationship is the model proposed by Panagiotakos and Fardis. The ratio between post-capping degrading stiffness and elastic stiffness (parameter α) is assumed equal to 0.03. The ratio between residual strength and maximum strength (parameter β) is assumed equal to 0.1.

Reference values of material properties are assumed from statistical analyses of the mechanical characteristics provided by the technical literature in order to be representative of the existing Italian building stock. In this work, a value of the compressive strength of concrete equal to 25 MPa and a Coefficient of Variation (CoV) of 31% has been set according to (Verderame et al., 2001; Masi and Vona, 2009). Also, reinforcement is assumed to be constituted by deformed bars. The a value for steel yield strength equal to 451 MPa and a Coefficient of

Variation (CoV) of 13% has been set according to STIL software (Verderame et al., 2012).

Values for infill mechanical characteristics based on the proposal of the Italian code (Circolare 617, 2009) for hollow clay brick panels have been set. Hence, assuming a full correlation between mechanical characteristics, the ratio between E_w and G_w is assumed equal to 10/3, whereas τ_{cr} is assumed as linearly dependent on G_w , assuming τ_{cr} equal to 0.3 and 0.4 MPa for G_w equal to 1080 and 1620 MPa, respectively. In particular, a value of the elastic modulus equal to 4500 MPa and a CoV of 30% have been adopted.

The influence of openings in decreasing lateral stiffness and strength of infill panels is taken into account through the introduction of control parameters reported in (Kakaletsis and Karayannis, 2009), according to the procedure extensively discussed in 3.3.2. The opening shape is assumed equal to the 25% of the corresponding infill length, regardless the opening type. The latter is assumed as a random discrete variable, as a function of the three types panel (solid, panel with window and balcony), with a uniform probability distribution. In such a way, considering a facade consisting of three bays, each of them will be characterized by a different opening type, namely solid panel, window opening and door opening.

Finally a thickness of external infill panels equal to 200mm is assumed and an thickness of internal infill panels for each one directions evaluated considering an internal infill percentage, $\rho_{w,int}$ equal to 50% of external one, for further detail see 3.3.2.

Damage States are defined according to the damage scale proposed by EMS-98 (Grünthal, 1998), defining analytical displacement thresholds corresponding to the damage to structural and non-structural elements, based on the mechanical interpretation of the reported description of damage. Hence, the key sentences describing the damage separately to infills and RC members reported in EMS-98 are translated into analytical displacement threshold through engineering

judgment, see Table 3-1. Note that, due to the assumed Shear-Type behaviour, the interstorey displacement leading to the attainment of each Damage State is the minimum between the values reported in Table 1 for infill panels and RC columns.

Definitely, the methodology described in 3.3.3-3.3.4 is applied, leading to the definition of Nonlinear Static Push-Over (SPO) curve, both in X and Y direction, of a Multi-linearization Curve by applying the equal energy rule, and of simplified Incremental Dynamic Analysis (IDA) curves according to ([Vamvatsikos and Cornell, 2006](#)). The latter allow to obtain a relationship between a seismic intensity measure (spectral ordinate) and an Engineering Demand Parameter (ductility).

Finally, Elastic spectra are the Uniform Hazard Newmark-Hall demand spectra provided in ([Eurocode 8-Part1](#)). Soil type A (stiff soil) is assumed (no amplification for stratigraphic effects). Hence, PGA value is evaluated from the corresponding spectral ordinate evaluated on the IDA-curve as a function of the capacity displacement for each DS according to Table 3-1.

In order to evaluate the influence of material characteristics and element capacity on the seismic response of the case study structure, the parameters reported in Table 3-3 are selected as Random Variables to carry out a sensitivity analysis:

Table 3-3: Parameters selected as Random Variables for sensitivity analysis

Variable	Symbol
Number of storeys	N_s
Building plan ratio	L_x/L_y
Elastic shear modulus of the infill	G_w
Secant stiffness to yield of RC columns	EI_y/EI_g
Ratio of the maximum moment capacity and the yield moment capacity of RC columns	M_c/M_y
Chord rotation at capping point of RC columns	θ_{cap}
Chord rotation at post-capping point of RC columns	θ_{pc}
Compressive strength of concrete	f_c
Steel yield strength	f_y
Lognormal standard deviation of distribution of R given μ	β_R

A lognormal distribution is assumed for all of the Random Variables. Each distribution is defined through the central (median) value and the Coefficient of Variation (CoV). Moreover, the number of storeys is assumed to range in the interval [2 4 6], whereas the building plan ratio, is assumed to range in the interval [1 2 3].

3.4.2 Results

Based on the assumed Random Variables, a sensitivity analysis is carried out, in this section, in order to investigate the influence of each variable on the seismic capacity of the case study structure. To this aim, two models are generated for each random variable assuming median-minus-standard-deviation and median-plus-standard-deviation values for the considered variable, and median values for the remaining variables.

Hence, the amount of the change in PGA capacity due to the change in each variable, compared with the model where median values are assigned to all variables (Model #1), is evaluated. For building plan ratio a value equal to 2 is assumed for (Model #1) and the

amount of the change in PGA capacity considering a value of building plan ratio respectively equal to 1 and 3 is evaluated.

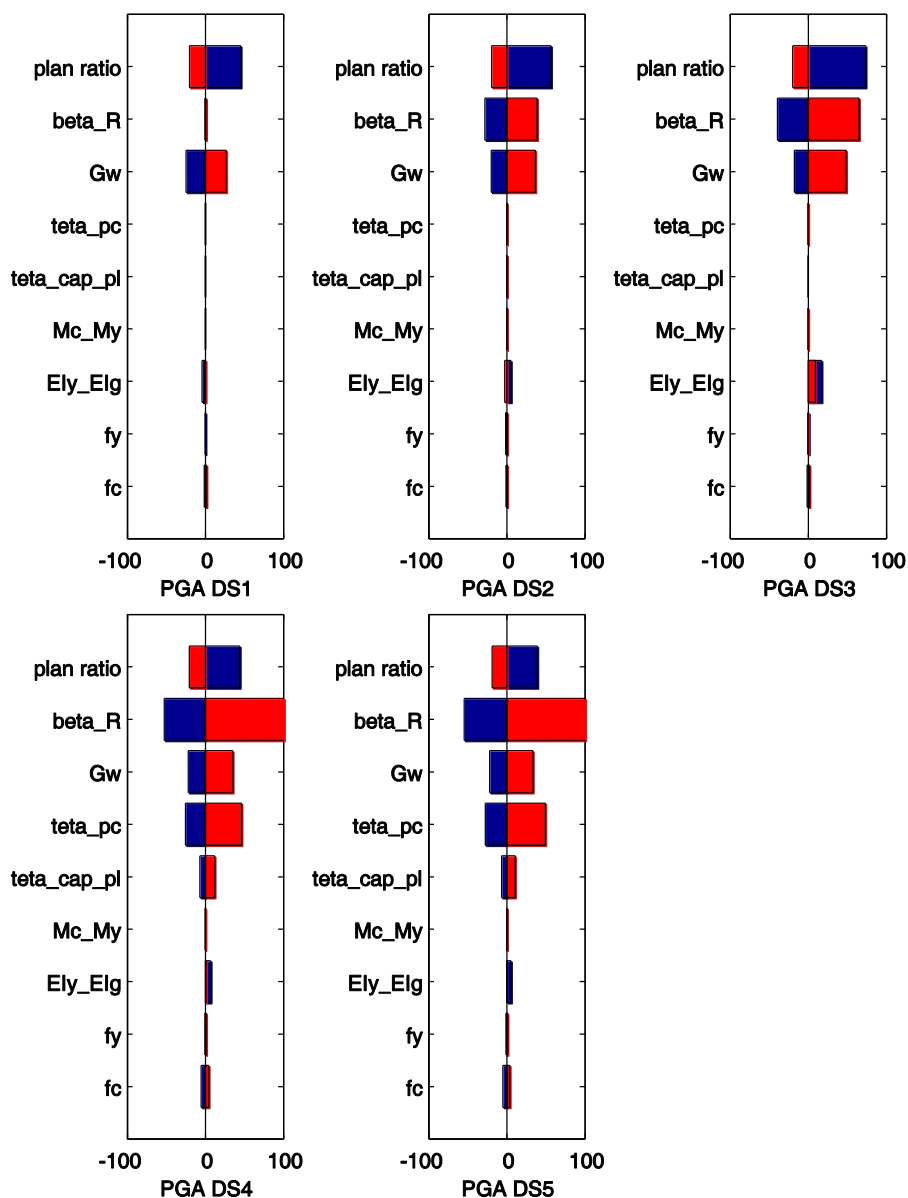


Figure 3-16: Results of sensitivity analysis for NC LS 2-Storeys Case-study Building

2-Storeys Case Study Building:

The sensitivity analysis shows that the increase in β_R produces an increase in PGA capacity. As a matter of fact, the higher β_R , accounting for the dispersion of IM (spectral ordinate) given EDP (ductility), the higher is the corresponding spectral ordinate and hence the PGA value.

Furthermore, it is to be noted that the higher is the EDP value the higher is the β_R . As a consequence, this effect is more pronounced for higher ductility value, namely for DS4-5. Obviously β_R does not affect DS1, since the corresponding displacements capacity affect the elastic branch of the quadrilinear backbones that mimics the Static Pushover, and consequently resulting in zero value for β_R . Vice versa if β_R decreases.

Moreover, $\theta_{cap,pl}$ and θ_{pc} , have a great influence on the PGA at DS4-5. As a matter of fact, it can be noted from Figure 3-12, that such a displacements allow to define the degrading branch of shear-displacement relationship for RC columns, and hence the displacement corresponding to a reduction of 20% of peak resistance and the displacement corresponding to zero resistance (equal to $\Delta_{cap,pl} + \Delta_{pc}$). This is clearly due to the fact the displacements capacity at DS4 and DS5 are directly given by the rotational capacity of columns, given the soft-storey collapse mechanism.

Thus, an increase in $\theta_{cap,pl}$ and θ_{pc} results in an increase in the displacements capacity at DS4 and DS5, leading to higher values of corresponding spectral ordinate through simplified IDA-curve and, hence, of relative PGA values. Vice versa if $\theta_{cap,pl}$ and θ_{pc} decrease.

When G_w increase, and correspondingly E_w , and τ_{cr} , several effects can be observed:

- the decrease of infill displacements capacity in DS1-2-3. As a matter of fact, due to fact that infill displacements capacity are typically lower than the corresponding RC columns ones, see Table 3-1, the former lead to the attainment of the corresponding

DS. In fact, the displacement leading to the attainment of each DS is the minimum between the values for infill panels and RC columns. Then, the increase of G_w produces a slight decrease in infill displacement capacity and consequently in DS1-2-3 displacement capacity;

-the increase in stiffness and strength leads to a lower T_{eff} and a higher $C_{s,max}$; this circumstance produce an increase in spectral ordinate and consequently an increase in PGA capacity, as it can be observed in Figure 3-18.

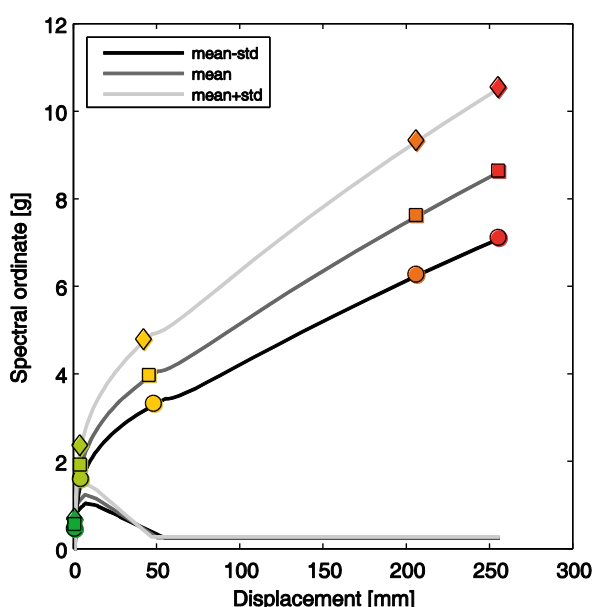


Figure 3-17: Simplified IDA-curves for 2-Storeys Case-study buildings in longitudinal direction (Lower, median and Upper value for G_w)

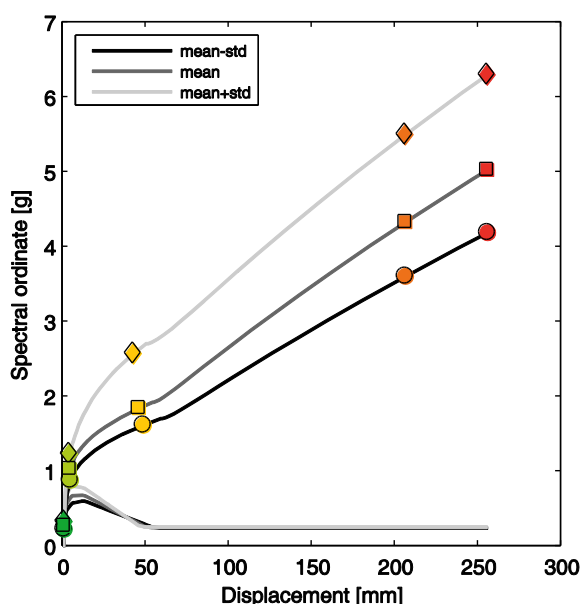


Figure 3-18: Simplified IDA-curves for 2-Storeys Case-study buildings in transversal direction (Lower, median and Upper value for G_w)

Moreover, the latter effect tends to prevail over the former, leading to a higher PGA value.

Similarly, it is to be noted that the increase of G_w affects also the PGA values at DS4-5, although the relative displacements capacity do not change as they are defined on RC Column shear-displacement relationship. Indeed, as it can be highlighted in Figure 3-18, the increase in stiffness and strength leads to a higher $C_{s,max}$, an increase in spectral ordinate and consequently an increase in PGA capacity for DS4-5. Vice versa if G_w decreases.

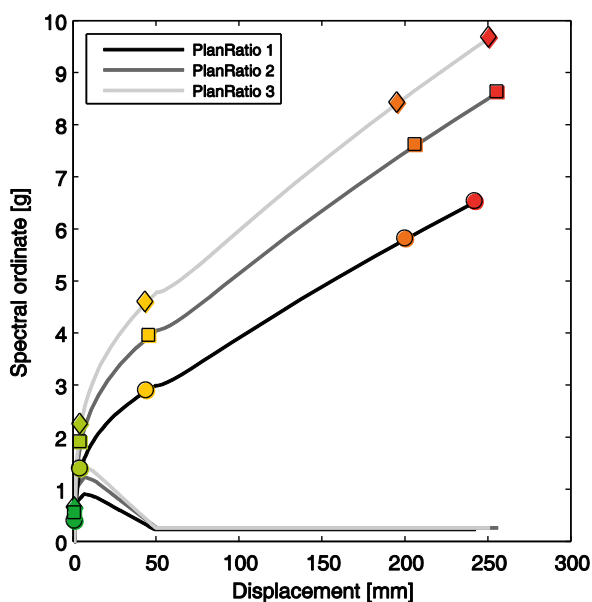


Figure 3-19: Simplified IDA-curves for 2-Storeys Case-study buildings in longitudinal direction (Plan ratio equal to 1, 2 and 3)

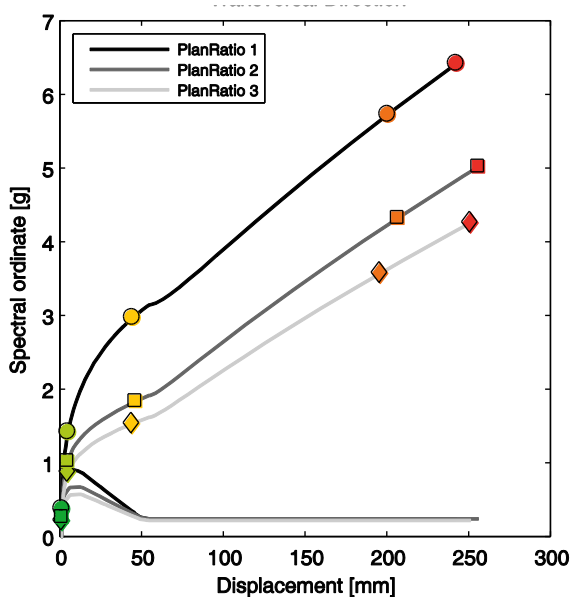


Figure 3-20: Simplified IDA-curves for 2-Storeys Case-study buildings in transversal direction (Plan ratio equal to 1, 2 and 3)

As it can be seen in Figure 3-16 the higher the plan ratio the lower is the PGA. As a matter of fact this effect is much more pronounced for a plan ratio changing from 1 to 2 (in blue in Figure 3-16), rather than from 2 to 3 (in red in Figure 3-16).

Hence, the amount of the change in PGA capacity due to the change in plan ratio respectively equal to 1 and 3, compared with the model where the plan ratio is equal to 2 and median value are assigned to all variables (Model #1), is evaluated.

It can be highlighted that the increase of plan ratio leads to a lower (higher) T_{eff} and a higher (lower) $C_{s,max}$ in transversal (longitudinal) direction; this circumstance produce an increase (decrease) in spectral ordinate and consequently an increase (decrease) in PGA capacity in transversal (longitudinal) direction, as it can be observed in Figure 3-20.

Since, fragility curves independent of the direction are obtained evaluating the minimum PGA capacities between longitudinal and transversal direction for each sampling, the increase of plan ratio globally produces a decrease in PGA capacity.

When f_c increase several effects can be observed:

- the increase of f_c produces a decrease of $\theta_{cap,pl}$ evaluated according to (Haselton et al., 2007 – Eq. 3.10), as it is a function of f_c through a power function with a base equal to 0.54;
- the increase of f_c produces a decrease of axial load ratio, ν . This circumstance produces an increase of $\theta_{cap,pl}$ evaluated according to (Haselton et al., 2007 – Eq. 3.10), as it is a function of ν through a power function with a base equal to 0.16.

Globally, the latter tends to prevail over the former, leading to a slightly higher PGA value as a function of a higher f_c value.

Finally, EI_y/EI_g and M_c/M_y have a negligible influence on PGA capacity, as they greatly affect displacement capacity of RC column at DS2-3. As a matter of fact, due to fact that infill displacements capacity are typically lower than the corresponding RC columns ones, the former

lead to the attainment of the corresponding DS. In fact, the displacement leading to the attainment of each DS is the minimum between the values for infill panels and RC columns.

Moreover, the latter effect tends to prevail over the former, leading to a higher PGA value.

Similarly, it is to be noted that the increase of G_w affects also the PGA values at DS4-5, although the relative displacements capacity do not change as they are defined on RC Column shear-displacement relationship. Indeed, as it can be highlighted in Figure 3-18, the increase in stiffness and strength leads to a higher $C_{s,max}$, an increase in spectral ordinate and consequently an increase in PGA capacity for DS4-5. Vice versa if G_w decreases.

4-Storeys and 6-storeys Case Study Building:

The sensitivity analysis shows that the parameters that greatly affect seismic capacity are β_R and $\theta_{cap,pl}$ and θ_{pc} . Moreover, it can be noticed a weaker influences of the parameters G_w and plan ratio unlike the case study 2-Storeys Case Study Building. As a matter of fact, with the number of storeys increasing, the strength and stiffness provided by structural elements (i.e., RC columns) increases, whereas the contribution of infills does not change significantly, since the latter is related to dimension of infill panels, which do not change with the height of the building. Therefore, with the number of storeys increasing, lateral strength and stiffness of building is mostly influenced by parameters related to RC columns' behaviour ($\theta_{cap,pl}$ and θ_{pc}), rather than to parameters related to infill panels' behaviour (G_w).

The sensitivity analysis shows that the increase in β_R produces an increase in PGA capacity, see Figure 3-21-Figure 3-22. Actually, the higher β_R , accounting for the dispersion of IM (spectral ordinate) given EDP (ductility), the higher is the corresponding spectral ordinate and hence the PGA value.

Furthermore, it is to be noted that the higher is the EDP value the higher is the β_R . As a consequence, this effect is more pronounced for higher ductility value, namely for DS4-5. Obviously β_R does not affect DS1, since the corresponding displacements capacity affect the elastic branch of the quadrilinear backbones that mimics the Static Pushover, and consequently resulting in zero value for β_R . Vice versa if β_R decreases.

Moreover, $\theta_{cap,pl}$ and θ_{pc} , have a great influence on the PGA at DS4-5, see Figure 3-21-Figure 3-22. As a matter of fact, it can be noted, that such a displacements allow to define the degrading branch of shear-displacement relationship for RC columns, and hence the displacement corresponding to a reduction of 20% of peak resistance and the displacement corresponding to zero resistance (equal to $\Delta_{cap,pl} + \Delta_{pc}$). This is clearly due to the fact the displacements capacity at DS4 and DS5 are directly given by the rotational capacity of columns, given the soft-storey collapse mechanism.

Thus, an increase in $\theta_{cap,pl}$ and θ_{pc} results in an increase in the displacements capacity at DS4 and DS5, leading to higher values of corresponding spectral ordinate through simplified IDA-curve and, hence, of relative PGA values. Vice versa if $\theta_{cap,pl}$ and θ_{pc} decrease.

When G_w increase, and correspondingly E_w , and τ_{cr} , an increase in stiffness and strength, and hence a lower T_{eff} and a higher $C_{s,max}$, can be observed. This circumstance produce an increase in spectral ordinate and consequently an increase in PGA capacity. The increase in G_w only affects DS1, see Figure 3-21-Figure 3-22, since the contribution of β_R and $\theta_{cap,pl}$ and θ_{pc} is negligible. With increasing level of damage, the influence of these parameters becomes predominant, and consequently the influence of G_w becomes negligible.

Similar arguments can be made regarding the plan ratio. As a matter of fact plan ratio has only a significant influence on seismic capacity on DS1 since the contribution of β_R and $\theta_{cap,pl}$ and θ_{pc} is negligible.

The amount of the change in PGA capacity due to the change in plan ratio respectively equal to 1 and 3, compared with the model where the plan ratio is equal to 2 and median value are assigned to all variables (Model #1), is evaluated.

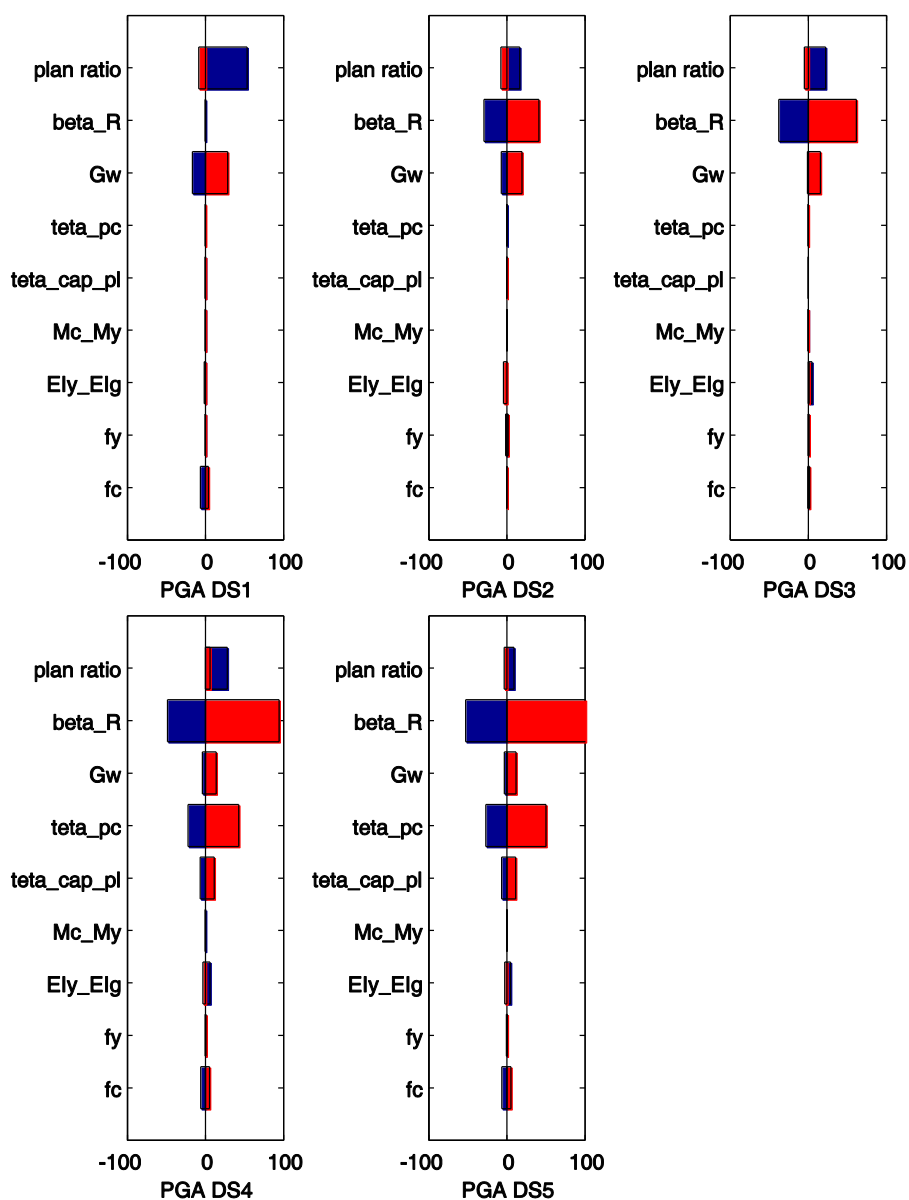


Figure 3-21: Results of sensitivity analysis for NC LS 4-Storeys Case-study Building

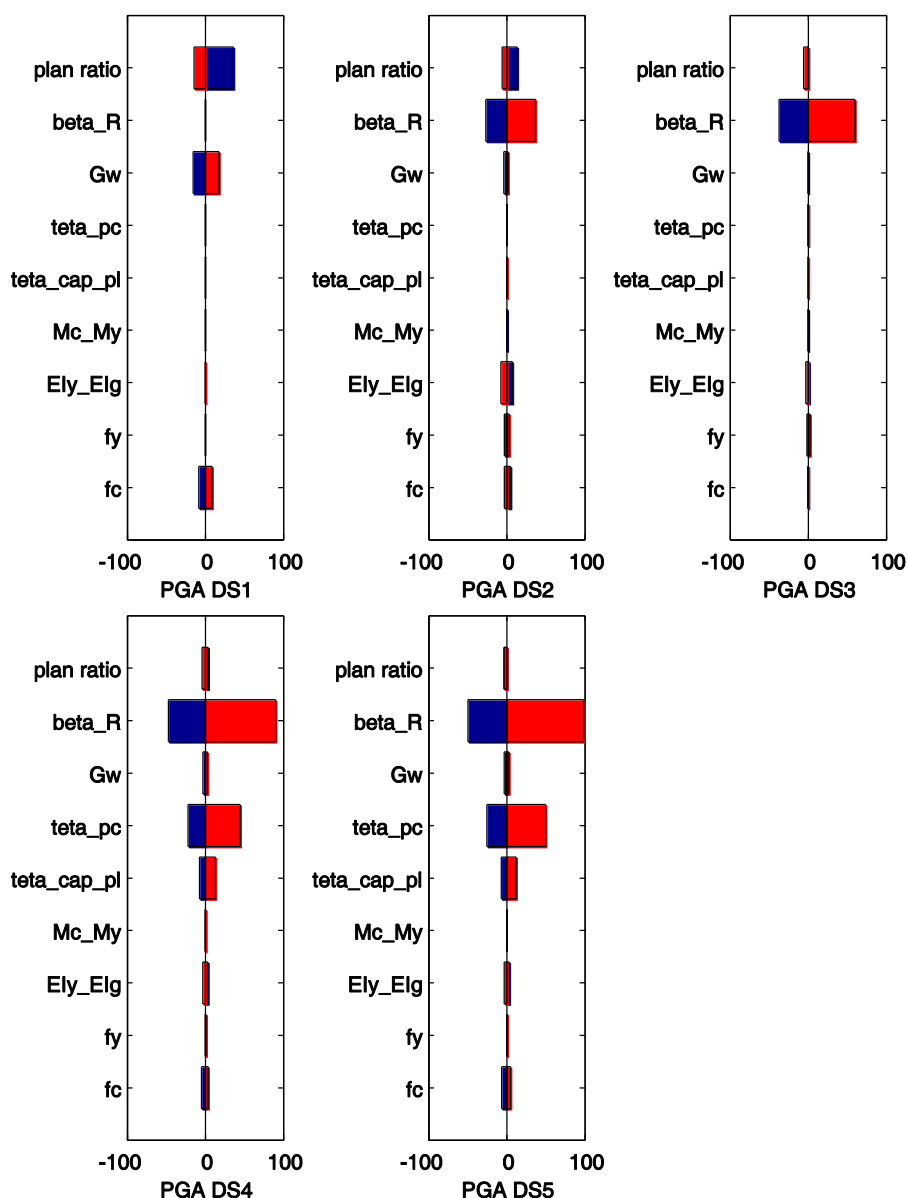


Figure 3-22: Results of sensitivity analysis for NC LS 6-Storeys Case-study Building

It can be highlighted that the increase of plan ratio leads to a lower (higher) T_{eff} and a higher (lower) $C_{s,max}$ in transversal (longitudinal)

direction; this circumstance produce an increase (decrease) in spectral ordinate and consequently an increase (decrease) in PGA capacity in transversal (longitudinal) direction.

Since, fragility curves independent of the direction are obtained evaluating the minimum PGA capacities between longitudinal and transversal direction for each sampling, the increase of plan ratio globally produces a decrease in PGA capacity.

When f_c increase a slight increase of PGA value can be observed.

Finally, EI_y/EI_g and M_c/M_y have a negligible influence on PGA capacity, as they greatly affect displacement capacity of RC column at DS2-3. As a matter of fact, due to fact that infill displacements capacity are typically lower than the corresponding RC columns ones, the former lead to the attainment of the corresponding DS. In fact, the displacement leading to the attainment of each DS is the minimum between the values for infill panels and RC columns.

3.5 Summary of results

An analytical procedure for seismic vulnerability assessment of RC buildings at large scale was described. The procedure is based on a simulated design procedure to define the structural model and on non-linear static analysis of a simplified structural model based on Shear-Type assumption to evaluate seismic capacity at different performance (i.e., displacement demand) levels. This approach allows to adopt interstorey drift as structural demand parameter for damage measure. Performance levels are assumed as corresponding to the observational-based DSs defined by EMS-98 scale ([Grünthal, 1998](#)). Uncertainties are taken into account adopting a simulation procedure based on Monte Carlo technique with LHS, including seismic demand, capacity models, and material characteristics, making it a relatively comprehensive yet still low computationally-demanding procedure, suitable for territorial scale applications. Note that further parameters could be assumed as input random variable – including geometrical

parameters – depending on the knowledge level, that is, on the amount of available information on building stock. Hence, the procedure has been illustrated to be applicable to differently (most probably less) detailed input data, allowing to analyze the sensitivity of the outcome of a seismic vulnerability assessment to the detail level of input data, see (Chapter 7 ;[Ricci et al., 2011](#); [Ricci et al., 2014](#)).

Possible future developments include the modelling of other sources of damage to RC buildings, such as the brittle failure modes affecting columns and beam-column joints – also due to the interaction with infill elements – and the out-of-plane vulnerability of infill panels.

3.6 References

- Berry M., Eberhard M.O., 2003. Performance models for flexural damage in reinforced concrete columns. Report No. UCB-PEER 2003-18, University of California, Berkeley, CA, USA.
- Biskinis D., Fardis M.N., 2010a. Deformations at flexural yielding of members with continuous or lap-spliced bars. *Structural Concrete*, 11(3), 128-138.
- Biskinis D., Fardis M.N., 2010b. Flexure-controlled ultimate deformations of members with continuous or lap-spliced bars. *Structural Concrete*, 11(2), 93-108.
- Borzi B., Crowley H., Pinho R., 2008b. The influence of infill panels on vulnerability curves for RC buildings. *Proceedings of the 14th World Conference on Earthquake Engineering*, Beijing, China, October 12-17. Paper 09-01-0111.
- Borzi B., Pinho R., Crowley H., 2008a. Simplified pushover-based vulnerability analysis for large scale assessment of RC buildings. *Engineering Structures*, 30(3), 804-820.
- Calvi G.M., 1999. A displacement-based approach for vulnerability evaluation of classes of buildings. *Journal of Earthquake Engineering*, 3(3), 411-438.
- CEN (2003) Eurocode 8: design of structures for earthquake resistance—Part 1: general rules, seismic actions and rules for buildings. European Standard EN 1998-1:2003. Comité Européen de Normalisation, Brussels
- Circolare del Ministero dei Lavori Pubblici. n. 617 del 2/2/2009 (2009) Istruzioni per l'applicazione delle "Nuove norme tecniche per le costruzioni" di cui al DM 14 gennaio 2008. (in italian)
- Cosenza E., Manfredi G., Polese M., Verderame G.M., 2005. A multi-level approach to the capacity assessment of existing RC buildings. *Journal of Earthquake Engineering*, 9(1), 1-22.
- Crowley H., Colombi M., Borzi B., Faravelli M., Onida M., Lopez M., Polli D., Meroni F., Pinho R., 2009. A comparison of seismic risk maps for Italy. *Bulletin of Earthquake Engineering*, 7(1), 149-190.

- Crowley H., Pinho R., Bommer J.J., 2004. A probabilistic displacement-based vulnerability assessment procedure for earthquake loss estimation. *Bulletin of Earthquake Engineering*, 2(2), 173-219.
- Crowley H., Pinho R., Bommer J.J., Bird, J.F., 2006. Development of a displacement-based method for earthquake loss assessment. ROSE Research Report No. 2006/01, IUSS Press, Pavia, Italy.
- Decreto Ministeriale del 14/1/2008: Approvazione delle nuove norme tecniche per le costruzioni. G.U. n. 29 del 4/2/2008 (in Italian)
- Decreto Ministeriale del 7/3/1981: Dichiarazione di zone sismiche nelle regioni Basilicata, Campania e Puglia. (in Italian)
- Decreto Ministeriale n. 40 del 3/3/1975. Approvazione delle norme tecniche per le costruzioni in zone sismiche. G.U. n. 93 dell'8/4/1975. (in Italian)
- Del Gaudio C., Ricci P., Verderame G.M., Manfredi G., 2015. Development and urban-scale application of a simplified method for seismic fragility assessment of RC buildings. *Engineering Structures*. Vol. 91, pp. 40-57. doi:10.1016/j.engstruct.2015.01.031
- Dolce M., Moroni C., 2005. La valutazione della vulnerabilità e del rischio sismico degli edifici pubblici mediante le procedure VC (vulnerabilità c.a.) e VM (vulnerabilità muratura), *Atti del Dipartimento di Strutture, Geotecnica, Geologia applicata all'ingegneria*, N. 4/2005. (in Italian)
- Dolšek M., Fajfar P., 2004a. Inelastic spectra for infilled reinforced concrete frames. *Earthquake Engineering and Structural Dynamics*. 33(15), 1395-1416.
- Dolšek M., Fajfar P., 2005. Simplified non-linear seismic analysis of infilled reinforced concrete frames. *Earthquake Engineering and Structural Dynamics*, 34(1), 49-66.
- Faccioli E., Pessina V. (editors), 2000. The Catania project: earthquake damage scenarios for a high risk area in the

- Mediterranean. CNR-Gruppo Nazionale per la Difesa dai Terremoti, Rome, Italy.
- Fajfar P., 1999. Capacity spectrum method based on inelastic demand spectra. *Earthquake Engineering and Structural Dynamics*, 28(9), 979-993.
 - Fardis M.N., Panagiotakos T.B., 1997. Seismic design and response of bare and masonry-infilled reinforced concrete buildings. Part II: infilled structures. *Journal of Earthquake Engineering*, 1(3), 475-503.
 - FEMA, 2001. HAZUS99 Technical Manual. Service Release 2. Federal Emergency Management Agency, Washington, D.C., USA.
 - Glaister S., Pinho R., 2003. Development of a simplified deformation-based method for seismic vulnerability assessment. *Journal of Earthquake Engineering*, 7(SI1), 107-140.
 - GNDT, 2000. Censimento di vulnerabilità a campione dell'edilizia corrente dei Centri abitati, nelle regioni Abruzzo, Basilicata, Calabria, Campania, Molise, Puglia e Sicilia. CNR-Gruppo Nazionale per la Difesa dai Terremoti, Rome, Italy.
 - Grünthal G., 1998. Cahiers du Centre Européen de Géodynamique et de Séismologie: Volume 15 – European Macroseismic Scale 1998. European Center for Geodynamics and Seismology, Luxembourg.
 - Guha-Sapir D., Vos F., 2011. Earthquakes, an epidemiological perspective on patterns and trends. In: Spence R., So E., Scawthorn C. (editors). *Human Casualties in Earthquakes. Advances in Natural and Technological Hazards Research*. Springer Science+Business Media B.V. 2011. DOI 10.1007/978-90-481-9455-1_2
 - Haselton, C.B., A.B. Liel, S. Taylor Lange, and G.G. Deierlein (2008). Beam-Column Element Model Calibrated for Predicting Flexural Response Leading to Global Collapse of RC Frame Buildings, PEER Report 2007/03, Pacific Engineering Research Center, University of California, Berkeley, California.

- Iervolino I., Manfredi G., Polese M., Verderame G.M., Fabbrocino G., 2007. Seismic risk of R.C. building classes. *Engineering Structures*, 29(5), 813-820.
- INGV-DPC S1, 2007. Progetto S1. Proseguimento della assistenza al DPC per il completamento e la gestione della mappa di pericolosità sismica prevista dall'Ordinanza PCM 3274 e progettazione di ulteriori sviluppi. Istituto Nazionale di Geofisica e Vulcanologia – Dipartimento della Protezione Civile, <http://esse1.mi.ingv.it> (in Italian)
- Kakaletsis D.J., Karayannis C.G., 2009. Experimental investigation of infilled reinforced concrete frames with openings. *ACI Structural Journal*, 106(2), 132-141.
- Kappos A.J., Stylianidis K.C., Pitilakis K., 1998. Development of seismic risk scenarios based on a hybrid method of vulnerability assessment. *Natural Hazards*, 17(2), 177-192.
- Kircher C.A., Nassar A.A., Kustu O., Holmes W.T., 1997a. Development of building damage functions for earthquake loss estimation. *Earthquake Spectra*, 13(4), 663-682.
- Kircher C.A., Reitherman R.K., Whitman R.V., Arnold C., 1997b. Estimation of earthquake losses to buildings. *Earthquake Spectra*, 13(4), 703-720.
- Lagomarsino, S., Giovinazzi, S. (2006). "Macroseismic and mechanical models for the vulnerability assessment of current buildings." *Bulletin of Earthquake Engineering*, 4(4), 415-443.
- Masi A., Vona M., 2009. Estimation of the in-situ concrete strength: provisions of the european and italian seismic codes and possible improvements. In: E. Cosenza (editor). *Eurocode 8 perspectives from the Italian standpoint workshop*. Doppiavoce, Naples, Italy, 2009. ISBN 978-88-89972-16-8. Pp. 67-77.
- McKay M.D., Conover W.J., Beckman R.J., 1979. A comparison of three methods for selecting values of input variables in the analysis of output from a computer code. *Technometrics*, 21(2), 239-245.

- Milutinovic, Z. V., Trendafiloski, G. S., 2003. “WP4 Vulnerability of Current Buildings”, Risk-UE Project: An advanced approach to earthquake risk scenarios with applications to different European towns.
- Mollaioli F., Bazzurro P., Bruno S., De Sortis A., 2009. Influenza della modellazione strutturale sulla risposta sismica di telai in cemento armato tamponati. Atti del XIII convegno ANIDIS “L’ingegneria sismica in Italia”, Bologna, Italy, June 28-July 2. Paper SM10-3. (in Italian)
- Noji E.K., 1997. The epidemiology of earthquakes: implications for vulnerability reduction, mitigation and relief. Proceedings of the international symposium on earthquakes and people's health: vulnerability reduction, preparedness and rehabilitation. Health Library for Disasters, World Health Organization, Kobe, Japan.
- Panagiotakos T.B., Fardis M.N., 2001. Deformation of reinforced concrete members at yielding and ultimate. *ACI Structural Journal*, 98(2), 135-148.
- Pecce M., Polese M., Verderame G.M., 2004. Seismic vulnerability aspects of RC buildings in Benevento. Proceedings of the Workshop on Multidisciplinary Approach to Seismic Risk Problems. Sant’Angelo dei Lombardi, Italy, September 22. In: Pecce M., Manfredi G., Zollo A., 2004. The many facets of seismic risk. Pp. 134-141. CRdC AMRA.
- Petal M., 2011. Earthquake casualties research and public education. In: Spence R., So E., Scawthorn C. (editors). *Human Casualties in Earthquakes. Advances in Natural and Technological Hazards Research*. Springer Science+Business Media B.V. 2011. DOI 10.1007/978-90-481-9455-1_3
- Pinho R., Bomber J.J., Glaister S., 2002. A simplified approach to displacement-based earthquake loss estimation analysis. Proceedings of the 12th European Conference on Earthquake Engineering, London, UK, September 9-13. Paper No. 738.
- Priestley M.J.N., 1997. Displacement-based seismic assessment of reinforced concrete buildings. *Journal of Earthquake Engineering*, 1(1), 157-192.

- Ricci P., 2010. Seismic vulnerability of existing RC buildings. PhD thesis, University of Naples Federico II, Naples, Italy.
- Ricci P., Del Gaudio C., Verderame G.M., Manfredi G., Pollino M., Borfecchia F., 2014. Seismic vulnerability assessment at urban scale based on different building stock data sources. In: M. Beer, I.S.K. Au, J.W. Hall (editors). *Vulnerability, Uncertainty, and Risk: Quantification, Mitigation, and Management*. American Society of Civil Engineers, 2014. ISBN 978-0-7844-1360-9. Pp. 1027-1038.
- Ricci P., Verderame G.M., Manfredi G., Pollino M., Borfecchia F., De Cecco L., Martini S., Pascale C., Ristatore E., James V., 2011. Seismic vulnerability assessment using field survey and Remote Sensing techniques. In: Murgante B., Gervasi O., Iglesias A., Taniar D., Apduhan B.O. (editors). *Computational Science and its Applications – ICCSA 2011*. Springer-Verlag Berlin Heidelberg, 2011. ISBN 978-3-642-21886-6. Volume 6783, Part II, pp. 109-124. doi:10.1007/978-3-642-21887-3_9
- Rossetto T., Elnashai A., 2003. Derivation of vulnerability functions for European-type RC structures based on observational data. *Engineering Structures*, 25(10), 1241-1263.
- Rota M., Penna A., Strobbia C., Magenes G., 2008. Direct derivation of fragility curves from Italian post-earthquake survey data. *Proceedings of the 14th World Conference on Earthquake Engineering*, Beijing, China, October 12-17. Paper 09-01-0148.
- Spence R., 2003. Earthquake risk mitigation in Europe: progress towards upgrading the existing building stock. In: *Proceedings of the 5th National Conference on Earthquake Engineering of Turkey*, Invited Lecture.
- Vamvatsikos D., Cornell C.A., 2006. Direct estimation of the seismic demand and capacity of oscillators with multi-linear static pushovers through IDA. *Earthquake Engineering and Structural Dynamics*, 35(9), 1097-1117.
- Verderame G.M., De Luca F., De Risi M.T., Del Gaudio C., Ricci P., 2012. A three level vulnerability approach for the damage assessment of infilled RC buildings: the Emilia 2012 case. ReLUIS, <http://www.reluis.it/>

- Verderame G.M., Manfredi G., Frunzio G., 2001. Le proprietà meccaniche dei calcestruzzi impiegati nelle strutture in cemento armato realizzate negli anni '60. Atti del X congresso nazionale ANIDIS "L'ingegneria Sismica in Italia", Potenza-Matera, Italy, September 9-13. (in Italian)
- Verderame G.M., Polese M., Mariniello C., Manfredi G., 2010. A simulated design procedure for the assessment of seismic capacity of existing reinforced concrete buildings. *Advances in Engineering Software*, 41(2), 323-335.
- Verderame G.M., Ricci P., Esposito M., Manfredi G., 2012. STIL v1.0 – Software per la caratterizzazione delle proprietà meccaniche degli acciai da c.a. tra il 1950 e il 2000. ReLUIS, <http://www.reluis.it/>
- Vorechovsky M., Novak D., 2009. Correlation control in small-sample Monte Carlo type simulations I: A simulated annealing approach. *Probabilistic Engineering Mechanics*, 24(3), 452-462.
- Whitman R.V., Anagnos T., Kircher C.A., Lagorio H.J., Lawson R.S., Schneider P., 1997. Development of a national earthquake loss estimation methodology. *Earthquake Spectra*, 13(4), 643-661.

Chapter 4

Avellino Municipality: a high detail level damage prediction

Rapid population growth and urbanization have made RC buildings the predominant type of construction in densely populated urban areas that are affected by disastrous earthquakes more and more frequently. Moreover, apart from their vulnerability, which is generally lower compared with masonry buildings, RC buildings are characterized by significantly higher fatality rates. These facts have led to a dramatic increase in the number of injuries and deaths in RC buildings, both in absolute terms and compared with masonry buildings, especially by the second half of the twentieth century (Noji, 1997; Spence, 2003; Guha-Sapir and Vos, 2011; Petal, 2011).

The Municipality of Avellino is constituted almost for the 80% by RC buildings, and it is characterized by high seismic hazard due to the numerous earthquakes that have taken place in the area. In this Municipality afield survey has been carried out, whose results had allowed to evaluate the seismic vulnerability for the whole RC Building stock.

Avellino is a town and Municipality, capital of the province of Avellino in the Campania region (southern Italy). Avellino was heavily struck by the 23 July 1930 Irpinia earthquake (Mw 6.72) and 23 November 1980 Irpinia-Basilicata earthquake (Mw 6.89). In the latter killed 2,914 people

were killed, more than 80,000 were injured and 280,000 homeless were counted. The quake hit an area extending from Vulture to Irpinia region involving the entire south-central area of Italy, up to Naples, leading the Italian Government to spend during the last thirty years around 30 billion of Euro for reconstruction.



Figure 4-1. Piazza del Popolo (Avellino), (a) 24 novembre 1980, (b), 2014

For this reason the entire area has been the object of several studies and research, among which the SIMURAI Project (Strumenti Integrati per il Multi Risk Assessment territoriale in ambienti urbani antropizzati, Integrated tools for large scale multi-risk assessment in urban anthropic environment), funded by the Italian Ministry of Research (MIUR), with the aim to apply a multi-hazard approach to the risk assessment in highly urbanized areas, to detect and interpret the phenomena of interaction between the elements constituting the urban fabric, for the purposes of the definition of the vulnerability of the whole anthropic system.

4.1 Field survey on building stock of Avellino city

In the following, data provided by the survey on the building stock of Avellino are shown and discussed. The survey was developed through specialized operators that filled a survey form subdivided in different sections, with an increasing level of detail.

The survey form includes the main parameters – among the ones that can be reasonably collected during a field survey – that may have a significant influence on building seismic capacity, addressing a particular attention to specific potential sources of seismic vulnerability.

The surveyed data have been acquired and managed through GIS technologies.

4.2 Analysis of building stock data

On the whole 1324 buildings have been surveyed. About 80% is composed of RC buildings, the remaining 20% for the majority of Masonry buildings and a little part of Steel and Combined buildings (Figure 4-2).

The survey is aimed at collecting all the data needed to define the seismic capacity of buildings, among which the most important are the age of construction, defining the codes and the rules used for the design, and the number of storeys, affecting the dynamic properties of buildings.

In Figure 4-2-Figure 4-5 the distribution of these parameters among the RC Buildings are reported. It is to be noted that in the period ranging from the '40-'50 up to the '80-'90 there was the greatest diffusion of the RC Buildings, at the turn of post-war economic development and reconstruction after the 1980 Irpinia earthquake. Indeed pre- and post-81 buildings respectively represent about the 56 and 44% of the RC building population whose age of construction was determined, which represent the 80% of the total.

In Figure 4-6 the percentages of RC buildings respecting the EC8 prescriptions about in plan-regularity are presented, where it appears that almost the whole sample is constituted exclusively by rectangular buildings.

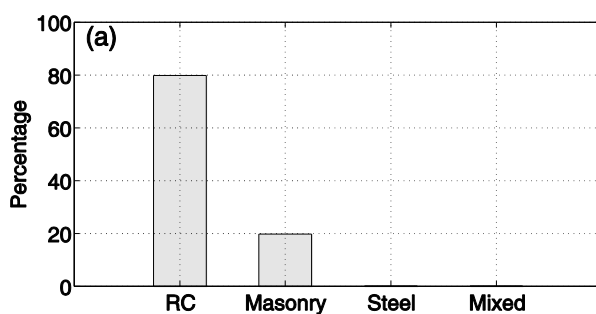


Figure 4-2: Distribution of building typologies.

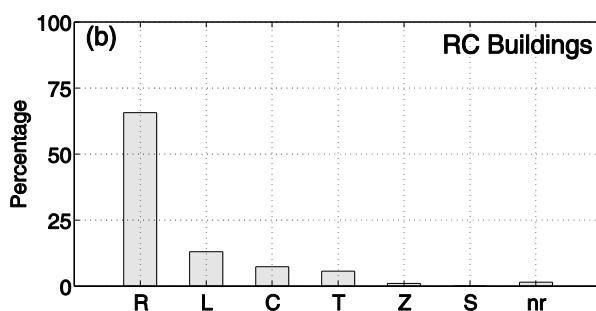


Figure 4-3: Distribution of plan morphologies.

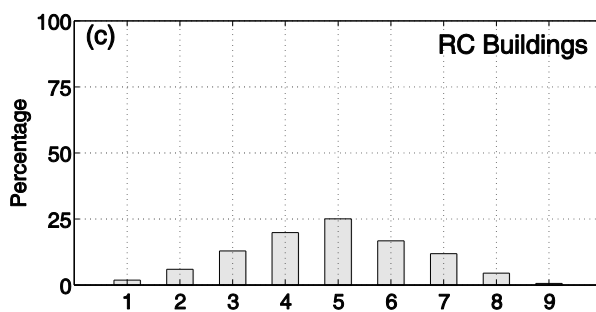


Figure 4-4: Distribution of number of storeys.

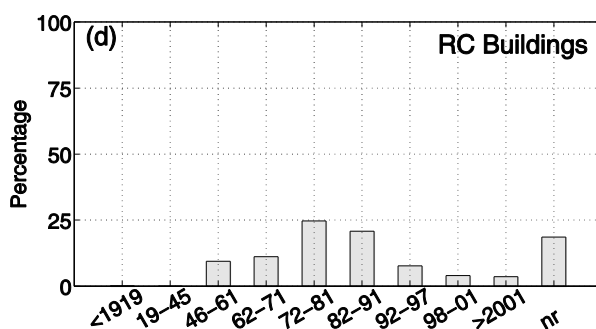


Figure 4-5. Distribution of: age of construction.

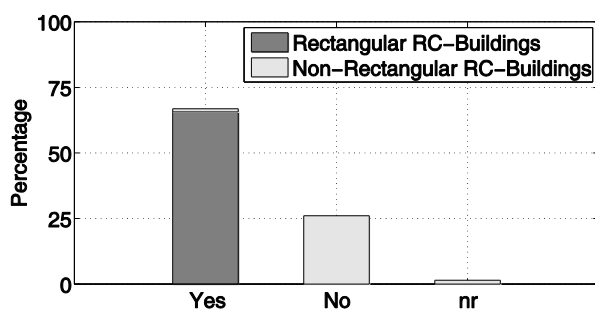


Figure 4-6. Percentages of RC buildings complying with EC8 prescriptions about in plan-regularity

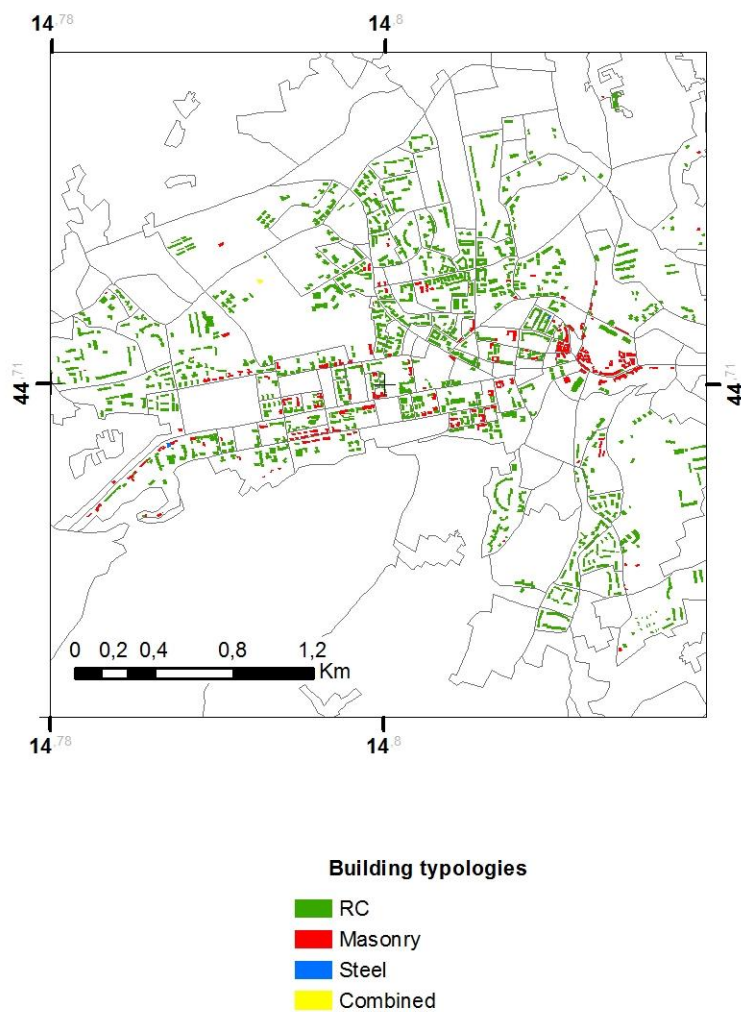


Figure 4-7: Spatial distribution at level of building of building typologies

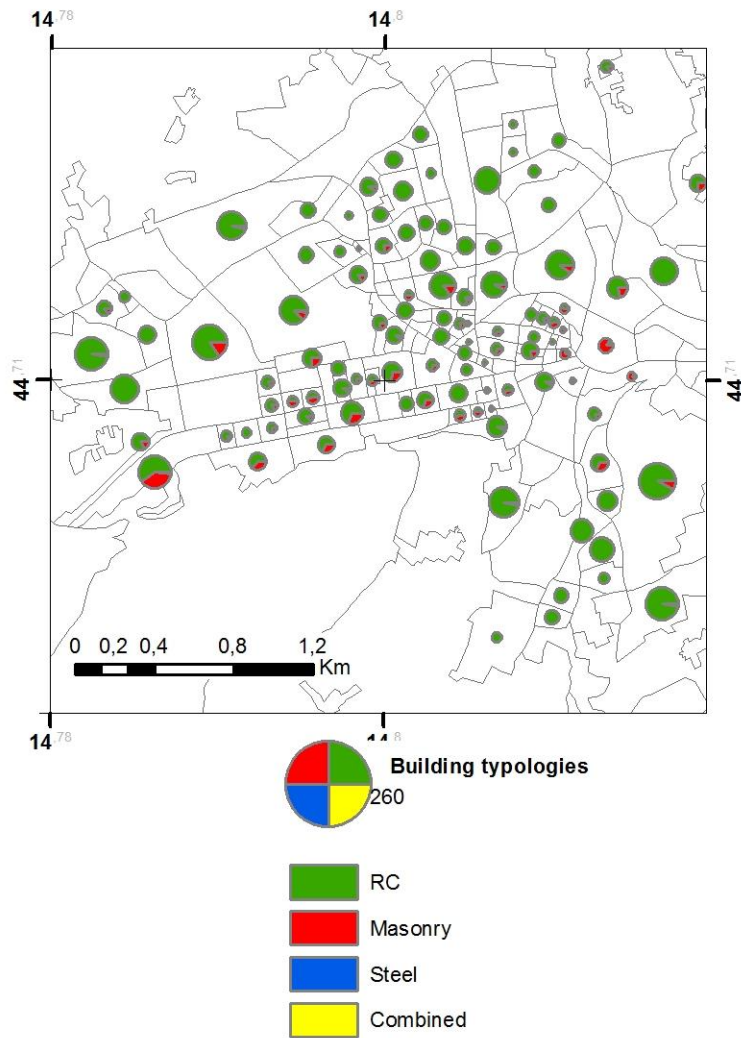


Figure 4-8: Spatial distribution at level of census cell of the building typologies

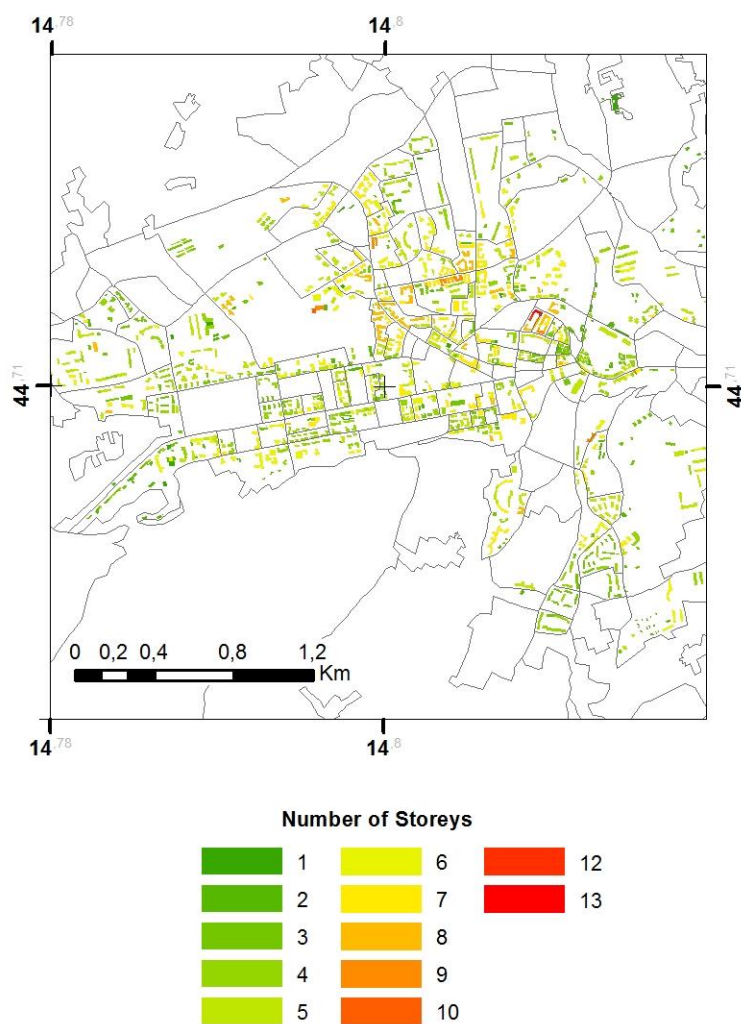


Figure 4-9: Spatial distribution at level of building of number of storeys

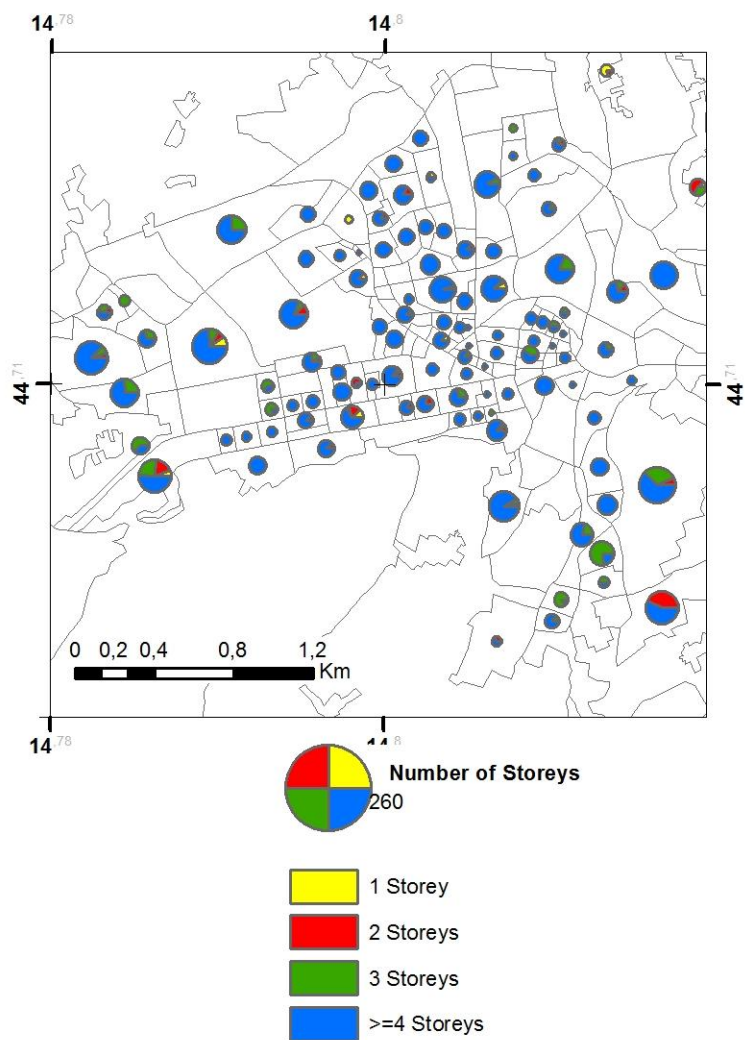


Figure 4-10: Spatial distribution at level of census cell of number of storeys

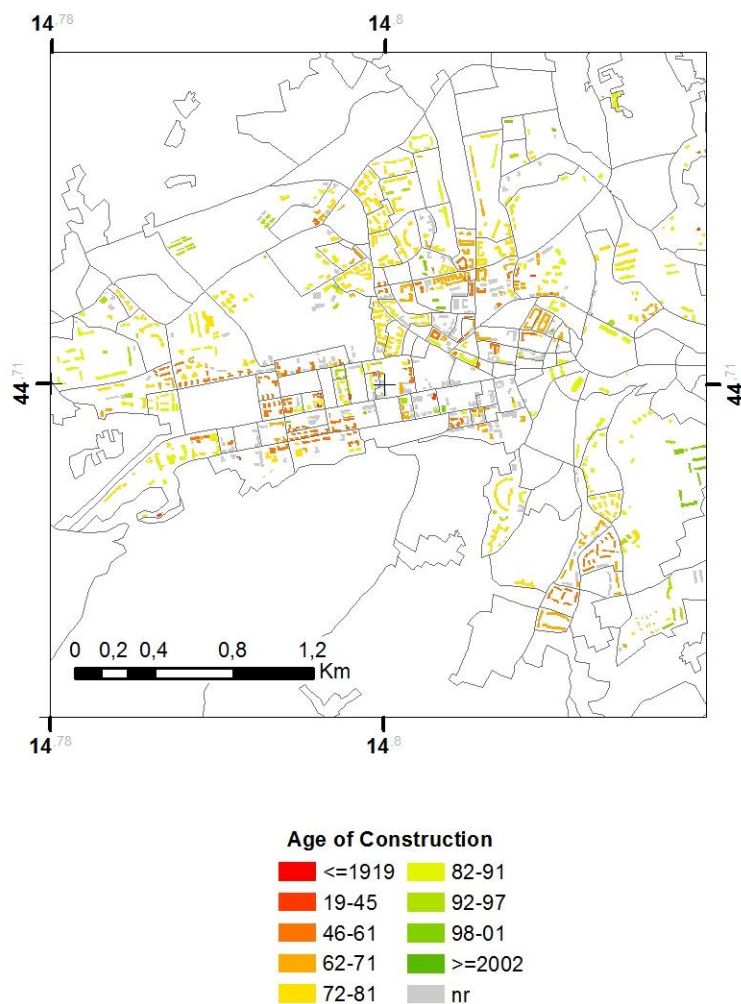


Figure 4-11: Spatial distribution at level of building of age of construction

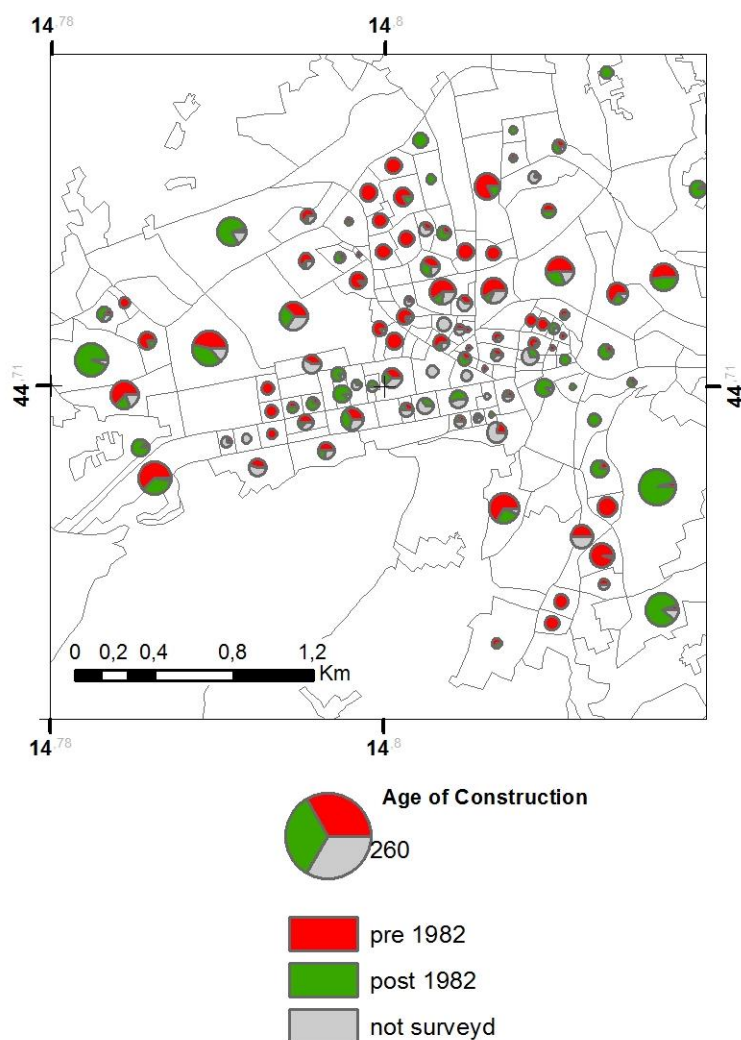


Figure 4-12: Spatial distribution at level of census cell of age of construction

Figure 4-7-Figure 4-12 shows the spatial distribution (grouped per census cell) of the same parameters previously analyzed at urban scale. The attention is focused on the central area of the Municipality, which was subjected to the field survey. Distribution of structural

typology per single building and within the single census cells are shown in Figure 4-7 and Figure 4-8, respectively.

Interesting observations can be made based on Figure 4-7. It can be observed that masonry buildings were mainly constructed at the beginning of the 20th century or before, or early after World War II, and are placed in the central area of the city. The period characterized by the first significant growth of the RC building stock is around 60s and 80s, and it involved mainly the northern area of the city, where a concentration of high-rise buildings can be found. Then, after the disastrous 23rd November 1980 Irpinia earthquake, an intense activity of reconstruction took place since the early 80s to the 90s, mainly in the central area where, close to masonry buildings, several post-1981 RC buildings can be found, which were constructed in replacement of the most heavily damaged masonry buildings. A further urban expansion affecting the south-eastern and north-western areas, constituted almost entirely by low-rise RC building dating from after 1981, can be observed.

In 1981 Avellino was also classified for the first time as seismic by the technical building code (DM 7/3/1981). This allows to make an important distinction between buildings dating from before 1981, which were designed for gravity loads only, and those dating from after 1981, designed according to seismic codes, although obsolete codes not accounting for Capacity Design rules.

As illustrated in section 3.5, the adopted procedure can be applied to data with different knowledge levels. In the case study illustrated herein (see section 4) the knowledge level is relatively high, and the geometrical characteristics of each single building can be assumed as deterministically known. Thus, it is only necessary to model the variability affecting material properties and capacity models, besides the uncertainty in seismic demand.

If the knowledge level is lower, it may be necessary to introduce some additional variables related, for instance, to the uncertainty in the geometrical model of the building. To this aim, statistical distributions providing the expected value and the corresponding variability of geometrical parameters are needed. These data can be drawn from statistical analysis of geometrical characteristics of surveyed existing building stocks. Also for this reason, it is interesting to analyze the data collected during the survey in the Municipality of Avellino about the inter-storey height at first and upper storeys, the average plan area, the plan ratio and the bay length, see Figure 4-18a-e.

It is to be noted that the inter-storey height at first storey shows a greater scatter compared to upper storeys. More than 80% of RC buildings are characterized by a value of inter-storey height at upper floor between 3.00 and 3.50 m with a mean value of 3.21 m and a CoV of about 7%, while inter-storey height at first storey shows a mean value of 3.58 m with a CoV more than doubled. The average plan area of RC buildings is around 400 m², and, as far as only rectangular RC buildings are concerned, the ratio between the larger and smaller plan dimension of the building is usually lower than 3. Bay length is typically around 4.40 m.

Interesting observations can be made looking at data concerning the distribution of infills. The opening percentage in infill panels at the bottom storeys of rectangular RC buildings is shown in Figure 4-18. This percentage was evaluated as the weighted average of the opening percentage on the four sides of the building. A peculiar trend is observed, characterized by two intermediate “peaks” corresponding to about 25 and 50%, due to the relatively high frequency of buildings fully infilled on two or three sides and without infills on the remaining sides. Note that a 100% opening percentage corresponds to “pilotis” buildings.

It is highlighted that the illustrated vulnerability assessment procedure has been applied at single building level based on the data about geometrical characteristics of each single building provided by the

field survey. Notwithstanding the previously provided distributions – based on the data collected during the survey in the Municipality of Avellino – are of fundamental importance in contributing to a priori information about the geometrical characteristics of buildings to be used when assessing the vulnerability at a large scale based on data with very low level of detail.

In the following, a comparison between the statistics collected from in situ survey data and those available in the technical-scientific literature is shown.

Comparing and cross-validating the data collected during the described in situ survey and data from other sources can be useful to the reader in order to check the reliability of the data, and to evaluate the possible use of other sources of data when a seismic vulnerability assessment at large scale is carried out and no field survey is available (Ricci et al., 2014).

However, in the present work the data from the in situ survey are used for an application of a simplified method for seismic vulnerability assessment of RC buildings on the Municipality of Avellino.

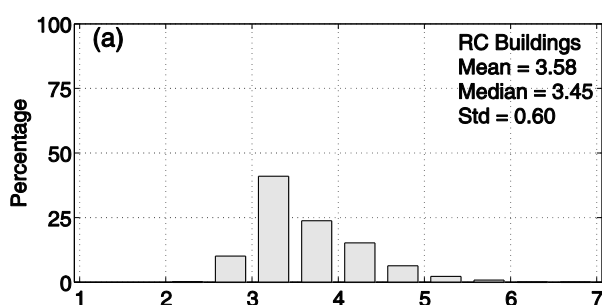


Figure 4-13: Distribution of inter-storey height at first storey.

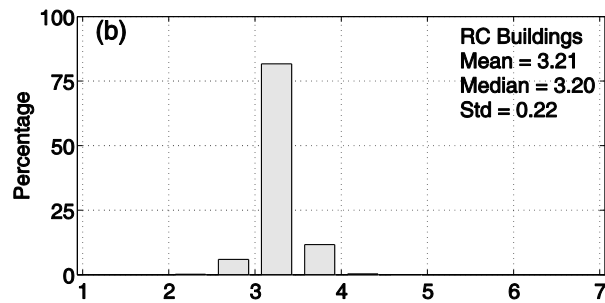


Figure 4-14: Distribution of inter-storey height at upper storeys.

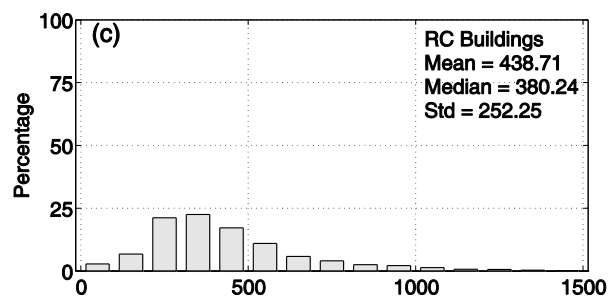


Figure 4-15: Distribution of average plan area.

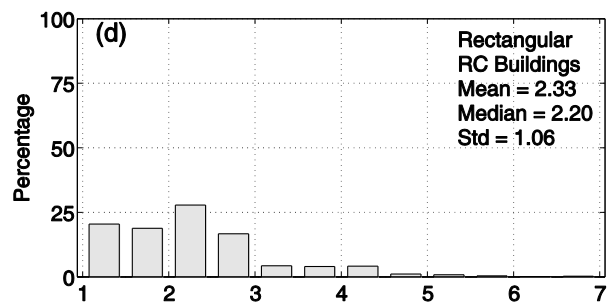


Figure 4-16: Distribution of plan ratio.

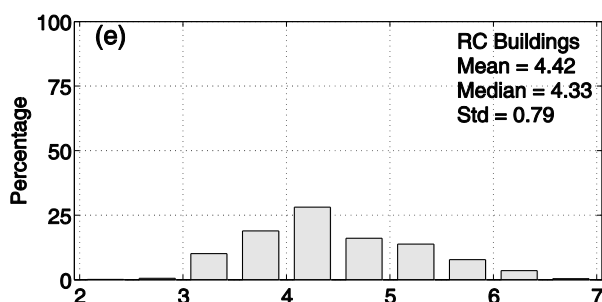


Figure 4-17: Distribution of bay length.

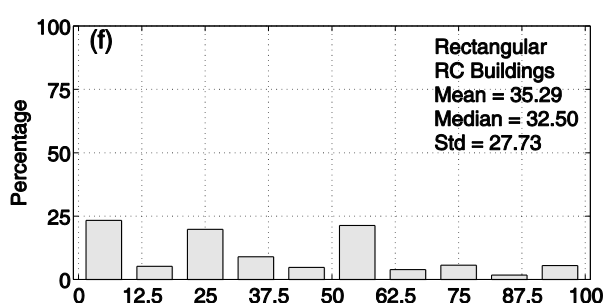


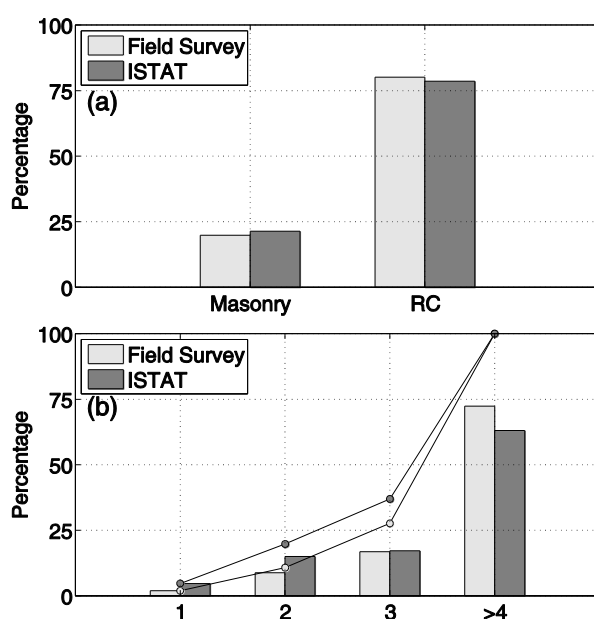
Figure 4-18. Distribution of opening percentage in infill panels at the bottom storey

4.2.1 Comparison with ISTAT data

The Italian National Institute of Statistics (Istituto Nazionale di Statistica, ISTAT) survey is a nation-wide census that provides information on citizens, foreign, buildings and dwellings. In particular the “14th general census of the population and dwellings” (14° Censimento generale della popolazione e delle abitazioni, ISTAT 2001) collected information about 57 millions of citizens, 13 millions of buildings and 27 millions of dwellings. Data about the number of storeys as well as characteristic of residential buildings, and in some cases even those non residential, were collected. This census provides the statistics of buildings, unlike previous census which provided statistics about dwellings, related to number of storeys (one-, two-, -three and (\geq four)-storey buildings), age of construction (typically with a decennial-rate)

and building typology (Masonry or RC buildings) for the spatial unit, that is the “census cell”. Nevertheless due to confidentiality requirements these statistics were presented in an aggregate manner, in which the information is not immediately identifiable as a function of the identified classes; for example, it is not possible to get the number of RC buildings in a cell dating back to a specific age of construction and characterized by a specific number of storeys, but only to know how many RC buildings, how many buildings dating back to that of construction and how many buildings with that number of storeys are present in that cell as a whole.

In the following the statistics for the 111 surveyed cells out of the 202 cells of Avellino from the ISTAT 2001 census are compared with the statistics obtained from the field survey carried out in the framework on the SIMURAI project. It is to be noted that a good matching can be observed with reference to the number of storeys and building typology (Figure 4-19a-b). More complex is the case of the age of construction, which was not surveyed in the 20% of cases (Figure 4-19c).



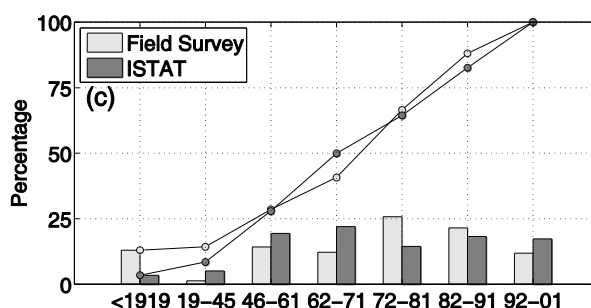


Figure 4-19. Comparison between the statistics obtained from the field survey carried out in the framework of the SIMURAI project and from the 14th general census (ISTAT): (a) building typology, (b) number of storeys, (c) age of construction

4.2.2 Comparison with LSU data

The project, built up between 1995 and 2000 thanks to employment initiatives based on participation in activities of public utility for disadvantaged subjects in labor market in the framework of Socially Useful Works (Lavori Socialmente Utili, LSU) sanctioned by Legislative Decree no. 468 (1997), provides a census of vulnerability of current buildings of built-up areas, in Abruzzo, Basilicata, Calabria, Campania, Molise, Puglia and Sicilia.

The surveys, carried out on municipalities within the regions with the highest seismic hazard in southern Italy, was promoted by Department of Civil Protection (Dipartimento della Protezione Civile, DPC) in collaboration with Italian Ministry of Labour and the National Group for Defence against Earthquakes (Gruppo Nazionale per la Difesa dai Terremoti, GNDT) of National Research Council (Consiglio Nazionale delle Ricerche, CNR). The project involved 1511 municipalities, in which a total of more than 40000 buildings were recorded, consisting for approximately 25% of public buildings and for the remaining part of private buildings. The survey activity also affected the city of Catania where the "Catania Project" was carried out (Faccioli and Pessina, 2000).

In Figure 4-20 the statistics on the age of construction and number of storeys surveyed in the framework of LSU and compared to the data collected in the Municipality of Avellino during SIMURAI project are presented. A good agreement between the two collection of data is observed, from which it can be deduced that the building stock of Avellino is representative of RC building stock in the twentieth century countrywide.

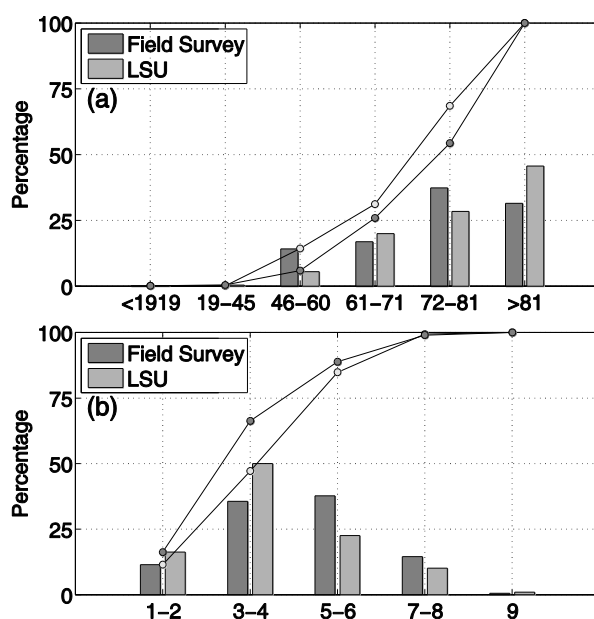


Figure 4-20. Comparison between the statistics obtained from the field survey carried out in the framework of the SIMURAI project and from LSU: (a) age of construction, (b) number of storeys

4.3 Input Data

In this section the methodology applied to a high level of detail of the data source is shown, given that geometric characteristics of each building are known by field survey.

The reference unit of the procedure is the building, for each of which geometrical model is completely defined through field survey data, namely number of storeys, bay length in longitudinal and transversal direction, interstorey height at first and upper storeys. Hence the structural model of the building is derived according to the age of construction, which allows to define design code prescriptions, professional practice and seismic classification of the area of interest at that time.

A *simulated design* according to (Verderame et al. 2010) is carried out. For this purpose seismic classification for the area is derived through ECS-it, which is a Geographic Information System (GIS) based on MATLAB® code that allows the visualization and the identification of the evolution of the seismic classification of the Italian territory from 1909 to 2003.

Actually, (DM 23/09/1981) classifies firstly the territory of the Municipality of Avellino in II Seismic Category.

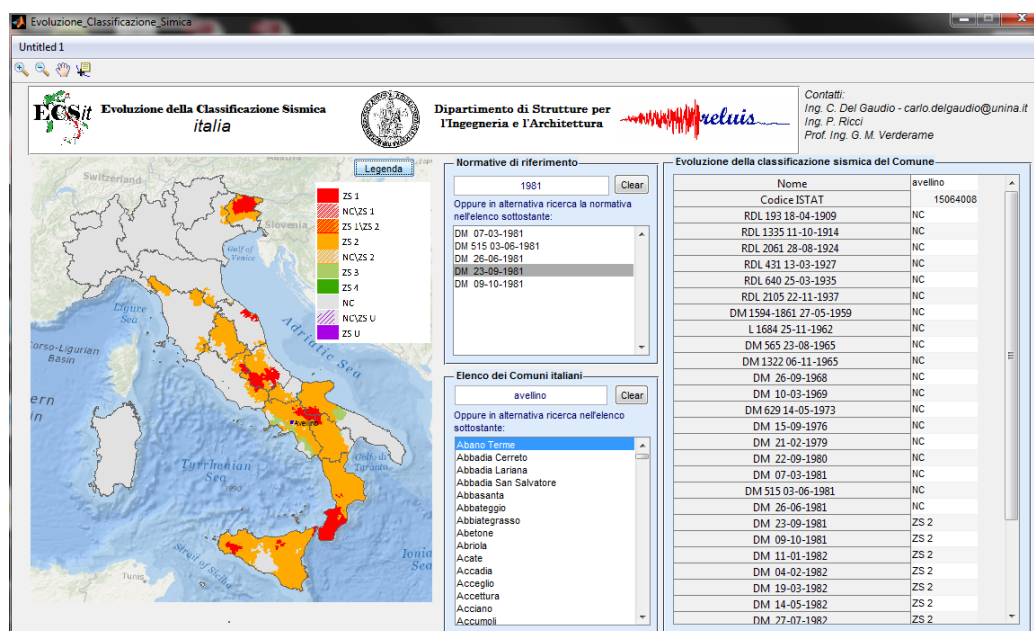


Figure 4-21: Evolution of seismic classification for the Municipality of Avellino through

ECS-it software based on MATLAB® code (<http://www.reluis.it/>)

Hence for RC Buildings dating back to before 1981 gravitational simulated design procedure has to be considered, whereas buildings constructed afterwards are designed by means of a seismic simulated procedure. For this purpose, it is necessary to assess the corresponding extent and distribution of lateral forces acting on the structure.

Hence, (DM 40/1975) ruled that buildings located in seismic category II have been designed according to a seismic intensity parameter $S = 9$, and a corresponding design base shear defined as

$$F = C \cdot W = \frac{S-2}{100} \cdot W = 0.07 \cdot W \quad \text{Eq 4-1}$$

where W was the building weight. Furthermore (DM 40/1975) introduces a linear force distribution proportional the sum of weight force acting from the basement to considered storey.

Then, element dimensions and element reinforcements are evaluated according to the procedure reported in 3.3.1.

Values of allowable stresses for steel and concrete employed in the simulated design procedure were determined according to the age of construction. As far as concrete is concerned, the allowable concrete stress for bending is assumed equal to

$$\sigma_c = 60 + \frac{R_{ck} - 150}{4} \quad \text{Eq 4-2}$$

Where R_{ck} is the cubic strength of concrete assumed equal to 25MPa in all cases. Hence, allowable compressive stress for axial load combined with bending is assumed equal to $0.7\sigma_c$. Moreover, the

concrete allowable stress used to determine column dimensions in the simulated design procedure was multiplied by a coefficient equal to 0.7 in the case of seismic design ([Pecce et al., 2004](#)).

Allowable steel stress ($\sigma_{s,adm}$) was calculated as the weighted average of the values corresponding to different steel typologies in time window corresponding to the surveyed age of construction, depending on the frequency of occurrence of each typology in this time window, according to the data reported in a statistical analysis of mechanical and typological characteristics of reinforcing steel used in Italy between 1950 and 1980 ([Verderame et al., 2010b](#)). For ages of construction above or below these limits, values corresponding to the most widely spread steel typologies in 1950 and 1980 were adopted, respectively, see Table 4-1.

Reinforcing steel typology (smooth or ribbed bars) was also determined as the most frequent typology in the time window corresponding to the surveyed age of construction, according to the data reported in ([Verderame et al., 2010b](#)).

Reference values of material properties usually come from statistical analyses of the mechanical characteristics provided by the technical literature. In the following, the choice of the statistical distributions adopted in this work for steel, concrete and infill materials is illustrated. These distributions are selected in order to be representative of the existing Italian building stock, therefore they will be used for the case study developed herein.

In ([Verderame et al., 2001](#); [Masi and Vona, 2009](#)) reliable statistics of the compressive strength of concrete used in Italy are presented. In this work, a value of 25 MPa for all ages of construction and a Coefficient of Variation (CoV) of 31% until 1981 has been set, while for buildings constructed after 1981 a CoV of 25% is assumed in order to reflect the higher reliability in the preparation of the concrete.

Statistics on steel yield strength are evaluated through STIL software ([Verderame et al., 2012](#)), providing statistics about main mechanical

characteristics of steel as a function of few parameters, such as the age of construction and the type of reinforcement (plain or ribbed bars). The latter is assumed to change with the age of construction: for buildings constructed before 1971 the reinforcement is assumed to be constituted by plain bars and subsequently by deformed bars.

The determination of infill material characteristics is affected by high difficulties and uncertainties, and literature does not offer enough experimental data. Values for mechanical characteristics based on the proposal of the Italian code ([Circolare 617, 2009](#)) for hollow clay brick panels have been set. Hence, assuming a full correlation between mechanical characteristics, the ratio between E_w and G_w is assumed equal to 10/3, whereas τ_{cr} is assumed as linearly dependent on G_w , assuming τ_{cr} equal to 0.3 and 0.4 MPa for G_w equal to 1080 and 1620 MPa, respectively. In particular, a value of the elastic modulus equal to 4500 MPa and a CoV of 30% have been adopted. The influence of openings in decreasing lateral stiffness and strength of infill panels is taken into account through a coefficient linearly dependent on the opening ratio, based on the experimental results reported in ([Kakaletsis and Karayannis, 2009](#)).

Age	Design	Reinforcement	$\sigma_{s,adm}$ [MPa]	f_y [MPa]	CoV [%]	f_c [MPa]	CoV [%]	E_{inf} [MPa]	CoV [%]
pre-1919	G	plain	140	325	20	25	31	4133	30
1919-45	G	plain	140	325	20				
1946-61	G	plain	173	336	22				
1962-71	G	plain	203	399	18				
1972-81	G	deformed	208	451	13	25	25	4133	30
1982-91	S	deformed	240	466	11				
1992-97	S	deformed	240	466	11				
1998-01	S	deformed	240	466	11				
post-2002	S	deformed	240	466	11				

Table 4-1. Type of design and material properties as a function of the age of construction

As far as the variables concerning the capacity models of RC elements, reference can be made to (Haselton et al., 2008), where a reliable and accurate model used to evaluate the performance of RC frame buildings up to collapse is developed. In this work a regression analysis is carried out on the experimental data from PEER (2005), leading to empirical functions relating seven calibrated model parameters for beams and columns to properties such as axial load, concrete strength, etc. The Authors also investigate uncertainty associated with each prediction identified by the logarithmic standard deviation and by the average of the ratio between the observed and predicted values, reported in

Table 4-2, assuming that the model parameters follow a lognormal distribution.

Table 4-2. Median and logarithmic standard deviation values of predicted to observed data for RC capacity model (Haselton et al, 2008)

Variable	$\mu_{\text{pred/obs}}$	$\beta_{\text{pred/obs}}$
EI_y / EI_g	0.95	0.28
M_c / M_y	0.97	0.10
θ_{cap}	1.02	0.54
θ_{pc}	1.00	0.72

Finally, the strength reduction factor R evaluated from R - μ - T relationship, back-applied to obtain PGA capacity from ductility capacity, is modelled as a Random Variable, too, according to (Vamvatsikos and Cornell, 2006).

A Monte Carlo simulation is used, and sampling of Random Variables is carried out through the efficient stratified Latin Hypercube Sampling (LHS) technique (McKay et al., 1979), adopting the “median” sampling scheme (Vorechovsky and Novak, 2009). In this way, a population of buildings is generated, each one corresponding to a different set of values of the defined Random Variables. Therefore, if

PGA capacity, at a given DS, is calculated for all the generated buildings, the corresponding cumulative frequency distributions of the obtained PGA capacity values provide the fragility curves in X and Y directions and at each DS. In the same way fragility curves independent of the direction can be obtained, through the evaluation of the cumulative frequency distribution of the minimum PGA capacities between longitudinal and transversal direction for each sampling.

Note that in the case study developed herein the shape of the acceleration response spectrum changes with the return period and it also depends on the coordinates at the site of interest and on stratigraphic conditions, due to the adopted seismic hazard data. Therefore, fragility curves are unavoidably site-dependent. PGA capacity values reported in the following (including fragility curves) are expressed in terms of PGA at the bedrock, already accounting for stratigraphic and topographic conditions.

In Figure 3-14 fragility curves at each different DS for a 1-storey building (ID 4799_B) situated in North-East area of Avellino Municipality are shown.

4.4 Evaluation of seismic hazard

Seismic hazard is evaluated according to (INGV-DPC S1, 2007), adopted by the Italian National Technical Standards (DM 14/1/2008). According to these provisions, seismic hazard is defined in terms of maximum horizontal expected acceleration in free field conditions on rigid soil with horizontal topographic surface, and in terms of the elastic acceleration response spectrum, with reference to pre-defined exceeding probability over the reference period.

The spectral shapes are defined according to the exceeding probability during the reference period (PVR), from the values of the following parameters referred to rigid horizontal site:

- a_g maximum acceleration at the site;

- F_0 maximum value of amplification factor of the horizontal acceleration spectrum;
- T_c^* value of the period corresponding to the beginning of the constant velocity branch of the spectrum.

These parameters, which are tabulated in Annex B of (DM 14/1/2008), are provided by (INGV, 2007) for the points of a nationwide grid, and for different return periods TR , falling into a target range between 30 and 2475 years, extremes included. Nevertheless, in this study there is the need to extend elastic demand spectra above and below the extreme values. To this aim, the formulations proposed for the interpolation procedure are also used to extrapolate the above mentioned parameters out of the given range of values, as in (Crowley et al., 2009). In this way, seismic hazard expressed in terms of PGA and elastic acceleration response spectrum at the bedrock is determined (Figure 4-22), but these values should be calculated taking into account the soil category at the site.

According to (DM 14/1/2008) five soil categories (from A to E) are defined based on the average shear wave velocity into the ground in the last 30 m ($V_{s,30}$). Soil category at each site has been provided by a microzonation study, which was already available for Avellino city. Then, stratigraphic effects are taken into account through coefficients depending on the soil category of the site of interest (Figure 4-23a).

Effects related to the topographic conditions are considered, too, by means of an amplifying coefficient depending on the topographic category (from T1 to T4), which is determined by spatial processing the DTM of the city in order to obtain the slope surface at any point (Figure 4-23b).

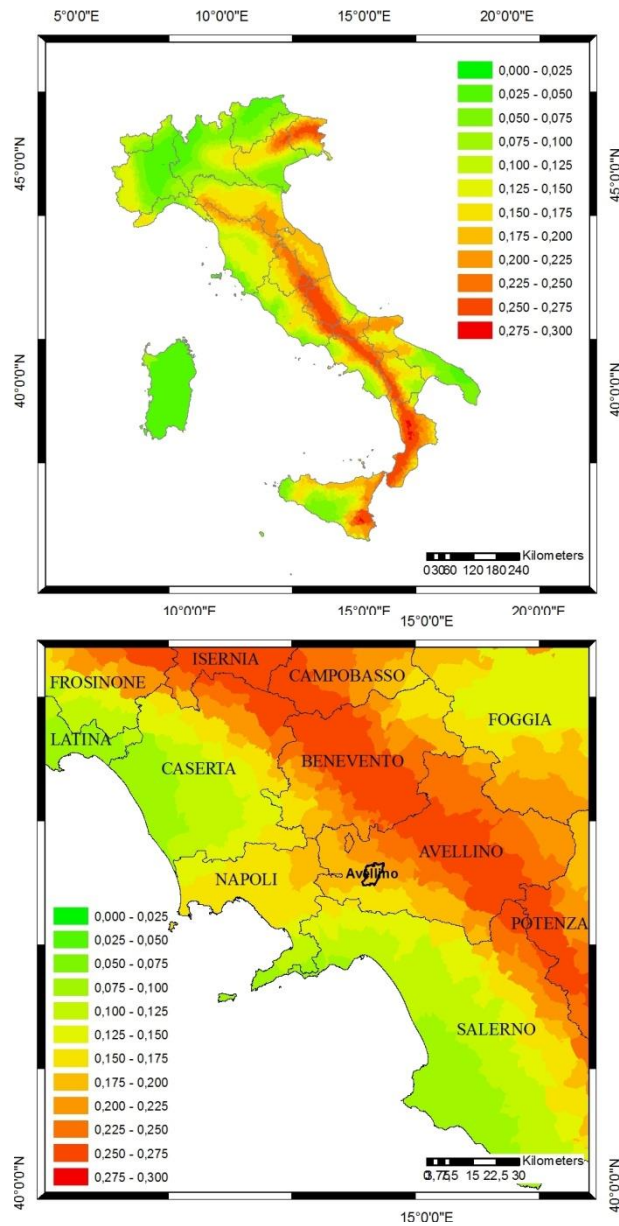


Figure 4-22.10% probability of exceedance in 50 years (return period of 475 years)
PGA[g] in Italy and in Campania region

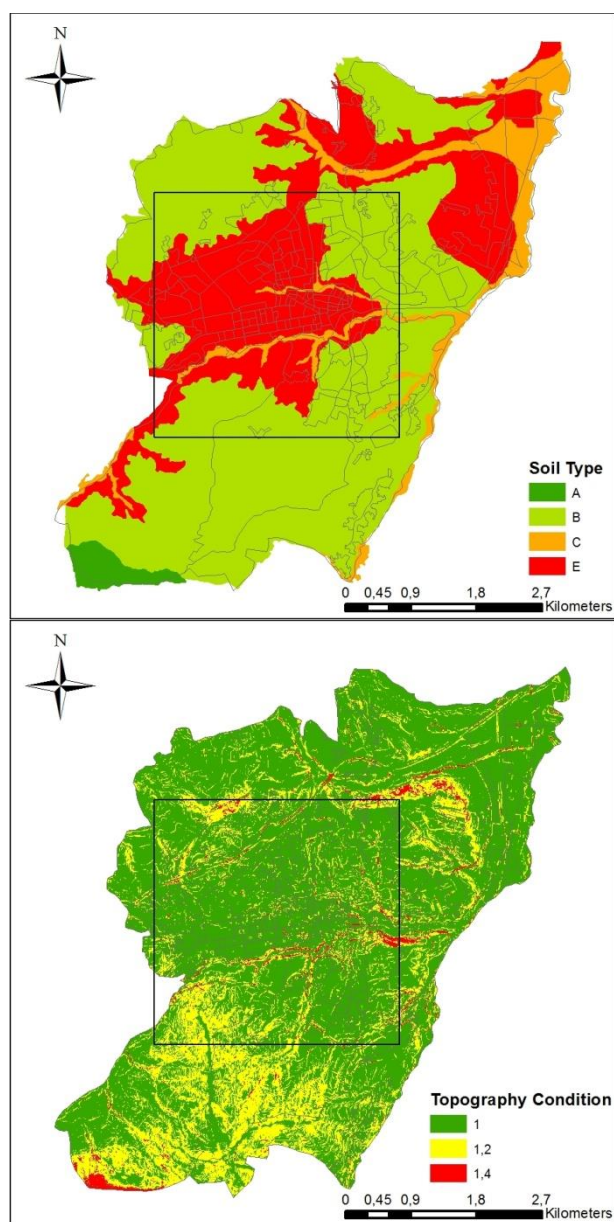


Figure 4-23. Stratigraphic and topographic soil conditions in Avellino city

4.5 Seismic vulnerability assessment

In the following, the results of the application of the above described vulnerability assessment procedure are reported. Fragility curve parameters and failure probability at different DSs in a time window of 1 year are presented, obtained by convolving the fragility curves of each single building with the hazard curve representing the exceeding probability of the adopted seismic intensity parameter (namely the PGA) in the chosen time window.

Note that in this application geometric characteristic of buildings (such as number of storeys, interstorey height, number of bays in each direction, bay length) are provided for each building by the detailed in situ survey, hence they are treated as deterministic parameters, whereas material properties, capacity models, and strength reduction factor R in R - μ - T relationship are modelled as Random Variables, according to Section 3.5. Moreover, fragility curves are evaluated at each Damage State for each single building independent of the direction, by assuming for each set of Random Variables sampled within the adopted Monte Carlo simulation procedure the minimum PGA capacity between the two main directions of the building, see Section 3.5.

The fragility curves, evaluated according to Section 3.5, are obtained as cumulative frequency distributions of the PGA capacity values at each DS. Such distributions can be fitted by lognormal cumulative distributions, depending on two parameters: the estimated median (μ , expressed in [g]) and logarithmic standard deviation (β) of PGA capacity. β controls the slope of the fragility curve: the smaller the value of β , the less variable the PGA capacity, and the steeper the fragility curve. The larger the value of β , the more variable the DS, and the flatter the fragility curve.

In Figure 4-24 a clear trend is observed looking at the median values reported as black circles, showing in all cases the higher vulnerability of taller buildings.

With the number of storeys increasing, the strength and stiffness provided by structural elements (i.e., RC columns) increases, whereas the contribution of infills does not change significantly, since the latter is related to dimension of infill panels, which do not change with the height of the building. Therefore, with the number of storeys increasing, lateral (effective) stiffness – which is the key parameter for seismic capacity at DS1 and DS2 – is less influenced by the contribution of infills. If seismic capacity is less sensitive to the presence of infills, variability in PGA capacity will be less sensitive to variability in infills' characteristics, too, resulting in lower β values.

As far as DS3 to DS5 are concerned, a significant increase in seismic fragility is observed with the number of storeys, especially when such number increases from lower or equal than 3 to greater or equal than 4, as suggested by failure probabilities.

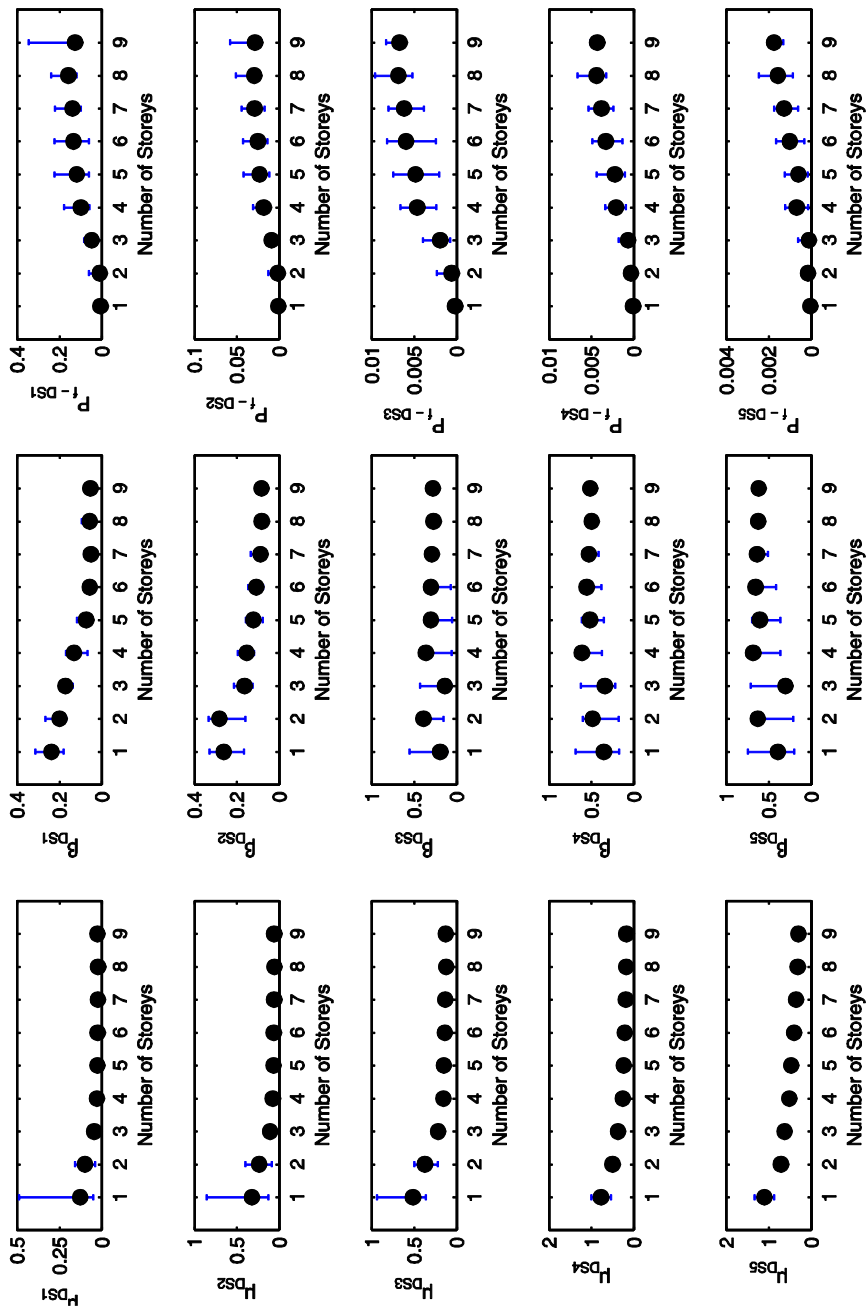


Figure 4-24. Median and lognormal standard deviation values of PGA Distribution (Fragility Curves) and Failure probabilities of surveyed RC buildings at each DS, as a function of the number of storeys

The influence of the age of construction can be observed for pre-1981 and post-1981 buildings. As a matter of fact, the introduction of seismic design prescriptions in Avellino city in 1981 results in an increase in lateral strength and displacement capacity of buildings, leading to higher vulnerability in pre-1981 buildings. The decreasing trend in seismic fragility for post-1981 buildings is readily observable looking at failure probabilities. The inversion shown by post-2002 buildings is mainly due to the fact that almost all of the buildings in this class are located on soil E. Generally speaking, in non-homogeneously sorted building databases the cross-correlation between different parameters that significantly affect seismic fragility (in this case, age of construction and soil type) can make it difficult to effectively highlight the influence of each single parameter, especially when the number of building in the classes is not very high.

Therefore, in order to analyze the influence of each parameter on the results, the application of the simplified method for seismic vulnerability assessment of the 1052 RC buildings for Avellino Municipality has been repeated removing the sensitivity to the soil condition, i.e. disregarding the information about the microzonation study and assuming that each building was placed on horizontal stiff soil (topographic category T1 and soil category A).

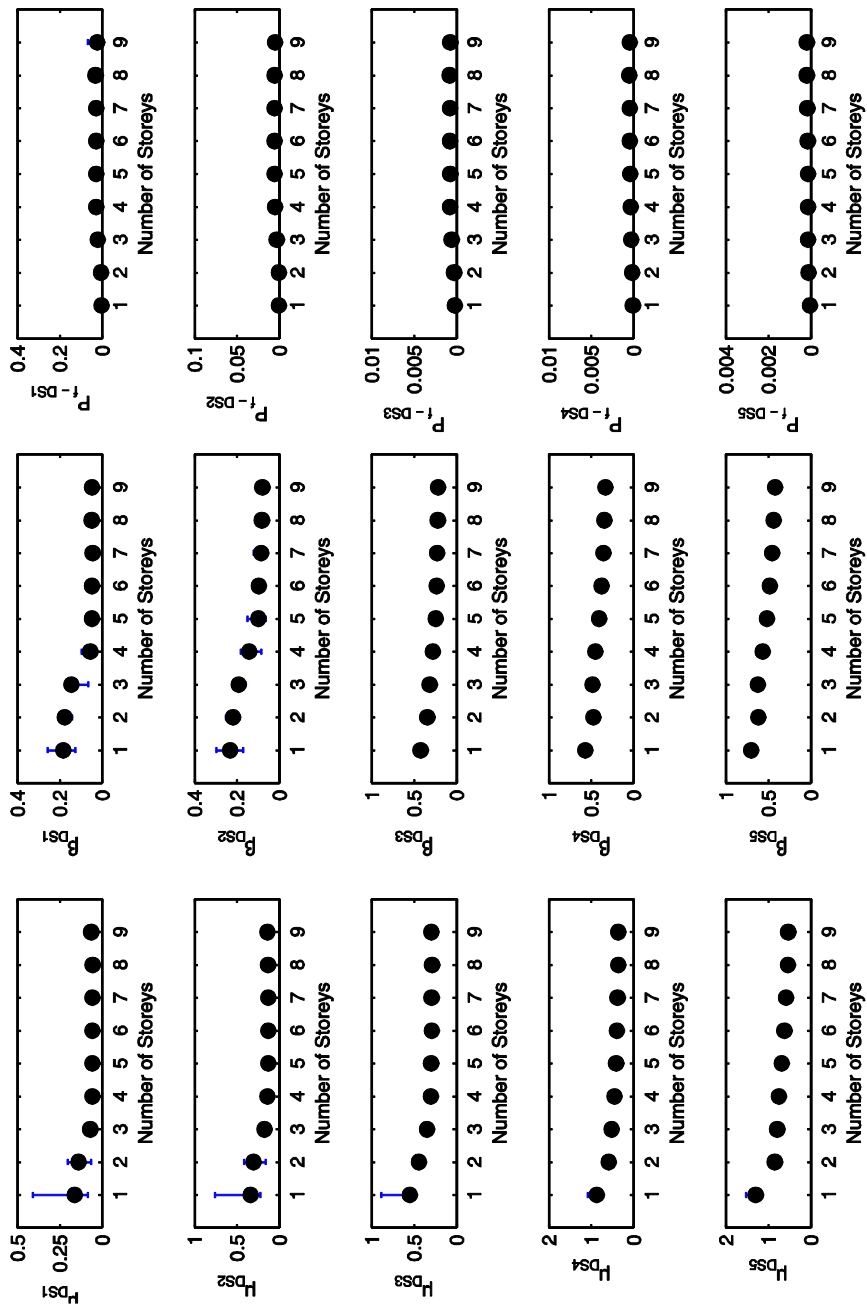


Figure 4-25. Median and lognormal standard deviation values of PGA Distribution (Fragility Curves) and Failure probabilities of surveyed RC buildings at each DS, as a function of the number of storeys, evaluated

From the comparison between Figure 4-24 and Figure 4-25 it can be observed how the general trends are confirmed, since in all cases the taller the buildings, the higher the vulnerability. At the same time, having removed the cross-correlation between the parameters, the trends appear much more regular, especially for the comparison in terms of logarithmic standard deviation for Damage States 3 to 5. Furthermore, as expected, an overall reduction in seismic fragility is observed, both in terms of increasing median PGA capacity and decreasing failure probability compared with Figure 4-25.

It is recalled that in some cases (about 20% of surveyed buildings) the age of construction was not determined. In these cases, a weighted average of the ages of construction of other buildings in the same census cell was calculated and this value was assumed also for the building of interest.

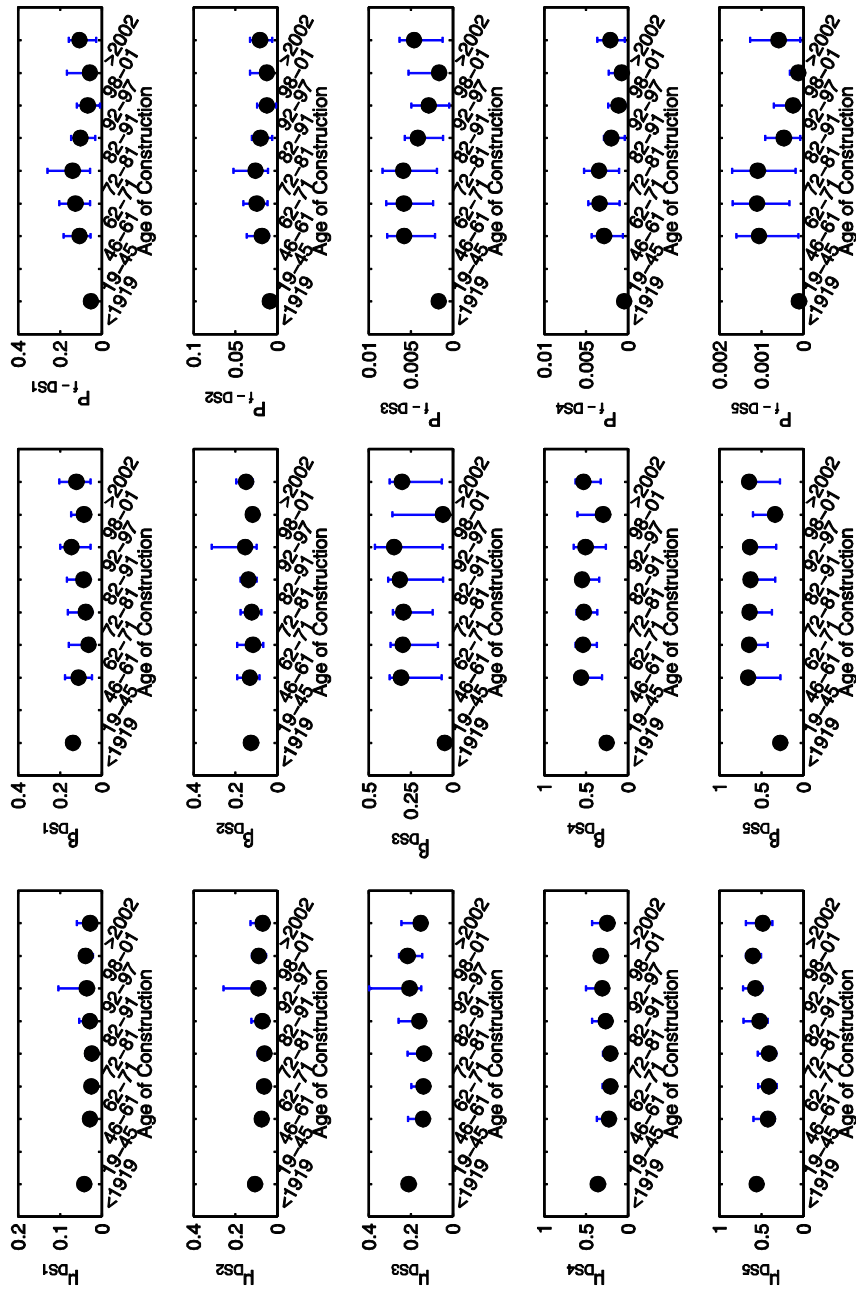


Figure 4-26. Median and lognormal standard deviation values of PGA Distribution (Fragility Curves) and Failure probabilities of surveyed RC buildings at each DS, as a function of the age of construction

The spatial distribution of annual failure probabilities within the area of the Municipality is shown in Figure 4-27.

Higher values of failure probabilities are observed in Central-Western and Northern areas. A clear influence of the difference in seismic hazard due to a different soil type (see Figure 4-23a) can be recognized, leading, as expected, to higher failure probabilities, on average, for buildings located on soil type E.

Significant differences in failure probabilities can be observed within areas characterized by the same soil type mainly due to differences in the number of storeys and the age of construction. This is the case of the Northern area where a concentration of high-rise buildings can be found, leading to significantly higher failure probabilities compared with the Central-Western area, although they are both located on soil type E. A further distinction can be made between the Central and the extreme Western areas: a majority of low/mid-rise pre-1981 is observed in the former, whereas low/mid-rise post-1981 are mainly present in the latter, leading to lower failure probabilities in the second case.

The lowest failure probabilities overall are observed in the extreme South-Eastern area, located on soil type B and populated by low/mid-rise post-1981 buildings.

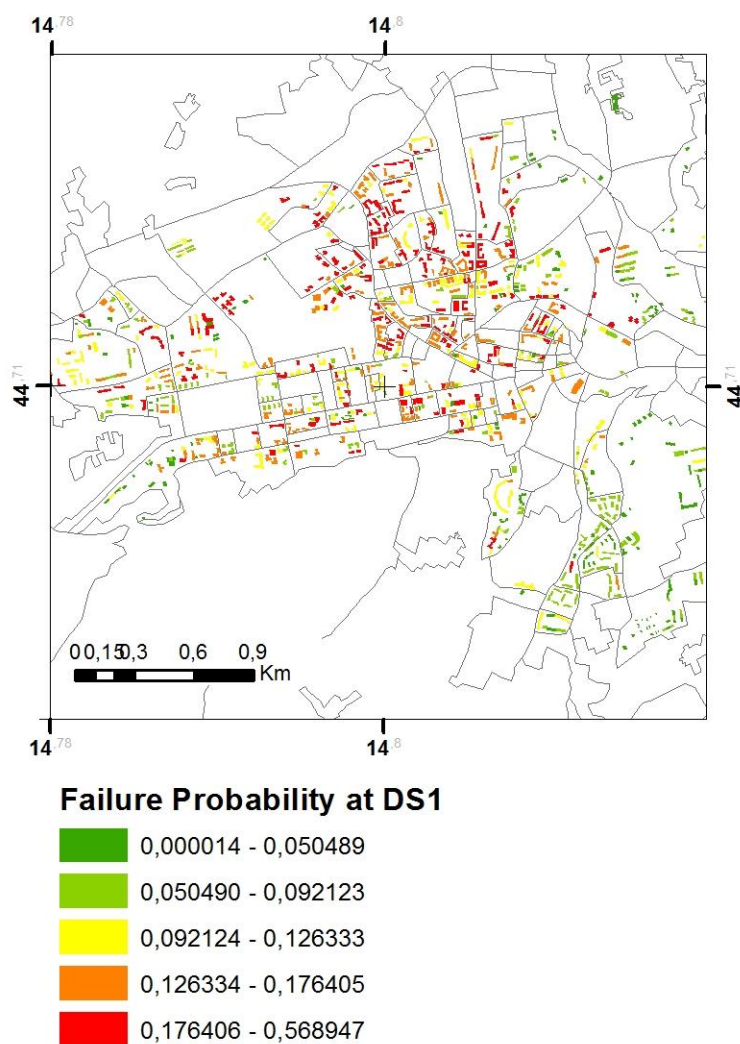


Figure 4-27: Failure probabilities of surveyed RC buildings at DS1

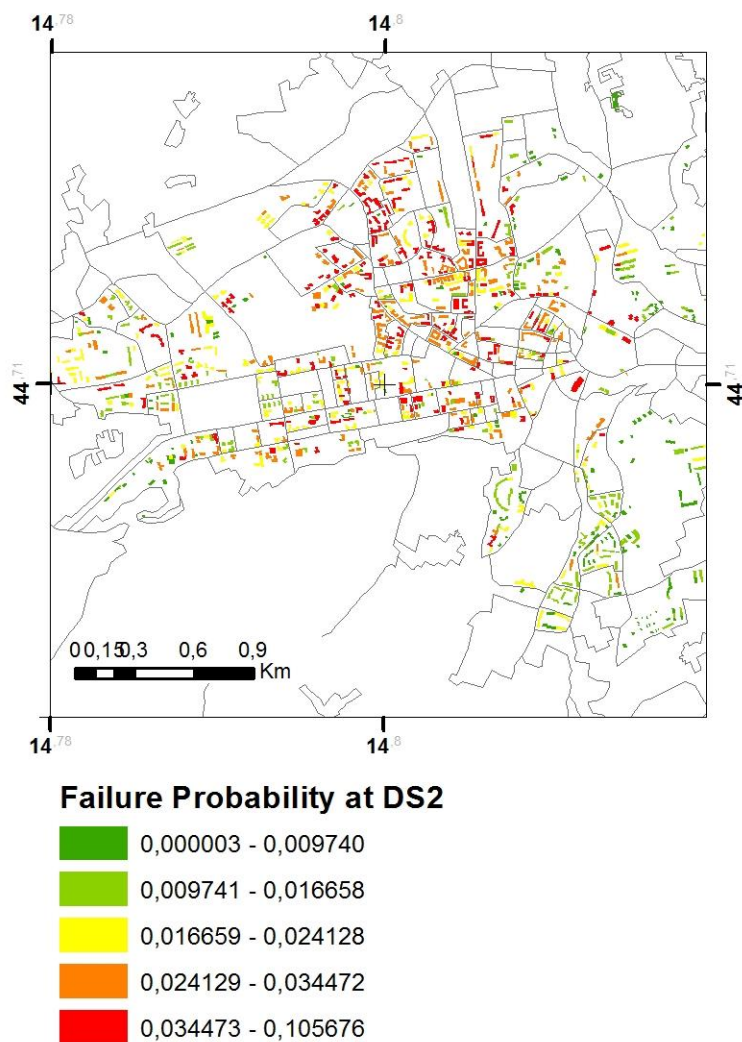


Figure 4-28: Failure probabilities of surveyed RC buildings at DS2

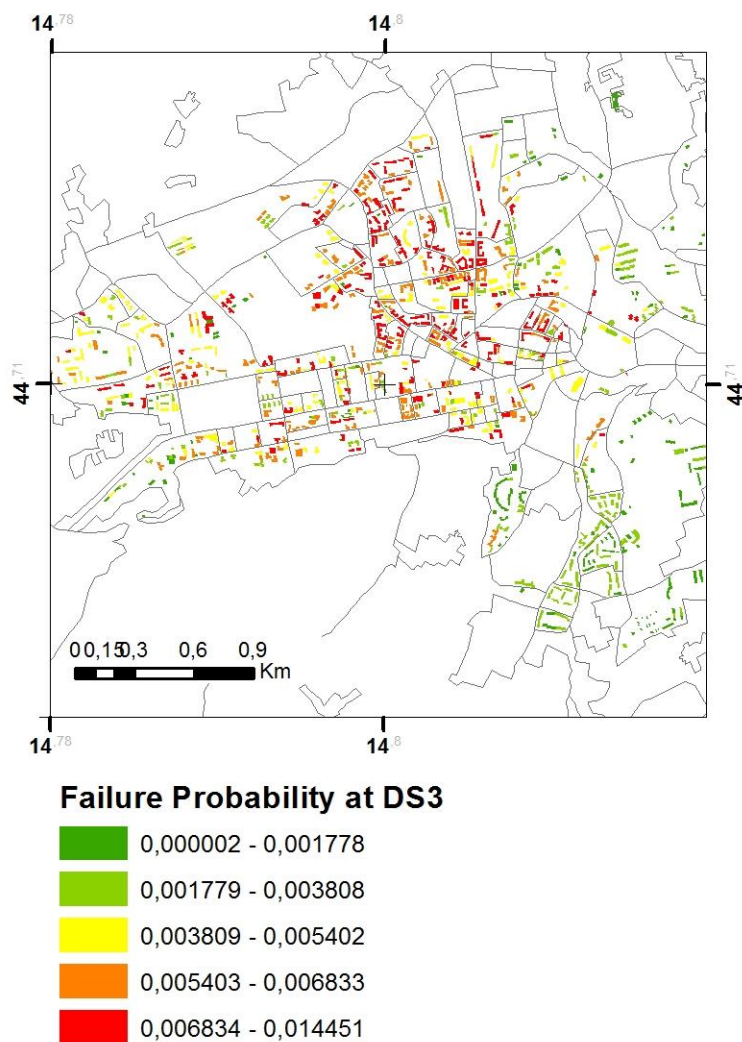


Figure 4-29: Failure probabilities of surveyed RC buildings at DS3

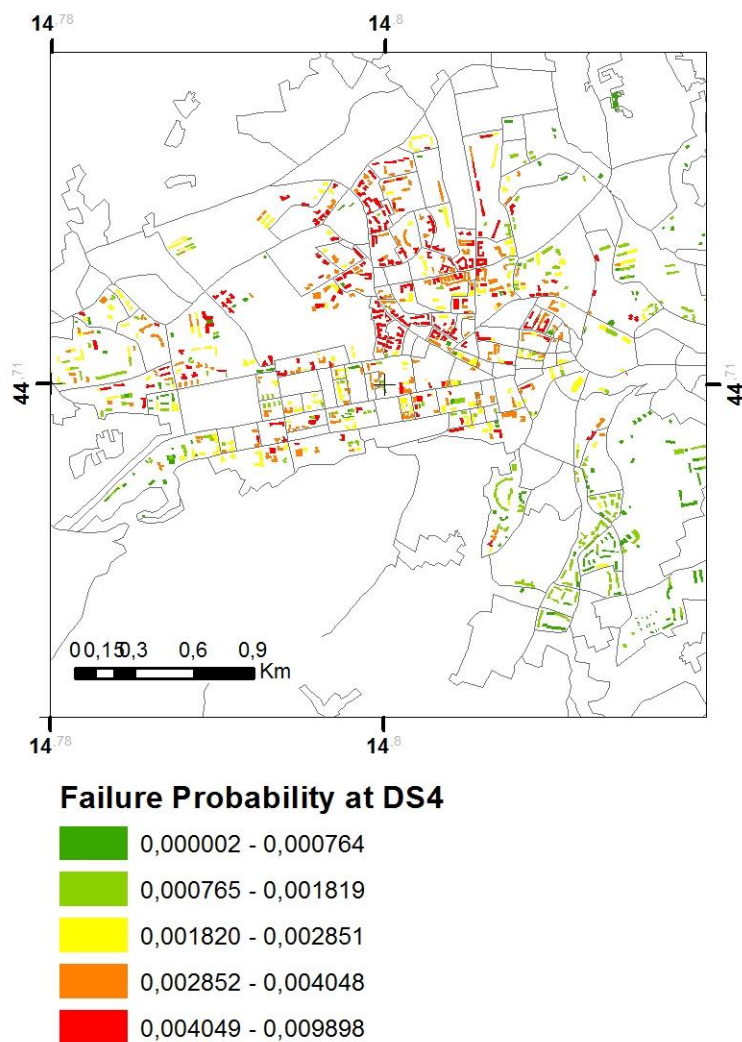


Figure 4-30: Failure probabilities of surveyed RC buildings at DS4

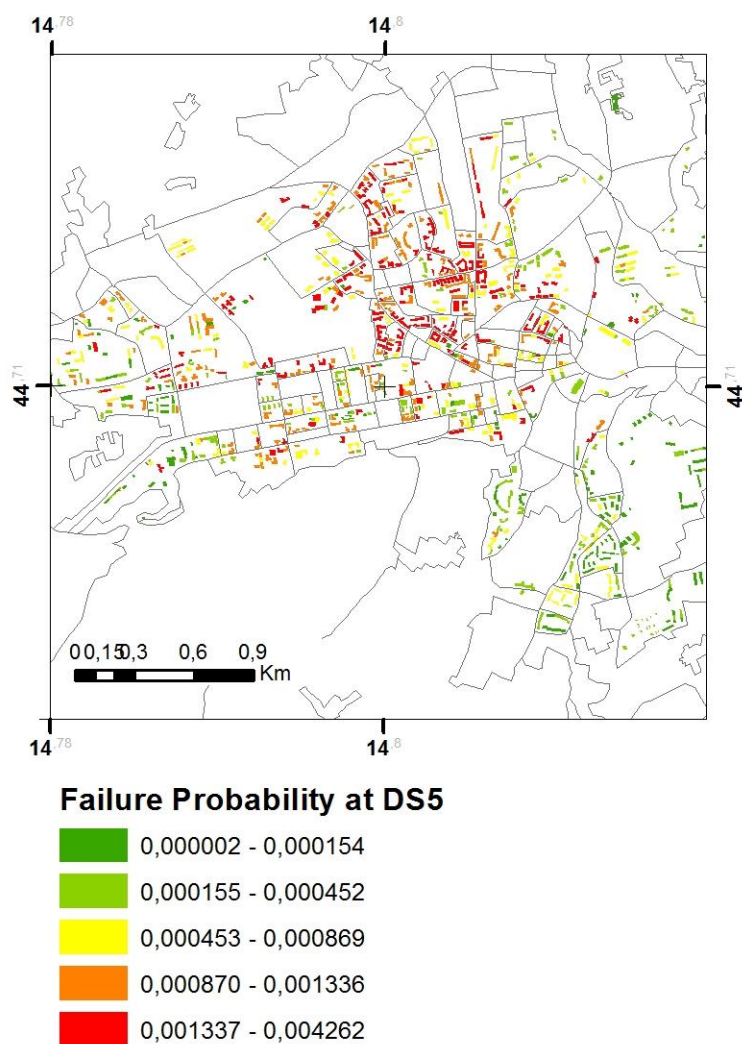


Figure 4-31: Failure probabilities of surveyed RC buildings at DS5

4.6 Comparison with fragility curves from literature

In this Section, analytical fragility curves derived for analyzed buildings are compared with fragility curves provided by other Authors. In order to carry out such a comparison, literature studies using the

same definition of damage levels adopted herein – that is, EMS-98 damage grades – must be considered.

Empirical methodologies by Lagomarsino and Giovinazzi (2006) and Rota et al. (2008) are thereby considered. In both cases, the Authors provide fragility curves for classes of buildings depending on structural typology, level of earthquake resistant design and number of storeys.

In particular, Lagomarsino and Giovinazzi (2006) provide fragility curves for Concrete Moment Frames as a function of the class of height (Low: $1 \leq N_{storeys} \leq 3$, Medium: $4 \leq N_{storeys} \leq 7$ or High: $N_{storeys} \geq 8$), and with or without Earthquake Resistant Design. In the former case sub-typologies are defined depending on the seismic category (I, II or III) and the ductility level (Low, Medium or High). Such fragility curves are derived from the DPMs implicitly defined by EMS-98 (see Section 2) assuming that PGA is correlated to the macroseismic intensity (I) through the following relationship:

$$PGA = c_1 c_2^{(I-5)} \quad \text{Eq 4-3}$$

with $c_1 = 0.03$ and $c_2 = 1.6$.

Similarly, Rota et al. (2008) provide fragility curves for RC buildings as a function of the class of height ($1 \leq N_{storeys} \leq 3$ or $N_{storeys} \geq 4$), and with or without seismic design; nevertheless, due to the reduced amount of data, no fragility curve is provided for RC buildings with seismic design and $N_{storeys} \geq 4$.

Based on the analysis of the RC building stock of Avellino, 72.6% of the buildings whose age of construction was surveyed belong to the class with $4 \leq N_{storeys} \leq 7$; among these, 56.6% is pre-1981 and 43.4% post-1981. The comparison is carried out for such classes, which are the most populated and representative of the whole building stock.

Note that the fragility curves were calculated herein for single buildings, whereas such a comparison with fragility curves from

literature has to be carried out for building classes. Then, mean fragility curves are derived for the analyzed buildings, grouping them in the above mentioned classes. Such mean curves are obtained by calculating at each Damage State the mean exceeding probability for all buildings within the class conditioned on PGA. Seismic fragility evaluated on horizontal stiff soil (see Section 4.3) is used for the comparison.

Then, Figure 4-33 reports a comparison between mean fragility curves evaluated herein for (i) pre- and (ii) post-1981 RC buildings with $4 \leq N_{storeys} \leq 7$ and fragility curves for (i) Medium-Rise Concrete Moment Frames without Earthquake Resistant Design ("RC1_M") and (ii) Medium-Rise Concrete Moment Frames with Earthquake Resistant Design in second seismic category with Low Ductility ("RC1-II_M DCL") from (Lagomarsino and Giovinazzi, 2006), see Table 4.

An acceptable agreement is observed between analytical fragility curves derived herein through POST procedure and empirical fragility curves from (Lagomarsino and Giovinazzi, 2006).

Compared with empirical data, median PGA capacities at Damage States 3 to 5 are very close or slightly lower for pre-1981 buildings, and vice versa for post-1981 buildings, whereas at Damage States 1 and 2 a better agreement is observed for pre-1981 buildings. Analytical curves show a lower variability, especially for Damage States 1 to 3; this is consistent with the relatively low number of buildings in the analyzed subset.

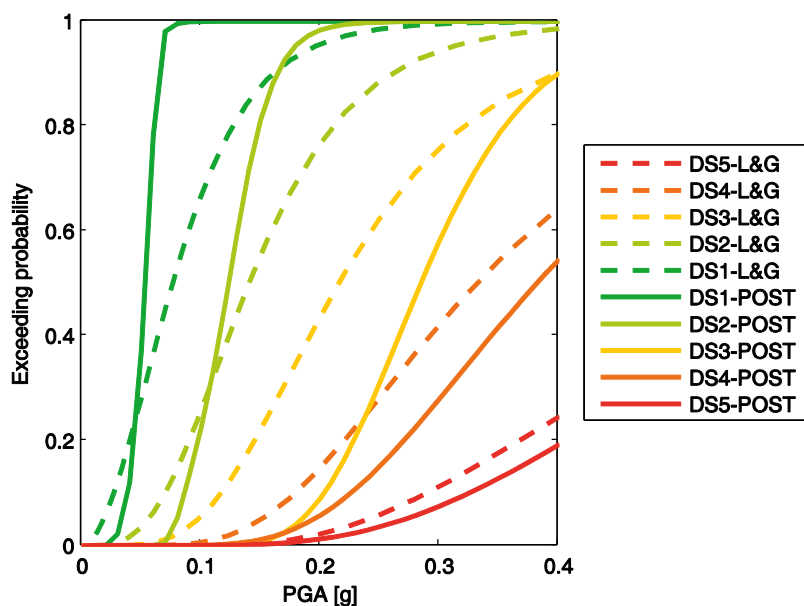


Figure 4-32: Comparison between mean fragility curves evaluated with POST and fragility curves provided by (Lagomarsino and Giovinazzi, 2006) for pre-1981 buildings with $4 \leq N_{\text{storeys}} \leq 7$

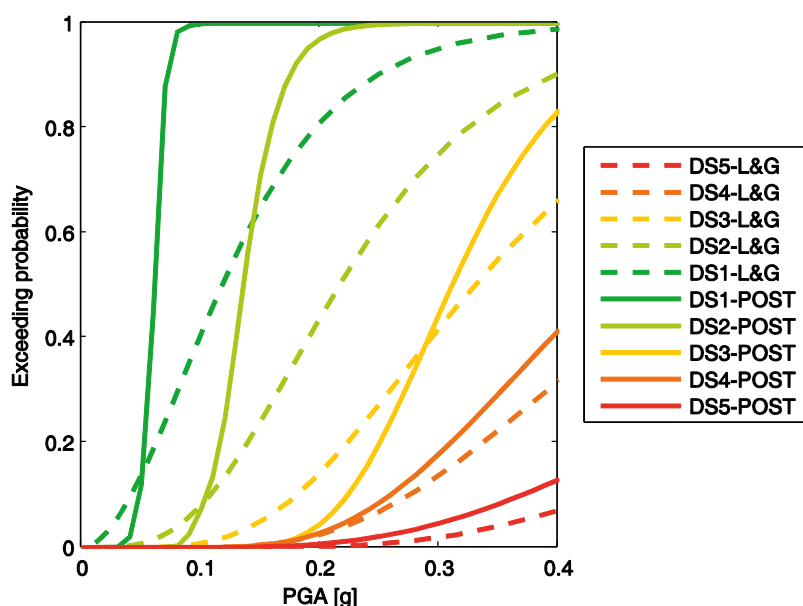


Figure 4-33. Comparison between mean fragility curves evaluated with POST and fragility curves provided by (Lagomarsino and Giovinazzi, 2006) for post-1981 buildings with $4 \leq N_{\text{storeys}} \leq 7$

Finally, Figure 4-34 reports a comparison between mean fragility curves evaluated herein for pre-1981 RC buildings with $4 \leq N_{\text{storeys}} \leq 7$ and fragility curves for Reinforced Concrete buildings without seismic design and with $N_{\text{storeys}} \geq 4$ (“RC4”) from (Rota et al., 2008), see Table 4. Also in this case a quite good agreement is observed, especially for heaviest Damage States. However, in (Rota et al., 2008) the Authors, when interpreting the level of damage reported on survey forms, considered only structural damage and ignored non-structural damage, whereas in the present study non-structural damage was explicitly accounted for, namely at Damage States 1 to 3 (see Section 3.4). This should be a reason for the lower seismic fragility in (Rota et al., 2008) compared with the analytical fragility evaluated herein at these Damage States.

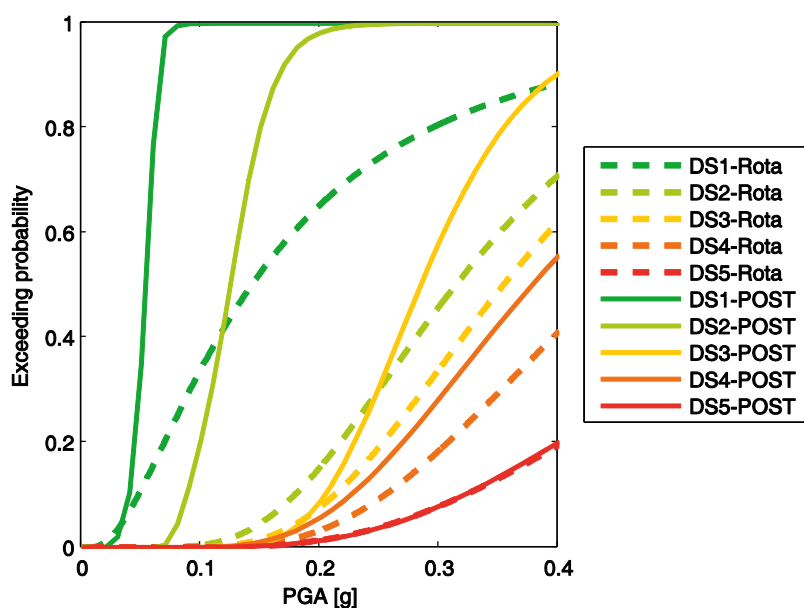


Figure 4-34. Comparison between mean fragility curves evaluated with POST and fragility curves provided by (Rota et al., 2008) for pre-1981 buildings with $4 \leq N_{storeys} \leq 7$

Table 4-3. Building classes used for seismic fragility comparison

POST	Lagomarsino and Giovinazzi (2006)	Rota et al. (2008)
Buildings with pre-1981 age of construction and $4 \leq N_{storeys} \leq 7$ from survey	Medium-Rise Concrete Moment Frames without Earthquake Resistant Design ("RC1_M")	Reinforced Concrete buildings without seismic design and with $N_{storeys} \geq 4$ ("RC4")
Buildings with post-1981 age of construction and $4 \leq N_{storeys} \leq 7$ from survey	Medium-Rise Concrete Moment Frames with Earthquake Resistant Design in second seismic category with Low Ductility ("RC1-II_M DCL")	-

4.7 Summary of remarks

The results of the application of the analytical procedure for seismic vulnerability assessment of RC buildings at large scale, which has been implemented in POST (PushOver on Shear Type models), a software based on MATLAB® code (Chapter 3 ,[Ricci, 2010](#), [Del Gaudio et al, 2015](#)), are reported. Fragility curve parameters and failure probability at different DSs in a time window of 1 year have been presented, obtained by convolving the fragility curves of each single building with the hazard curve representing the exceeding probability of the adopted seismic intensity parameter (namely the PGA) in the chosen time window.

The procedure was applied to building stock data provided by the field survey carried out within the framework of the SIMURAI Research Project ([2010](#)). Comparison between such data and further literature sources – including census statistics – show a reasonable agreement, thus supporting the reliability of collected data. The procedure was shown to be able to model the influence of key parameters on seismic fragility. Namely, as far as structural characteristics are concerned, the influence of number of storeys and age of construction was illustrated. These parameters also determined the spatial distribution of areas most prone to seismic risk within the Municipality, together with the local amplification of seismic hazard due to soil conditions. Finally, a comparison with observational data is illustrated in order to test the reliability of numerical results and to allow validation and calibration of the analytical methodology.

4.8 References

- ATC, 1985. Earthquake damage evaluation data for California. Report ATC-13, Applied Technology Council, Redwood City, California, USA.
- Benedetti D., Petrini V., 1984. Sulla vulnerabilità di edifici in muratura: proposta di un metodo di valutazione. L'industria delle Costruzioni, 149(1), 66-74. (in Italian)
- Borzi B., Crowley H., Pinho R., 2008b, The influence of infill panels on vulnerability curves for RC buildings. Proceedings of the 14th World Conference on Earthquake Engineering, Beijing, China, October 12-17. Paper 09-01-0111.
- Borzi B., Pinho R., Crowley H., 2008a. Simplified pushover-based vulnerability analysis for large scale assessment of RC buildings. Engineering Structures, 30(3), 804-820.
- Braga F., Dolce M., Liberatore D., 1982. A statistical study on damaged buildings and an ensuing review of the MSK-76 scale. Proceedings of the 7th European Conference on Earthquake Engineering, Athens, Greece. Pp. 431-450.
- Calvi G.M., 1999. A displacement-based approach for vulnerability evaluation of classes of buildings. Journal of Earthquake Engineering, 3(3), 411-438.
- Calvi G.M., Pinho R., Magenes G., Bommer J.J., Restrepo-Veléz L.F., Crowley H., 2006. The development of seismic vulnerability assessment methodologies for variable geographical scales over the past 30 years. ISET Journal of Earthquake Technology, 43(3), 75-104.
- Circolare del Ministero dei Lavori Pubblici. n. 617 del 2/2/2009 (2009) Istruzioni per l'applicazione delle "Nuove norme tecniche per le costruzioni" di cui al DM 14 gennaio 2008. (in Italian)

- Colombi M., Borzi B., Crowley H., Onida M., Meroni F., Pinho R., 2008. Deriving vulnerability curves using Italian earthquake damage data. *Bulletin of Earthquake Engineering*, 6(3), 485-504.
- Cosenza E., Manfredi G., Polese M., Verderame G.M., 2005. A multi-level approach to the capacity assessment of existing RC buildings. *Journal of Earthquake Engineering*, 9(1), 1-22.
- Crowley H., Colombi M., Borzi B., Faravelli M., Onida M., Lopez M., Polli D., Meroni F., Pinho R., 2009. A comparison of seismic risk maps for Italy. *Bulletin of Earthquake Engineering*, 7(1), 149-190.
- Crowley H., Pinho R., 2004. Period-height relationship for existing european reinforced concrete buildings. *Journal of Earthquake Engineering*, 8(1), 93-119.
- Crowley H., Pinho R., 2006. Simplified equations for estimating the period of vibration of existing buildings. *Proceedings of the 1st European Conference on Earthquake Engineering and Seismology*, Geneva, Switzerland, September 3-8. Paper No. 1122.
- Crowley H., Pinho R., Bommer J.J., 2004. A probabilistic displacement-based vulnerability assessment procedure for earthquake loss estimation. *Bulletin of Earthquake Engineering*, 2(2), 173-219.
- Crowley H., Pinho R., Bommer J.J., Bird, J.F., 2006. Development of a displacement-based method for earthquake loss assessment. *ROSE Research Report No. 2006/01*, IUSS Press, Pavia, Italy.
- Del Gaudio C., Ricci P., Verderame G.M., Manfredi G., 2015. Development and urban-scale application of a simplified method for seismic fragility assessment of RC buildings. *Engineering Structures*. Vol. 91, pp. 40-57. doi:10.1016/j.engstruct.2015.01.031

- Di Pasquale G., Orsini G., 1997. Proposta per la valutazione di scenari di danno conseguenti ad un evento sismico a partire dai dati ISTAT. Atti dell'VIII convegno ANIDIS "L'ingegneria sismica in Italia", Taormina, Italy, September 21-24. Vol. 1, pp. 477–486. (in Italian)
- Di Pasquale G., Orsini G., Romero R.W., 2005. New developments in seismic risk assessment in Italy. Bulletin of Earthquake Engineering, 3(1), 101-128.
- Dolce M., Masi A., Marino M., Vona M., 2003. Earthquake damage scenarios of the building stock of Potenza (southern Italy) including site effects. Bulletin of Earthquake Engineering, 1(1), 115-140.
- Dolce M., Moroni C., 2005. La valutazione della vulnerabilità e del rischio sismico degli edifici pubblici mediante le procedure VC (vulnerabilità c.a.) e VM (vulnerabilità muratura), Atti del Dipartimento di Strutture, Geotecnica, Geologia applicata all'ingegneria, N. 4/2005. (in Italian)
- Faccioli E., Pessina V. (editors), 2000. The Catania project: earthquake damage scenarios for a high risk area in the Mediterranean. CNR-Gruppo Nazionale per la Difesa dai Terremoti, Rome, Italy.
- Faccioli E., Pessina V., Calvi G.M., Borzi B., 1999. A study on damage scenarios for residential buildings in Catania city. Journal of Seismology, 3(3), 327-343.
- Fajfar P., 1999. Capacity spectrum method based on inelastic demand spectra. Earthquake Engineering and Structural Dynamics, 28(9), 979-993.
- FEMA, 2001. HAZUS99 Technical Manual. Service Release 2. Federal Emergency Management Agency, Washington, D.C., USA.
- Giovinazzi S., 2005. The vulnerability assessment and the damage scenario in seismic risk analysis. PhD Thesis, Technical

- University Carolo-Wilhelmina at Braunschweig, Braunschweig, Germany and University of Florence, Florence, Italy.
- Glaister S., Pinho R., 2003. Development of a simplified deformation-based method for seismic vulnerability assessment. *Journal of Earthquake Engineering*, 7(SI1), 107-140.
 - GNDT, 1993. Rischio sismico di edifici pubblici. Parte I: aspetti metodologici. CNR-Gruppo Nazionale per la Difesa dai Terremoti, Rome, Italy.
 - Grant D., Bommer J.J., Pinho R., Calvi G.M., 2006. Defining priorities and timescales for seismic intervention in school buildings in Italy. ROSE Research Report No. 2006/03, IUSS Press, Pavia, Italy.
 - Grünthal G., 1998. Cahiers du Centre Européen de Géodynamique et de Séismologie: Volume 15 – European Macroseismic Scale 1998. European Center for Geodynamics and Seismology, Luxembourg.
 - Haselton, C.B., A.B. Liel, S. Taylor Lange, and G.G. Deierlein (2008). Beam-Column Element Model Calibrated for Predicting Flexural Response Leading to Global Collapse of RC Frame Buildings, PEER Report 2007/03, Pacific Engineering Research Center, University of California, Berkeley, California.
 - Hassan A.F., Sozen M.A., 1997. Seismic vulnerability assessment of low-rise buildings in regions with infrequent earthquakes. *ACI Structural Journal*, 94(1), 31-39.
 - Iervolino I., Manfredi G., Polese M., Verderame G.M., Fabbrocino G., 2007. Seismic risk of R.C. building classes. *Engineering Structures*, 29(5), 813-820.
 - INGV-DPC S1, 2007. Progetto S1. Proseguimento della assistenza al DPC per il completamento e la gestione della mappa di pericolosità sismica prevista dall'Ordinanza PCM 3274 e progettazione di ulteriori sviluppi. Istituto Nazionale di Geofisica

- e Vulcanologia – Dipartimento della Protezione Civile, <http://esse1.mi.ingv.it> (in Italian)
- JBDPA, 1990. Standard for seismic capacity assessment of existing reinforced concrete buildings. Japanese Building Disaster Prevention Association, Ministry of Construction, Tokyo, Japan.
 - Kakaletsis D.J., Karayannis C.G., 2009. Experimental investigation of infilled reinforced concrete frames with openings. *ACI Structural Journal*, 106(2), 132-141.
 - Kappos A.J., Pitilakis K., Stylianidis K.C., 1995. Cost-benefit analysis for the seismic rehabilitation of buildings in Thessaloniki, based on a hybrid method of vulnerability assessment. *Proceedings of the 5th International Conference on Seismic Zonation, Nice, France, October 17-19. Vol. 1*, pp. 406-413.
 - Kappos A.J., Stylianidis K.C., Pitilakis K., 1998. Development of seismic risk scenarios based on a hybrid method of vulnerability assessment. *Natural Hazards*, 17(2), 177-192
 - Kircher C.A., Nassar A.A., Kustu O., Holmes W.T., 1997. Development of building damage functions for earthquake loss estimation. *Earthquake Spectra*, 13(4), 663-682.
 - Kircher C.A., Reitherman R.K., Whitman R.V., Arnold C., 1997. Estimation of earthquake losses to buildings. *Earthquake Spectra*, 13(4), 703-720.
 - Lagomarsino, S., Giovinazzi, S. (2006). "Macroseismic and mechanical models for the vulnerability assessment of current buildings." *Bulletin of Earthquake Engineering*, 4(4), 415-443.
 - Masi A., 2003. Seismic vulnerability assessment of Gravity Load Designed R/C frames. *Bulletin of Earthquake Engineering*, 1(3), 371-395.
 - Masi A., Vona M., 2009. Estimation of the in-situ concrete strength: provisions of the european and italian seismic codes and possible improvements. In: E. Cosenza (editor). *Eurocode 8*

- perspectives from the Italian standpoint workshop. Doppiavoce, Naples, Italy, 2009. ISBN 978-88-89972-16-8. Pp. 67-77.
- Mouroux P., Le Brun B., 2006. Presentation of RISK-UE project. Bulletin of Earthquake Engineering, 4(4), 323-339.
 - Ordaz M., Miranda E., Reinoso E., Pérez-Rocha L.E., 2000. Seismic Loss estimation model for Mexico City. Proceedings of the 12th World Conference on Earthquake Engineering, Auckland, New Zealand, January 30-February 4. Paper No. 1902.
 - Orsini G., 1999. A model for buildings' vulnerability assessment using the Parameterless Scale of Seismic Intensity (PSI). Earthquake Spectra, 15(3), 463-483.
 - Ozdemir P., Boduroglu M.H., Ilki A., 2005. Seismic safety screening method. Proceedings of the International Workshop on Seismic Performance Assessment and Rehabilitation of Existing Buildings (SPEAR), Ispra, Italy, April 4-5. Paper No. 23.
 - Park Y.J., Ang A.H.S., 1985. Mechanistic seismic damage model for reinforced concrete. ASCE Journal of Structural Engineering, 111(4), 722-739.
 - Pinho R., Bomber J.J., Glaister S., 2002. A simplified approach to displacement-based earthquake loss estimation analysis. Proceedings of the 12th European Conference on Earthquake Engineering, London, UK, September 9-13. Paper No. 738.
 - Priestley M.J.N., 1997. Displacement-based seismic assessment of reinforced concrete buildings. Journal of Earthquake Engineering, 1(1), 157-192.
 - Rossetto T., Elnashai A., 2003. Derivation of vulnerability functions for European-type RC structures based on observational data. Engineering Structures, 25(10), 1241-1263.
 - Rossetto T., Elnashai A., 2005. A new analytical procedure for the derivation of displacement-based vulnerability curves for

- populations of RC structures. *Engineering Structures*, 7(3), 397-409.
- Rota, M., A. Penna, and C. L. Strobbia. "Processing Italian damage data to derive typological fragility curves." *Soil Dynamics and Earthquake Engineering* 28.10 (2008): 933-947.
 - Sabetta F., Goretti A., Lucantoni A., 1998. Empirical fragility curves from damage surveys and estimated strong ground motion. *Proceedings of the 11th European Conference on Earthquake Engineering*, Paris, France, September 6-11.
 - Sabetta F., Pugliese A., 1987. Attenuation of peak horizontal acceleration and velocity from Italian strong-motion records. *Bulletin of the Seismological Society of America*, 77(5), 1491-1513.
 - Sabetta F., Pugliese A., 1996. Estimation of response spectra and simulation of nonstationary earthquake ground motions. *Bulletin of the Seismological Society of America*, 86(2), 337-352.
 - Singhal A., Kiremidjian A.S., 1996. Method for probabilistic evaluation of seismic structural damage. *ASCE Journal of Structural Engineering*, 122(12), 1459-1467.
 - Singhal A., Kiremidjian A.S., 1998. Bayesian updating of fragilities with application to RC frames. *ASCE Journal of Structural Engineering*, 124(8), 922-929.
 - Spence R.J.S., Coburn A.W., Sakai S., Pomonis A., 1991. A parameterless scale of seismic intensity for use in the seismic risk analysis and vulnerability assessment. *International Conference on Earthquake, Blast and Impact*, Manchester, UK, September 19-20. Pp. 19-30.
 - Verderame G.M., De Luca F., Ricci P., Manfredi G., 2010. Preliminary analysis of a soft storey mechanism after the 2009 L'Aquila earthquake. *Earthquake Engineering and Structural Dynamics*. DOI: 10.1002/eqe.1069

- Verderame G.M., Manfredi G., Frunzio G., 2001. Le proprietà meccaniche dei calcestruzzi impiegati nelle strutture in cemento armato realizzate negli anni '60. Atti del X congresso nazionale ANIDIS "L'ingegneria Sismica in Italia", Potenza-Matera, Italy, September 9-13. (in Italian)
- Verderame G.M., Ricci P., Esposito M., Manfredi G., 2012. STIL v1.0 – Software per la caratterizzazione delle proprietà meccaniche degli acciai da c.a. tra il 1950 e il 2000. ReLUIS, <http://www.reluis.it/>
- Whitman R.V., Anagnos T., Kircher C.A., Lagorio H.J., Lawson R.S., Schneider P., 1997. Development of a national earthquake loss estimation methodology. *Earthquake Spectra*, 13(4), 643-661.
- Whitman R.V., Reed J.W., Hong S.T., 1973. Earthquake Damage Probability Matrices. *Proceedings of the 5th World Conference on Earthquake Engineering*, Rome, Italy, June 25-29. Vol. 2, pp. 2531-2540.
- Yakut A., 2004. Preliminary seismic performance assessment procedure for existing RC buildings. *Engineering Structures*, 26(10), 1447-1461.

Chapter 5

Pettino area: a single-building comparison with observed post-earthquake damage

5.1 Introduction

Among natural disasters, earthquakes represent one of the most unpredictable phenomena even lethal and devastating from the economic and social standpoint. Earthquakes are in fact able to produce effects in spread geographical areas far away from the epicentral areas in which the phenomenon triggers. Obviously the consequences in terms of casualties and in terms of direct and indirect damage to the structures and infrastructures are a function of the degree of urbanization and the demographic level of the affected areas, as well as the quality and type of housing, which is connected substantially to the presence or absence of seismic codes for constructions. Indeed the ten most recent and catastrophic earthquakes of the last 40 years have covered the continent of Asia (China, Pakistan, Iran, Armenia) and Latin America (Peru, Guatemala) representing the mostly developing countries characterized by bad quality of housing ([Guha-Sapir and Vos, 2011](#)).

For this reason there is an increasing interest in the creation of seismic risk maps able to produce on one side damage scenario in order to provide and guide the emergency response and assistance to

people affected by an event seismic, on the other able to allow the identification and delimitation of the areas most prone at risk and to address the planning of seismic upgrading of existing structures and lead a proper building design through the upgrading of technical standards.

In the following, a simplified analytical method for the seismic fragility assessment of Reinforced Concrete buildings at large scale is presented. The proposed method is based on a simulated design procedure to define the structural model and on non-linear static analysis of a simplified structural model based on Shear-Type assumption to evaluate seismic capacity. Damage States are defined according to the observational-based Damage States provided by the European Macroseismic Scale (EMS-98) (Grünthal, 1998). Presence of infills is considered, both taking into account their influence on the structural response and evaluating the damage to such non-structural elements.

Hence the methodology has been used for the assessment of a damage scenario for a sample of 131 buildings located in L'Aquila Municipality. Uncertainties in seismic demand, material characteristics, and capacity models are taken into account through a Monte Carlo simulation technique. Fragility curves are obtained for each building, leading to the evaluation of damage scenario through the values of the PGA from the shake map of the event provided by INGV (<http://shakemap.rm.ingv.it/shake/index.html>).

In fact, a database of 131 reinforced concrete (RC) buildings collected after 2009 L'Aquila earthquake, in the neighborhood of Pettino, has been derived. For each building the outcomes of official usability and damage inspections collected by Italian National Civil Protection right after the event are available. Furthermore additional data about the locationing and plan dimensions of buildings collected during independent field surveys (Polidoro, 2010) have allowed the construction of a geo-referencing database.

The comparison in terms of damage scenario has allowed on one side the validation of the methodology, especially for what concerns the correspondence between the displacement thresholds and the relative damage observed on the individual element, columns and infill panels, on the other side the validation of the results obtained by the application of the methodology.

5.2 Derivation of Building database from Survey form data

The database considered in this study is made of 131 infilled RC MRF frames located in Pettino neighborhood in L'Aquila. Pettino area was very close to the epicenter of the mainshock event of L'Aquila 2009 earthquake. On April 6, 2009 in the area between the Municipalities of Colle Roio, Genzano and Collesalvatore, affecting also most of Central Italy, was recorded by the National Institute of Geophysics and Vulcanology an earthquake of moment magnitude 6.3 M_w , i.e. according to the scale of local magnitude 5.9 M_l . Just after the earthquake survey campaigns of the damage, emergency response and usability of buildings were performed, through the damage inspections form derived from the Italian National Civil Protection ([Baggio et al., 2007](#)).

Hereinafter the damage inspection form is shown and a description of database characteristics are provided.

Just after an earthquake, thousands and thousands of buildings can be damaged and further shocks can occur. Therefore there is firstly the need to make a quickly estimation of damage to buildings, so as to determine the capacity of the structure to withstand further shocks of equal intensity, or to assess the capacity of the structure to withstand the vertical loads in the damaged configuration. At the same time, the inspectors must provide a usability judgment on the building to allow people keep living indoor, in order to reduce the people's discomfort and stop the emergency phase.

For these reasons in most of seismic prone areas in the world, different methodologies are date back to almost the same period, the end of the 1970s and sometimes revised, due to lessons learnt after each destructive earthquake.

In Italy, as reported in (Goretti and Di Pasquale, 2006) a research program aimed at introducing a first level usability and damage inspection form started in 1995, but when 1997 Umbria-Marche earthquake struck, the form was in a preliminary version. The form was then revised and tested after Pollino 1998 earthquake, whereas its final version was published in (Baggio et al., 2007) and reported in (DPCM 8/7/2014).

The aim of usability judgment in the post-earthquake emergency is to supply a safety evaluation of buildings affected by the earthquake, essentially based on an expert judgment and carried out in a short time, based on a simple visual inspection.

The evaluation is essentially based on three fundamental aspects:

- i.definition of the reference earthquake, to which the building must withstand if subjected to a further shock, defined as the maximum intensity resentful to the site during the sequence;
- ii.definition of the vulnerability of the building,
- iii.building damage assessment based on a simple visual inspection (no damage; slight damage; medium-severe damage; very heavy damage and/or collapse).

The inspection form is divided into operative sections. The first three sections give general information to allow identification of the building, in addition to information regarding its geometrical, typological and morphological characteristics. Sections 3 and 4 supply information respectively about the vulnerability of the building and the size and extension of damage due to the earthquake. Section 8 instead reports the outcome of usability that the inspector must provide based on damage to structural and non-structural elements, as well as to damage

resulting from geotechnical conditions and risk arising from external causes.

In particular in section 4 of inspection form the apparent damage observed on the structural (vertical structures, floors, stairs and roofs) and non-structural components (partition and infills) during the survey, being it pre-existent or related to the earthquake. The reference to the infill panels as non-structural elements is exclusively of a formal nature, as it is assumed in the manual that infill panel especially for RC moment resisting frame buildings may modify the resistance and/or the response of the structure.

Furthermore, in addition to providing information about the extent of the damage the inspection form provides also information on its extension, evaluating the percentage of the building affected by each of damage grade (Figure 5-1).

The definition of the observed damage grades is based on the EMS98 scale, including six possible damage grades (from D0-no damage to D5- destruction) referred to the whole building, based on the level and on the extension of structural and non structural damage in the building. Despite that, the inspection form reports 3 damage levels, combining level D2 with D3 and D4 with D5.

Level Extension Component		DAMAGE									
		D4-D5 Very heavy or collapse			D2-D3 Medium or heavy			D1 Slight			D0 Null
		> 2/3	1/3 - 2/3	< 1/3	> 2/3	1/3 - 2/3	< 1/3	> 2/3	1/3 - 2/3	< 1/3	
		A	B	C	D	E	F	G	H	I	
1	Vertical structures	■	■	■	■	■	■	■	■	■	○
2	Horizontal structures	■	■	■	■	■	■	■	■	■	○
3	Stairs	■	■	■	■	■	■	■	■	■	○
4	Roof	■	■	■	■	■	■	■	■	■	○
5	URM Infill walls	■	■	■	■	■	■	■	■	■	○
6	Pre-existing damage	■	■	■	■	■	■	■	■	■	○

Figure 5-1: Damage classification according to (Baggio 2007)

In the following, it is illustrated and discussed in detail how the qualitative EMS-98 description of damage, which reports a detailed damage pattern both for infill panels and RC columns, has been explicitly translated, for each element and for each damage state, to a detailed estimate of the amplitude and extension of the cracks, so as to allow through a simple visual inspection to relate the extension of a crack to a building damage state.

- D1 slight damage: it is a damage that does not affect significantly the capacity of the structure and does not affect the stability of the non-structural elements which could harm to occupants because of their fall. This damage state is related with a slight but widespread damage on the beams (up to 1 mm), a very slight damage on the columns (< 0.5 mm). Regarding the infill it is assumed that this DS corresponds to the first detachment of the infill panel from surrounding RC structure (up to 2 mm) and at a slight diagonal cracking of the panel itself (< 1 mm).
- D2-D3 medium-severe damage: it is a damage that changes significantly the capacity of the structure, which nevertheless does not lead to partial-collapse/collapse of the main structural

components. Despite that the extent of the damage is such that it is possible the falling of non structural objects. This damage state is related to flexural cracks in beams up to 4-5 mm, cracks in columns and in shear walls up to 2-3 mm. Moreover, damage is such as to cause the beginning of buckling of the compressed bars in columns, the spalling of the concrete cover and sometimes to the attainment of residual displacement of columns. At the same time, damage to infill panels at this stage is very severe. Diagonal cracks up to few mm, evident crushing at the corners in contact with the bearing structures and sometimes localised failure of the panel can be observed.

-D4-D5 very heavy damage: it is a damage that significantly modifies the capacity of the structure, which could lead to partial or total collapse of the main structural components.

In the following statistics about geometrical, typological and morphological characteristics, as well as for what concerning the damage of the buildings object of this study. The 131 buildings selected are all regular in plan and elevation and fully infilled according to data reported in post-earthquake inspection forms by Italian National Civil Protection ([Polidoro 2010](#), [De Luca et al., 2014](#)). In Figure 5-3 a general overview of Pettino area in the Municipality of L'Aquila. In the same figure buildings plane shape is shown in addition to Peak Ground Acceleration data according to the evaluation provided by Istituto Nazionale di Geofisica e Vulcanologia,

(<http://shakemap.rm.ingv.it/shake/index.html>).

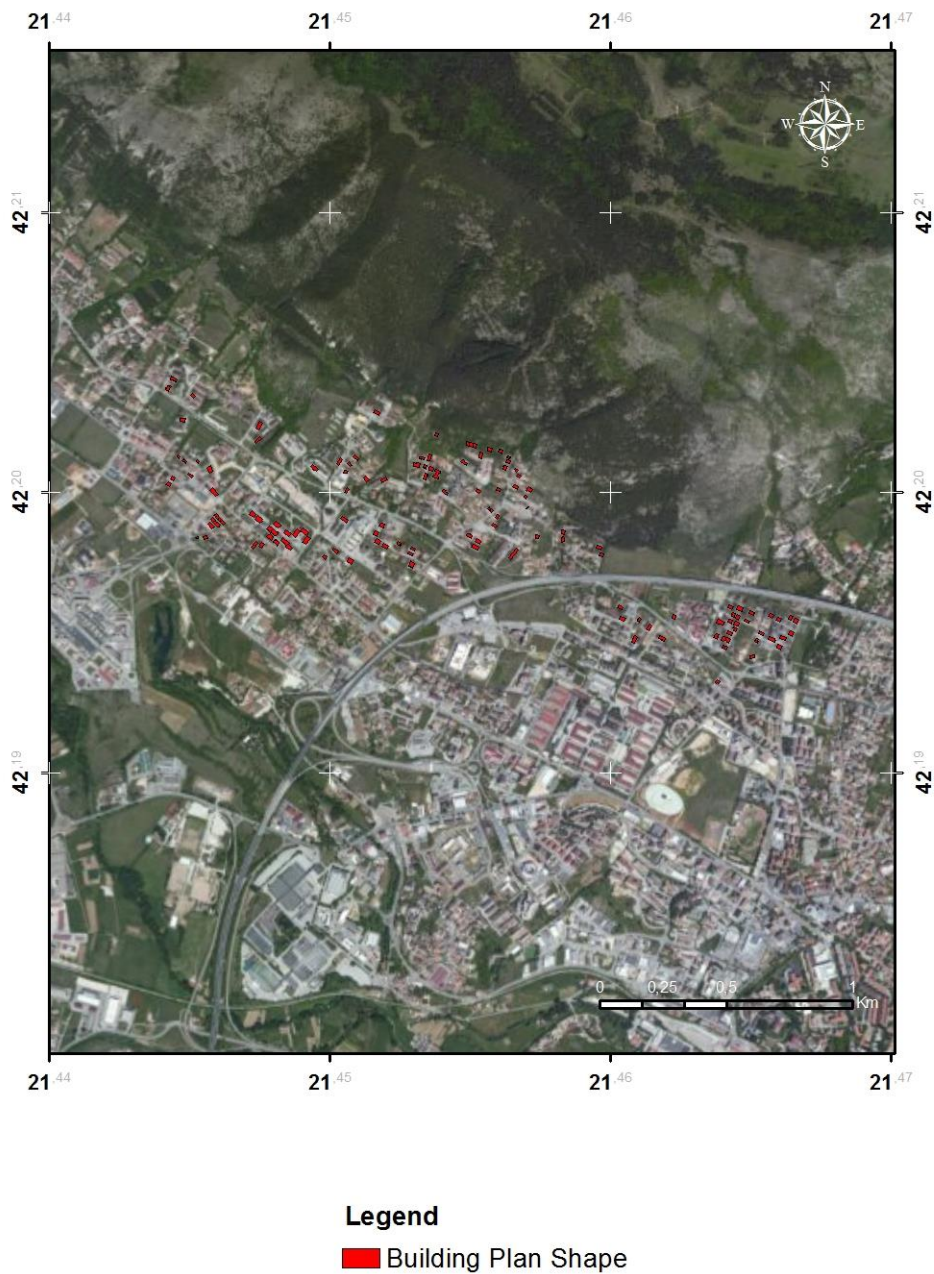


Figure 5-2: Map of Pettino area with indication of building plan area

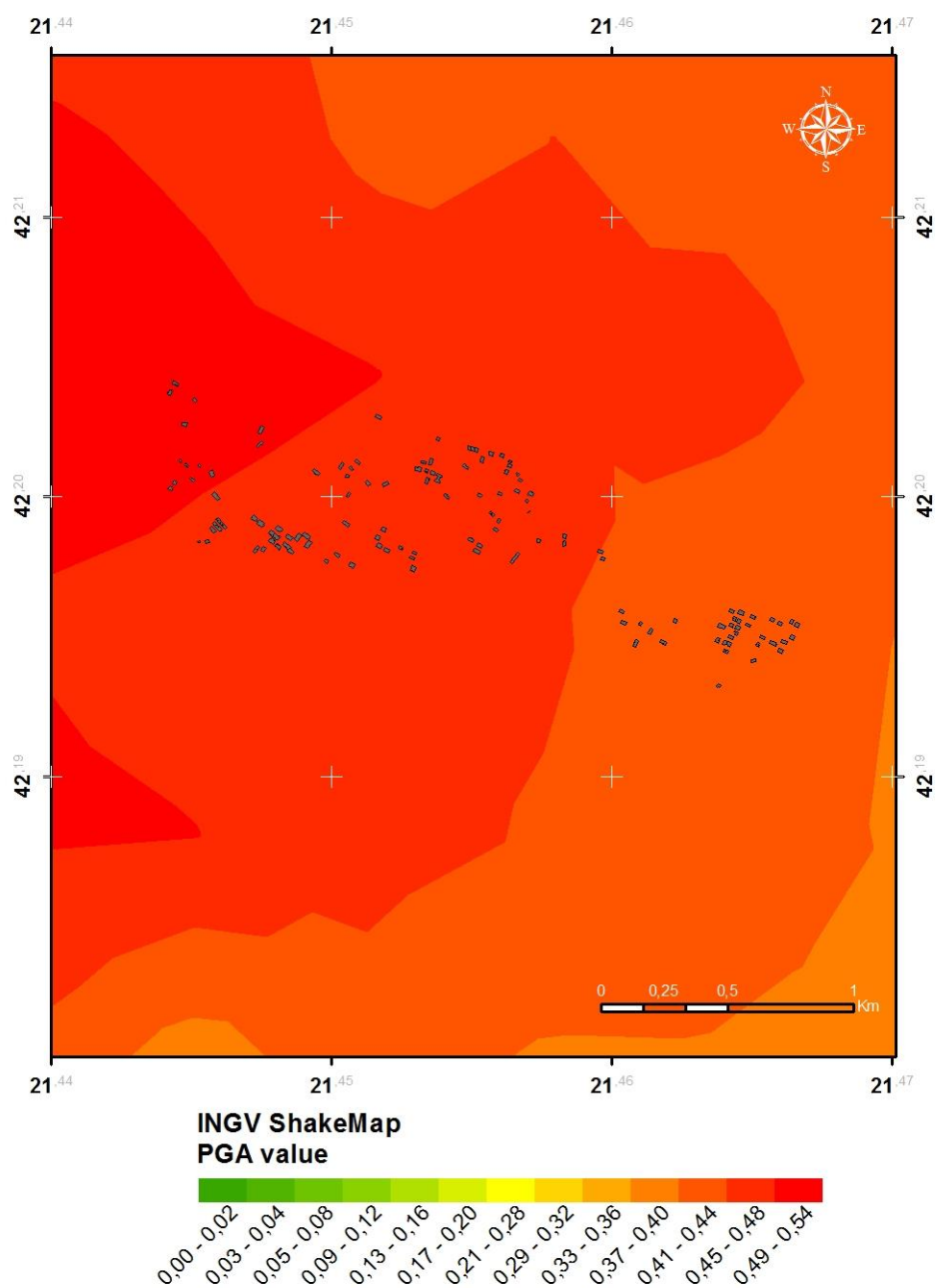


Figure 5-3: Map of Pettino area with indication of building plan area and shake map data according to (<http://shakemap.rm.ingv.it/shake/index.html>).

Moreover from the data specified in Section 2 of the inspection form information about total number of storeys, average storey height and age of construction.

The 131 RC buildings are located in Pettino area in the Municipality of L'Aquila, and are mainly built in the twenty years at the turn of the 70 and 90 (about 75%), have a regular and compact plan and are characterized mainly by a number of floors between 3 and 4 (in about 65% of cases) as shown in Figure 5-7-Figure 5-7.

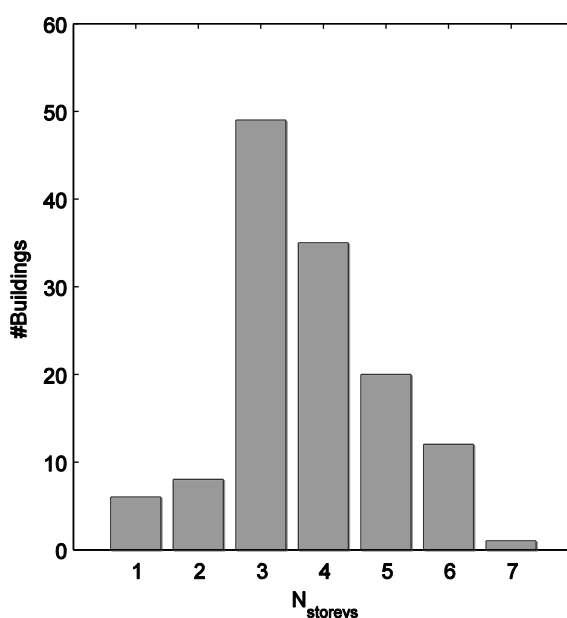


Figure 5-4: Distribution of number of floors for the 131 buildings of database located in Pettino area.

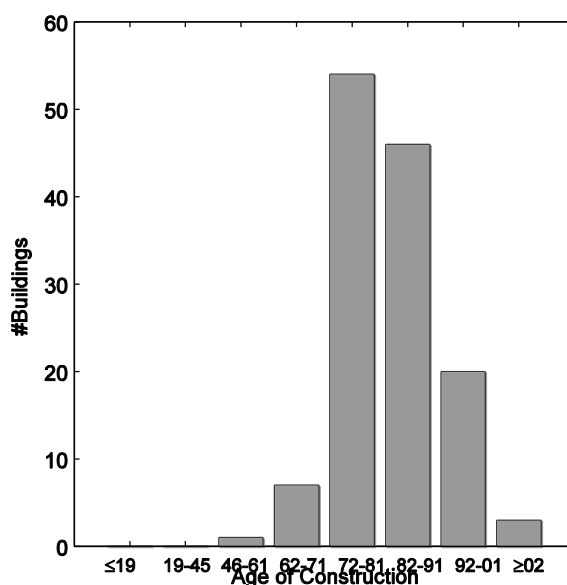


Figure 5-5: Distribution of age of construction for the 131 buildings of database located in Pettino area.

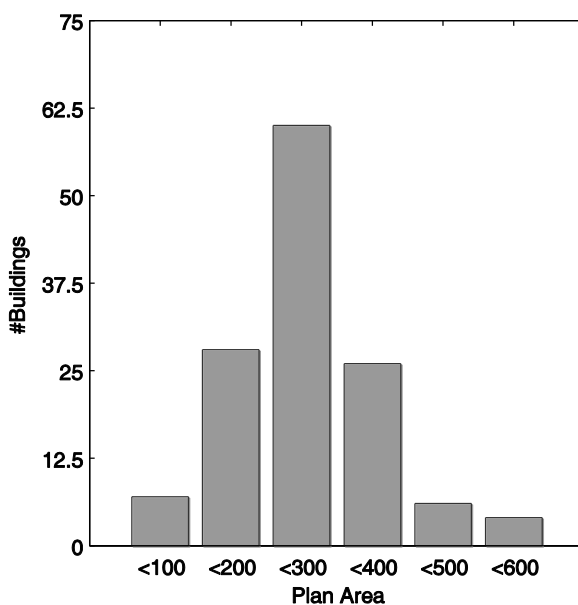


Figure 5-6: Distribution of Plan area for the 131 buildings of database located in Pettino area.

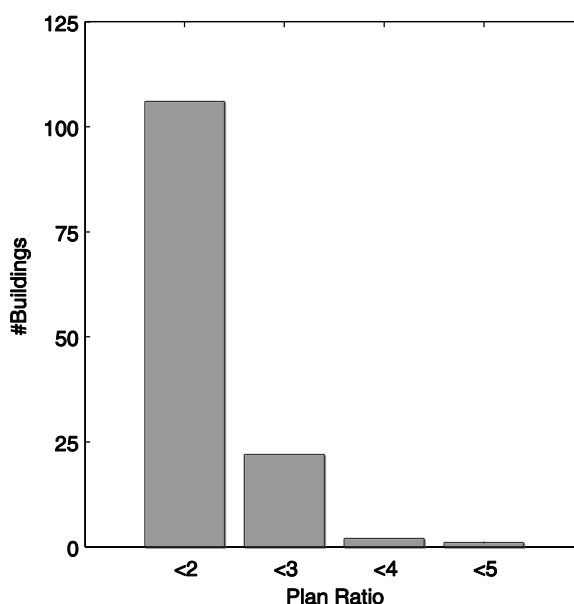
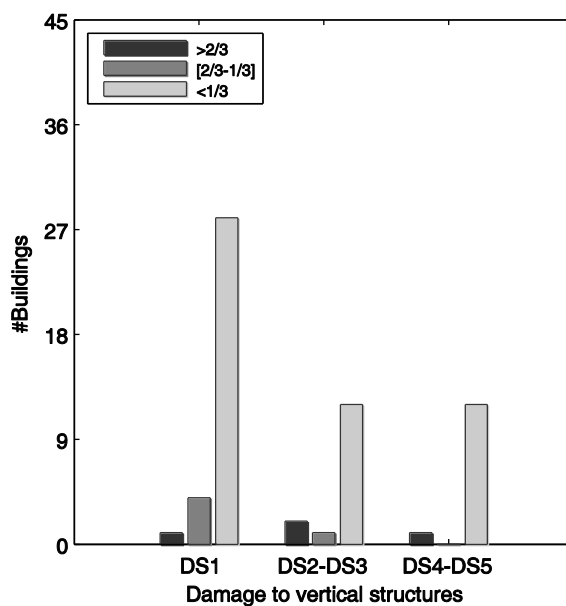
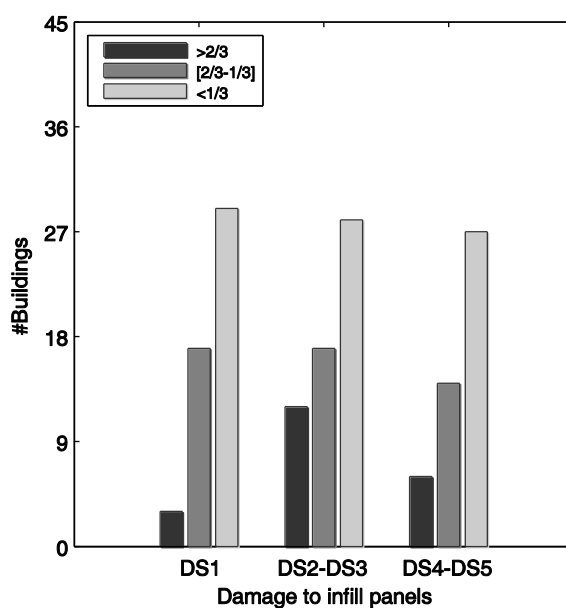


Figure 5-7: Distribution of Building Plan ratio (d) for the 131 buildings of database located in Pettino area.

Furthermore, from the data specified in Section 4 of the inspection form information about damage can be deduced. In particular, in 50% of the buildings is not detected damage to vertical structures, whereas in the remaining cases a concentrated damage is detected, limited to more than one third of the elements, and usually of slight extent (Figure 5-8). Notwithstanding a mainly severe and widespread damage to infill panels can be observed.



(a)



(b)

Figure 5-8: Damage distribution to vertical structures (a) and to infill panels (b) for the 131 buildings of the database deduced from survey (Baggio et al., 2007) with the

indication of the damage extension

Finally, section 8 of the inspection form reports the usability judgments for the surveyed building. It is worth noting that Italian classification has six possible outcomes, see Table 5-1, while in other countries, such as Japan, California, or Greece, only three alternatives are available, see (Goretti and Di Pasquale, 2006). As an example, in California the possible outcomes of usability surveys, not including information on damage, are inspected, restricted use, and unsafe.

The aim of usability judgment in the post-earthquake emergency is to supply a short term safety evaluation of damaged buildings. Thus, a “usable” building is essentially able to withstand a further seismic shock and/or is essentially able to support the gravity loads in the damaged configuration, safeguarding the lives of their occupants. The larger number of outcomes in the Italian forms is aimed at increasing the number of buildings, or some of its parts (see PARTIALLY USABLE in Table 5-1), that can be used with or without short-term countermeasures. The circumstance of limiting the number of buildings unusable aims to end shortly the emergency condition and allow the population to return to their homes and restore normal social functions of affected areas.

Table 5-1: Italian building classification for post-earthquake usability [from Goretti and Di Pasquale (2006)]

A	USABLE	Building can be used without measures. Small damage can be present, but
B	USABLE WITH COUNTERMEASURES	Building has been damaged, but can be used when short term countermeasures
C	PARTIALLY USABLE	Only a part of the building can be safely used
D	TEMPORARY UNUSABLE	Building to be re-inspected in more detail. Unusable until the new inspection
E	UNUSABLE	Building can not be used due to high structural, non-structural or geotechnical
F	UNUSABLE FOR EXTERNAL RISK	Building can be used in relation to its damage level, however it can not be used

The outcome of inspection forms for the database is shown in Figure 5-9. Most of buildings are classified as B and E (usable with countermeasures, and unusable), respectively. Only 12 buildings are classified as A (usable).

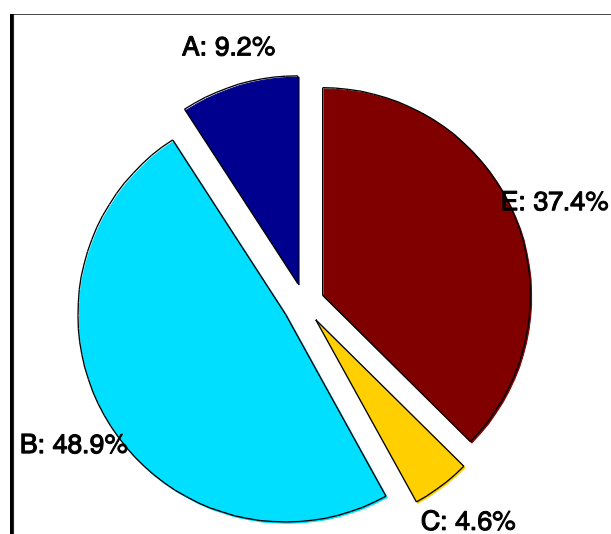


Figure 5-9: Usability outcomes for the 131 buildings of the database deduced from survey form AEDES (Baggio et al., 2007)

Finally, the usability outcome providing information on the safety of the building can therefore be related to the estimation of the monetary losses arising from the strengthening and / or the reconstruction of the building. Indeed, the usability outcome is more related to the economic damage, that to building structural damage.

Therefore, in order to derive a seismic risk scenario from the results of inspection form, it should then refer to structural and non-structural elements damage. It is to be noted that the latter is based on the European Macroseismic Scale EMS98, which includes six possible damage grades (from D0-no damage to D5- destruction) for the building. Hence it is possible to interpret a posteriori the results of inspection form to derive damage grade for the building. In the following, it is illustrated and discussed in detail how to derive damage grade from the observed damage reported in inspection form separately for RC columns and infill panels.

Infill Panel:

- Grade1 – Negligible to slight damage: this condition, corresponding in EMS-98 to fine cracks in infill panels, can be related to DS1, namely to the first detachment of the infill panel from surrounding RC structure (up to 2 mm) and at a slight diagonal cracking of the panel itself (< 1 mm);
- Grade2 – Moderate damage: this condition, corresponding in EMS-98 to cracks in partition and infill walls, can be related to DS2-DS3, defined by diagonal cracks, evident crushing at the corners in contact with the bearing structures and sometimes localised failure of the panel;
- Grade3 – Substantial to heavy damage: this condition, corresponding in EMS-98 to large cracks in partition and infill walls, failure of individual infill panels, can be related to DS4-DS5, defined by the failure of infill panels.
- RC Column. For the definition of EMS-98 Grades starting from RC columns damage reported in inspection forms reference is

made to the scheme reported in (Rota et al, 2007, Dolce et al, 1999):

- Grade1 – Negligible to slight damage: this condition, corresponding in EMS-98 to fine cracks in plaster over frame members, can be related to DS1, represented by a very slight damage on the columns (< 0.5 mm);
- Grade2 – Moderate damage: this condition, corresponding in EMS-98 to cracks in columns, can be related to a damage equal to DS2-DS3 for a limited number of columns (less than 33%);
- Grade3 – Substantial to heavy damage: this condition, corresponding in EMS-98 to Cracks in columns, Spalling of concrete cover, buckling of reinforced rods, coincides with that described in AEDES manual as DS2-DS3. Hence it can be related to a damage equal to DS2-DS3 for a most of columns (at least 33%);
- Grade4 – Very heavy damage: this condition, corresponding in EMS-98 to large cracks in structural elements, can be put in relation with an exacerbation of damage represented by DS4-DS5 for the majority of columns (less than 66%);
- Grade5 – Destruction: this condition, corresponding in EMS-98 to collapse of ground floor or parts of building can be related to a damage equal to DS4-DS5 for all columns (at least 66%).

Therefore, for each building, namely, for each inspection form, a different Grade for RC columns and infill panels can be obtained. The heaviest Grade between the two represents the Grade for the whole building. In Figure 5-10 damage grades outcomes for the 131 buildings are reported. It is to be noted that most of buildings is subject to a damage lies between Grade1 and Grade3 (83%), while only a small percentage in Grade1 (7%) and Grade4 (9%) and a negligible percentage in Grade5 (1%).

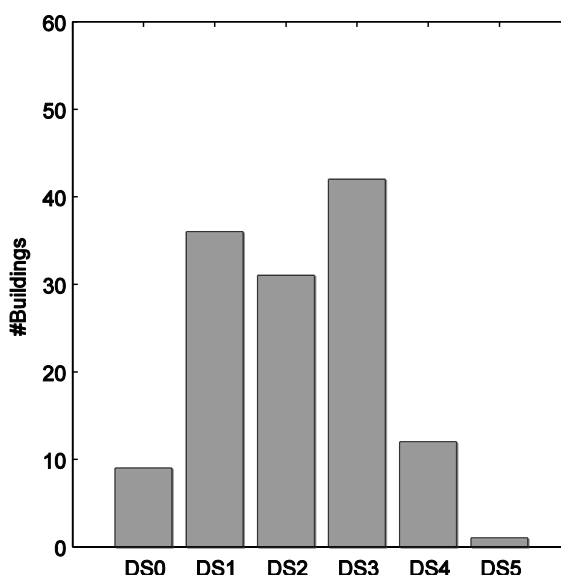


Figure 5-10: Damage State outcomes for the 131 buildings of the database

5.3 Seismic vulnerability methods at large scale

The analysis of the data of the last 100 years shows that there is a reduction in the number of deaths caused by natural disasters, while on the other hand there is an increase in economic losses. This trend persists even considering economic losses normalised to current (as of 2000) US dollars (Scawthorn, 2010). Among the main reasons of these trends there is the concentration of people in large cities as well as the improvements in the quality of buildings, in the emergency management and the medical treatment.

Actually, in the last decades the inhabitants of rural areas move in urban areas, leading to the depopulation of the former and the formation of highly urbanized metropolitan cities. Hence, when natural disasters affect uninhabited territories they produce less loss, but when such phenomena affect a densely populated areas, the result is a catastrophe of enormous dimensions, as occurred with the Haiti earthquake of 2010.

Consequently, there is an increasingly attention to the regional losses models to undertake hazard and risk assessments and to evaluate the economic impact of natural disasters on the territory.

In Italy, the scientific community has made considerable progress in the evaluation of seismic hazard ([INGV-DPC S1, 2007](#)) which allowed the preparation of seismic hazard maps for the whole country for different probabilities of occurrence. This has also affected the evaluation of seismic vulnerability, allowing the creation and development of vulnerability mechanical models. Traditionally, in fact models of seismic vulnerability differ in mechanical and empirical models, or models that use a combination of the two approaches that can be defined hybrid models.

Previously seismic vulnerability models based their development on the diffusion of hazard maps defined in terms of macroseismic damage scale (Medvedev-Sponheuer-Karnik (MSK) scale, European Macroseismic Scale (EMS-98) ([Grünthal et al, 2008](#))).

In fact, these methods are obtained through nonlinear regression analysis from damage data collected during past earthquakes as a function of macroseismics intensity measure, which in turns are obtained from damage itself, resulting an interdependence between macroseismic intensity and observed damage.

The result of this regression is represented by a probability of exceeding of a damage threshold, in discrete form (Damage Probability Matrix) or continuous (vulnerability curves).

Furthermore, the derivation of vulnerability curves requires large quantities of damage data, for the investigated structural typology, for an extended interval of seismic intensity. Nevertheless, the accuracy of empirical methods may be affected by the unavailability of a sufficient database of damage observations, which usually consists of heterogeneous data. Typically, in fact, the most populated class is characterized by the damage data deriving from low-intensity earthquakes.

On the other hand, the mechanical methods provide a direct relationship between seismic intensity and observed damage through the derivation of a model with a direct physical meaning. In the past, mechanical methods were not very developed because the relative computation burden was prohibitive, with reference to the technology of the time.

The advances in technology, greatly reducing the relative computational burden, have made increasingly advantageous the use of such methods. Furthermore, mechanical methods typically require a greater amount of input data with a greater level of detail.

Furthermore, the development of the attenuation laws in terms of spectral ordinates and the corresponding derivation of hazard maps has further promoted the development of mechanical methods. Among these, for example, the so-called capacity-spectrum-based methods (CSM) which rely on the identification of a performance point resulting from the intersection between the capacity curve of an equivalent non linear s.d.o.f. system (obtained from the response curve of the building) and the earthquake demand curve, adequately reduced, both represented in a spectral acceleration versus displacement domain, (Lagomarsino and Giovinazzi, 2006; Borzi et al., 2008).

In particular, the method reported in (Borzi et al., 2008) combines the definition of a pushover curve using a simplified mechanics-based procedure – similar to (Cosenza et al., 2005) – with a displacement-based approach. A set of random variables is defined, including geometrical dimensions, material properties and design loads. Uncertainty in seismic demand is taken into account, too.

In (Cosenza et al., 2005) for each building class, defined as a function of age of construction and number of storeys, a number of building models is generated by means of a simulated design procedure, based on the probabilistic distribution of the structural (geometrical and mechanical) parameters. Seismic capacity is determined in terms of base shear coefficient and global drift for the

determined collapse mechanism. However, in this study no fragility curve is provided. In ([Iervolino et al., 2007](#)) a complete seismic risk assessment framework is presented. In order to investigate the building class capacity, geometrical and mechanical characteristics of the buildings are identified as random variables, and corresponding intervals are assumed. A simulated design procedure and a static pushover analysis are carried out for the generated buildings. Using a Response Surface Method, seismic risk is finally computed considering the number of buildings for which the displacement capacity is exceeded by the displacement demand.

In this Section, vulnerability methods at large scale are used to derive seismic scenario, the latter compared with observed damage resulting from post-earthquake survey through inspection form. In the following mechanical and empirical methods are considered, some of them using the same definition of damage levels adopted herein – that is, EMS-98 damage grades ([Lagomarsino and Giovinazzi, 2006](#), [Rota et al, 2008](#)) and another one deriving the building structural response from a physical model as herein ([Borzi et al., 2008](#)).

First, Rota et al. (2008) provides fragility curves from data on structural damage (the Authors do not explicitly take into account non-structural damage) for about 150000 buildings collected during the main Italian earthquakes of the last 30 years (1980 Irpinia, Abruzzo 1984 Molise 1997 Pollino 1998 Molise 2002). The outcomes of inspection forms have been collected and processed in order to obtain the Damage Probability Matrix (DPMs) and fragility curves for typological classes characteristics of Italian building stock through non-linear regression.

The Authors provide fragility curves for RC buildings as a function of the class of height ($1 \leq N_{storeys} \leq 3$ or $N_{storeys} \geq 4$), and with or without seismic design; nevertheless, due to the reduced amount of data, no fragility curve is provided for RC buildings with seismic design and $N_{storeys} \geq 4$. In particular, building typology is defined as a function of

the age of construction: according to the Authors solely buildings constructed after 1975 in a Municipality classified as Seismic Zone can be considered seismic.

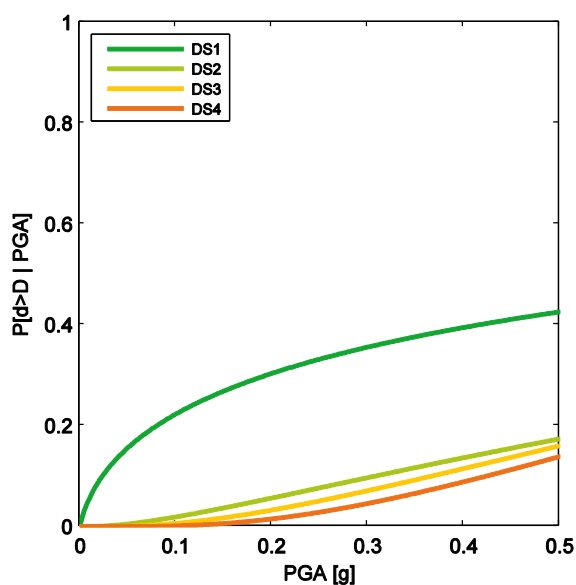


Figure 5-11: Fragility curves provided by (Rota et al., 2008) for low-rise Reinforced Concrete buildings with seismic design.

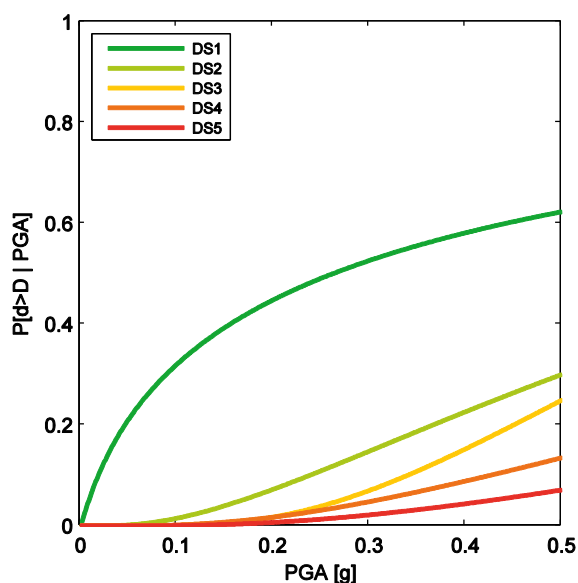


Figure 5-12: Fragility curves provided by (Rota et al., 2008) for low-rise Reinforced Concrete buildings without seismic design.

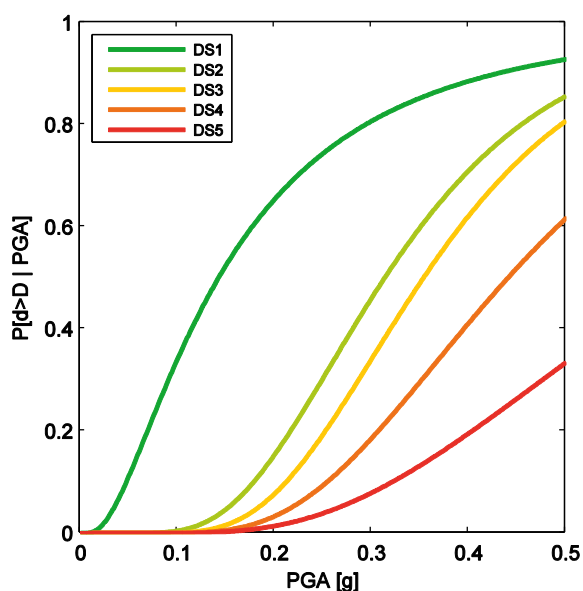


Figure 5-13: Fragility curves provided by (Rota et al., 2008) for high-rise Reinforced Concrete buildings without seismic design.

Figure 5-11 and Figure 5-12 reports fragility curves for low-rise Reinforced Concrete buildings ($N_{storeys} < 4$) with and without seismic design, “RC1” and “RC2” typologies from (Rota et al., 2008) and Figure 5-13 for high-rise Reinforced Concrete buildings ($N_{storeys} \geq 4$) without seismic design “RC4” typology.

Then the Simplified Pushover-Based Earthquake Loss Assessment (SP-BELA) method (Borzi et al., 2008) combines the definition of a pushover curve using a simplified mechanics-based procedure (Cosenza et al., 2005) with the displacement-based framework proposed by (Priestley, 1997; Calvi, 1999) in order to define seismic capacity of building for different limit conditions.

Three limit state conditions have been taken into account: light damage, significant damage and

collapse. In addition a non-structural limit condition referred to infill panels is considered.

- Non-structural Light damage limit state (NSLS): interstorey rotation capacity between 0.1% and 0.3% for driftsensitive partition walls;

- Light damage structural limit state (LS1): The rotation capacity is limited by the chord rotation corresponding to yielding according to (Panagiotakos and Fardis, 2001; Eurocode 8);

Significant damage (LS2) and Collapse damage (LS3): The chord rotation capacity is limited to 3/4 and 4/4, respectively, of the ultimate rotation capacity according to (Panagiotakos and Fardis, 2001; Eurocode 8).

Hence fragility curves are derived from comparison between demand and capacity to define the proportion of buildings of the dataset that survive the considered limit conditions.

Furthermore, SP-BELA has been further developed in order to approximately account for the presence of infill panels in (Borzi et al., 2008b). It is assumed that the panels have an influence on the lateral resistance of the building up to the yield limit state, considering RC

columns and infill panels acting in parallel, the latter with a linear elastic behaviour. Hence, the only way the influence of infill panels is accounted for is that they are assumed to increase the lateral strength of the building up to the yielding of the RC structure.

Figure 5-14 and Figure 5-15 report fragility curves for RC Regularly distributed infill panels buildings non-seismically designed and seismically designed with a lateral force $c=10\%$ respectively, reported with circle marker from (Borzi et al., 2008b) and the relative fitted curves with a lognormal distribution obtained through a nonlinear regression procedure according to procedure reported in (Porter et al., 2007).

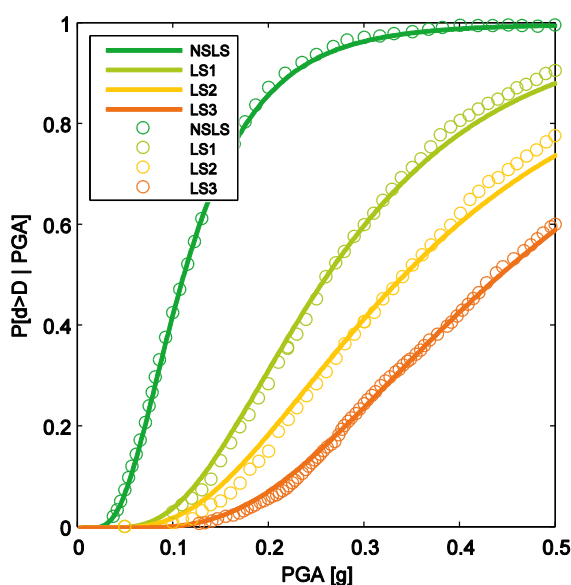


Figure 5-14: Fragility curves provided by (Borzi et al., 2008b) for RC Regularly distributed infill panels buildings non-seismically designed with a lateral force $c=10\%$.

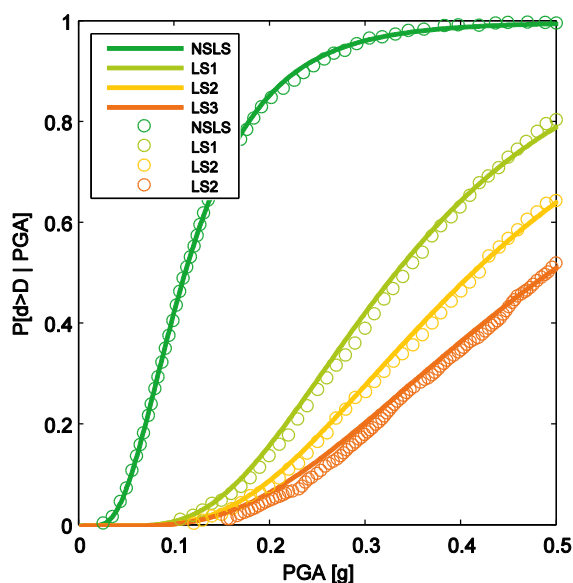


Figure 5-15: Fragility curves provided by (Borzi et al., 2008b) for RC Regularly distributed infill panels buildings seismically designed with a lateral force $c=10\%$.

Finally, Lagomarsino and Giovinazzi (2006) combines a “macroseismic” and a “mechanical” method. In both cases, the adopted building typological classification essentially corresponds to the EMS-98 proposal. Following the macroseismic approach, vulnerability and fragility curves, respectively providing the expected (mean) damage grade for each building class and the probability of having each discrete damage grade as a function of macroseismic intensity, are derived from the DPMs implicitly defined by EMS-98. The mechanical approach is based on CSM, employing bilinear single degree of freedom (SDOF) capacity curves representative of each building class, which are derived from seismic design code lateral-force design requirements, factors like redundancies and conservatism, and the true strength of materials rather than the nominal ones. Hence, fragility curves are derived from the comparison between demand and capacity, the latter defined as a function of capacity curve.

Figure 5-16 and Figure 5-17 reports fragility curves for Low and Medium-Rise Concrete Moment Frames with Earthquake Resistant Design in second seismic category with Low Ductility, “RC1-II_L DCL” and “RC1-II_M DCL” typologies from (Lagomarsino and Giovinazzi, 2006).

In the same figures with the dashed line, fragility curves obtained considering the modifiers of the vulnerability index for soil category B are reported.

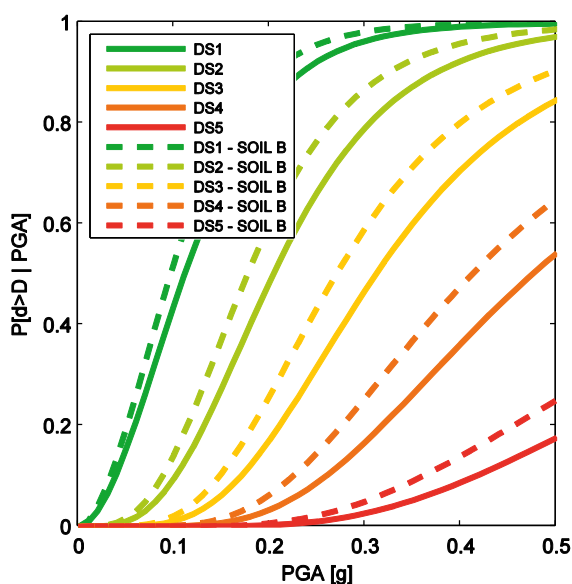


Figure 5-16: Fragility curves provided by (Lagomarsino and Giovinazzi, 2006) for Low-Rise Concrete Moment Frames with ERD in second seismic category with Low Ductility.

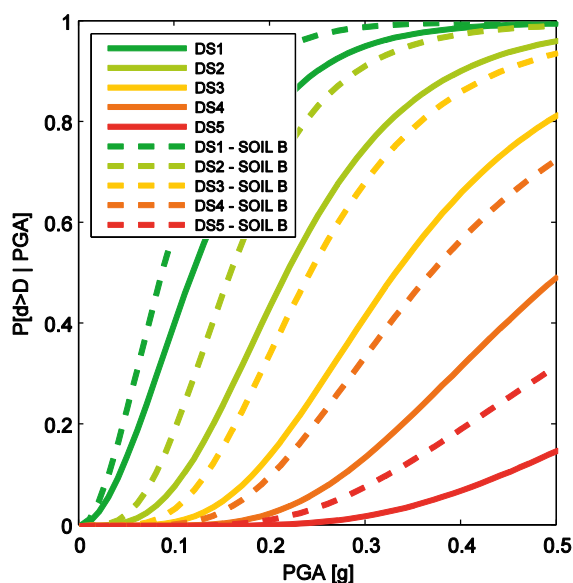


Figure 5-17: Fragility curves provided by ([Lagomarsino and Giovinazzi, 2006](#)) for Medium-Rise Concrete Moment Frames with ERD in second seismic category with Low Ductility.

5.4 Simplified methodology for seismic vulnerability of existing RC buildings: PushOver on Shear Type models (POST)

In the following the Simplified methodologies for seismic vulnerability assessment of building stocks – which has been implemented in POST (PushOver on Shear Type models), a software based on MATLAB® code (Section 3.3, [Ricci, 2010](#), [Del Gaudio et al, 2015](#)) – is recalled. The methodology is based on the following step:

- a simulated design procedure to evaluate the building structural characteristics based on few data such as number of storeys, global dimensions and type of design ([Verderame et al. 2010](#));
- The assumption of a Shear Type behaviour to evaluate in closed form the non-linear static response ([Ricci, 2010](#)).
- The assessment of the seismic capacity is evaluated trough the derivation of a simplified IDA-curve ([Vamvatsikos and Cornell,](#)

2006), leading to the construction of fragility curves and based on the mechanical interpretation of the DSs described by the European Macroseismic Scale (EMS-98) (Grünthal, 1998).

Hence, results from the application of the simplified procedure illustrated in Section 3.3 on rectangular RC buildings in Pettino are illustrated. To this aim, material characteristics (steel, concrete and infills), capacity models for RC members and dispersion of IM given EDP (Vamvatsikos and Cornell, 2006) will be considered as Random Variables.

The reference unit of the procedure is the building.

5.4.1 Input data

The considered buildings are symmetric in plan, both in longitudinal (X) and in transversal (Y) direction. Number of storeys, longitudinal dimension, L_x , and transversal dimension, L_y , in addition to the surface area, have been made available from survey data. Hence, the number of bays in longitudinal and transversal direction is evaluated in correspondence with the value that minimizes the deviation from a target value of the bay length equal to 5 m. Interstorey height is assumed equal to 3.0 m.

The structural model of buildings, located in the Municipality of L'Aquila (42°21'14.43"N 13°23'31.17"E), are defined by means of a simulated design procedure according to code prescriptions and design practices in force at the age of construction. The latter has been derived from AEDES survey form.

(RDL n431/1927) classifies firstly the territory of the Municipality of L'Aquila in II Seismic Category. The classification of the municipality of L'Aquila has remained unchanged over the years, until 2003 when the (OPCM 3274/2003) confirmed the seismic classification in II category, as reported by ECS-it (Figure 5-18), which is a Geographic Information System (GIS) based on MATLAB® code that allows the visualization

and the identification of the evolution of the seismic classification of the Italian territory from 1909 to 2003.

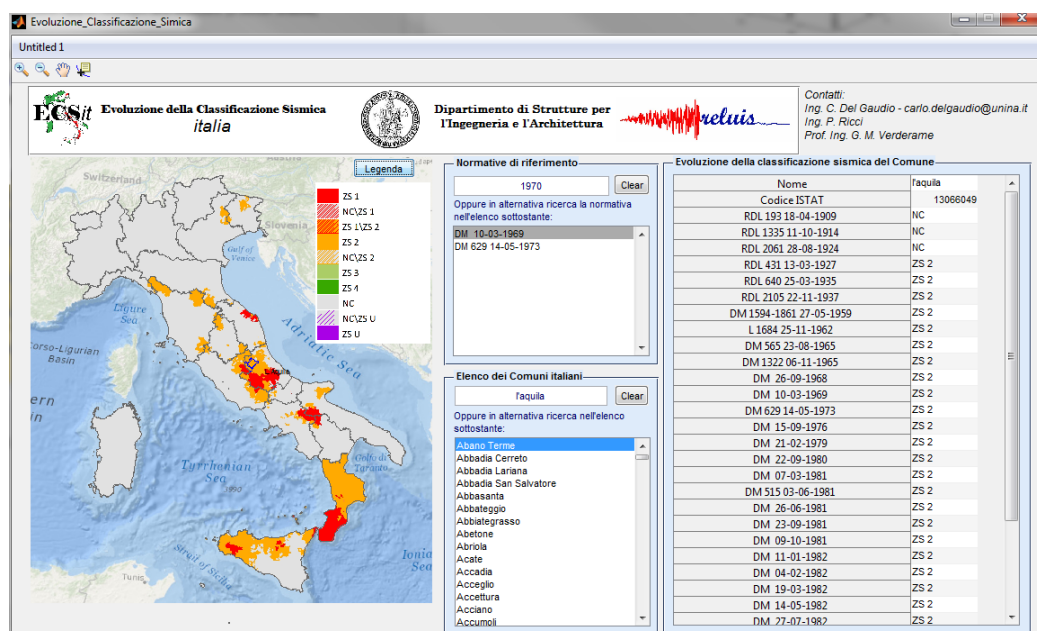


Figure 5-18: Evolution of seismic classification for the Municipality of L'Aquila through ECS-it software based on MATLAB® code (<http://www.reluis.it/>)

Hence for RC Buildings dating back to before 1927 gravitational simulated design procedure has to be considered, whereas buildings constructed afterwards are designed by means of a seismic simulated procedure. For this purpose, it is necessary to assess the corresponding extent and distribution of lateral forces acting on the structure.

(RDL 431/1927) ruled that building, in seismic category II, should be design considering horizontal forces to be applied in structural analysis equal to 1/10 of the corresponding weight for heights up to 15 meters, or equal to 1/8 for higher heights. Later, (RDL 640/1935) ruled a base

shear coefficient equal to 0.07 for buildings located in L'Aquila, whatever the height of the building and the number of floors.

These values were confirmed by ([Law n.1684/1962](#)).

Hence, ([DM 40/1975](#)) ruled that buildings located in seismic category II have been designed according to a seismic intensity parameter $S = 9$, and a corresponding design base shear defined as

$$F = C \cdot W = \frac{S-2}{100} \cdot W = 0.07 \cdot W \quad \text{Eq 5-1}$$

where W was the building weight. Furthermore ([DM 40/1975](#)) introduces a linear force distribution proportional the sum of weight force acting from the basement to considered storey.

Then, element dimensions and element reinforcements are evaluated according to the procedure reported in 3.3.1.

Values of allowable stresses for steel and concrete employed in the simulated design procedure were determined according to the age of construction. As far as concrete is concerned, the allowable concrete stress for bending is assumed equal to

$$\sigma_c = 60 + \frac{R_{ck} - 150}{4} \quad \text{Eq 5-2}$$

Where R_{ck} is the cubic strength of concrete assumed equal to 25MPa in all cases. Hence, allowable compressive stress for axial load combined with bending is assumed equal to $0.7\sigma_c$. Moreover, the concrete allowable stress used to determine column dimensions in the simulated design procedure was multiplied by a coefficient equal to 0.7 in the case of seismic design ([Pecce et al., 2004](#)).

Allowable steel stress ($\sigma_{s,adm}$) was calculated as the weighted average of the values corresponding to different steel typologies in time window corresponding to the surveyed age of construction, depending

on the frequency of occurrence of each typology in this time window, according to the data reported in a statistical analysis of mechanical and typological characteristics of reinforcing steel used in Italy between 1950 and 1980 (Verderame et al., 2010b). For ages of construction above or below these limits, values corresponding to the most widely spread steel typologies in 1950 and 1980 were adopted, respectively, see Table 5-2.

Reinforcing steel typology (smooth or ribbed bars) was also determined as the most frequent typology in the time window corresponding to the surveyed age of construction, according to the data reported in (Verderame et al., 2010b).

Reference values of material properties usually come from statistical analyses of the mechanical characteristics provided by the technical literature. In the following, the choice of the statistical distributions adopted in this work for steel, concrete and infill materials is illustrated. These distributions are selected in order to be representative of the existing Italian building stock, therefore they will be used for the case study developed herein.

In (Verderame et al., 2001; Masi and Vona, 2009) reliable statistics of the compressive strength of concrete used in Italy are presented. In this work, a value of 25 MPa for all ages of construction and a Coefficient of Variation (CoV) of 31% until 1981 has been set, while for buildings constructed after 1981 a CoV of 25% is assumed in order to reflect the higher reliability in the preparation of the concrete.

Statistics on steel yield strength are evaluated through STIL software (Verderame et al., 2012), providing statistics about main mechanical characteristics of steel as a function of few parameters, such as the age of construction and the type of reinforcement (see Table 5-2). The latter is assumed to change with the age of construction: for buildings constructed before 1971 the reinforcement is assumed to be constituted by plain bars and subsequently by deformed bars.

Age	Design	Reinforcement	$\sigma_{s,adm}$ [MPa]	f_y [MPa]	CoV [%]	f_c [MPa]	CoV [%]	E_{inf} [MPa]	CoV [%]
pre-1919	G	plain	140	325	20	25	31	4133	30
1919-45	G	plain	140	325	20				
1946-61	G	plain	173	336	22				
1962-71	G	plain	203	399	18				
1972-81	G	deformed	208	451	13	25	25	4133	30
1982-91	S	deformed	240	466	11				
1992-97	S	deformed	240	466	11				
1998-01	S	deformed	240	466	11				
post-2002	S	deformed	240	466	11				

Table 5-2. Type of design and material properties as a function of the age of construction

Values for infill mechanical characteristics based on the proposal of the Italian code ([Circolare 617, 2009](#)) for hollow clay brick panels have been set. Hence, assuming a full correlation between mechanical characteristics, the ratio between E_w and G_w is assumed equal to 10/3, whereas τ_{cr} is assumed as linearly dependent on G_w , assuming τ_{cr} equal to 0.3 and 0.4 MPa for G_w equal to 1080 and 1620 MPa, respectively. In particular, a value of the elastic modulus equal to 4500 MPa and a CoV of 30% have been adopted.

The influence of openings in decreasing lateral stiffness and strength of infill panels is taken into account through the introduction of control parameters reported in ([Kakaletsis and Karayannis, 2009](#)), according to the procedure extensively discussed in 3.3.2. The opening shape is assumed equal to the 25% of the corresponding infill length, regardless the opening type. The latter is assumed as a random discrete variable, as a function of the three types panel (solid, panel with window and balcony), with a uniform probability distribution. In such a way, considering a facade consisting of three bays, each of them will be characterized by a different opening type, namely solid panel, window opening and door opening.

Finally a thickness of external infill panels equal to 200mm is assumed and an thickness of internal infill panels for each one directions evaluated considering an internal infill percentage, $\rho_{w,int}$ equal to 50% of external one, for further detail see 3.3.2.

Afterwards, a tri-linear envelope is assumed for the moment-rotation model, with cracking and yielding as characteristic points. Behaviour is linear elastic up to cracking and perfectly-plastic after yielding (see Figure 3-6).

Moment at yielding (M_y) is calculated in closed form by means of the first principles-based simplified formulations proposed in proposed in ([Fardis, 2007](#) – Section 3.2.2.2, Eqs. 3.33 to 3.37). Rotation at yielding (θ_y) is univocally identified by M_y and the secant stiffness to yield provided by ([Haselton et al., 2007](#)– Section 3.2.4.1, Eq. 3.1). The

Authors also investigate uncertainty associated with each prediction identified by the logarithmic standard deviation and by the average of the ratio between the observed and predicted values, reported in Table 5-3, assuming that the model parameters follow a lognormal distribution.

Table 5-3: Median and logarithmic standard deviation values of predicted to observed data for RC capacity model (Haselton et al, 2008)

Variable	$\mu_{pred/obs}$	$\beta_{pred/obs}$
EI_y/EI_g	0.95	0.28
M_c/M_y	0.97	0.10
θ_{cap}	1.02	0.54
θ_{pc}	1.00	0.72

Damage States adopted in the proposed analytical methodology are defined according to the damage scale proposed by European Macroseismic Scale (EMS-98) (Grünthal, 1998).

To this aim, analytical displacement thresholds corresponding to the damage to structural and non-structural elements described by EMS-98, based on the mechanical interpretation of the reported description of damage are assumed.

Table 5-4 reports, for each one of the five EMS-98 damage grades, key sentences describing the damage to infills and RC members, respectively, and the corresponding assumed analytical displacement threshold. Note that, due to the assumed Shear-Type behaviour, the interstorey displacement leading to the attainment of each Damage State is the minimum between the values reported in Table 5-4 for infill panels and RC columns.

Damage States		Infill panels		RC columns	
		EMS 98 description	Displacement threshold	EMS 98 description	Displacement threshold
DS1	GRADE 1: Negligible to slight damage	<i>Fine cracks in partitions and infills</i>	Δ_{cr}^{inf}	<i>Fine cracks in plaster over frame members</i>	Δ_{cr}^{RC}
DS2	GRADE 2: Moderate damage	<i>Cracks in partition and infill walls.</i>	Δ_{max}^{inf}	<i>Cracks in columns</i>	Δ_y^{RC}
DS3	GRADE 3: Substantial to heavy damage	<i>Large cracks in partition and infill walls, failure of individual infill panels</i>	Δ_{ult}^{inf}	<i>Spalling of concrete cover, buckling of reinforced rods</i>	$\Delta_{spalling}^{RC}$ $\Delta_{buckling}^{RC}$
DS4	GRADE 4: Very heavy damage	-	-	<i>Large cracks in structural elements with compression failure of concrete and fracture of rebars</i>	First attainment of $\Delta_{collapse}^{RC}$
DS5	GRADE 5: Destruction	-	-	<i>Collapse of ground floor or parts of buildings</i>	Last attainment of $\Delta_{collapse}^{RC}$

Table 5-4. Displacement thresholds at the assumed Damage States, based on the mechanical interpretation of the damage grades described by EMS 98

It is to be noted that the analytical displacement thresholds reported in 3.3.5, corresponding to the damage to non-structural elements described by EMS-98, are assumed to correspond to characteristic point of the corresponding lateral force-displacement response. Displacement threshold at DS1 is assumed to correspond to the end of the initial elastic branch of the lateral force-displacement response (Δ_{cr}^{inf}), whereas displacement threshold at DS2 is assumed to correspond to the maximum resistance point on the backbone of the lateral force-displacement response (Δ_{max}^{inf}). Finally displacement threshold at DS3 is assumed to correspond to the end of the post-peak degrading branch in the lateral force-displacement response (Δ_{ult}^{inf}).

Damage scenario derived from fragility curves, obtained by adopting these displacement thresholds to define the damage to non-structural elements, and from the shake map of event, according to procedure reported in Section 5.5, is reported in Figure 5-19.

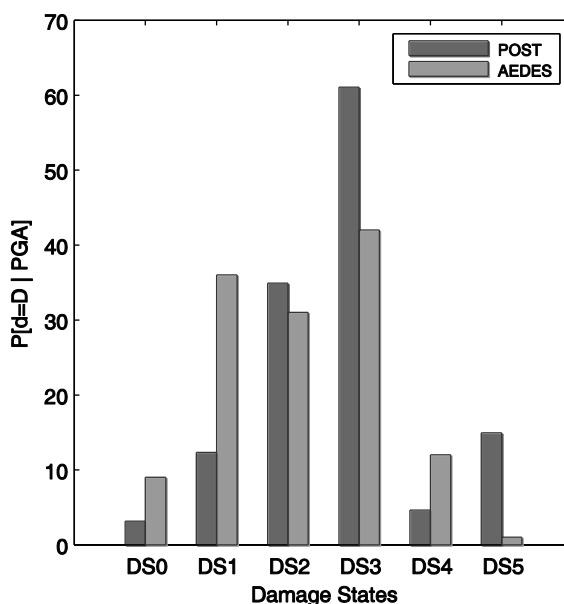


Figure 5-19: Comparison of the damage predicted by POST methodology, obtained by adopting these displacement thresholds to define the damage to non-structural

elements, and observed damage.

This scenario is compared in figure with that derived from observed damage resulting from AEDES inspection forms. It is to be noted that the results produce unsatisfactory results, especially for DS1 and DS3. Actually, predicted damage scenario derived from the assumed displacement thresholds, produces an underestimation of about 65% of the number of buildings characterized by a negligible-slight damage and an overestimation of about 45% of the number of buildings characterized by a substantial-heavy damage.

Note that generally speaking, not necessarily the displacement thresholds, defining the damage to elements must correspond with characteristic points of the corresponding response curve. In this way, alternative approaches to estimate damage to non-structural elements by relating it with the exceeding of proper displacement threshold have been researched.

In particular, Colangelo has extensively dealt with this aspect and in (Colangelo, 2013) probabilistic distributions of the drift at certain degrees of damage to non-structural masonry infills on the basis of the pseudo-dynamic tests on the infilled frames are derived.

Therefore, in the following a parametric analysis for a reference infill panel in order to compare the displacement thresholds corresponding to characteristic point of the lateral force-displacement response with those reported in (Colangelo, 2013) is presented.

In order to derive a probabilistic distribution, a reference infill panel, with geometrical characteristic equal to 3000x5000x200 mm ($H_w \times L_w \times s_w$), and mechanical characteristic obtained as a function of E_w , assumed to follow a lognormal distribution probability function with a mean value of the elastic modulus equal to 4500 MPa and a CoV of 30%. Hence, assuming a full correlation between mechanical characteristics, G_w is assumed equal to 10/3 of E_w , whereas τ_{cr} is assumed as linearly dependent on G_w , assuming τ_{cr} equal to 0.3 and 0.4 MPa for G_w equal to 1080 and 1620 MPa, respectively. In Figure 5-20, with a black line the lateral load-Drift relationship for the median

model can be observed, whereas with gray lines the lateral load-Drift relationships by varying E_w .

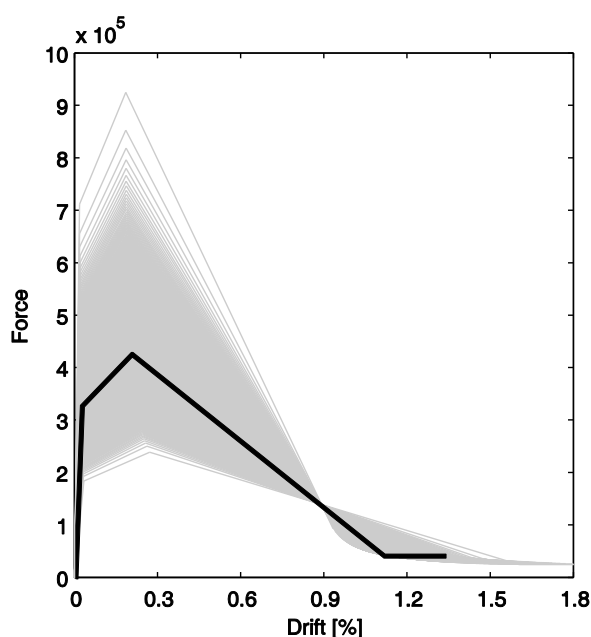


Figure 5-20: Results of parametric analysis on lateral force-displacement relationship for infill panels

It can be observed that the variation of E_w produces a strong variation in strengths but also stiffnesses of the infill behavior, and hence a slight variation in the corresponding drifts.

In Table 5-5 the probabilistic distribution of drift threshold corresponding to the damage to non-structural elements as a consequence of the variation of E_w are reported.

Table 5-5: Definition of infills Drift thresholds.

•	• Mean [%]	• CoV
• DS1	• 0.0236	• 8.82%
• DS2	• 0.2062	• 5.84%
• DS3	• 1.1276	• 8.27%

Furthermore, in Table 5-6, probabilistic distributions of the drift at certain degrees of damage to non-structural masonry infills according to (Colangelo, 2013), are reported.

Table 5-6. Definition of infills Drift thresholds [%] from (Colangelo, 2013).

•	• Mean [%]	• CoV
• 1 st State	• 0,029	• 59,9%
• 2 nd State	• 0,350	• 96,5%
• 3 rd State	• 1,618	• 23,7%

In particular, in Table 5-6 the mean value and Coefficient of Variation of Drift values corresponding to a certain degree of damage to non-structural infill panel are reported. The first row of Table 5-6 can be related to the onset of cracking in the bricks, associated with the first noticeable reduction of stiffness, whereas the second row can be related to moderate cracks before attaining the maximum strength. Finally, third row of Table 5-6 is related to the failure of panel, identified with a damage state in which so many broken bricks that repair is unreasonable.

It can be noted that the mean values and especially the CoVs reported in Table 5-6 are higher than those reported in Table 5-5, corresponding to characteristic point of the infill lateral force-displacement response.

In the following, the mean and CoV values reported in Table 5-6 are assumed to define analytical displacement thresholds, corresponding to the damage to non-structural elements described by EMS-98, and reported in Table 5-4.

Definitely, the methodology described in 3.3.3-3.3.4 is applied, leading to the definition of Nonlinear Static Push-Over (SPO) curve, both in X and Y direction, of a Multi-linearization Curve by applying the equal energy rule, and of simplified Incremental Dynamic Analysis (IDA) curves according to (Vamvatsikos and Cornell, 2006). The latter allow to obtain a relationship between a seismic intensity measure (spectral ordinate) and an Engineering Demand Parameter (ductility).

Finally, Elastic spectra are the Uniform Hazard Newmark-Hall demand spectra provided in (Eurocode (CEN)). Soil type B (as reported in De Luca et al. 2014, Chioccarelli et al. 2009) is assumed. Hence, PGA value is evaluated from the corresponding spectral ordinate evaluated on the IDA-curve as a function of the capacity displacement for each DS according to Table 5-4.

Hence a Monte Carlo simulation is used, and sampling of Random Variables is carried out through the efficient stratified Latin Hypercube Sampling (LHS) technique (McKay et al., 1979), adopting the “median” sampling scheme (Vorechovsky and Novak, 2009). In this way, a population of buildings is generated, each one corresponding to a different set of values of the defined Random Variables (for further details see 3.3.6), regarding (i) Material properties (see Table 5-4), (ii) Capacity models (see table Table 5-3) and (iii) displacement threshold for infill panels (see Table 5-6).

Finally record to record variability can be estimated directly through the dispersion of IM given EDP (Vamvatsikos and Cornell, 2006). Thus, the effect of aleatory randomness can be estimated through SPO2IDA, evaluating IDA-curve-84% and IDA-curve-16%.

Therefore, if PGA capacity, at a given DS, is calculated for all the generated buildings, the corresponding cumulative frequency distributions of the obtained PGA capacity values provide the fragility curves in X and Y directions and at each DS. In the same way fragility curves independent of the direction can be obtained, through the evaluation of the cumulative frequency distribution of the minimum PGA

capacities between longitudinal and transversal direction for each sampling.

Note that the fragility curves were calculated herein for single buildings, whereas the fragility curves reported above (Figure 5-11, Figure 5-12 and Figure 5-13; Figure 5-14 and Figure 5-15; Figure 5-16 and Figure 5-17) are for building classes. Then, *mean* fragility curves (Figure 5-21 and Figure 5-22) are derived for the analyzed buildings, grouping them as a function of number of storeys. Such mean curves are obtained by calculating at each Damage State the mean exceeding probability for all buildings within the class conditioned on PGA. Seismic fragility evaluated on horizontal soil type B.

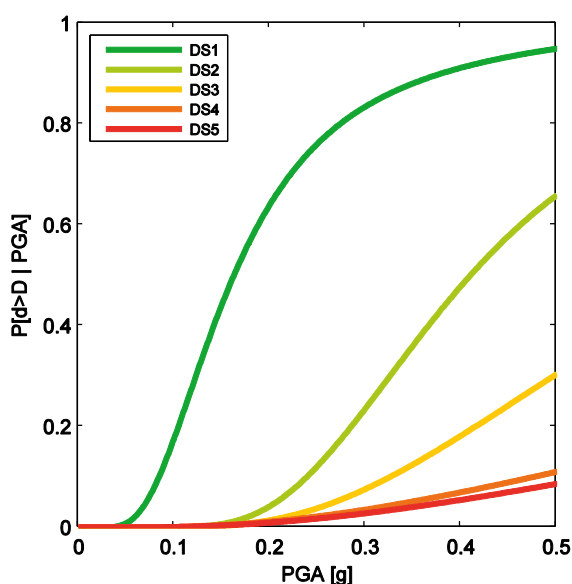


Figure 5-21: Mean fragility curves according to POST Methodology for Low-Rise class for the 131 Buildings of Pettino area.

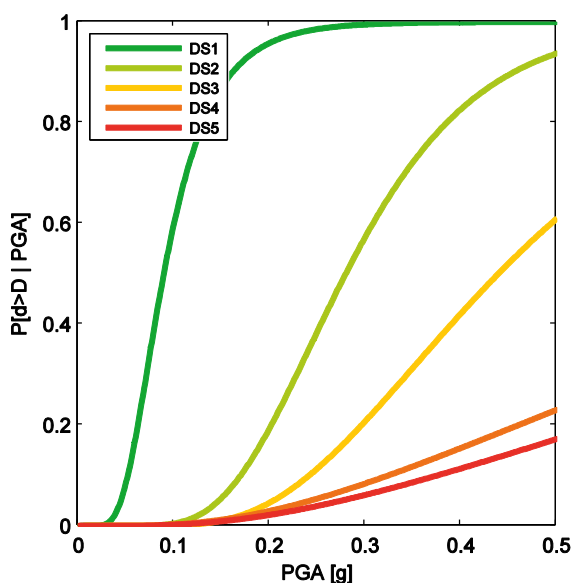


Figure 5-22: Mean fragility curves according to POST Methodology for Medium-Rise class for the 131 Buildings of Pettino area.

5.5 Analysis of results

In this Section, vulnerability methods at large scale are used to derive seismic damage scenario for 131 Buildings located in Pettino area in the Municipality of L'Aquila. In particular mechanical and empirical methods are considered, some of them using the same definition of damage levels adopted herein – that is, EMS-98 damage grades (Lagomarsino and Giovinazzi, 2006, Rota et al, 2008) and another one deriving the building structural response from a physical model as herein (Borzi et al., 2008).

Damage scenarios are derived from fragility curves and from the shake map of the seismic event, which struck the area on 6/4/2009 provided by INGV (<http://shakemap.rm.ingv.it/shake/index.html>).

Each scenario is compared with observed damage resulting from post-earthquake survey through inspection form. Note that fragility curves derived herein are for single buildings, whereas such a

comparison with fragility curves from literature has to be carried out for building classes.

Seismic fragility evaluated on horizontal soil type B is used. Indeed soil type of a station of the National Accelerometric Network (Rete Accelerometrica Nazionale, RAN) in the area was classified according to cross-hole test results as type B, see ([De Luca et al. 2014](#), [Chioccarelli et al. 2009](#)) for more details.

Then a distribution of damage for each building from each DS fragility curve and the value of PGA, evaluated for each building from shake map of the event, can be derived. This distribution detect the probability of building to show each DS used to derive fragility curves, or similarly the percent of building of the population of building characterized by each DS, generated through the set of values of the defined Random Variables used to derive the fragility curve.

Figure 5-23 and Figure 5-24 show the damage distribution for the whole database derived summing up all damage distributions for the 131 buildings. This scenario is compared in figure with that derived from observed damage resulting from post-earthquake survey. It is to be noted the good agreement between the observed and predicted results.

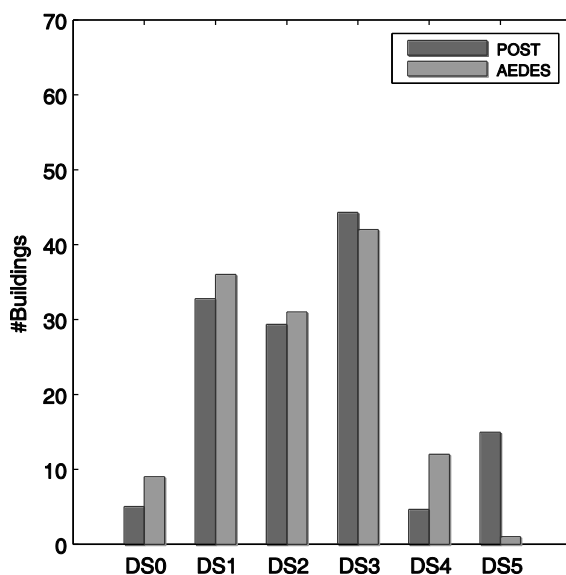


Figure 5-23: Comparison of the cumulative distribution of damage predicted by POST methodology and observed damage.

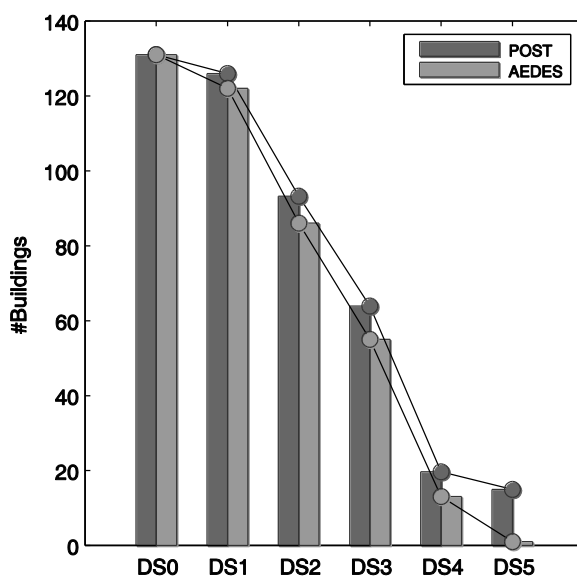


Figure 5-24: Comparison of the cumulative distribution of damage predicted by POST methodology and observed damage.

Similarly damage scenario derived from ([Rota et al., 2008](#), [Lagomarsino and Giovinazzi, 2006](#), [Borzi et al., 2008](#)) are obtained from fragility curves and shake map of the event. Nevertheless, this fragility curves are derived for building classes, defined as a function of structural typology, level of earthquake resistant design and number of storeys.

Figure 5-25 and Figure 5-26 show the comparison between observed damage and damage scenario obtained from fragility curves reported in ([Rota et al., 2008](#)).

It is to be noted that due to the reduced amount of data, no fragility curve is provided for RC buildings with seismic design and $N_{storeys} \geq 4$. Nevertheless, although L'Aquila was classified Seismic Zone for the first time in 1927 according to Royal Decree n°431, only buildings constructed after 1975 can be considered seismic, as reported by Authors. Notwithstanding for high-rise seismic design RC Buildings are assumed for the derivation of damage scenario the fragility curves for high-rise building class without seismic design.

Figure 5-25 and Figure 5-26 report the comparison between observed and predicted damage scenario from ([Rota et al., 2008](#)), resulting in a poor agreement between the results. In effect the predicted damage scenario is extremely conservative for the heaviest damages and at the same time not very cautionary for what concerning the absence of damage.

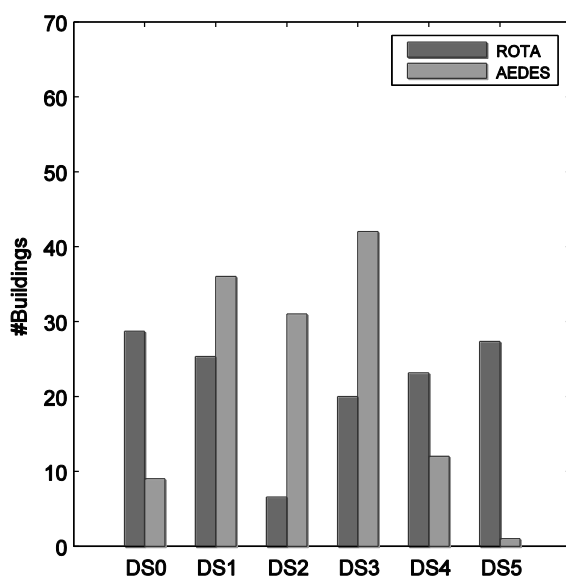


Figure 5-25: Comparison of the distribution of damage predicted by (Rota et al., 2008) methodology and observed damage.

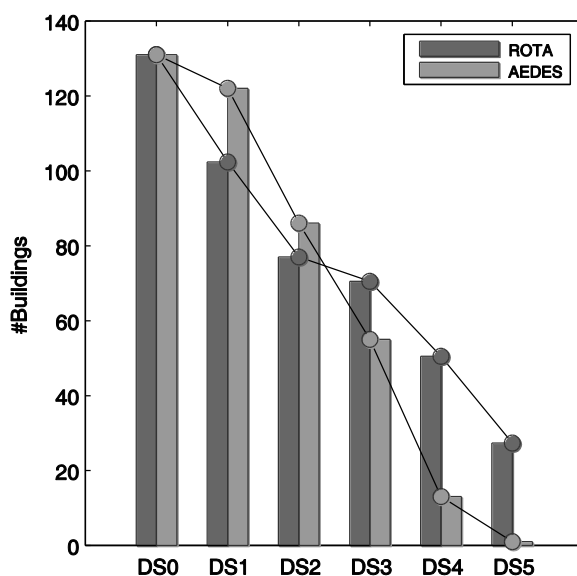


Figure 5-26: Comparison of the cumulative distribution of damage predicted by (Rota et al., 2008) methodology and observed damage.

Figure 5-27 and Figure 5-28 reports the comparison between observed and predicted damage scenario from (Lagomarsino and Giovinazzi, 2006), resulting in a poor agreement between the results, as the predicted damage results extremely conservative.

Damage scenario is derived using Low and Medium-Rise Concrete Moment Frames with Earthquake Resistant Design in second seismic category with Low Ductility, “RC1-II_L DCL” and “RC1-II_M DCL” typologies for soil type B.

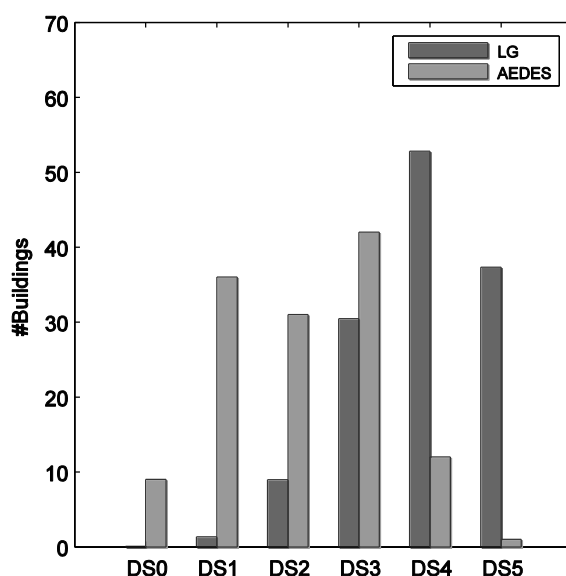


Figure 5-27: Comparison of the distribution of damage predicted by (Lagomarsino and Giovinazzi, 2006) methodology and observed damage.

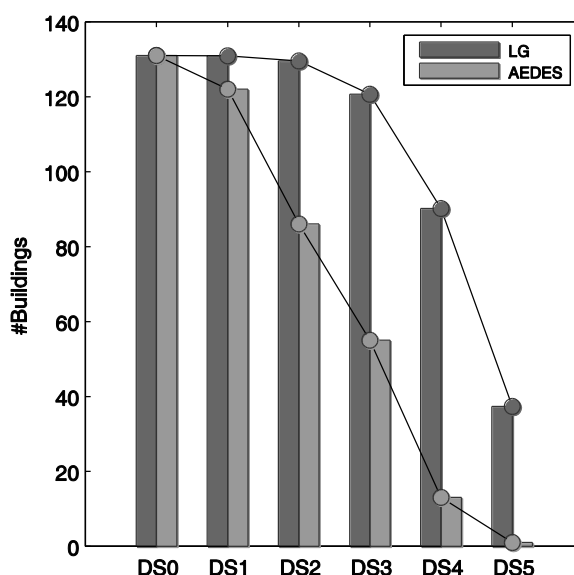


Figure 5-28: Comparison of the cumulative distribution of damage predicted by (Lagomarsino and Giovinazzi, 2006) methodology and observed damage.

Finally, in order to make a comparison between observed and predicted damage scenario from (Borzi et al., 2008b), it has to be defined a correspondence between limit states presented by Authors and the corresponding damage grades dell'EMS-98. Indeed as highlighted in previous section, Authors define displacement thresholds related to technical code (DM 14/1/2008, Eurocode (CEN 2003)), unlike this work where displacement thresholds have been set using the definition of EMS-98 damage Grade.

Table 5-7 shows the corresponding between displacement thresholds, EMS-98 damage Grade and AEDES damage states. Second column reports the interpretation a posteriori of the results of inspection form to derive damage grade for the damaged building from (Rota et al., 2008). Third column reports the correspondence assumed between analytical displacement threshold assumed in this work and EMS-98 damage Grade. Fifth column reports the damage limit states

identified on the capacity curve as a function of the yielding and of the ultimate displacements from (Lagomarsino and Giovinazzi, 2006).

In the following, it is illustrated and discussed in detail how limit states from (Borzi et al., 2008b) can be translated into EMS-98 damage grades:

- Non-structural Light damage limit state (NSLS): defined corresponding to an interstorey rotation capacity between 0.1% and 0.3% for drift sensitive partition walls, which in (Colangelo, 2013) is related to a moderate damage prior to the achievement of the peak resistance of infill panel;
- Light damage structural limit state (LS1): defined corresponding to yielding chord rotation (Panagiotakos and Fardis, 2001; Eurocode 8), can be related to a moderate damage of vertical structures;
- Significant damage (LS2): defined corresponding to 3/4 of ultimate chord rotation (Panagiotakos and Fardis, 2001; Eurocode 8). As ultimate displacement capacity can be related conventionally to a 20% drop of peak resistance on force-displacement envelope, 3/4 of ultimate displacement capacity can be approximately related to peak resistance, corresponding to concrete cover spalling and bar buckling of longitudinal bars phenomena, namely EMS-98 heavy damage.

EMS-98	AEDES Inspection form		POST		Borzi		L&G
	Infills	RC Columns	Infills	RC Columns	Infills	RC Columns	
Grade1	DS1 <1/3 DS1 1/3-2/3 DS1 >2/3	DS1 <1/3 DS1 1/3-2/3 DS1 >2/3	Δ_{cr}^{inf}	Δ_{cr}^{RC}	NSLS	LS1	0.7 Δ_y
Grade2	DS2-DS3 <1/3 DS2-DS3 1/3-2/3 DS2-DS3 >2/3	DS2-DS3 <1/3 DS2-DS3 1/3-2/3 DS2-DS3 >2/3	Δ_{max}^{inf}	Δ_y^{RC}			1.5 Δ_y
Grade3	DS4-DS5 <1/3 DS4-DS5 1/3-2/3 DS4-DS5 >2/3	DS2-DS3 1/3-2/3 DS2-DS3 >2/3	Δ_{ult}^{inf}	$\Delta_{spalling}^{RC}$ $\Delta_{buckling}^{RC}$		LS2	0.5 ($\Delta_y + \Delta_u$)
Grade4		DS4-DS5 <1/3 DS4-DS5 1/3-2/3		$\Delta_{collapse}^{RC1}$			Δ_u
Grade5		DS4-DS5 >2/3		$\Delta_{collapse}^{RC2}$			
1: first attainment							
2: Last attainment							

Table 5-7: The equivalence in the association of Damage States between EMS98 and investigated methodologies (POST; Rota et al., 2008; Lagomarsino and Giovinazzi, 2006; Borzi et al., 2008b)

Figure 5-29 reports the comparison between observed and predicted damage scenario from (Borzi et al., 2008b), resulting in a quite-good agreement between the results, although it does not allow the definition of the Heaviest damage and collapse of building.

Damage scenario is derived using RC Regularly distributed infill panels buildings non-seismically designed and seismically designed with a base shear coefficient $C=0.10$ respectively.

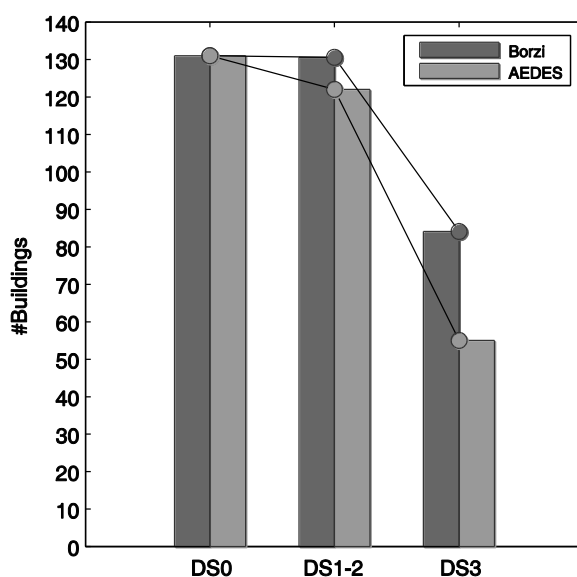


Figure 5-29: Comparison of the damage predicted by (Borzi et al., 2008b) methodology and observed damage.

5.6 Summary of remarks

In this section, the results of the application of a simplified analytical methodology for large scale seismic fragility assessment of RC buildings are shown.

The methodology, implemented in POST (PushOver on Shear Type models), a software based on MATLAB® code (Chapter 3, Ricci, 2010, Del Gaudio et al, 2015), accounts explicitly for the damage to structural and non-structural (infill) elements.

Then, the methodology has been used for the assessment of a damage scenario for a sample of 131 buildings located in L'Aquila Municipality. Uncertainties in seismic demand, material characteristics, and capacity models are taken into account through a Monte Carlo simulation technique. Fragility curves are obtained for each building, leading to the evaluation of damage scenario through the values of the PGA from the shake map of the event provided by INGV.

The database has been made of 131 RC buildings collected after 2009 L'Aquila earthquake, in the neighborhood of Pettino. For each building the outcomes of official usability and damage inspections collected by Italian National Civil Protection right after the event are available. Furthermore additional data about the locationing and plan dimensions of buildings collected during independent field surveys ([Polidoro, 2010](#)) have allowed the construction of a geo-referencing database.

The methodology is applied to the database and a comparison between predicted and observed damage is shown. The comparison has allowed the validation of the methodology, especially for what concerns the correspondence between the displacement thresholds and the relative damage observed on the individual element, columns and infill panels.

The comparison shows a generally good agreement between predicted and observed damage. Such a kind of comparison is of fundamental importance in validation of an analytical methodology aimed at large scale applications.

5.7 References

- Baggio C, Bernardini A, Colozza R, Coppari S, Corazza L, Della Bella M, Di Pasquale G, Dolce M, Goretti A, Martinelli A, Orsini G, Papa F, Zuccaro G (2007) Field manual for post-earthquake damage and safety assessment and short term countermeasures (Pinto A, Taucer F eds), Translation from Italian: Goretti A, Rota M, JRC Scientific and Technical Reports, EUR 22868 EN-2007
- Borzi B., Pinho R., Crowley H., 2008a. Simplified pushover-based vulnerability analysis for large scale assessment of RC buildings. *Engineering Structures*, 30(3), 804-820.
- Calvi GM. A displacement-based approach for vulnerability evaluation of classes of buildings. *Journal of Earthquake Engineering* 1999;3(3):411–38.
- CEN (2005) Eurocode 8: design of structures for earthquake resistance—Part 3: assessment and retrofitting of buildings. European Standard EN 1998-3:2005. Comité Européen de Normalisation, Brussels.
- Chioccarelli E, De Luca F, Iervolino I (2009) Preliminary study on L'Aquila earthquake ground motion records, V5.20. <http://www.reluis.it/>
- Circolare del Ministero dei Lavori Pubblici. n. 617 del 2/2/2009 (2009) Istruzioni per l'applicazione delle "Nuove norme tecniche per le costruzioni" di cui al DM 14 gennaio 2008. (in italian)
- Cosenza E., Manfredi G., Polese M., Verderame G.M., 2005. A multi-level approach to the capacity assessment of existing RC buildings. *Journal of Earthquake Engineering*, 9(1), 1-22.
- Del Gaudio C., Ricci P., Verderame G.M., Manfredi G., 2015. Development and urban-scale application of a simplified method for seismic fragility assessment of RC buildings.

- Engineering Structures. Vol. 91, pp. 40-57.
doi:10.1016/j.engstruct.2015.01.031
- De Luca, Flavia, Gerardo M. Verderame, and Gaetano Manfredi.
"Analytical versus observational fragilities: the case of Pettino (L'Aquila) damage data database." *Bulletin of Earthquake Engineering* (2014): 1-21.
 - Decreto Del Presidente Del Consiglio Dei Ministri 8 luglio 2014.
Istituzione del Nucleo Tecnico Nazionale (NTN) per il rilievo del danno e la valutazione di agibilità nell'emergenza post-sismica e approvazione dell'aggiornamento del modello per il rilevamento dei danni, pronto intervento e agibilità per edifici ordinari nell'emergenza post-sismica e del relativo manuale di compilazione. GU Serie Generale n.243 del 18-10-2014. (in Italian)
 - Decreto Ministeriale del 14/1/2008 (2008) Approvazione delle nuove norme tecniche per le costruzioni. G.U. n. 29 del 4/2/2008 (in Italian)
 - Decreto Ministeriale del 24/1/1986 (1986) Istruzioni relative alla normativa tecnica per le costruzioni in zona sismica. G.U. n. 108 del 12/5/1986 (in Italian)
 - Decreto Ministeriale n. 40 del 3/3/1975 (1975) Approvazione delle norme tecniche per le costruzioni in zone sismiche. G.U. n. 93 dell'8/4/1975 (in Italian)
 - Goretti A, Di Pasquale G (2006) Technical emergency management. In: Oliveira CS, Roca A, Goula X (eds) *Assessing and managing earthquake risk*, chapter 16. Springer
 - Grünthal G., 1998. *Cahiers du Centre Européen de Géodynamique et de Séismologie: Volume 15 – European Macroseismic Scale 1998*. European Center for Geodynamics and Seismology, Luxembourg.
 - Guha-Sapir D., Vos F., 2011. Earthquakes, an epidemiological perspective on patterns and trends. In: Spence R., So E.,

- Scawthorn C. (editors). Human Casualties in Earthquakes. Advances in Natural and Technological Hazards Research. Springer Science+Business Media B.V. 2011. DOI 10.1007/978-90-481-9455-1_2.
- Haselton, C.B., A.B. Liel, S. Taylor Lange, and G.G. Deierlein (2008). Beam-Column Element Model Calibrated for Predicting Flexural Response Leading to Global Collapse of RC Frame Buildings, PEER Report 2007/03, Pacific Engineering Research Center, University of California, Berkeley, California.
 - Iervolino I., Manfredi G., Polese M., Verderame G.M., Fabbrocino G., 2007. Seismic risk of R.C. building classes. Engineering Structures, 29(5), 813-820.
 - INGV-DPC S1 (2007). "Progetto S1. Proseguimento della assistenza al DPC per il completamento e la gestione della mappa di pericolosità sismica prevista dall'Ordinanza PCM 3274 e progettazione di ulteriori sviluppi." Istituto Nazionale di Geofisica e Vulcanologia – Dipartimento della Protezione Civile, <http://esse1.mi.ingv.it> (in Italian)
 - Kakaletsis D.J., Karayannis C.G., 2009. Experimental investigation of infilled reinforced concrete frames with openings. ACI Structural Journal, 106(2), 132-141.
 - Lagomarsino, S., Giovinazzi, S. (2006). "Macroseismic and mechanical models for the vulnerability assessment of current buildings." Bulletin of Earthquake Engineering, 4(4), 415-443.
 - Masi A., Vona M., 2009. Estimation of the in-situ concrete strength: provisions of the european and italian seismic codes and possible improvements. In: E. Cosenza (editor). Eurocode 8 perspectives from the Italian standpoint workshop. Doppiavoce, Naples, Italy, 2009. ISBN 978-88-89972-16-8. Pp. 67-77.
 - Ordinanza del Presidente del Consiglio dei Ministri n. 3274 del 20/3/2003 (2003) Primi elementi in materia di criteri generali per la classificazione sismica del territorio nazionale e di

- normative tecniche per le costruzioni in zona sismica. G.U. n. 105 dell'8/5/2003 (in Italian)
- Polidoro B (2010) MSc Thesis. La valutazione della vulnerabilità sismica: il caso di Pettino (AQ), University of Naples Federico II. Advisors: Manfredi G, Iervolino I, Martinelli A, Verderame GM. <http://wpage.unina.it/iuniervo> (in Italian).
 - Priestley MJN. Displacement-based seismic assessment of reinforced concrete buildings. Journal of Earthquake Engineering 1997;1:157–92.
 - Regio Decreto Legge n. 2105 del 22/11/1937 (1937) Norme tecniche di edilizia con speciali prescrizioni per le località colpite dai terremoti. G.U. n. 298 del 27/12/1937 (in Italian)
 - Regio Decreto Legge n. 431 del 13/3/1927 (1927) Norme tecniche ed igieniche di edilizia per le località colpite dai terremoti. G.U. n. 82 dell'8/4/1927 (in Italian)
 - Regio Decreto Legge n. 573 del 29/4/1915 (1915) Che riguarda le norme tecniche ed igieniche da osservarsi per i lavori edilizi nelle località colpite dal terremoto del 13 gennaio 1915. G.U. n. 117 dell'11/5/1915 (in Italian)
 - Regio Decreto Legge n. 640 del 25/3/1935 (1935) Nuovo testo delle norme tecniche di edilizia con speciali prescrizioni per le località colpite dai terremoti. G.U. n. 120 del 22/5/1935 (in Italian)
 - Regio Decreto Legge n. 682 del 3/4/1930 (1930) Nuove norme tecniche ed igieniche di edilizia per le località sismiche. G.U. n. 133 del 7/6/1930 (in Italian).
 - Rossetto, T., and Elnashai A., 2003. "Derivation of vulnerability functions for European-type RC structures based on observational data." Engineering structures 25.10: 1241-1263.
 - Rota, M., A. Penna, and C. L. Strobbia. "Processing Italian damage data to derive typological fragility curves." Soil Dynamics and Earthquake Engineering 28.10 (2008): 933-947.

- Scawthorn C., 2011, Disaster Casualties – Accounting for Economic Impacts and Diurnal Variation. In: Spence R., So E., Scawthorn C. (editors). Human Casualties in Earthquakes. Advances in Natural and Technological Hazards Research. Springer Science+Business Media B.V. 2011. DOI 10.1007/978-90-481-9455-1_2.
- Vamvatsikos D., Cornell C.A., 2006. Direct estimation of the seismic demand and capacity of oscillators with multi-linear static pushovers through IDA. Earthquake Engineering and Structural Dynamics, 35(9), 1097-1117.
- Verderame G.M., Manfredi G., Frunzio G., 2001. Le proprietà meccaniche dei calcestruzzi impiegati nelle strutture in cemento armato realizzate negli anni '60. Atti del X congresso nazionale ANIDIS "L'ingegneria Sismica in Italia", Potenza-Matera, Italy, September 9-13. (in Italian)
- Verderame G.M., Polese M., Mariniello C., Manfredi G., 2010. A simulated design procedure for the assessment of seismic capacity of existing reinforced concrete buildings. Advances in Engineering Software, 41(2), 323-335.
- Verderame G.M., Ricci P., Esposito M., Manfredi G., 2012. STIL v1.0 - Software per la caratterizzazione delle proprietà meccaniche degli acciai da c.a. tra il 1950 e il 2000. ReLUIS, <http://www.reluis.it/>

Chapter 6

L'Aquila Province: a class-oriented large scale comparison with post-earthquake damage

6.1 Introduction

On April 6, 2009 at 3:32, an earthquake, with a moment magnitude (M_w) of 6.3 and with its epicenter in the area between the town of Colle Roio, Genzano and Collesalvino, hits a large part of 'Central Italy, in particular the Central Apennine area bordering the L'Aquila basin and most part of L'Aquila province.

The earthquake caused 309 victims, about 1,600 injured, more than 65,000 people needing assistance and about 30,000 long term homeless ([Dolce 2010](#)).

Just after the event a field survey, aimed at evaluating the building immediate occupancy and the structural and non-structural damage, was performed. The assessment was carried out using the AeDES form ([Baggio et al. 2007](#); [Goretti and Di Pasquale 2002](#)).

The damage and usability assessment was managed by the Italian Civil Protection Department, with a substantial support from Regions, Provinces, Municipalities, Firemen, ReLuis, Eucentre, National Chambers of Engineers, Architects and Surveyors and National Research Council.

Hence, the information collected through the survey form had allowed the implementation of a Geographical Information System (GIS) database of more than 70,000 buildings (Dolce et al, 2015a; Dolce et al, 2015b), from the about (78,062) survey forms collected soon after the Earthquake, since sometimes repeated inspections were performed on the same building because of aftershocks, inaccurate inspections or errors in building identification. After 3 months from the event, more than 70,000 buildings were inspected.

In the following the distributions of the main parameters present in survey form will be shown. In particular information on typological, morphological and geometrical characteristics of buildings, in addition to information on damage to buildings will be shown.

The data collected will be analyzed in detail, showing the distribution for the whole database and at the level of each municipality.

The implementation of the database had allowed, on the one hand, the derivation of empirical fragility curves for RC buildings, derived from statistical elaboration of survey data collected just after the earthquake of 6 April 2009, considering different building typologies.

Hence, the procedure of section 3.3– which has been implemented in POST (PushOver on Shear Type models), a software based on MATLAB® code (Ricci, 2010, Del Gaudio et al., 2015) – is applied, considering the survey data collected in the database as input parameters. Therefore, the derivation of mechanical fragility curves for building classes and the derivation of seismic damage scenario from the Shake Map of the event is shown.

Afterward, the seismic damage scenario is compared with survey data on damage of RC buildings in order to assess the reliability of the results of the application of the methodology

6.2 Derivation of Building database from Survey form data

In this section data deriving from AEDES survey form (Baggio et al. 2007) will be presented and discussed.

The aims of the survey form is to guide the inspector to the definition of a Usability outcome of the building, which had significant implications on both the emergency management and the reconstruction phase. Indeed the usability outcome is used to define the short term safety/occupancy assessment of buildings, namely if the building is able to safely withstand an aftershocks, as well as the emergency countermeasures to be taken in order to reduce the risk for people.

The form consists of nine sections containing information on the building identification, dimension, age, use, structural type and observed damage to structural and non-structural components (see Table 6-1). The data collected in each section of survey form will be analyzed in detail hereinafter.

Table 6-1: indication of the sections that compose the survey form ([Baggio et al. 2007](#))

SECTION 1	Building identification
SECTION 2	Building description
SECTION 3	Typology
SECTION 4	Damage to structural elements and short term countermeasures carried out
SECTION 5	Damage to non structural elements and short term countermeasures carried out
SECTION 6	External damage due to other constructions and short term countermeasures carried out
SECTION 7	Soil and foundations
SECTION 8	Usability judgment
SECTION 9	Other observations

6.2.1 Section 1: Building identification

This section contains information concerning the identification of both the building and its survey. In this section is possible to unambiguously identify the building through ISTAT data identifying the municipality (region, province and municipality), together with the aggregate number and the building number. The combination of these two identification codes allows the information management, even in a nationally unified database. Furthermore, in this section cadastral data

(sheet, allegato and parcels) have to be supplied together with the address of the building, and its position relative to other buildings for building aggregates.

The database contains information on over 70,000 buildings located on 129 municipalities in the provinces of L'Aquila (88.8%), Teramo (7.1%), Pescara (4.1%) and very few buildings in the province of Chieti. Among these 102 municipalities are located in the province of L'Aquila. In addition, the number of the buildings inspected through the survey form is not graded uniformly on the territory. In fact the buildings inspected in the Municipality of L'Aquila represent respectively the 34% and the 38.3% of the buildings of the database and of those inspected in the province of L'Aquila (see Figure 6-1).

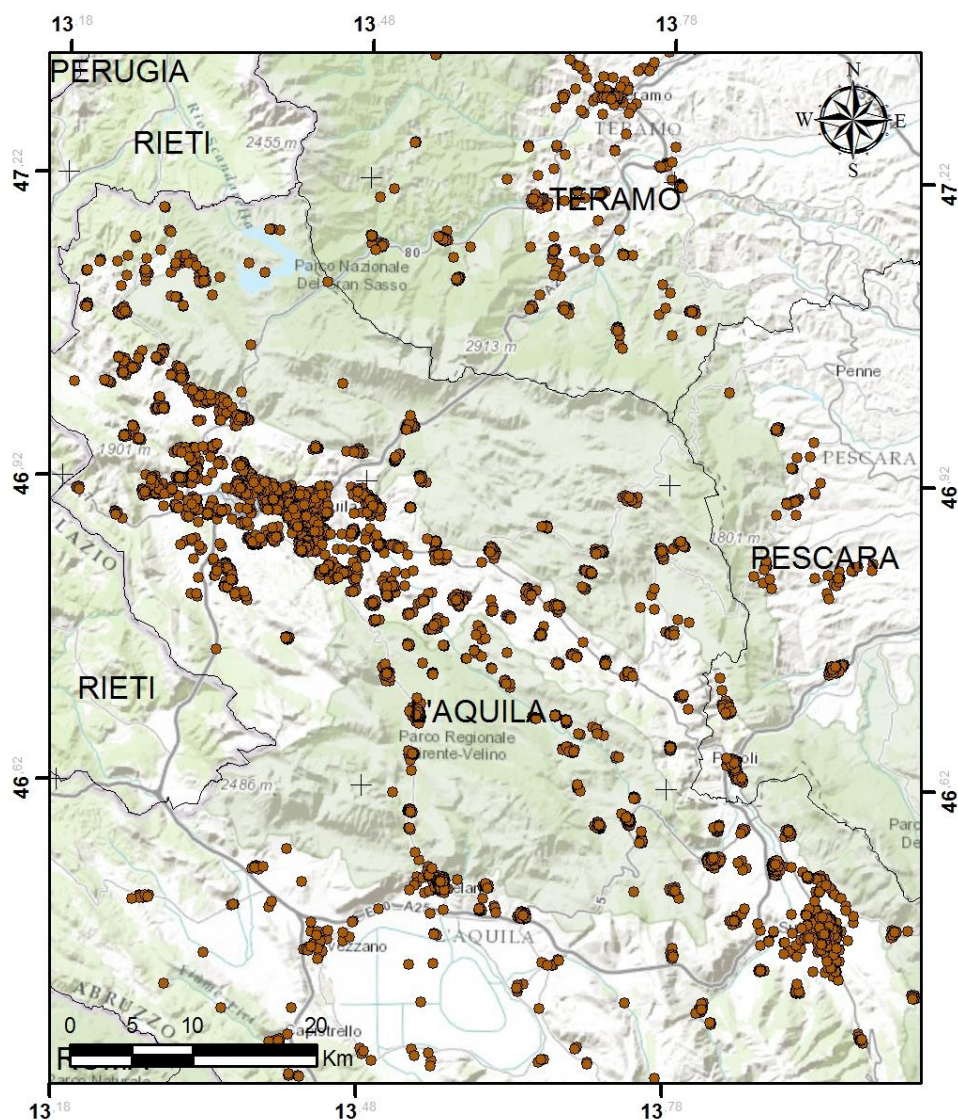


Figure 6-1: Map of L'Aquila area with indication of surveyed buildings after the 6/4/2009 earthquake

6.2.2 Section 2: Building description

Section 2 collects information concerning metrical data, age, with indication of the period of construction and eventually of renovation of the building, as well as type of use and exposure. Metrical data must include the total number of storeys including basements, the number of basements, the average storey height and the average storey surface. The total number of storeys refers to those which can be counted starting from the foundation level. Basements floors are defined as those having an elevation above the ground level (i.e. the average elevation in case of buildings on slope) lower than half of the total storey height.

In particular over 65% of the whole sample of buildings were masonry buildings and 18% RC or Steel buildings. The remaining were buildings with mixed structure or with undetectable resistant System. It can be noted from Table 6-2 that the percentage of RC buildings of L'Aquila Municipality is much greater of that of the remaining surveyed Municipalities. This circumstance can be related to the different construction practices that affect the areas. As it will be see in the following the building stock of L'Aquila and neighborhood Municipalities located in the homonymous basin is characterized by a modern residential housing with respect to that of the Municipalities located in the mountain areas of National Park of Gran Sasso and Monti della Laga (North-East) and Natural Regional Park Sirente–Velino (South-East), characterized mostly by a rural and ancient housing.

Table 6-2: Structural Typology Distribution for the whole building database

	Masonry (%)	RC (%)	Steel (%)	Mixed (%)
All	65.16%	17.04%	0.75%	7.47%
L'Aquila	50.93%	28.20%	1.54%	7.71%
Other Municipalities	72.50%	11.29%	0.34%	7.34%

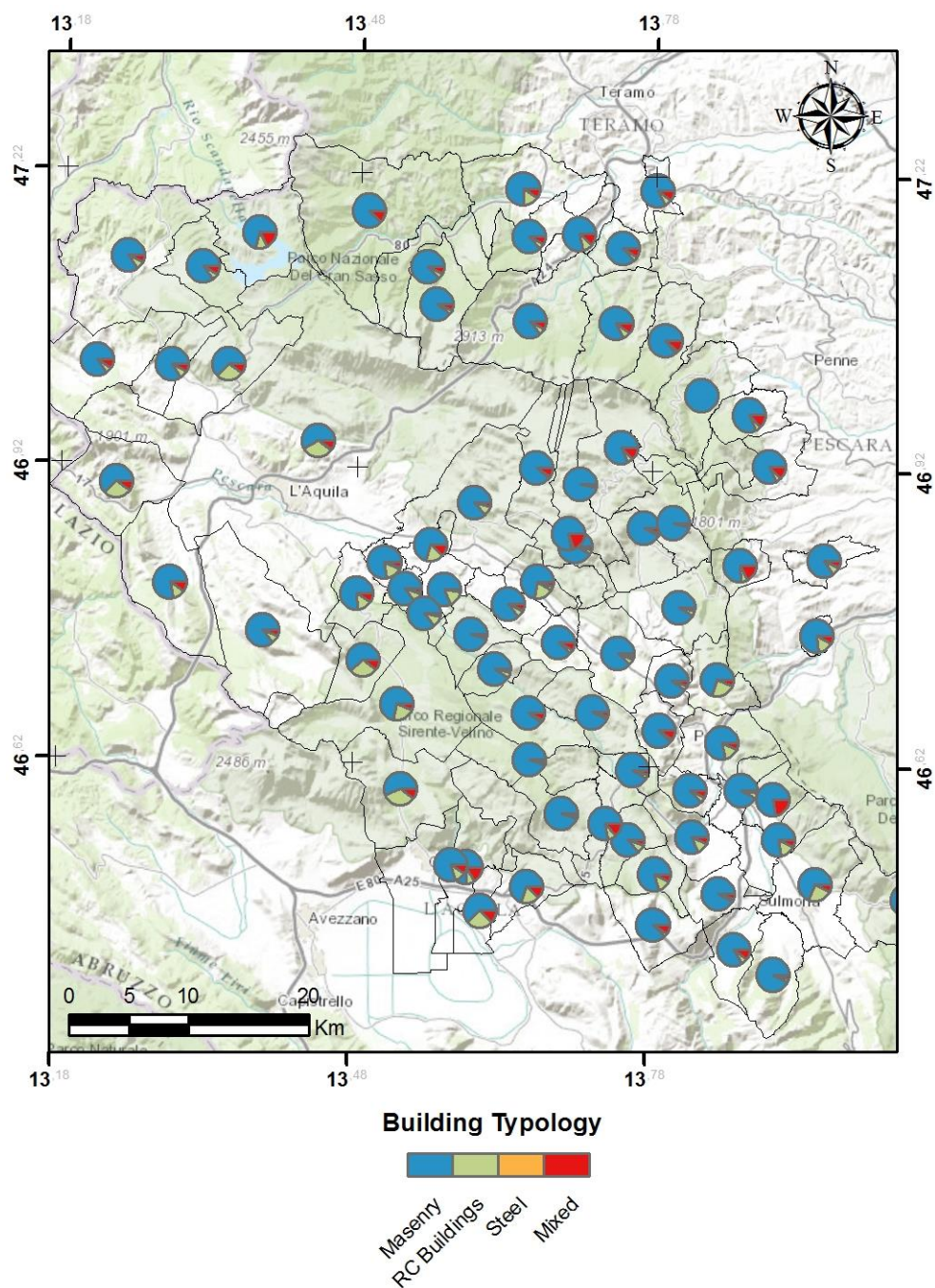


Figure 6-2: Structural Typology Distribution for each Municipality

It can be noted from Figure 6-2 that L'Aquila (28.2%) and the Municipality in the close proximity (Scoppito 26.6%, Rocca di Mezzo 19.8%, Pizzoli 24.6%) are characterized by significant percentage of RC surveyed buildings. On the contrary, the Municipalities located on the Central Apennine area are mainly characterized by Masonry or Mixed surveyed buildings, namely Ofena and Capestrano and the other municipalities of the National Park of Gran Sasso and Monti della Laga and Natural Regional Park Sirente–Velino, situated respectively in the North-East and South-East of L'Aquila.

Table 6-3: Number of Storeys Distribution for the whole building database

	1	2	3	4	5	>6
All	10.87%	29.75%	39.34%	14.53%	2.67%	1.47%
L'Aquila	16.42%	26.87%	34.96%	13.59%	3.39%	2.65%
Other Municipalities	8.00%	31.24%	41.60%	15.02%	2.30%	0.86%

Furthermore, in Figure 6-3 the distribution of number of storeys over the whole database is shown. It can be noted a modal value equal to three regardless of Building Typologies.

Figure 6-4 shows the distribution of number of storeys in the study area. It can be noted analogous trends observed for building typology. As a matter of fact, the buildings surveyed in the L'Aquila basin are characterized by a modal value of number of storeys higher than that of buildings located in mountain areas falling in the National Park of Gran Sasso and Monti della Laga and Natural Regional Park Sirente–Velino, characterized by a modal value of the number around two (see Figure 6-4).

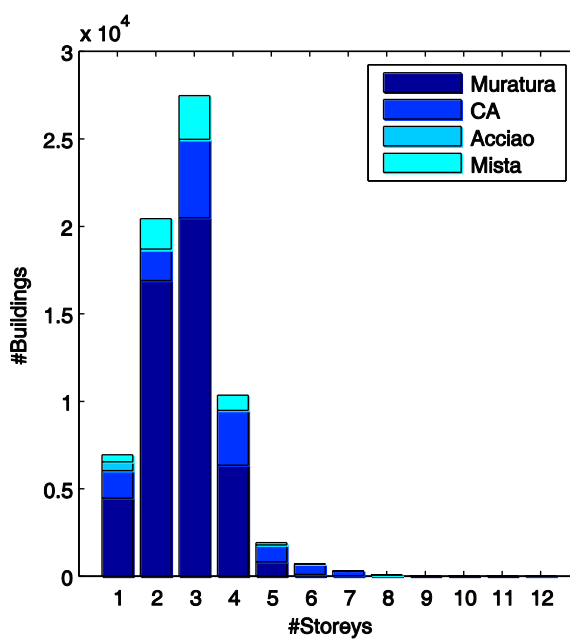


Figure 6-3: Number of Storeys Distribution for the whole building database

In Figure 6-5 the distribution of number of basement is shown. It can be noted that the 65,1% of surveyed building is not equipped with Basements floors, while 17,0% of Building are characterized by 1 Basements floor.

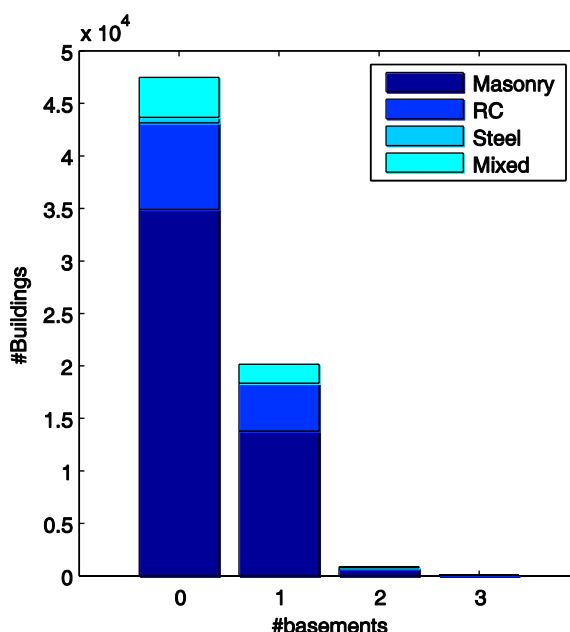


Figure 6-5: Number of Basement Distribution for the whole building database

Figure 6-6 show the distribution of average storey surface of the whole database. The latter represent the average value better representing the total volume, namely the value better characterising the average surface among all storeys.

It can be noted that the modal value of the average storey surface is equal to "<50" and "130" m^2 respectively for Masonry and RC Structure.

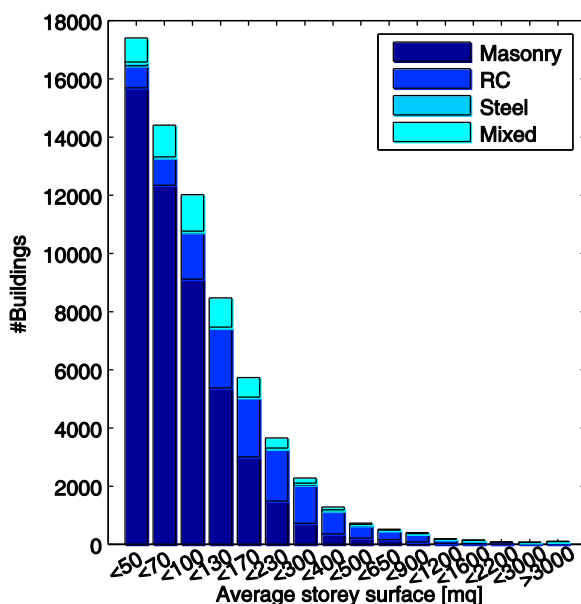


Figure 6-6: Average storeys surface Distribution for the whole building database

Table 6-4: Average storey surface Distribution for the whole building database

	≤70	[70-130]	[130-230]	[230-400]	>400
All	46.5%	29.3%	13.3%	5.0%	3.2%
L'Aquila	35.7%	29.7%	17.9%	7.7%	5.3%
Other Municipalities	34.4%	19.2%	7.2%	2.4%	1.4%

Moreover, Figure 6-7 and Figure 6-8 show the distribution of age of construction and renovation, the latter identifying the year in which the building has been subject to a renovation process significant from the structural point of view ([Baggio et al, 2007](#)), for the whole database.

It can be noted how most of Masonry Buildings are dated before 1919, while most of RC Building are dated later 1971. Furthermore the 38.8% of Masonry Buildings and the 47.9% of Mixed Buildings has been subjected over the years to a renovation process approximately

since the early 1946. For RC buildings, this percentage is just 5.7%, and the process of renovation is started since the early 1970.

Table 6-5: Age of construction Distribution for the whole building database

	≤1919	19-45	46-61	62-71	72-81	82-91	92-01	≥2001
All	44.45%	10.86%	7.18%	7.24%	9.59%	8.48%	5.35%	3.90%
L'Aquila	26.87%	8.37%	7.82%	9.81%	13.93%	13.03%	8.12%	6.86%
Other Municipalities	53.52%	12.14%	6.85%	5.92%	7.36%	6.13%	3.92%	2.37%

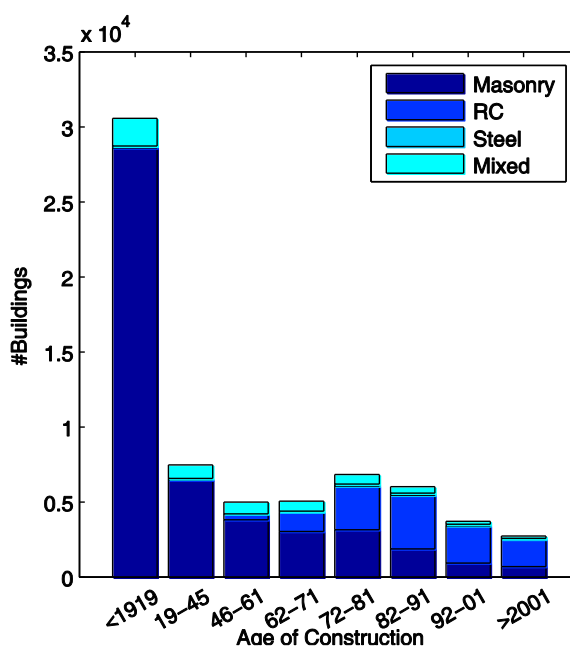


Figure 6-7: Age of construction Distribution for the whole building database

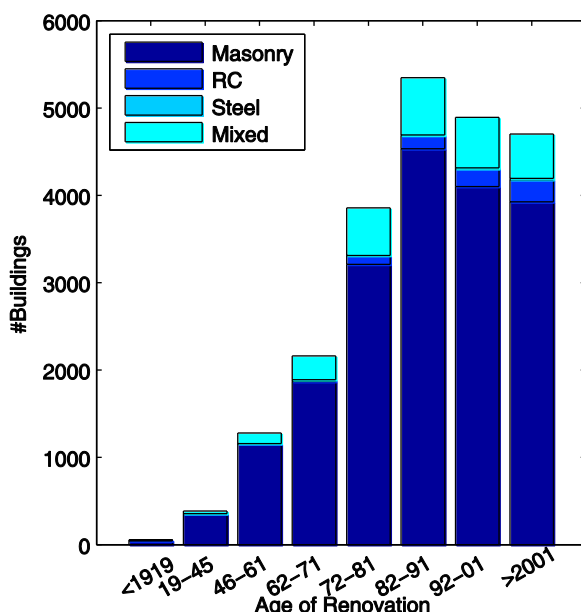


Figure 6-8: Age of renovation Distribution for the whole building database

Finally, Figure 6-9 shows the spatial distribution of age of construction in the study area. It is to be noted that L'Aquila basin area is characterized by a greater number of recently constructed buildings, while the Municipalities located near the National Park of Gran Sasso and Monti della Laga and Natural Regional Park Sirente–Velino are characterized by dating no later than 1946-1961, with a number of storeys not greater than 2 and typically made up of masonry building with a limited average storey surface.

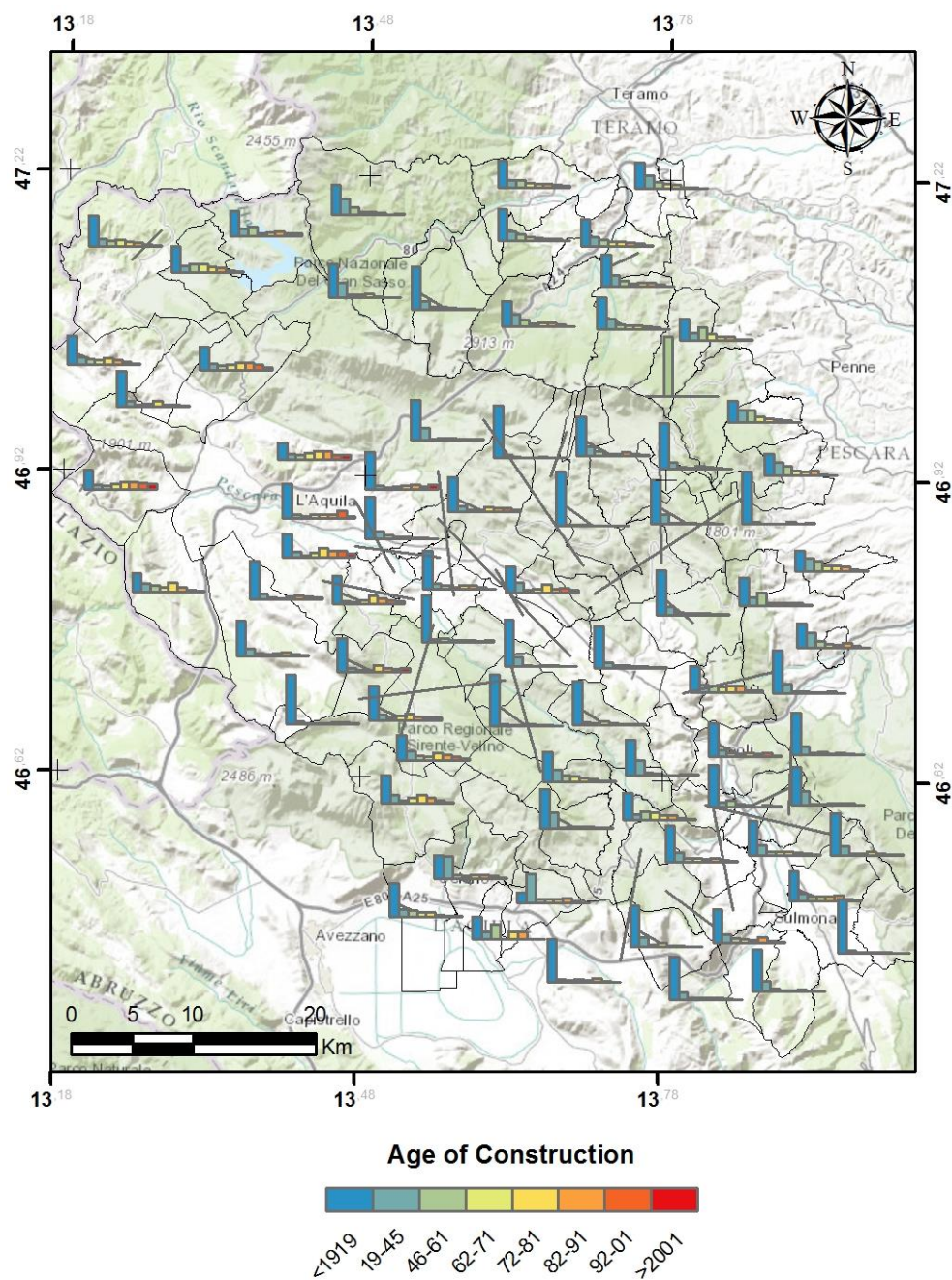


Figure 6-9: Age of construction Distribution for each Municipality

For what concerns use, section 2 allows to distinguish residential from the offices use, referring to private offices, namely banks, professional activities. Moreover public and strategic services use and strategic use is considered, the latter related to Civil Protection functions, such as hospitals, municipalities, firemen barracks. Finally, warehouse use is considered too, related to location used for storing material, where no fixed staff is present excluding garages or basements belonging to houses. In Figure 6-10 the distribution of Use is reported, in which buildings with non-exclusive uses have been excluded. It can be noted that the most of these are residential (61.9%), regardless of the building typology, while the 9.4%, mainly consisting of masonry buildings, are warehouse.

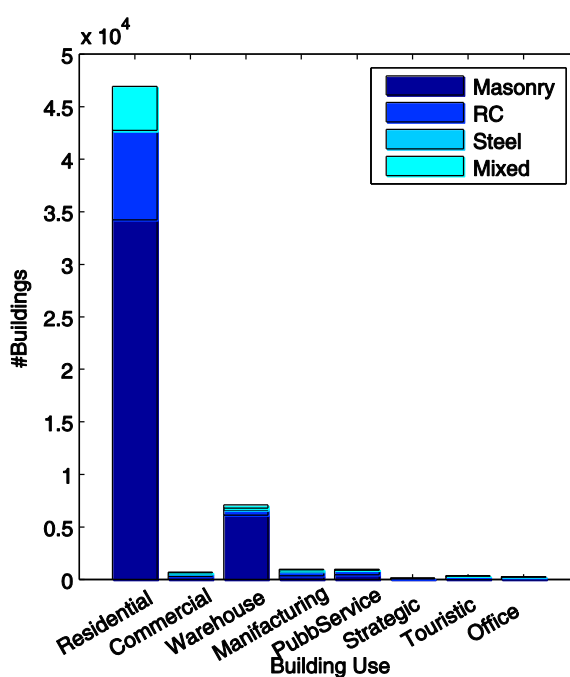


Figure 6-10: Use Distribution for the whole building database

6.2.3 Section 3: Typology

Section 3 of the survey form allow the identification of the structural system of building, which may influence the building seismic response and hence its vulnerability. In particular for masonry buildings the latter is evaluated based on the quality of vertical bearing structure (materials, mortar, construction quality) and on the typology of horizontal structure, subdivided into flexible, semirigid and rigid, in their plane. Usually, reinforced concrete floors are considered as rigid, those realised with iron beams and hollow clay tiles as semirigid, those realised with iron beams supporting shallow arch vaults or wooden floors are considered flexible (see Figure 6-11).

<div><div>Horizontal Structures</div><div>Vertical structures</div></div>		Unknown	Masonry buildings						
			Irregular layout or bad quality (stones, pebble,...)		Regular layout and good quality (Hwen stones, bricks,..)		Isolated columns	Mixt	Strengthened
			Without ties or tie beams	With ties or tie beams	Without ties or tie beams	With ties or tie beams			
		A	B	C	D	E	F	G	H
1	Unknown	○	□	□	□	□	SI	□	□
2	Vaults without ties	□	□	□	□	□	○	G1	H1
3	Vaults with ties	□	□	□	□	□		□	□
4	Flexible floors	□	□	□	□	□	NO	G2	H2
5	Semirigid floors	□	□	□	□	□	○	□	□
6	Rigid floors	□	□	□	□	□		G3	H3

Figure 6-11: Masonry building classification

According to their seismic behavior, masonry buildings can be classified as poor, medium and good quality buildings (Mas-A, Mas-B, Mas-C). The classification is based on the characteristics of the vertical and the horizontal components, described in Section 3 of the AeDES form ([Dolce et al, 2015](#)).

Horizontal structures	Vertical structures			
	Irregular layout or bad quality (stones, pebble,...)		Regular layout and good quality (Hwen stones, bricks,...)	
	Without ties or tie beams	With ties or tie beams	Without ties or tie beams	With ties or tie beams
Vaults without ties	A	A	A	B
Vaults with ties	A	B	A	B
Flexible floors	A	B	A	B
Semirgrid floors	A	B	B	C
Rigid floors	B	B	C	C

Figure 6-12: Masonry building classification (A = most vulnerable, C = less vulnerable) from (Dolce et al, 2015).

Finally RC and Steel buildings are characterized as having the entire bearing structure in reinforced concrete or steel, respectively. Mixed type buildings are characterized by a vertical bearing structure that includes both RC and masonry components, either on the same floor or at different floors.

6.2.4 Section 4: Damage to structural elements and short term countermeasures carried out

Section 4 reports the apparent, that can be observed on the structural components during the survey. It can be pre-existent or related to the earthquake. The damage is related to structural components, namely vertical and horizontal structures, stairs and roof, in addition to non-structural components (infills and partitions), which may modify the resistance and/or the response of the structure, in particular for frame structures, see Figure 6-13.

Moreover, the survey form allows not only the identification of the damage grade but also its relative extension. To this aim, it is necessary to appropriately combine the relative damage extension in each floor

and the number of damaged storeys, in order to estimate the relative extension to be assigned to each damage grade.

<div>Level Extension</div> <div>Component</div>		DAMAGE									
		D4-D5 Very heavy or collapse			D2-D3 Medium or heavy			D1 Slight			D0 Null
		> 2/3	1/3 - 2/3	< 1/3	> 2/3	1/3 - 2/3	< 1/3	> 2/3	1/3 - 2/3	< 1/3	
		A	B	C	D	E	F	G	H	I	
1	Vertical structures	■	■	■	■	■	■	■	■	■	○
2	Horizontal structures	■	■	■	■	■	■	■	■	■	○
3	Stairs	■	■	■	■	■	■	■	■	■	○
4	Roof	■	■	■	■	■	■	■	■	■	○
5	URM Infill walls	■	■	■	■	■	■	■	■	■	○
6	Pre-existing damage	■	■	■	■	■	■	■	■	■	○

Figure 6-13: Damage classification according to (Baggio 2007)

The definition of the observed damage grades is based on the European Macroseismic Scale EMS98, integrated with the additional specifications introduced in the past in the (GNDT 1986, GNDT 1993) survey forms. The EMS98 scale includes six possible damage grades (from D0-no damage to D5-destruction) referred to the whole building, based on the level and on the extension of structural and non-structural damage in the building.

Nevertheless, the survey form introduces a damage classification graduated on three damage levels, combining level D2 with D3 and D4 with D5, and reporting its extension for each structural and non-structural component.

Hereinafter it will be explicitly reported the description of the damage grades provided in the AEDES field manual (Baggio 2007) since subsequently it will be derived a damage grades for the whole building starting from the damage classification and its extension for each

structural and non-structural component according with the contents of the EMS98.

- D1 slight damage: it is a damage that does not affect significantly the capacity of the structure and does not jeopardise the occupants safety due to falling of non structural elements; the damage is slight when the falling of objects can immediately be avoided. Reinforced concrete: slight cracks in the beams (up to 1 mm), widespread, but not vertical, cracks (< 0.5 mm) in columns or in partitions. Cracks up to 2 mm due to separation of the infill walls from the structures, slight diagonal cracks in the infills (< 1 mm).
- D2-D3 medium-severe damage: it is a damage that changes significantly the capacity of the structure, without getting close to the limit of partial collapse of the main structural components. Possible falling of non structural objects. Reinforced concrete: flexural cracks in beams up to 4-5 mm, cracks in columns and in shear walls up to 2-3 mm, beginning of buckling of the compressed bars in the columns, with spalling of the concrete cover, just perceptible residual out of plumb. Evident cracks (> 2 mm) in infill walls due to the separation from the structure, diagonal cracks up to few mm, evident crushing at the corners in contact with the bearing structures, sometimes with localised expulsion of material.
- D4-D5 very heavy damage: it is a damage that significantly modifies the capacity of the structure, bringing it close to the limit of partial or total collapse of the main structural components. This state is characterised by damages heavier than the previous ones, including collapse.

6.2.5 Section 5: Damage to non structural elements and short term countermeasures carried out

In Section 5, the presence of damage to non structural component is registered together with the presence of existing short term

countermeasures. The damage caused by the earthquake to non structural components is important both for the usability classification and for the estimate of the repair costs. Typical damages to non structural components are those concerning plasters, coatings, stuccos, false ceilings, infill panels, non structural roof components, covering, eaves and parapets. Damages to the water, gas or electricity plants are also included.

6.2.6 Section 6: External damage due to other constructions and short term countermeasures carried out

In Section 6, reference is made to factor of risk related to damage to components that are external to the building under survey. Danger may derive from instability of adjacent buildings (risk of collapses or objects falling), or from unsafe conditions of the distribution systems.

6.2.7 Section 7: Soil and foundations

In Section 7, qualitative information concerning the soil and the foundation, needed for the geotechnical risk evaluation, are collected, namely the description of the morphology of the site where the building is located and the possible presence of visible soil instabilities, related to instable slope or to the building foundations, whether in the case this has been triggered by the earthquake or it is already existing.

6.2.8 Section 8: Usability judgment

Section 8 provides synthetic information on Structural risk related to the bearing elements (vertical structures, horizontal structures, infill panels) and non-structural risk, related to partition walls, tiles, chimneys, technological networks, in addition to external risk, induced by possible partial or total collapses of adjacent buildings on the building under study or on the streets leading to it, and geotechnical risk, related to the conditions of soil and foundations.

This information which briefly summarize what is reported in a more detailed manner in sections 4 to 7 allow the inspector to provide a usability judgment for the surveyed building.

The aim of usability judgment in the post-earthquake emergency is to supply a short term safety evaluation of damaged buildings. Thus, a “usable” building is essentially able to withstand a further seismic shock and/or is essentially able to support the gravity loads in the damaged configuration, safeguarding the lives of their occupants. The larger number of outcomes in the Italian forms is aimed at increasing the number of buildings, or some of its parts (see PARTIALLY USABLE in Table 6-6), that can be used with or without short-term countermeasures. The circumstance of limiting the number of buildings unusable aims to end shortly the emergency condition and allow the population to return to their homes and restore normal social functions of affected areas.

Table 6-6: Possible usability outcomes from (Baggio 2007)

A	USABLE	Building can be used without measures. Small damage can be present, but negligible risk for human life
B	USABLE WITH COUNTERMEASURES	Building has been damaged, but can be used when short term countermeasures are provided
C	PARTIALLY USABLE	Only a part of the building can be safely used
D	TEMPORARY UNUSABLE	Building to be re-inspected in more detail. Unusable until the new inspection
E	UNUSABLE	Building can not be used due to high structural, non-structural or geotechnical risk for human life. Not necessarily imminent risk of total collapse.
F	UNUSABLE FOR EXTERNAL RISK	Building can be used in relation to its damage level, however it can not be used due high risk caused by external factors (heavy damaged

In Figure 6-14 the distribution of the usability outcomes, from A to F, for masonry, reinforced concrete and mixed type buildings is shown. As expected, masonry buildings exhibit a higher percentage of outcomes E (unusable) and F (unusable for external risk), when compared to reinforced concrete buildings. While outcome E can be ascribed to the higher vulnerability of masonry buildings, outcome F is due to the larger fraction of masonry buildings in historical centres, where the external risk is more recurrent.

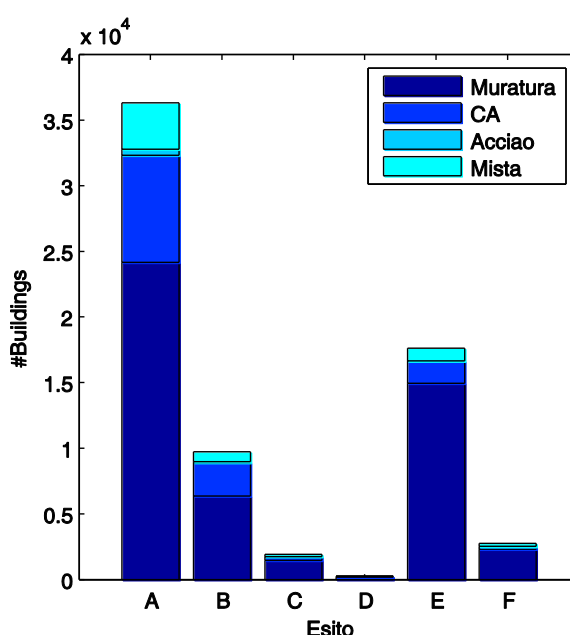


Figure 6-14: Usability outcomes Distribution for the whole building database

In order to facilitate the comparison with international standards the usability classification can be modified, so that Usable = Green = A, Restricted Use = Jellow = B+C, Unusable = Red = D + E + F. In Table 6-7: Usability outcomes Distribution for the whole building database are reported the outcomes in terms of usable, restricted usable and unusable judgments for masonry, reinforced concrete and mixed type

buildings are shown. The usability outcomes are, in percentage, much more frequent in RC and Steel buildings. The fact that the percentage of restricted use RC buildings are more frequent than in the other case can be related to the implications of the damage to infill panels and to non-structural components for the usability classification.

Table 6-7: Usability outcomes Distribution for the whole building database

	Masonry	RC	Steel	Mixed	All
Usable	48.89%	63.17%	79.01%	62.72%	52.97%
Restricted Use	15.79%	21.97%	13.58%	16.35%	16.98%
Unasable	35.32%	14.86%	7.41%	20.93%	30.04%

Finally, the spatial distribution of usability judgment is shown in Figure 6-15. It is to be noted a concentration of unusable buildings in area of L'Aquila basin, where are located the epicentral areas. Moreover in these areas has been developed a relatively recent housing, characterized by a number of floors and a surface area typically higher than those of surrounding areas.

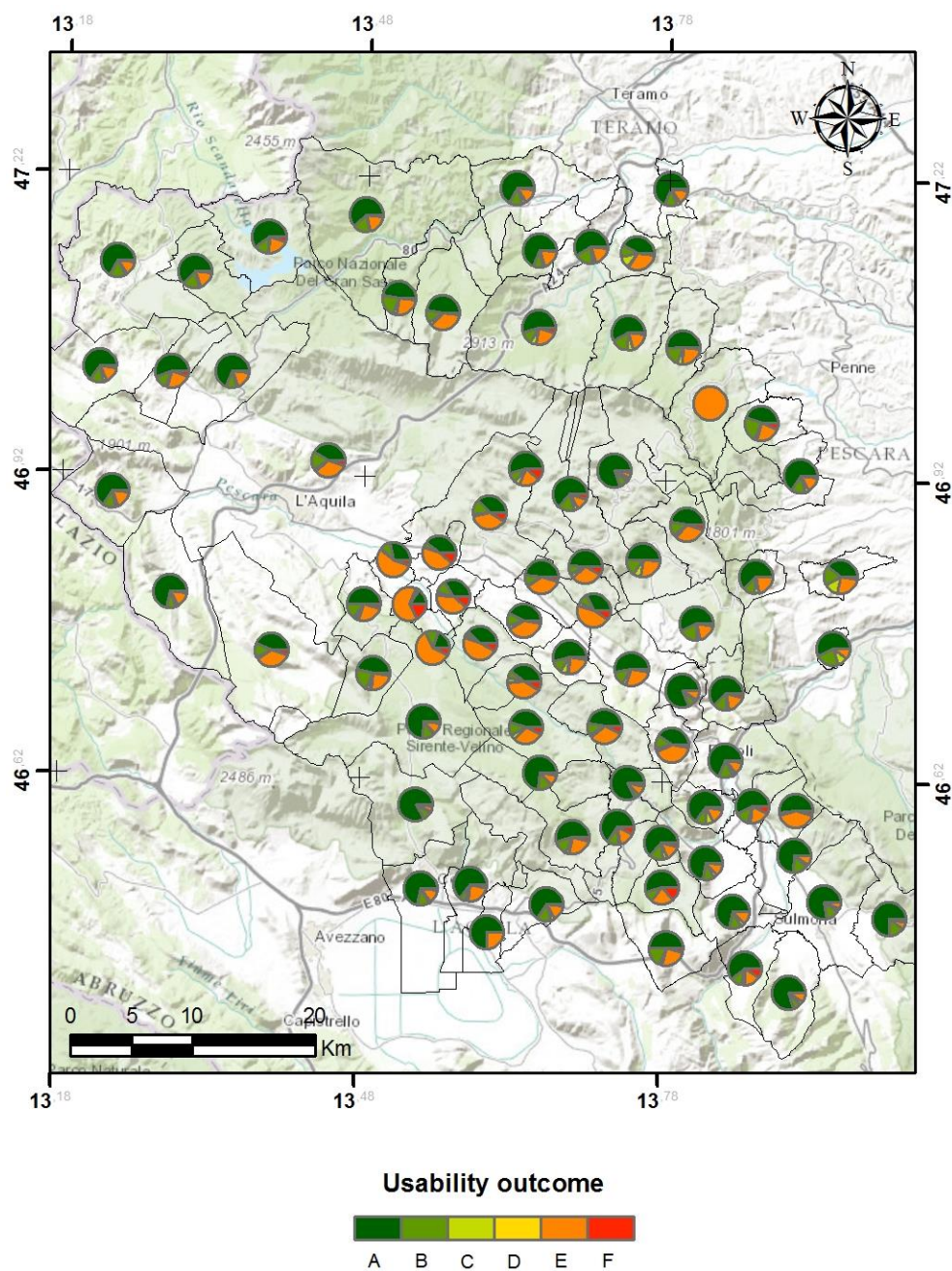


Figure 6-15: Usability outcomes Distribution for each Municipality

6.3 Residential RC buildings Database

In section 6.5, POST procedure (PushOver on Shear Type models) (Ricci, 2010, Del Gaudio et al., 2015) is applied, considering the survey data collected in the database as input parameters. POST procedure is a simplified methodology for seismic vulnerability assessment of RC buildings, that starting from a simulated design procedure based on few data allows to evaluate in closed-form the non-linear static response of building. The assessment of the seismic capacity is based on the mechanical interpretation of the damage states described by the EMS-98 (Grünthal, 1998) through the simplified IDA curves derived from (Vamvatsikos and Cornell, 2006). Hence the methodology allow to take into account the influence of infill panel both in the definition of the non-linear static response of building and seismic capacity.

In present section, the 78,062 survey forms (Dolce et al, 2015a; Dolce et al, 2015b) will be elaborated in order to derive the input parameters for seismic vulnerability assessment of RC building stock of L'Aquila area through POST methodology.

Hence, in the following the statistics about residential RC buildings (8463) are shown. In Figure 6-16 and Figure 6-17 the distributions of number of storeys and number of basements are shown. It can noted that 56.7% of building is characterize by a number of storeys not greater than three, while 62.5% of building is devoid of a basement floor and 36.8% has one basement floor.

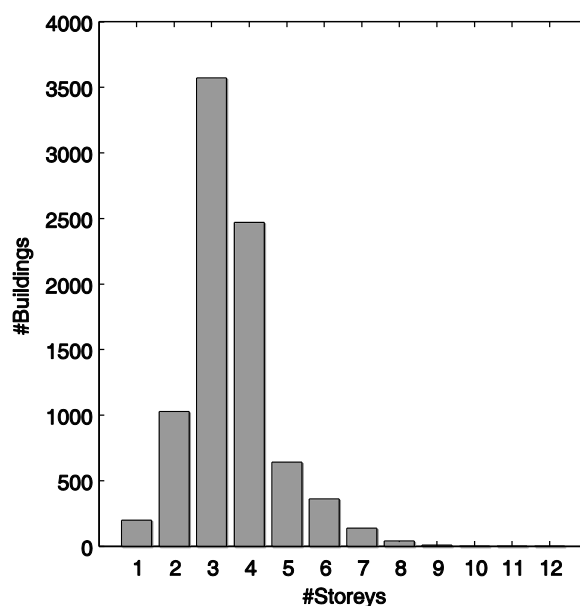


Figure 6-16: Number of Storeys Distribution for the RC residential buildings

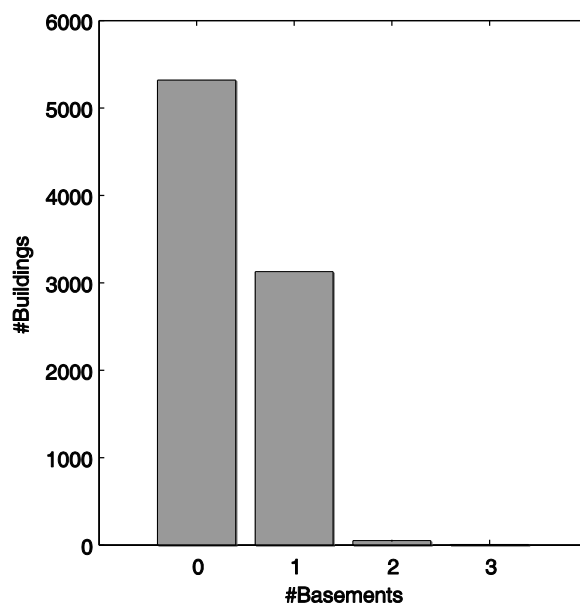


Figure 6-17: Number of Basements Distribution for the RC residential buildings

Figure 6-18 and Figure 6-19 show the distribution of age of construction and renovation. It can be noted that just the 1.2% of residential RC building is dated before 1945, while 72.9% is dated between 1972 and 2001. Furthermore, just the 4% of the considered dataset is subjected to a renovation process after the 1982, while in very rare cases have occurred previously.

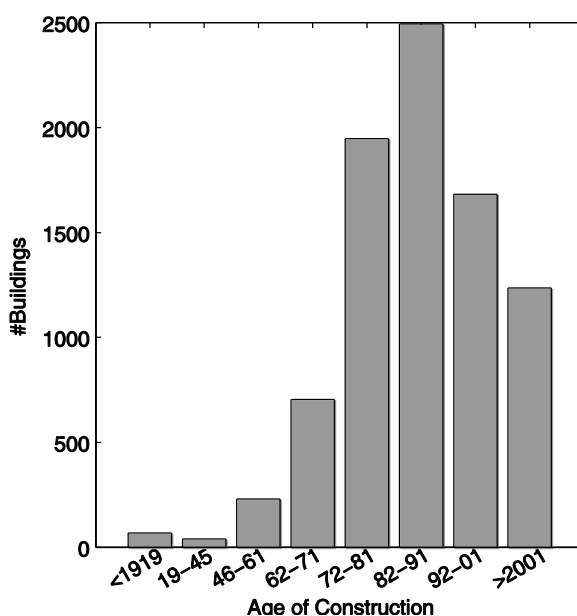


Figure 6-18: Age of construction Distribution for the RC residential buildings

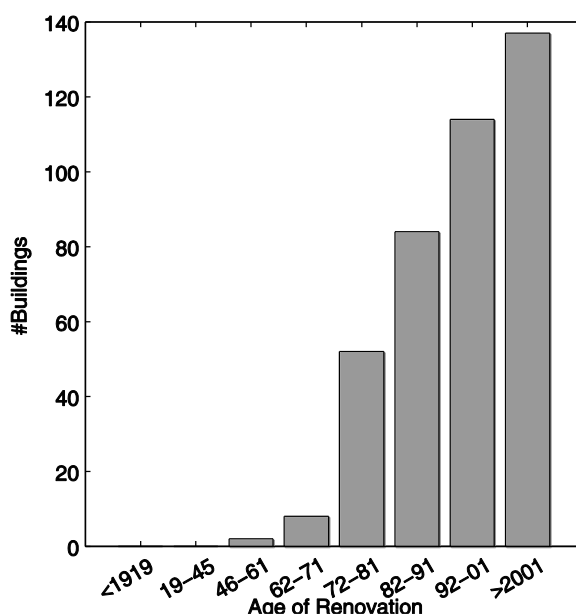


Figure 6-19: Age of renovation Distribution for the RC residential buildings

Figure 6-20 shows the distribution of average storey surface. It can be noted that 48.8% of buildings is characterized by an average storey surface less than 130 m², while the 49.7% between 130 and 500 m².

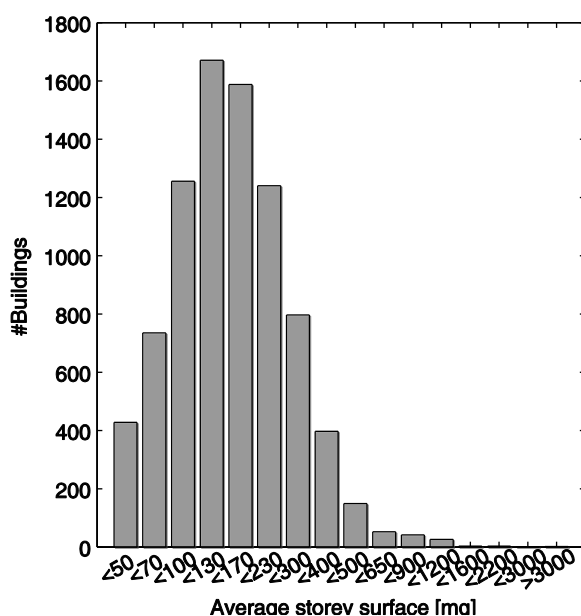


Figure 6-20: Average storey surface Distribution for the RC residential buildings

Definitely in Figure 6-21 the distribution of usability outcomes is shown. It can be shown that the 64.9%, 21.2% and 13.8 of residential RC buildings is respectively Usable, Restricted Usable and Unusable.

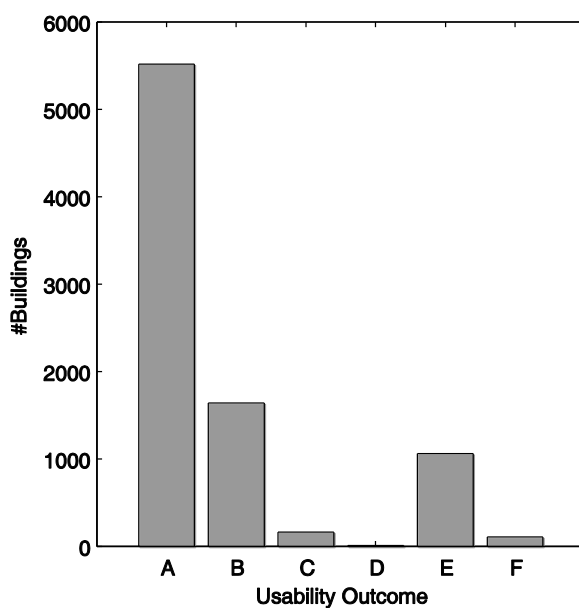


Figure 6-21: Usability outcomes Distribution for the RC residential buildings

6.4 Observed damage scenario

In the case of class/regional scale seismic scenario analysis vulnerability data are typically represented by means of statistical analysis of post earthquake damage surveys (Rossetto and Elnashai, 2003; Rota et al., 2007).

In the present section, empirical fragility curves are derived from statistical elaboration of the surveys data collected after the 6/4/2009 earthquake (see Section 6.3) according to the methodology described in (Porter et al., 2007). This approach converts Eq 6-1 to a linear regression problem by taking the inverse Gaussian cumulative distribution function of each side and fitting a line to the data (for further details see (Porter et al., 2007); “probability paper” in (Ang and Tang 1975)):

$$F_{dm}(edp) = P[DM \geq dm | EDP = edp] \quad \text{Eq 6-1}$$

$$F_{dm}(edp) = \Phi\left(\frac{\log(edp/x_m)}{\beta}\right) \quad \text{Eq 6-2}$$

where Φ denotes the standard normal (Gaussian) cumulative distribution function, x_m denotes the median value of the distribution, and β denotes the logarithmic standard deviation.

In order to derive observational fragilities the damage grades D0, D1, D2, D3, D4 and D5 have been obtained from the data collected in the AeDES form (Baggio et al., 2007), where, however, the only condensed damage grades (D0, D1, D2–D3 and D4–D5) are reported.

In (Dolce et al, 2015) an observed damage distribution is introduced as a function of the condensed damage grades and a series of parameters, which provide the transition from D2 to D3 and from D4 to D5, assumed constant for all the buildings belonging to a specific class in a given locality and related to the mean damage of the class in the selected location.

In the present work, a different procedure is derived starting from the condensed damage grades (D0, D1, D2–D3 and D4–D5) reported for vertical structures and infill panels in AeDES form, taking into account also the extension of the damage level.

In particular, it is to be noted that condensed damage grades are derived from the European Macroseismic Scale EMS98, which includes six possible damage grades (from D0-no damage to D5- destruction) for the building. Hence, it is possible to interpret a posteriori the results of inspection form to derive damage grade for the building. In the following, it is illustrated and discussed in detail how to derive damage grade from the observed damage reported in inspection form separately for RC columns and infill panels.

Infill Panel:

- Grade1 – Negligible to slight damage: this condition, corresponding in EMS-98 to fine cracks in infill panels, can be related to DS1, namely to the first detachment of the infill panel from surrounding RC structure (up to 2 mm) and at a slight diagonal cracking of the panel itself (< 1 mm);
- Grade2 – Moderate damage: this condition, corresponding in EMS-98 to cracks in partition and infill walls, can be related to DS2-DS3, defined by diagonal cracks, evident crushing at the corners in contact with the bearing structures and sometimes localised failure of the panel;
- Grade3 – Substantial to heavy damage: this condition, corresponding in EMS-98 to large cracks in partition and infill walls, failure of individual infill panels, can be related to DS4-DS5, defined by the failure of infill panels.

RC Column. For the definition of EMS-98 Grades starting from RC columns damage reported in inspection forms reference is made to the scheme reported in ([Rota et al, 2007](#), [Dolce et al, 1999](#)):

- Grade1 – Negligible to slight damage: this condition, corresponding in EMS-98 to fine cracks in plaster over frame

members, can be related to DS1, represented by a very slight damage on the columns (< 0.5 mm);

- Grade2 – Moderate damage: this condition, corresponding in EMS-98 to cracks in columns, can be related to a damage equal to DS2-DS3 for a limited number of columns (less than 33%);
- Grade3 – Substantial to heavy damage: this condition, corresponding in EMS-98 to Cracks in columns, Spalling of concrete cover, buckling of reinforced rods, coincides with that described in AEDES manual as DS2-DS3. Hence it can be related to a damage equal to DS2-DS3 for a most of columns (at least 33%);
- Grade4 – Very heavy damage: this condition, corresponding in EMS-98 to large cracks in structural elements, can be put in relation with an exacerbation of damage represented by DS4-DS5 for the majority of columns (less than 66%);
- Grade5 – Destruction: this condition, corresponding in EMS-98 to collapse of ground floor or parts of building can be related to a damage equal to DS4-DS5 for all columns (at least 66%).

Therefore, for each building, namely, for each inspection form, a different Grade for RC columns and infill panels can be obtained. The heaviest Grade between the two represents the Grade for the whole building.

In Figure 6-22 damage grades outcomes for the Residential RC buildings (8342) are reported. It is to be noted that most of buildings is subject to a damage lies between DS0 and DS1 (about 76%), a not negligible percentage in D2 and DS3 (about 20%) and a little percentage in DS4 and DS5 (about 2%).

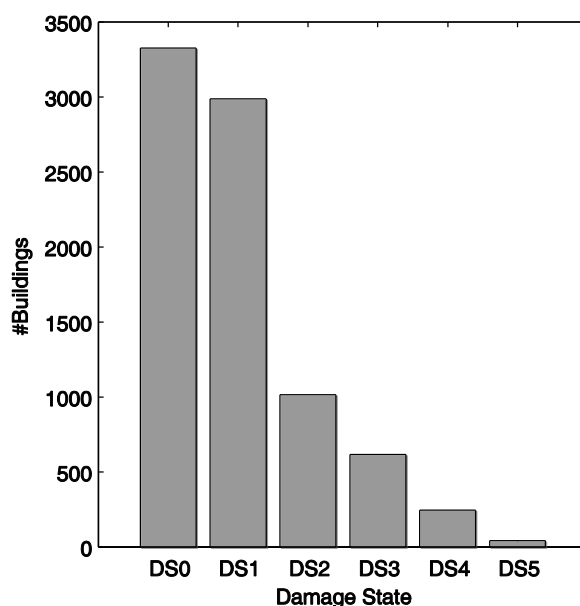


Figure 6-22: Damage grades Distribution for the Residential RC buildings

Moreover, for each residential RC building of the database a PGA value was extrapolated from the shake map provided by INGV (<http://shakemap.rm.ingv.it/shake/index.html>).

Then, buildings are grouped bins by ranges of PGA. The assumed bin subdivision ranges from 0.1 to 0.55g, with steps of 0.05.

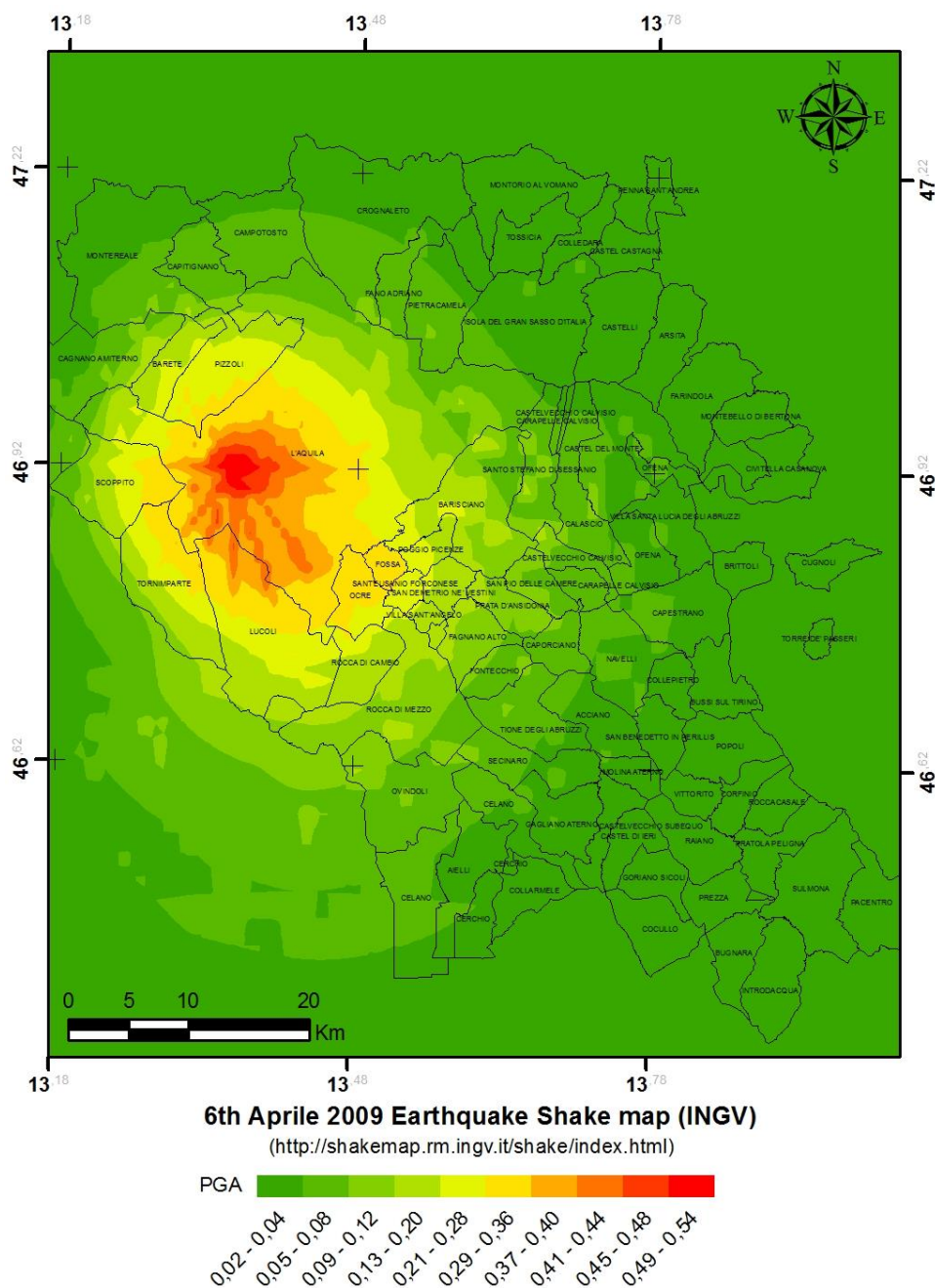


Figure 6-23: Map of L'Aquila area and shake map data according to <http://shakemap.rm.ingv.it/shake/index.html>

In this study, four different classes of buildings has been defined, as reported in Table 6-9, as a function of the number of storeys (less or equal to 3 and greater than 3) and of the age of construction (prior to or after 1981), which is related to design code enforced.

Hence, a linear regression between the points defined by the logarithm of average PGA value, defined as the average PGA of buildings located in that particular bin, and the cumulative distribution function of the fraction of buildings that exceed each DS. The regression parameters derived in this manner allow to evaluate the parameters of lognormal fragility curve for that particular DS. For example in Figure 6-24 the derivation of the parameters of lognormal fragility curve for the RC-LH-NS building class (Age of construction before of 1981 and $N_s \leq 3$) are derived.

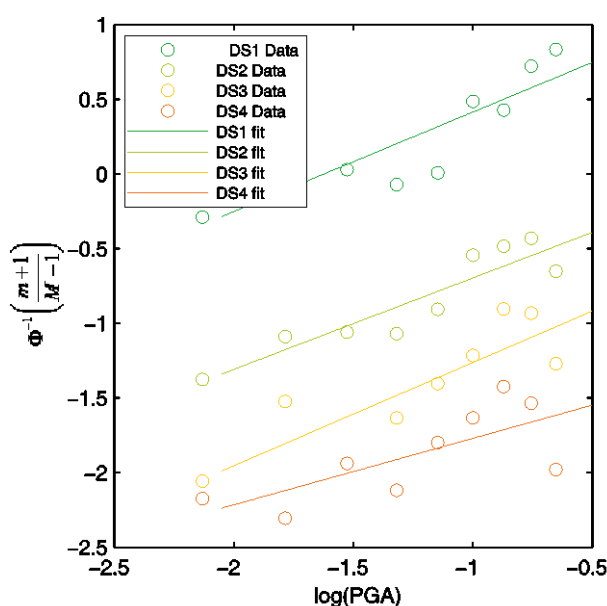


Figure 6-24: Linear regression parameters for the evaluation of lognormal distributions for DS1-DS4 according to (Porter et al., 2007) for RC-LH-NS building class.

Indeed, for each of the class of building defined in Table 6-8, the procedure previously illustrated is repeated. Hence in Table 6-8, the parameters of lognormal fragility curves (μ , exponential value of lognormal mean; β , lognormal standard deviation) for each class of building are reported.

Table 6-8: Parameters of observational lognormal fragility curves for the class of building

	DS1		DS2		DS3	
	μ	β	μ	β	μ	β
RC-LH-NS	0.2	1.4	1.1	1.5	2.2	1.4
	1	6	6	9	5	1
RC-LH-S	0.3	1.7	8.7	2.8		
	6	4	5	0		
RC-MH-NS	0.1	1.1	0.4	0.9	0.6	0.7
	3	2	1	8	4	5
RC-MH-S	0.0	1.7	0.5	1.4	1.2	1.4
	9	2	1	9	7	6

In Figure 6-25-Figure 6-28 the fragility curves for the class of building previously defined are shown.

Nevertheless, since the data quality is not homogenous, this simple linear regression procedure could lead to not reliable results. In fact, the subdivision of the available data into different building classes and PGA bins has the effect of reducing the size of some samples. In order to investigate the reliability of the procedure appropriate weights are introduced. Firstly, a weighted linear regression employing the number of buildings in each bin as weight (indicated in figures with the suffix 'Weight'). Secondly, the assessment of uncertainties of the damage distribution for each PGA bin and each class of building, through the bootstrap technique ([Efron and Tibshirani, 1994](#)) is evaluated. For this purpose, each building class data set is resampled with substitution to generate several samples of the same size, which are then analysed in order to estimate the standard deviation of each damage state probability. Hence, the weighted linear regression is set employing the

inverse of the estimated standard deviation in each bin as weight (indicated in figures with the suffix 'std').

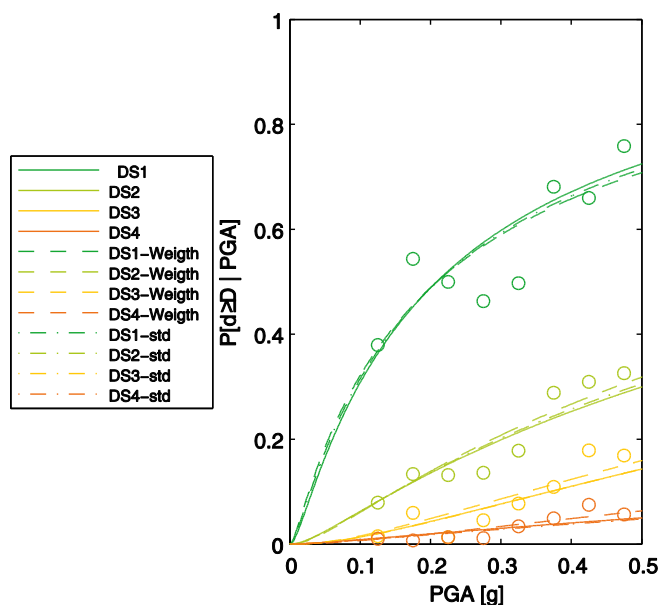


Figure 6-25: Observational fragility curves for pre-1981 buildings with $3 \leq N_{\text{stores}}$ (RC-LH-NS)

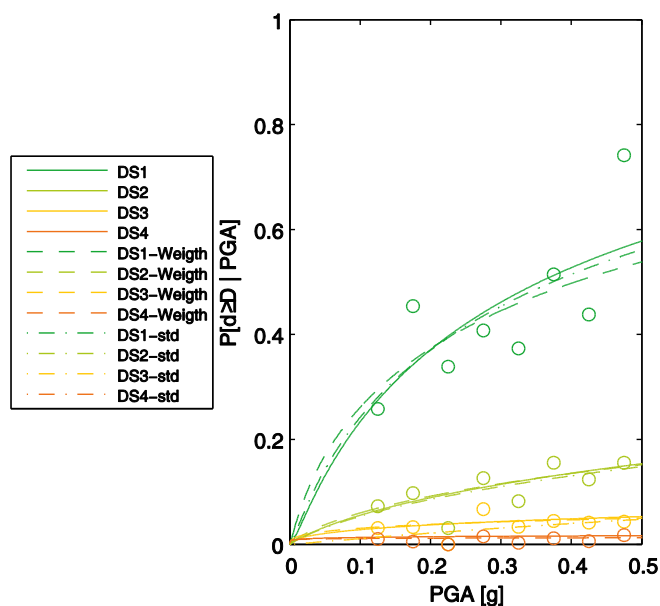


Figure 6-26: Observational fragility curves for post-1981 buildings with $3 \leq N_{\text{storeys}}$ (RC-LH-S)

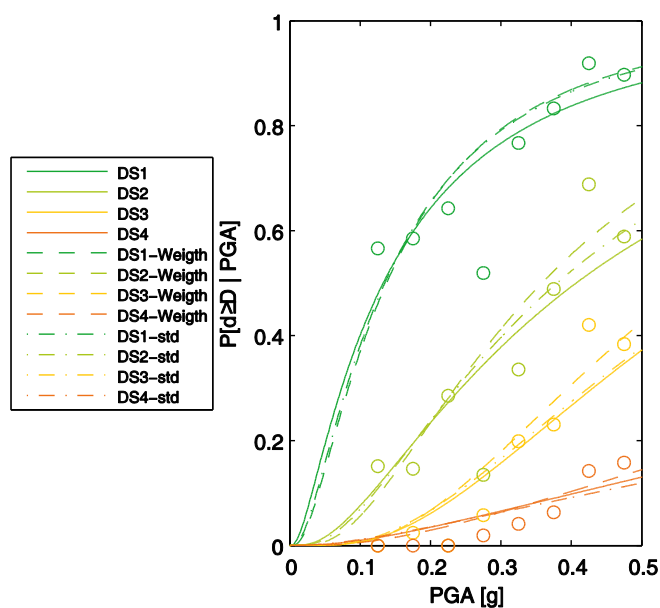


Figure 6-27: Observational fragility curves for pre-1981 buildings with $N_{\text{storeys}} > 3$ (RC-LH-S)

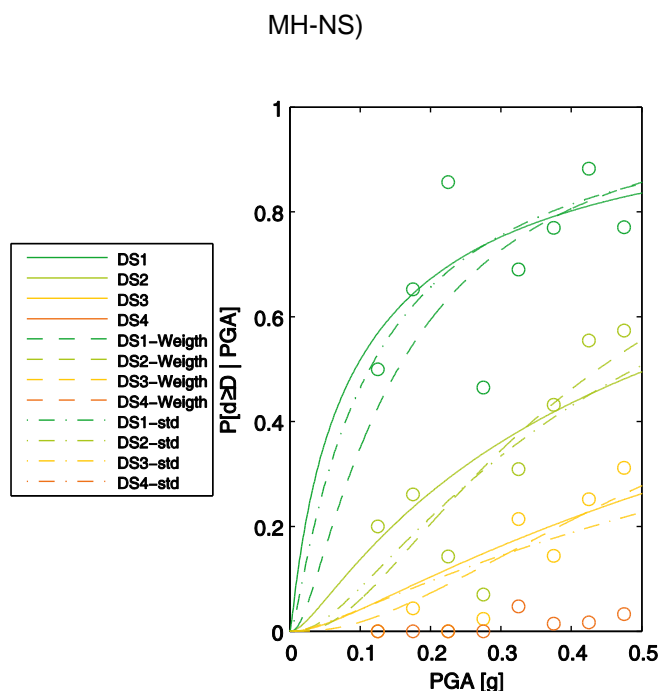


Figure 6-28: Observational fragility curves for post-1981 buildings with $N_{\text{stores}} > 3$ (RC-MH-S)

As a matter of fact, the effect of the weights is less important for the class of building characterized by a large amount of data, namely the RC-LH-NS class with the 41.7% of residential RC buildings, while it can strongly improve the quality of results for typologies with smaller observed samples, as for RC-MH-S with the 7.6% of buildings.

6.5 Predicted damage scenario

In the present section fragility curves for building class characteristic of L'Aquila building stock are derived. In particular, the results of survey forms, collected in a GIS database (see section 6.2), are employed to define the random variables in order to completely define global dimensions of buildings within the class.

Hence, seismic vulnerability assessment of infilled RC building through POST (PushOver on Shear Type models) methodology (section 3.3, [Ricci, 2010](#), [Del Gaudio et al, 2015](#)), has been derived. The methodology is essentially based on a simulated design procedure to evaluate the geometrical and structural model of the building based on few data such as number of storeys, global dimensions and type of design ([Verderame et al. 2010](#)). Building non-linear static response is evaluated through a closed-form procedure starting from non-linear behavior of structural (RC columns) and non-structural components (infill panels), considering acting in parallel, thanks to the simplified assumption of a Shear Type behavior.

The assessment of the seismic capacity is based on the mechanical interpretation of the damage states described by the European Macroseismic Scale (EMS-98) ([Grünthal, 1998](#)) through the simplified IDA curves derived from ([Vamvatsikos and Cornell, 2006](#)). Hence the methodology allow to take into account the influence of infill panel both in the definition of the non-linear static response of building and seismic capacity, relating displacement thresholds on the non-linear behavior of infill sub-assemblages, selected on mechanical basis and experimentally validated, to the description of damage reported in EMS98.

The methodology allows the probabilistic seismic demand evaluation for single building, through the introduction of random variables related to material properties, capacity models, both for RC columns and infill panels, and seismic response.

Actually, material characteristics of an existing building, should be categorized as an epistemic uncertainties, since they can only be characterized from laboratory or in-situ tests.

For what concerns capacity models, these are invariably imperfect mathematical idealizations of reality and contain uncertain errors. Their parameters are usually assessed through a process of “fitting” these sub-models to observed data (experimental tests). The relative uncertainty in the model is a mixture of aleatory and epistemic model uncertainties.

Analogously, uncertainty related to seismic response is evaluated through a series of incremental dynamic analysis ([Vamvatsikos and Cornell, 2006](#)), a parametric analysis method that estimates seismic demand and capacity by subjecting different structural models, namely SDOF systems with a variety of quadrilinear backbones that mimics the Static Pushover, to several ground motion records, each scaled to multiple levels of intensity ([Vamvatsikos and Cornell, 2002](#)). In such a way, the Authors have shown the influence of the SPO curve on the dynamic behavior and at the same time allow to supply the variability of seismic response (spectral ordinate) as a function of demand parameters which monitors the structural response of the model, or vice versa.

Hence, following a Monte Carlo simulation technique procedure the methodology is iteratively repeated. In any single run, a realization of random variable is sampled according to the marginal distributions chosen to define its variability. Accordingly, in any single run the building non-linear static response (Static pushover analysis) is derived and seismic capacity is evaluated. Therefore, at the end of the simulation, once PGA capacity at a given damage state is calculated for all the runs, the corresponding cumulative frequency distributions provide the fragility curves at each damage state.

Furthermore, given a single defined building, some variables can be assumed as Random Variables because their values cannot be known in a deterministic manner, for lack of knowledge or because their

definition may require an excessive cost or it can not be easily and quickly determined.

In the following the definition of the class is based on parameters which affect the seismic behaviour of the buildings, while they are available at a large scale.

6.5.1 Definition of building class

Generally speaking, within an engineering analysis model the lack of knowledge part of the uncertainty can be represented in the model by introducing auxiliary non-physical variables (Der Kiureghian and Ditlevsen, 2009). In such a way, homogeneous classes of buildings can be defined, identifying the parameters that greatly influence their seismic fragility.

Obviously, the choice of the parameters defining the class, is necessarily conditioned by the available level of information.

The variability within a class takes into account the variability between the fragility of different buildings in the same class (intra-variability), apart from the variability between the fragility of different classes of building.

It can be stated that the fragility of a building should coincide with the fragility of the class to which it belongs, unless of some deviations between the fragility of buildings belonging to the same class, which in theory should be as limited as possible. Such deviations are greater the higher is the heterogeneity within the class of the parameters that greatly influence the seismic fragility. This heterogeneity is in turn necessarily conditioned by the available level of information.

In this regard, it is worth highlighting that does not exist a clear distinction between fragility of building and fragility of class of building. This distinction is greatly ascribable to the nature and the extent of the involved uncertainties, and is in turn mainly attributable to the available level of information.

To this aim, the definition of the class should be based on parameters which affect the seismic behaviour of the buildings, while they are available at a large scale. The very simple features which may be directly related to the seismic assessment are number of storeys and design code enforced at time of construction.

In this study, four different classes of buildings have been defined, as reported in Table 6-9, as a function of the number of storeys (less or equal to 3 and greater than 3) and of the age of construction (prior to or after 1981), which is related to design code enforced. Effectively, the (DM 3/3/1975) can be considered as the first modern seismic design in Italy (Rota et al, 2007).

Table 6-9: Definition of Building Class

	Pre 1981	Post 1981
$N_{storeys} \leq 3$	RC_LH_NS	RC_LH_S
$N_{storeys} > 3$	RC_MH_NS	RC_MH_S

Hence, for each Building class using the Monte Carlo simulation technique procedure additional variables have to be set, in order to define the geometrical configuration of the Building class.

Hence, for each Building and for each run of the procedure a virtual building is defined by a realization of the vector of random variables, which may also include plan dimensions, bay lengths and inter-storey height, in addition to material properties, and variables related to capacity models and seismic response.

Therefore, at the end of the simulation, once PGA capacity at a given damage state is calculated for all the runs, the corresponding cumulative frequency distributions provide the fragility curves for the considered building class (see Table 6-9) at each damage state.

Hence, the fragility curve for a building class relative to a DS can be used to estimate the probability of exceeding of that particular DS for the building representative of the class, or alternatively to assess the fraction of buildings within the class expected to exceed that particular damage state.

6.5.2 Geometrical model for the building class

In the following seismic vulnerability assessment of RC building stock for L'Aquila area is derived. Hence, the individuation of building classes is performed in section 6.5.1 in order to derive fragility curves and damage scenario at urban scale.

This circumstance is due to the fact that the application concerns with spatially extended and numerous populations of buildings (8463). Hence, it can be considerably time-consuming and would require a large amount of input data with a high level of detail to perform the application at the level of individual building. The latter is a very restrictive condition, since the available input data for this application are not characterized by a level of detail such as to provide the geometric model of the single building. Indeed, input data are derived from the AEDES survey form ([Baggio et al, 2007](#)) collected just after the earthquake of 6/4/2009, see section 6.3.

Hence, the parameters defining plan dimensions, namely bay lengths and inter-storey height, are assumed as random variables in addition to material properties, and variables related to capacity models and seismic response.

Obviously, the result in terms of fragility curves is sensitive to changes in correlations among the input random variables. Therefore, it is essential to precisely capture the input correlations in the simulated values.

The choice of these variables is made according to correlation value that affect the building of that particular class, so as at the end of the simulation, the virtual population of building, extracted at each single

run through the definition of random variables, exactly reflects the characteristics of surveyed buildings for the class considered according to AEDES form, see section 6.2.

Thus, Monte Carlo type simulation approaches with sampling of correlated data from their distributions is performed.

First of all, the availability of a detailed database on the characteristic of building stock of L'Aquila area has allowed to estimate the correlation between geometrical and morphological building parameters and hence to incorporate this correlation in the Monte Carlo type simulation.

It is to be noticed from Figure 6-30, which reports data about number of storeys and Average storey surface for RC residential buildings, that a strong correlation between the parameters exists. As a matter of fact increasing the number of storeys a significant increase in the Average storey surface can be observed. This circumstance can be related to the fact that low-class of building ($N_s \leq 3$) is characterized by a non-intensive housing typically constituted from single-family home with a limited Average storey surface, whereas medium-class of building ($N_s > 3$) is characterized by a residential housing constituted from multi-family home with an Average storey surface ranging from 230 to 500 m².

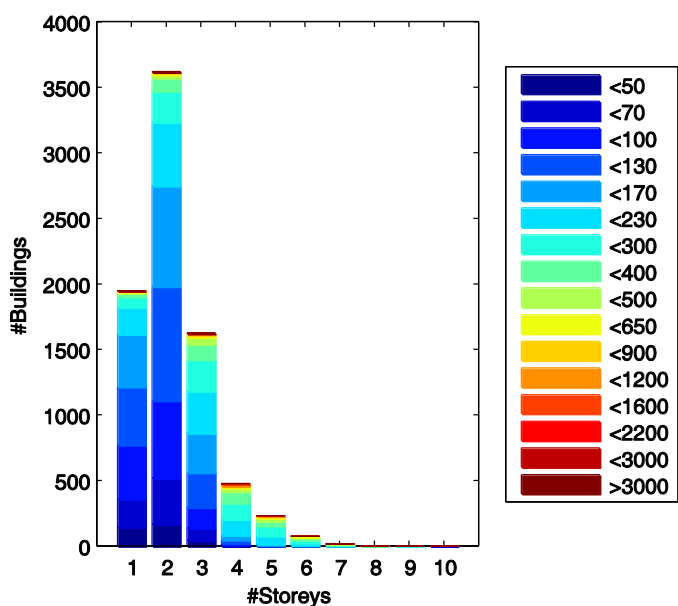


Figure 6-29: Distribution of plan area depending on number of storeys for residential RC Building of L'Aquila area

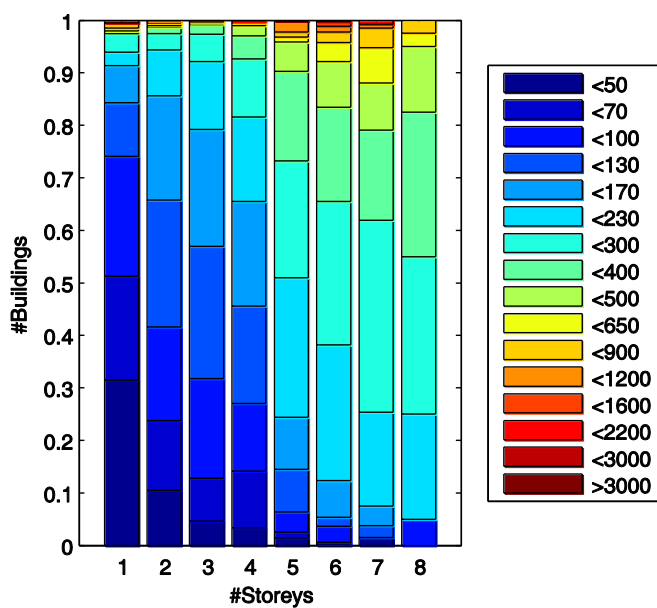


Figure 6-30: Percentage distribution of plan area depending on number of storeys for

residential RC Building of L'Aquila area

Figure 6-32 shows the distribution of number of storeys and age of construction for residential RC buildings. It can be highlighted a uniform development in the years of the construction industry for buildings with a number of storeys less than 5, constituting the 86% of the whole sample.

From Figure 6-32 it may appear that in 60-70 years there has been an increase in construction with a higher number of storeys, in particular for numbers of storeys greater than 6. However, these data are not very significant from a statistical standpoint, representing not more than 2% of the whole sample.

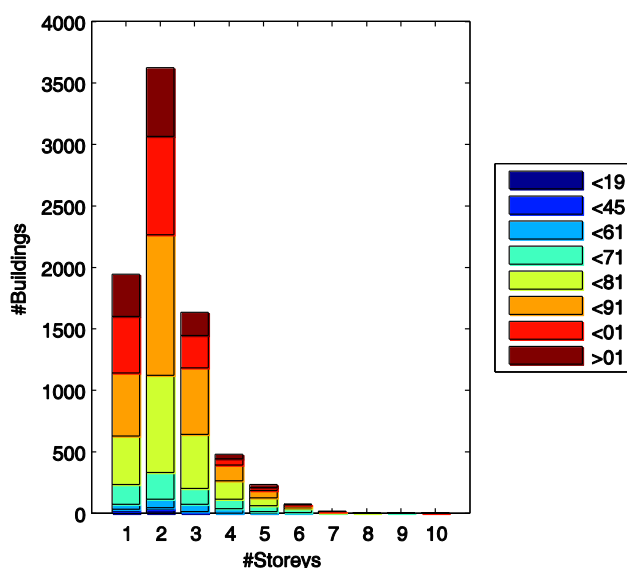


Figure 6-31: Correlation between Number of storeys and age of construction for residential RC Building of L'Aquila area

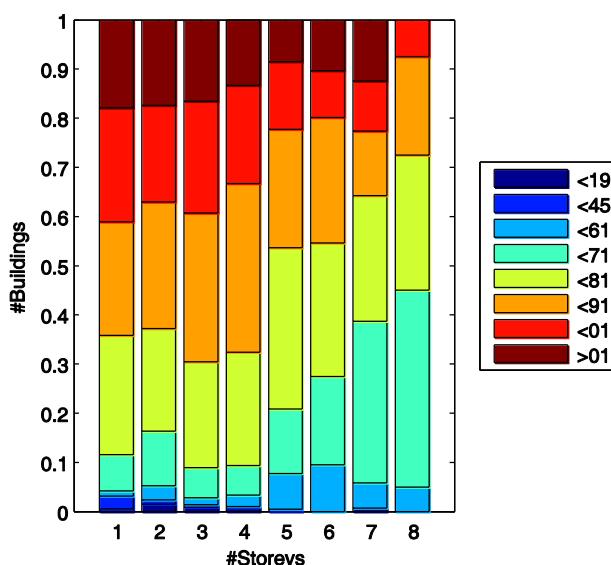


Figure 6-32: Correlation between Number of storeys and age of construction for residential RC Building of L'Aquila area

Finally, Figure 6-34 shows the distribution of age of construction with the average area surface for residential RC buildings. It can be observed a slight correlation between the parameters. In Particular, excluding buildings built prior to 1945, representing just over 1% of the sample, it can be observed increasing age of construction from 1945 until 2000, a slight reduction in the Average storey surface of building.

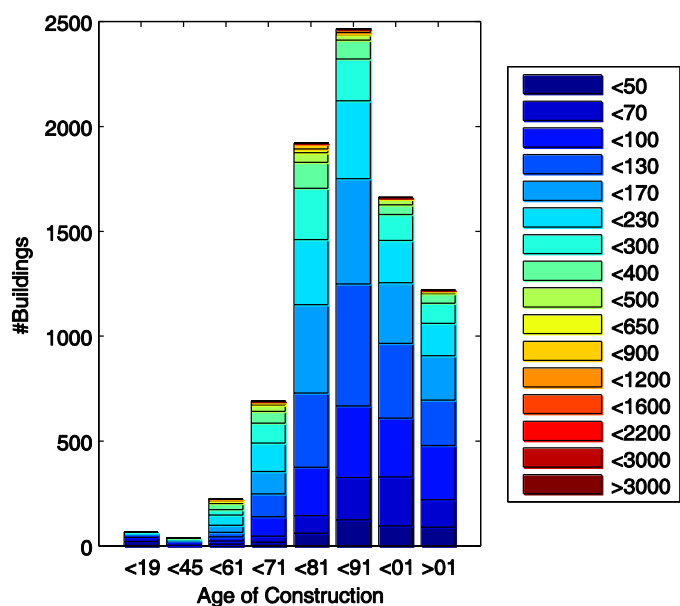


Figure 6-33: Correlation between age of construction and average storey surface for residential RC Building of L'Aquila area

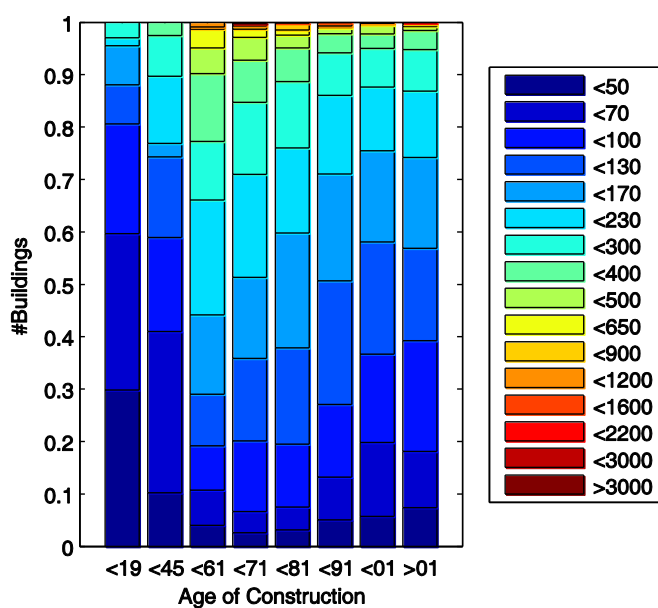


Figure 6-34: Correlation between age of construction and average storey surface for

residential RC Building of L'Aquila area

In conclusion, looking at the data collected through the AEDES survey form after the L'Aquila earthquake for residential RC buildings, that there is a strong correlation between the number of storeys and the relative average storey surface of the buildings, while there is a weak correlation between the age of construction and Average storey surface and a very slight correlation between the number of storeys and age of construction of residential RC buildings.

In the following, this information will be used in the Monte Carlo approach in order to change the random variables that will define the geometry and structural typology of the buildings of the class, in order to take into account such dependencies.

For this purpose, an analogy between the statistical mechanics of large multivariate physical systems and combinatorial optimization is used to develop a strategy for the optimal ordering of samples to control the correlation structure. The problem of optimal sample ordering is solved by the so-called Simulated Annealing method using a Monte Carlo procedure ([Vorechovský and Novák, 2009](#)).

The Simulated Annealing method originated in the early 1980s when ([Kirkpatrick et al., 1983](#)) and ([Cerný, 1982](#); [Cerný, 1985](#)) independently explored an analogy between the physical annealing process in solids and the task of solving large combinatorial optimization problems. Annealing, in metallurgy, refers to a heat treatment that alters the microstructure of a material causing changes in properties such as strength and hardness. It causes a solid in a heat bath to enter low energy states. In this process, the solid is first heated to melting point and then slowly cooled until the low energy ground state is reached.

The imposition of a prescribed correlation matrix into a sampling scheme can be understood as an optimization problem: we want to minimize the difference between the target correlation matrix and the actual correlation matrix.

In the algorithm proposed by (Vorechovský and Novák, 2009), the first step (mutation) is performed by a transition called a swap from the initial configuration to the actual configuration. A swap (or a trial) is a small change to the arrangement of random variables. It is done by randomly interchanging a pair of two random variable. Such a change to the arrangement of samples requires the recalculation of correlation coefficients to update the objective function, difference between the correlation target matrix actual correlation matrix. One swap may or may not lead to a decrease in the objective function. The procedure is repeated minimizing the objective function, namely until the actual correlation matrix is equal to the target correlation matrix.

Nevertheless, in order to completely define the geometrical model of building, in addition to Average storey surface and number of storeys, is necessary to define its plan ratio to detect the relative dimension in plan. Unfortunately, plan ratio is not reported in AEDES survey form, although it is a parameter which can greatly affect the response of the building.

Then, since it was available a subset (131 buildings) of the whole sample located in the area of Pettino in the municipality of L'Aquila, for which in addition to the parameters obtained from the survey form was also known the building plan morphology based on a digital regional technical land-use map (see Section 5.2), it is assumed that the relation between average storey surface and plan ratio, see Figure 6-35, is somehow representative of the whole sample of buildings.

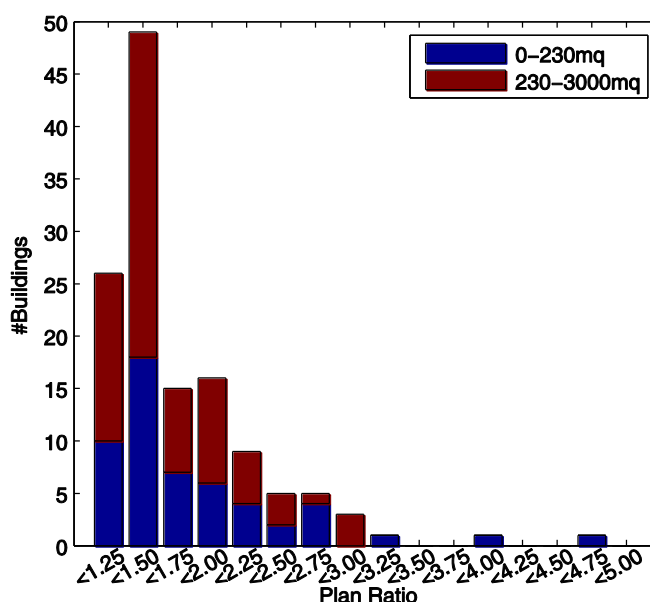


Figure 6-35: Correlation between plan ratio and average storey surface for 131 Building of Pettino area

6.5.3 Input data

In the following the input parameters defining the classes of building are reported. The considered buildings are symmetric in plan, both in longitudinal (X) and in transversal (Y) direction. Number of storeys, age of construction, average storey surface and plan ratio, are assumed as random variables and for each run of Monte Carlo simulation technique procedure their realization is obtained from survey data according to what extensively reported in section 6.5.2.

Hence, the number of bays in longitudinal and transversal direction is evaluated in correspondence with the value that minimizes the deviation from a target value of the bay length equal to 5 m. Interstorey height is assumed equal to 3.0 m.

The structural model of buildings, located in the Municipality of L'Aquila (42°21'14.43"N 13°23'31.17"E), is defined by means of a

simulated design procedure according to code prescriptions and design practices in force at the age of construction. Hence, for each building class once the variable related to age of construction has been extracted the corresponding type of design is obtained, namely Gravitational or Seismic. In the case of seismic design the base shear coefficient and the distribution of lateral forces are derived based on the code in force at the age of construction of building for the corresponding seismic category of the Municipality where the building is located. Accordingly, element dimensions and reinforcements are derived. For further detail see section 5.4.1.

Reference values of material properties are assumed from statistical analyses of the mechanical characteristics provided by the technical literature ([Verderame et al., 2001](#); [Masi and Vona, 2009](#); [Verderame et al., 2012](#)), see Table 5-2.

Values for infill mechanical characteristics based on the proposal of the Italian code ([Circolare 617, 2009](#)) for hollow clay brick panels have been set. Hence, assuming a full correlation between mechanical characteristics, the ratio between E_w and G_w is assumed equal to 10/3, whereas τ_{cr} is assumed as linearly dependent on G_w , assuming τ_{cr} equal to 0.3 and 0.4 MPa for G_w equal to 1080 and 1620 MPa, respectively. In particular, a value of the elastic modulus equal to 4500 MPa and a CoV of 30% have been adopted.

The influence of openings in decreasing lateral stiffness and strength of infill panels is taken into account through the introduction of control parameters reported in ([Kakaletsis and Karayannis, 2009](#)), according to the procedure extensively discussed in 3.3.2. The opening shape is assumed equal to the 25% of the corresponding infill length, regardless the opening type. The latter is assumed as a random discrete variable, as a function of the three types panel (solid, panel with window and balcony), with a uniform probability distribution. In such a way, considering a facade consisting of three bays, each of them will be

characterized by a different opening type, namely solid panel, window opening and door opening.

Finally a thickness of external infill panels equal to 200mm is assumed and an thickness of internal infill panels for each one directions evaluated considering an internal infill percentage, $\rho_{w,int}$ equal to 50% of external one, for further detail see 3.3.2.

Afterwards, a tri-linear envelope is assumed for the moment-rotation model, with cracking and yielding as characteristic points. Behaviour is linear elastic up to cracking and perfectly-plastic after yielding (see Figure 3-6).

Moment at yielding (M_y) is calculated in closed form by means of the first principles-based simplified formulations proposed in proposed in (Fardis, 2007 – Section 3.2.2.2, Eqs. 3.33 to 3.37). Rotation at yielding (θ_y) is univocally identified by M_y and the secant stiffness to yield provided by (Haselton et al., 2007– Section 3.2.4.1, Eq. 3.1). The Authors also investigate uncertainty associated with each prediction identified by the logarithmic standard deviation and by the average of the ratio between the observed and predicted values, reported in Table 5-3, assuming that the model parameters follow a lognormal distribution.

Damage States adopted in the proposed analytical methodology are defined according to the damage scale proposed by EMS-98 (Grünthal, 1998).

To this aim, analytical displacement thresholds corresponding to the damage to structural and non-structural elements described by EMS-98, based on the mechanical interpretation of the reported description of damage are assumed.

Table 5-4 reports, for each one of the five EMS-98 damage grades, key sentences describing the damage to infills and RC members, respectively, and the corresponding assumed analytical displacement threshold. Note that, due to the assumed Shear-Type behaviour, the interstorey displacement leading to the attainment of each Damage

State is the minimum between the values reported in Table 5-4 for infill panels and RC columns.

Then, analytical displacement thresholds, corresponding to the damage to non-structural elements described by EMS-98, are assumed from the mean and CoV values reported in Table 5-6.

Definitely, the methodology described in 3.3.3-3.3.4 is applied, leading to the definition of Nonlinear Static Push-Over (SPO) curve, both in X and Y direction, of a Multi-linearization Curve by applying the equal energy rule, and of simplified Incremental Dynamic Analysis (IDA) curves according to (Vamvatsikos and Cornell, 2006). The latter allow to obtain a relationship between a seismic intensity measure (spectral ordinate) and an Engineering Demand Parameter (ductility).

Finally, Elastic spectra are the Uniform Hazard Newmark-Hall demand spectra provided in (Eurocode (CEN)). Soil type B (as reported in De Luca et al. 2014, Chioccarelli et al. 2009) is assumed. Hence, PGA value is evaluated from the corresponding spectral ordinate evaluated on the IDA-curve as a function of the capacity displacement for each DS according to Table 5-4.

Hence a Monte Carlo simulation is used, and sampling of Random Variables is carried out through the efficient stratified Latin Hypercube Sampling (LHS) technique (McKay et al., 1979), adopting the “median” sampling scheme (Vorechovsky and Novak, 2009). In this way, a population of buildings is generated, each one corresponding to a different set of values of the defined Random Variables, regarding

- i. *Number of storeys, age of construction, average storey surface and plan ratio* according to Simulated Annealing method (Vorechovský and Novák, 2009) in order to account for correlations among the input random variables, see Section 6.5.2;
- ii. *Material properties* (see Table 5-4),
- iii. *Capacity models* (see table Table 5-3);
- iv. *Displacement threshold for infill panels* (see Table 5-6);

v. *Seismic response* according to (Vamvatsikos and Cornell, 2006), see Eq 3-14.

Therefore, if PGA capacity, at a given DS, is calculated for all the generated buildings, the corresponding cumulative frequency distributions of the obtained PGA capacity values provide the fragility curves in X and Y directions and at each DS. In the same way fragility curves independent of the direction can be obtained, through the evaluation of the cumulative frequency distribution of the minimum PGA capacities between longitudinal and transversal direction for each sampling.

Note that the fragility curves calculated herein are for building classes, see Table 6-9. Then, the exponential value of lognormal mean, μ , and the lognormal standard deviation, β , for each class are reported in Table 6-10.

Table 6-10: Parameters of lognormal fragility curves for the class of building

	DS1		DS2		DS3		DS4		DS5	
	μ	β	μ	β	μ	β	μ	β	μ	β
RC_LH_NS	0.21	0.62	0.50	0.56	0.70	0.65	1.66	0.94	1.94	0.96
RC_LH_S	0.22	0.58	0.51	0.55	0.71	0.63	1.68	0.93	1.97	0.96
RC_MH_NS	0.09	0.41	0.27	0.35	0.36	0.41	0.81	0.71	1.00	0.77
RC_MH_S	0.11	0.45	0.29	0.36	0.39	0.41	0.86	0.71	1.05	0.76

6.6 Comparison and Analysis of Results

In this Section, fragility curves derived from POST methodology, see Table 6-10, in addition to fragility curves derived from ([Lagomarsino and Giovinazzi, 2006](#), [Rota et al, 2008](#)), are used to derive seismic damage scenario for residential RC Buildings of L'Aquila area, which has been subjected to a field survey just after the Earthquake that hits the area in 06/04/2009.

Each scenario is compared with observed damage resulting from AEDES inspection form ([Baggio et al., 2007](#)).

Note that fragility curves are derived herein for building classes, see Section 6.5.1 for further detail. The latter are evaluated considering a horizontal soil type B. Indeed soil type of a station of the National Accelerometric Network (Rete Accelerometrica Nazionale, RAN) in the area was classified according to cross-hole test results as type B, see ([De Luca et al. 2014](#), [Chioccarelli et al. 2009](#)) for more details.

Then distribution of damage for each building is derived according the following steps: (i) identification of the class to which the building belongs, based on the number of storeys and at the age of construction; (ii) identification of the corresponding fragility curves for each DS; (iii) evaluation of PGA for each building from shake map of the event, Figure 6-23; (iv) derivation of building damage distribution.

Thus identifying the fragility of the building with the fragility of the class to which it belongs, seismic scenario can be considered as the probability that the building has to be characterized by that damage level. Conversely, it can be considered as the percentage of buildings belonging to that building class characterized by that the damage level.

Ultimately, the fragility curves of building class are used to detect the damage scenario of single building from the value of PGA, obtained from ShakeMap, at which the building has been subjected during the seismic event of 06/04/2009.

Figure 6-37 shows the damage distribution for the whole database derived summing up all damage distributions for the whole residential RC building dataset. Then, the predicted and observed scenario are compared, the latter derived interpreting a posteriori the condensed damage grades (D0, D1, D2–D3 and D4–D5) reported for vertical structures and infill panels in AeDES form in order to derive DSs according to EMS98, see Section 6.4. It is to be noted the good agreement between the observed and predicted results.

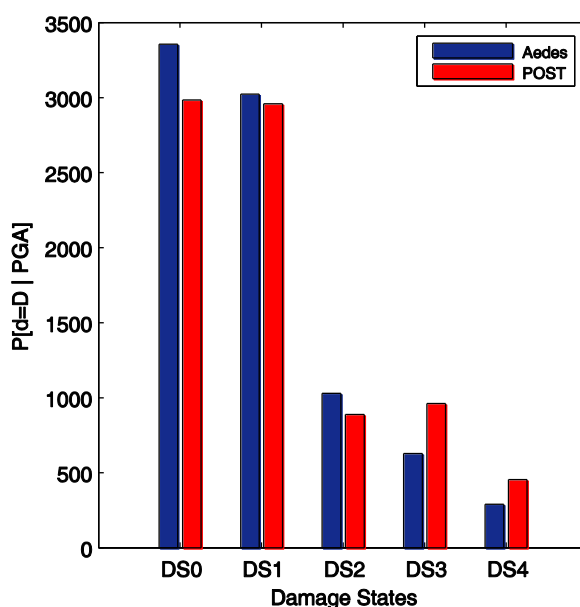


Figure 6-36: Distribution of predicted damage according to POST methodology and observed damage

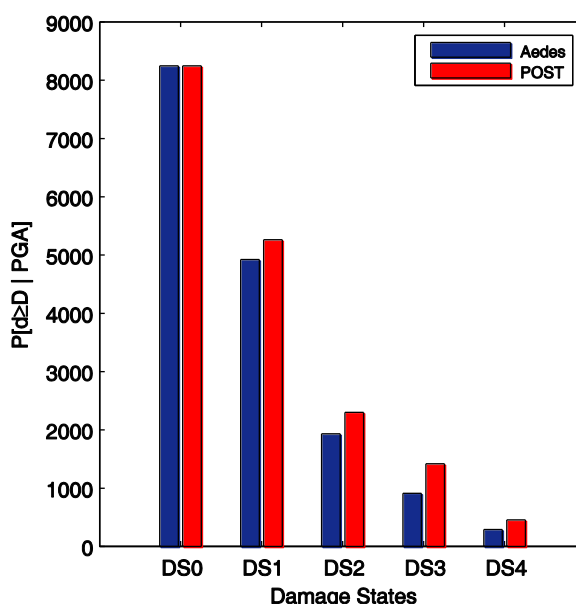


Figure 6-37: Cumulative distribution of predicted damage according to POST methodology and observed damage.

Figure 6-39 reports the comparison between observed and predicted damage scenario from the procedure reported in ([Lagomarsino and Giovinazzi, 2006](#)), briefly mentioned in section 5.3.

Damage scenario is derived using Low and Medium-Rise Concrete Moment Frames with Earthquake Resistant Design in second seismic category with Low Ductility, “RC1-II_L DCL” and “RC1-II_M DCL” typologies for soil type B.

Figure 6-41 reports the comparison between observed and predicted damage scenario from ([Lagomarsino and Giovinazzi, 2006](#)), resulting in a poor agreement between the results, as the predicted damage results extremely conservative.

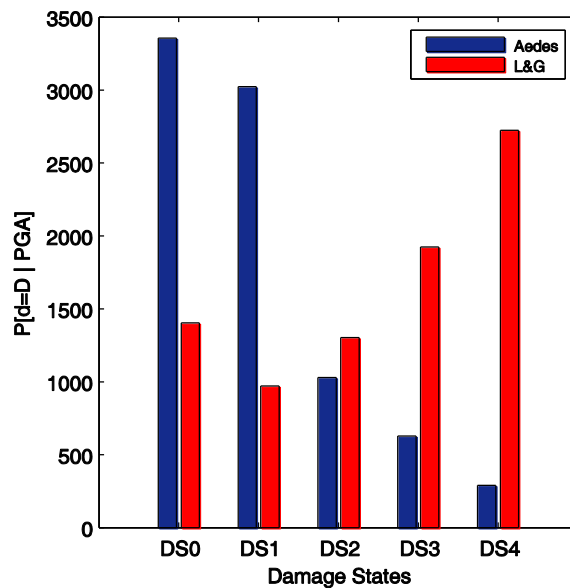


Figure 6-38: Distribution of predicted damage according to (Lagomarsino and Giovinazzi, 2006) methodology and observed damage

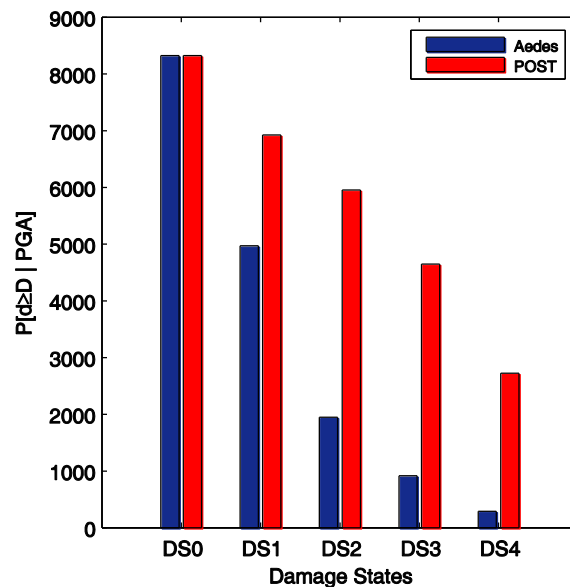


Figure 6-39: Cumulative distribution of predicted damage according to (Lagomarsino and Giovinazzi, 2006) methodology and observed damage methodology and observed

damage.

Figure 6-41 shows the comparison between observed damage and damage scenario obtained from fragility curves obtained through the procedure reported in (Rota et al., 2008), briefly mentioned in section 5.3.

It is to be noted that due to the reduced amount of data, no fragility curve is provided for RC buildings with seismic design and $N_{storeys} \geq 4$. Hence buildings falling in this class (buildings constructed after 1981 characterized by a $N_{storeys} \geq 4$) are excluded from the hereinafter comparison of results. Therefore, the comparison of Figure 6-41 deals with 7994 buildings in contrast to what previously shown.

Therefore, fragility curves for low- and medium-rise non-seismically designed RC Building (when constructed before 1975), “RC2” and “RC4” typologies, and for low-rise seismically designed RC Building (when constructed before 1975), “RC1” typology, are herein adopted.

Figure 6-41 reports the comparison between observed and predicted damage scenario from (Rota et al., 2008), resulting in a quite good agreement between the results. In effect the predicted damage scenario detects a higher number of buildings in DS0 and DS4 than those actually observed through the AEDES inspection form, to the detriment of the remaining DSs.

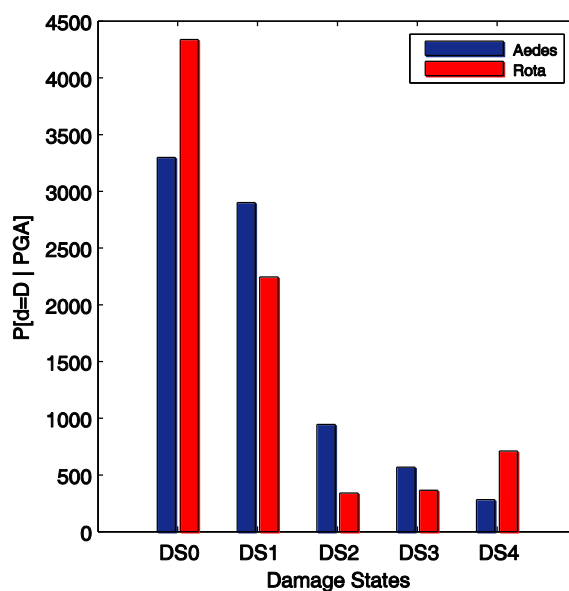


Figure 6-40: Distribution of predicted damage according to (Rota et al., 2008) methodology and observed damage methodology and observed damage.

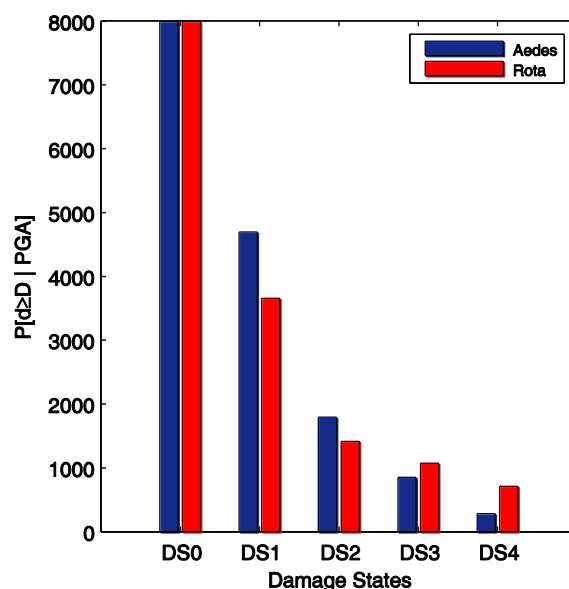


Figure 6-41: Cumulative distribution of predicted damage according to (Rota et al., 2008) methodology and observed damage methodology and observed damage.

Hereinafter damage scenarios subdivided into PGA bins, ranging from a 0 value up to a maximum value of 0.55g, with an increase of 0.05g, the same used in Section 6.4 to derive empirical fragility curves, are shown.

Figure 6-42 shows the damage distribution according to POST methodology derived summing up all damage distributions for each PGA bin for the whole residential RC building dataset.

It can be noted that the higher the value of PGA for an assigned DS the higher is the number of buildings characterized by that particular DS. Vice versa for DS0, where the opposite trend can be observed.

On the other hand, Figure 6-43 shows the observed damage scenario derived from DS for each building according to EMS98 obtained from the condensed damage grades reported for vertical structures and infill panels in AeDES. Hence, Figure 6-43 reports for each PGA bin and for each DS the number of buildings characterized by that particular DS and a value PGA from ShakeMap included in that PGA bin.

It can be highlighted comparing the results from Figure 6-42 and Figure 6-43, namely between predicted and observed damage, a good agreement between the data for DS2-DS3-DS4, while a less satisfactory agreement for DS0-DS1.

In particular, predicted damage scenario tends to overestimate the number of buildings in DS0 for low PGA values compared to observed damage scenario, and underestimate for high PGA values. Vice versa predicted damage scenario tends to underestimate the number of buildings in DS1 for low PGA value compared to observed damage scenario, and overestimate for high PGA value

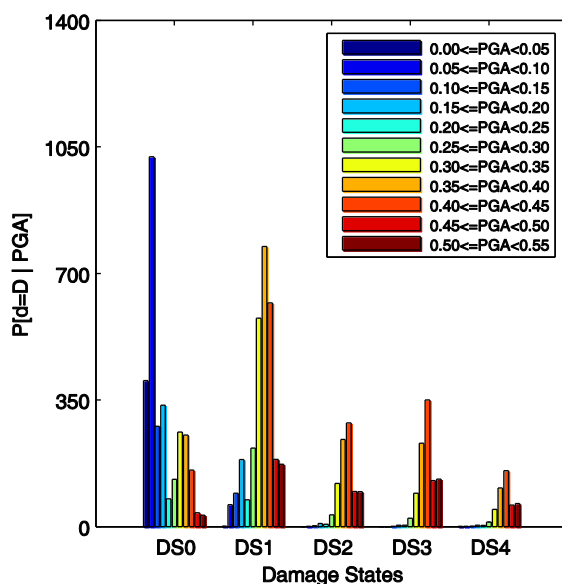


Figure 6-42: Damage Scenario from POST methodology subdivided into PGA bins

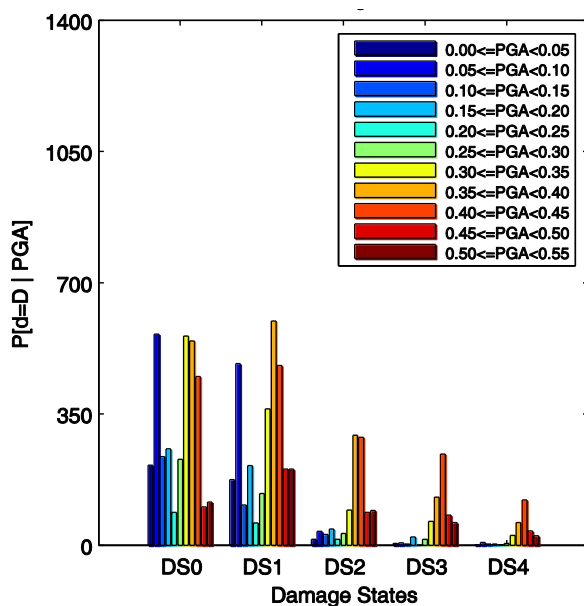


Figure 6-43: Damage Scenario derived from AEDES inspection forms subdivided into PGA bins

Therefore, in order to better investigate these trends, hereinafter the same results are shown presenting a direct comparison between predicted and observed scenario for each DS for the different PGA bins.

Figure 6-44 shows the comparison between the damage scenarios for DS0.

It can be noticed in Figure 6-44 that the POST methodology leads to an overestimation in the number of buildings characterized by DS0 and a PGA value between 0 and 0.1g, variable between 83 and 93% compared to those detected through AEDES inspection form. Vice versa, the POST methodology leads to an underestimation in the number of buildings characterized by DS0 and a PGA value between 0.35 and 0.45g, variable between 50 and 70% compared to those detected through AEDES inspection form.

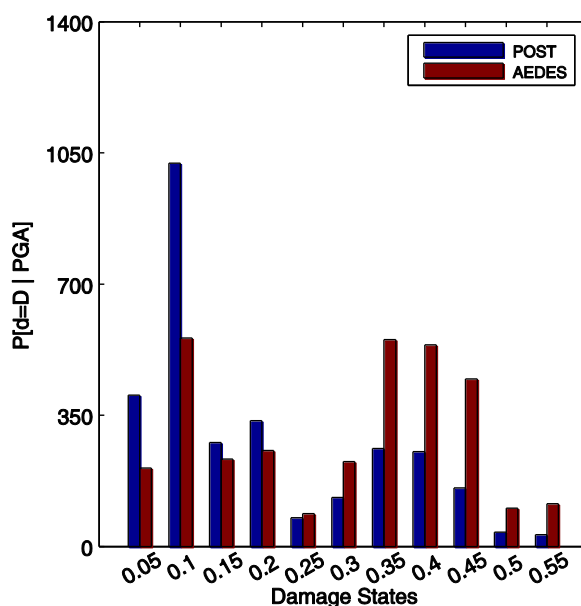


Figure 6-44: Comparison of the damage predicted by POST methodology and observed damage subdivided into PGA for DS0

Similarly, Figure 6-45 shows the comparison between the damage scenarios for DS1.

It can be noticed in Figure 6-45 that the POST methodology leads to an underestimation in the number of buildings characterized by DS1 and a PGA value between 0 and 0.1g, variable between 87 and 99% compared to those detected through AEDES inspection form. Vice versa, the POST methodology leads to an overestimation in the number of buildings characterized by DS1 and a PGA value between 0.35 and 0.45g, variable between 31 and 60% compared to those detected through AEDES inspection form.

This circumstance is probably related to logarithmic standard deviation (β) of DS1 fragility curve. As a matter of fact, β controls the slope of the fragility curve: the smaller the value of β , the less variable the PGA capacity, and the steeper the fragility curve. The larger the value of β , the more variable the DS, and the flatter the fragility curve. Hence, an increase in the β value would produce a flatter fragility curve, and hence an improvement in results for DS0 and DS1.

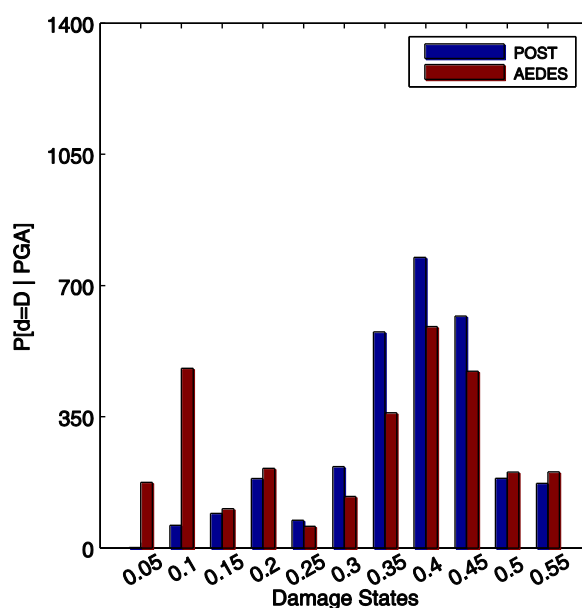


Figure 6-45: Comparison of the damage predicted by POST methodology and

observed damage subdivided into PGA for DS1

Figure 6-46, Figure 6-47 and Figure 6-48 show the comparison between the damage scenarios for DS2, DS3 and DS4.

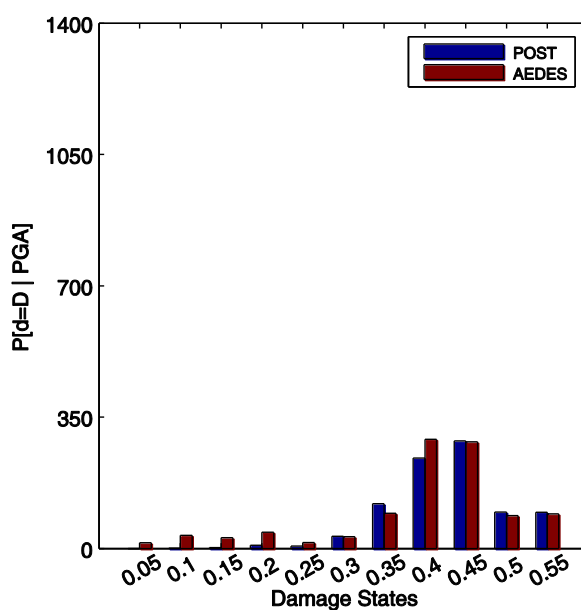


Figure 6-46: Comparison of the damage predicted by POST methodology and observed damage subdivided into PGA for DS2

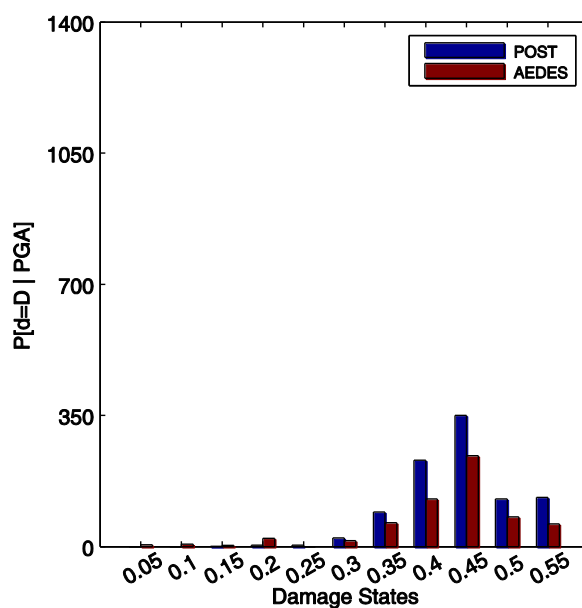


Figure 6-47: Comparison of the damage predicted by POST methodology and observed damage subdivided into PGA for DS3

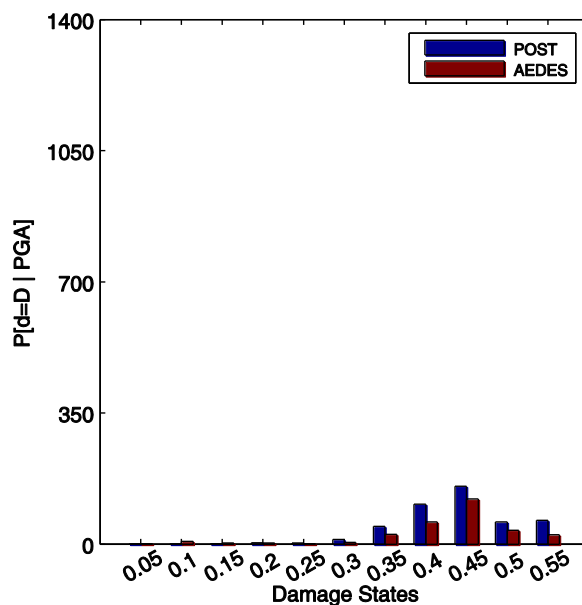


Figure 6-48: Comparison of the damage predicted by POST methodology and observed damage subdivided into PGA for DS4

Therefore, it can be argued that there is a good agreement between predicted and damage scenario, see Figure 6-41. The former is derived summing up all damage distributions evaluated for each single building from fragility curves, Table 6-10, for the whole residential RC building dataset. The latter is derived interpreting a posteriori the condensed damage grades (D0, D1, D2–D3 and D4–D5) reported for vertical structures and infill panels in AeDES form in order to derive DSs according to EMS98, see Section 6.4.

Hence, predicted and observed damage scenarios are subdivided into PGA bins, ranging from a 0 value up to a maximum value of 0.55g, with an increase of 0.05g.

It has been shown that POST methodology provides an overestimation of number of buildings in DS0 for low PGA value and an underestimation for high PGA values, and vice versa for DS1.

From one hand, this circumstance globally leads to a good result, because the errors are compensated each other. On the other hand, this circumstance can be related to a low value of logarithmic standard deviation (β) of DS1 fragility curve. As a matter of fact, increasing the β value would produce a flatter fragility curve, and hence an improvement in results for DS0 and DS1.

Finally hereinafter damage scenarios for the building class introduced in Table 6-9, are shown. In particular, four different classes of RC buildings have been defined, as a function of the number of storeys ($LH=N_s \leq 3$ and $MH=N_s > 3$) and of the age of construction (NS when buildings are dated before 1981; S when buildings are dated after 1981).

Figure 6-49 shows the damage distribution according to POST methodology derived summing up all damage distributions for the class to which the building belongs for the whole residential RC building dataset.

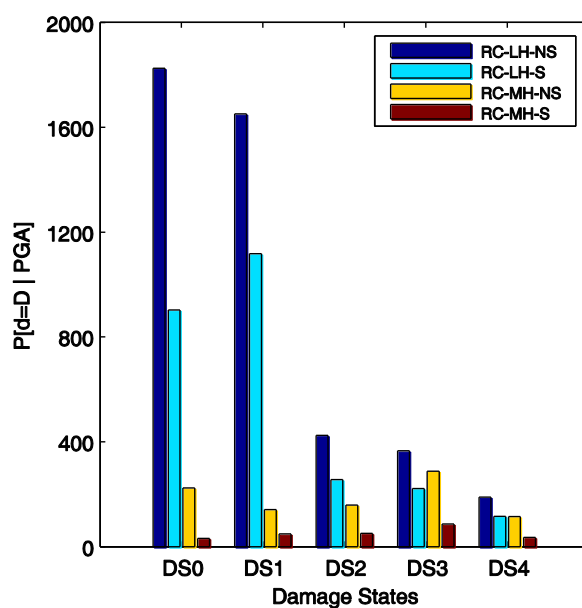


Figure 6-49: Damage Scenario derived from POST methodology subdivided for building classes

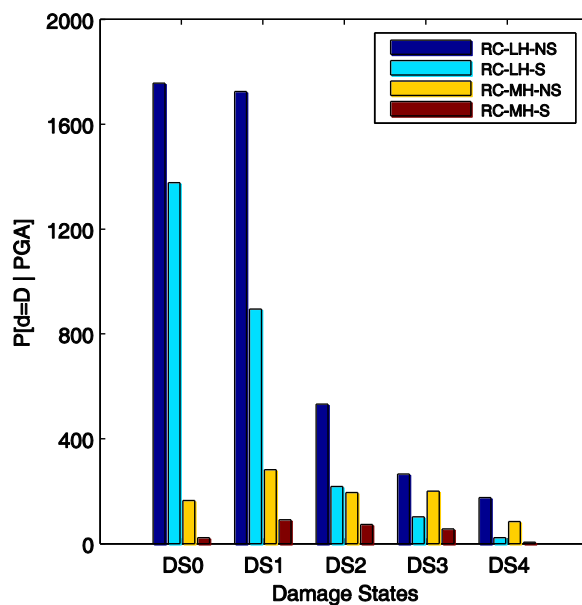


Figure 6-50: Damage Scenario derived from AEDES inspection forms subdivided for building classes

It can be noted that building classes are not homogeneously sorted in the database. As a matter of fact most of buildings belongs to the RC-LH-NS and RC-LH-S class (54.0% and 34.7%), while 11% of the buildings belong to RC-MH-NS class and just 3% of the buildings belong to RC-MH-S class.

Analogously, Figure 6-50 shows some results obtained from DS for each building according to DS according to EMS98 derived from the condensed damage grades reported for vertical structures and infill panels in AeDES.

Furthermore, in Figure 6-51-Figure 6-54 the comparison between predicted and observed damage for the different classes, separately, are shown.

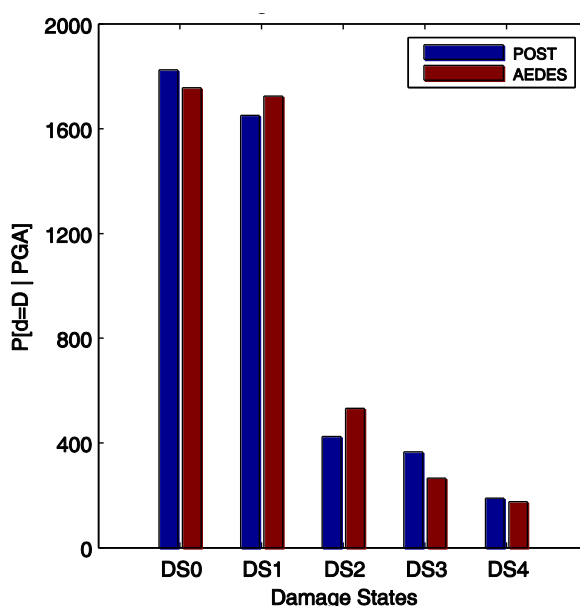


Figure 6-51: Comparison of the damage predicted by POST methodology and observed damage for RC-LH-NS class

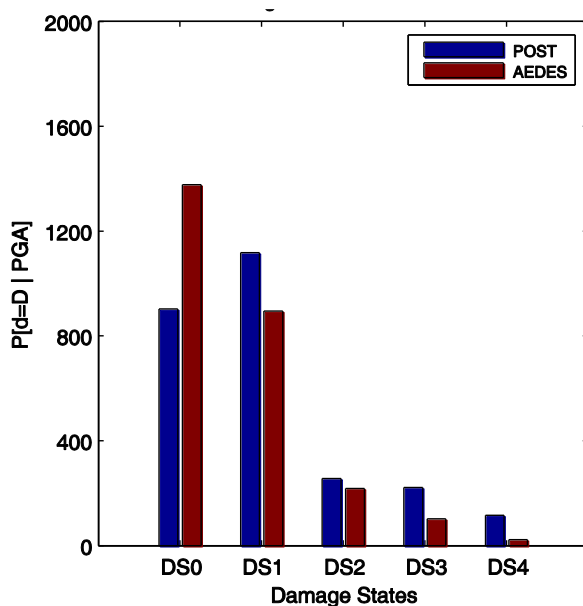


Figure 6-52: Comparison of the damage predicted by POST methodology and observed damage for RC-LH-S class

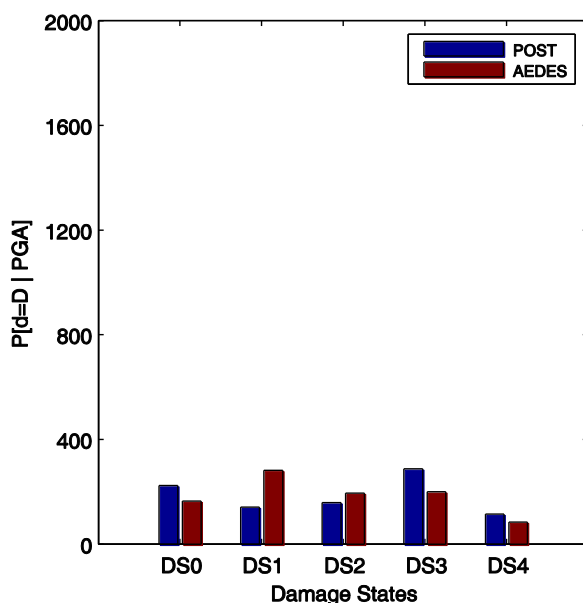


Figure 6-53: Comparison of the damage predicted by POST methodology and observed damage for RC-MH-NS class

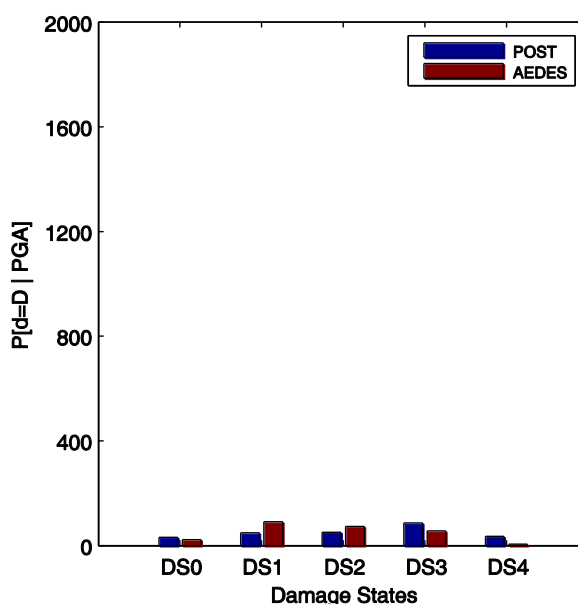


Figure 6-54: Comparison of the damage predicted by POST methodology and observed damage for RC-MH-S class

It can be noticed that a good correspondence between predicted and observed damage scenario for most statistically significant building classes, namely RC-LH-NS (Figure 6-51) and RC-LH-S (Figure 6-52). A slight underestimation of the number of buildings characterized by DS0 and a corresponding overestimation of number of buildings characterized by DS1 for the RC-LH-S class according to POST methodology can be observed. This circumstance can be related, as previously stated, to the value of logarithmic standard deviation (β) of DS1 fragility curve.

Finally, a fairly good agreement between predicted and observed damage scenarios for RC-MH-NS (Figure 6-53) and RC-MH-S (Figure 6-54) classes can be observed. Generally speaking, since building classes are not homogeneously sorted in the database, the comparison between results can be misleading because of the cross-correlation between different parameters, namely the number of storeys and PGA demand. As a matter of fact, this condition is particularly emphasized

for the RC-MH-NS class, which buildings are not-homogeneously spatially distributed on the territory leading to an irregular distribution of PGA from ShakeMap, see Figure 6-55, due to the fact that high-rise RC building dated after 1981 are mainly located in the epicentral area, in the L'Aquila basin, see Figure 6-4 and Figure 6-9.

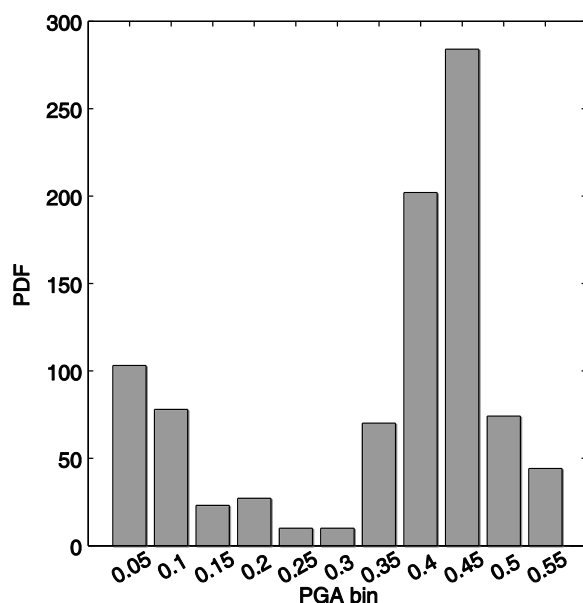


Figure 6-55: Distribution of PGA from ShakeMap for RC-MH-NS class

6.7 Summary of remarks

In this section, the derivation of a Geographical Information System (GIS) database of more than 70,000 buildings ([Dolce et al, 2015a](#); [Dolce et al, 2015b](#)), from the about (78,062) AEDES survey forms collected soon after the 2009 Earthquake that hits L'Aquila area has been shown. The data collected will be analyzed in detail, showing the distribution for the whole database and at the level of each municipality. Hence distributions on typological, morphological and geometrical

characteristics of buildings, in addition to information on damage to buildings have been shown.

Then, empirical fragility curves for RC buildings, from statistical elaboration of survey data collected just after the earthquake of 6 April 2009, considering different building typologies, have been derived.

Hence, the methodology, implemented in POST (PushOver on Shear Type models), a software based on MATLAB® code (Chapter 3 ,[Ricci, 2010](#), [Del Gaudio et al, 2015](#)) – is applied, considering the survey data collected in the database as input parameters. Therefore, the derivation of mechanical fragility curves for building classes and the derivation of seismic damage scenario from the Shake Map of the event is shown. Hence, fragility curves derived from POST methodology, in addition to fragility curves derived from ([Lagomarsino and Giovinazzi, 2006](#), [Rota et al, 2008](#)), are used to derive seismic damage scenario for residential RC Buildings of L'Aquila area. Each scenario is compared with observed damage resulting from AEDES inspection form ([Baggio et al., 2007](#)). The comparison of results shows a good agreement between predicted and observed damage.

6.8 References

- Ang, A. H. S., and Tang, W. H., 1975. Probability Concepts in Engineering Planning and Design, Vol. 1—Basic Principles, John Wiley & Sons, New York.
- Baggio C, Bernardini A, Colozza R, Coppari S, Corazza L, Della Bella M, Di Pasquale G, Dolce M, Goretti A, Martinelli A, Orsini G, Papa F, Zuccaro G, 2007. Field manual for post-earthquake damage and safety assessment and short term countermeasures (Pinto A, Taucer F eds), Translation from Italian: Goretti A, Rota M, JRC Scientific and Technical Reports, EUR 22868 EN-2007
- Del Gaudio C., Ricci P., Verderame G.M., Manfredi G., 2015. Development and urban-scale application of a simplified method for seismic fragility assessment of RC buildings. Engineering Structures. Vol. 91, pp. 40-57. doi:10.1016/j.engstruct.2015.01.031
- CEN (2003) Eurocode 8: design of structures for earthquake resistance—Part 1: general rules, seismic actions and rules for buildings. European Standard EN 1998-1:2003. Comité Européen de Normalisation, Brussels
- Cerný V. A, 1982. Thermodynamical approach to the traveling salesman problem: An efficient simulation algorithm. Tech. rep., (Bratislava, Czechoslovakia): Comenius University.
- Cerný V., 1985. Thermodynamical approach to the traveling salesman problem: An efficient simulation algorithm. Journal of Optimization Theory and Applications; 45(1):41_51. doi:10.1007/BF00940812.
- Chioccarelli E, De Luca F, Iervolino I, 2009. Preliminary study on L'Aquila earthquake ground motion records, V5.20. <http://www.reluis.it/>
- Circolare del Ministero dei Lavori Pubblici. n. 617 del 2/2/2009 (2009) Istruzioni per l'applicazione delle "Nuove norme

- tecniche per le costruzioni” di cui al DM 14 gennaio 2008. (in italian)
- De Luca F, Verderame GM, and Manfredi G, 2014. "Analytical versus observational fragilities: the case of Pettino (L'Aquila) damage data database." *Bulletin of Earthquake Engineering* (2014): 1-21.
 - Decreto Ministeriale n. 40 del 3/3/1975 (1975) Approvazione delle norme tecniche per le costruzioni in zone sismiche. G.U. n. 93 dell'8/4/1975 (in Italian)
 - Der Kiureghian, Armen, and Ove Ditlevsen. "Aleatory or epistemic? Does it matter?." *Structural Safety* 31.2 (2009): 105-112.
 - Dolce M, 2010. Emergency and post-emergency management of the Abruzzi earthquake. In: 14th European conference on earthquake engineering, Ohrid, Macedonia, 3–8 September 2010, published in MGarevski, A Ansal (eds) *Earthquake engineering in Europe*, Springer. doi:10.1007/978-90-481-9544-2_19
 - Dolce M, Masi A, Goretti A., 1999. Damage to buildings due to 1997 Umbria-Marche earthquake. In: Bernardini, editor. *Seismic damage to masonry buildings*. Rotterdam: Balkema; 1999.
 - Dolce M., and Goretti A., 2015a. "Building damage assessment after the 2009 Abruzzi earthquake." *Bulletin of Earthquake Engineering* (2015): 1-24.
 - Dolce M., Manfredi G., 2015b. *Libro bianco sulla ricostruzione privata fuori dai centri storici nei comuni colpiti dal sisma dell'Abruzzo del 6 aprile 2009*, ISBN 978-88-89972-50-2, Doppiavoce, Napoli, 2015. In press. (in italian)
 - Efron B, Tibshirani RJ., 1994. *An introduction to the bootstrap*. London: Chapman & Hall/CRC.
 - Fardis M.N., Panagiotakos T.B., 1997. *Seismic design and response of bare and masonry-infilled reinforced concrete*

- buildings. Part II: infilled structures. *Journal of Earthquake Engineering*, 1(3), 475-503.
- Fardis, Michael N. Seismic design, assessment and retrofitting of concrete buildings: based on EN-Eurocode 8. Vol. 8. Springer Science & Business Media, 2009.
 - GNDT, 1993. Seismic Risk of Public Buildings, Part I: Methodology. Tipografia Moderna, Bologna, Italy (in Italian).
 - GNDT, Emilia-Romagna Region, Tuscany Region, 1986. Field Manual for the completion of the building vulnerability GNDT form. Litografia della Giunta Regionale (in Italian).
 - Goretti A, Di Pasquale G, 2002. An overview of post-earthquake damage assessment in Italy. In: EERI invitational workshop an action plan to develop earthquake damage and loss data protocols, 19–20 September. Pasadena, CA
 - Grünthal G., 1998. Cahiers du Centre Européen de Géodynamique et de Séismologie: Volume 15 – European Macroseismic Scale 1998. European Center for Geodynamics and Seismology, Luxembourg.
 - Haselton, C.B., A.B. Liel, S. Taylor Lange, and G.G. Deierlein (2008). Beam-Column Element Model Calibrated for Predicting Flexural Response Leading to Global Collapse of RC Frame Buildings, PEER Report 2007/03, Pacific Engineering Research Center, University of California, Berkeley, California.
 - Kakaletsis D.J., Karayannis C.G., 2009. Experimental investigation of infilled reinforced concrete frames with openings. *ACI Structural Journal*, 106(2), 132-141.
 - Kirkpatrick S, Gelatt CD, Vecchi MP., 1983. Optimization by simulated annealing. *Science*;220(4598):671_80 .
 - Masi A., Vona M., 2009. Estimation of the in-situ concrete strength: provisions of the european and italian seismic codes and possible improvements. In: E. Cosenza (editor). Eurocode 8 perspectives from the Italian standpoint

- workshop. Doppiavoce, Naples, Italy, 2009. ISBN 978-88-89972-16-8. Pp. 67-77.
- McKay M.D., Conover W.J., Beckman R.J., 1979. A comparison of three methods for selecting values of input variables in the analysis of output from a computer code. *Technometrics*, 21(2), 239-245.
 - Porter K, Kennedy R, and Bachman R., 2007. "Creating fragility functions for performance-based earthquake engineering." *Earthquake Spectra* 23.2: 471-489.
 - Ricci P., 2010. Seismic vulnerability of existing RC buildings. PhD thesis, University of Naples Federico II, Naples, Italy.
 - Rossetto T, Elnashai, 2003. AS. Derivation of vulnerability functions for European-type RC structures based on observational data. *Engineering Structures*;25:1241–63.
 - Rossetto, T., and Elnashai A., 2003. "Derivation of vulnerability functions for European-type RC structures based on observational data." *Engineering structures* 25.10: 1241-1263.
 - Rota, M., A. Penna, and C. L. Strobbia. "Processing Italian damage data to derive typological fragility curves." *Soil Dynamics and Earthquake Engineering* 28.10 (2008): 933-947.
 - Vamvatsikos D, Cornell CA., 2002. Incremental dynamic analysis. *Earthquake Engineering and Structural Dynamics*; 31(3):491–514.
 - Vamvatsikos D., Cornell C.A., 2006. Direct estimation of the seismic demand and capacity of oscillators with multi-linear static pushovers through IDA. *Earthquake Engineering and Structural Dynamics*, 35(9), 1097-1117.
 - Verderame G.M., Manfredi G., Frunzio G., 2001. Le proprietà meccaniche dei calcestruzzi impiegati nelle strutture in cemento armato realizzate negli anni '60. Atti del X congresso nazionale ANIDIS "L'ingegneria Sismica in Italia", Potenza-Matera, Italy, September 9-13. (in Italian)

- Verderame G.M., Polese M., Mariniello C., Manfredi G., 2010. A simulated design procedure for the assessment of seismic capacity of existing reinforced concrete buildings. *Advances in Engineering Software*, 41(2), 323-335.
- Verderame G.M., Ricci P., Esposito M., Manfredi G., 2012. STIL v1.0 – Software per la caratterizzazione delle proprietà meccaniche degli acciai da c.a. tra il 1950 e il 2000. ReLUIS, <http://www.reluis.it/>
- Vořechovský, M., and D. Novák., 2009. "Correlation control in small-sample Monte Carlo type simulations I: A simulated annealing approach." *Probabilistic Engineering Mechanics* 24.3: 452-462.

Chapter 7

Seismic vulnerability assessment at urban scale based on field survey, remote sensing and census data

In this study, a seismic vulnerability assessment at urban scale is carried out in a high-seismic city in Southern Italy using building stock data from different sources, namely (in a growing order of accuracy): census data providing information on buildings aggregate for relatively large spatial units (census cells); data from an airborne Remote Sensing mission carried out over the municipality, providing a detailed estimate of 3D geometric parameters of buildings; data from a field survey, provided detailed information on geometrical and structural characteristics of each single building. Such data are used, within a multilevel approach, in order to evaluate the influence of the detail level of input data on seismic vulnerability assessment at urban scale. To this aim, data from the detailed field survey are assumed as a reference, and when using Remote Sensing data, due to the lack of information affecting such data source, some of the input parameters to the seismic vulnerability assessment procedure are assumed as random variables (e.g., the age of construction, which is not known for single buildings when data other than field survey are used). The use of hybrid data sources is investigated, too, assuming that Remote Sensing are integrated not only with census data, but also with data from a (less detailed) field survey. Hence, the error introduced by the use of less detailed (but easier, faster and less expensive to collect) data is

analyzed and discussed in order to evaluate the reliability of alternative data sources within a cost/benefit approach to large scale seismic risk assessment.

7.1 Introduction

During last years, a growing interest is addressed to time- and money-saving procedures and technologies providing an acceptably reliable knowledge of building stock characteristics for large scale seismic risk assessment. “Level Zero” knowledge data as census data are usually available (for instance, for the whole Italian territory), but they are quite rough and they are provided in aggregate form for census cells. The most reliable and detailed data are provided by in-situ field surveys, but they are usually quite expensive to be collected. Remote Sensing methodologies are intensely developing. They are used (as in the present study) for data collection on building stock characteristics aimed at seismic vulnerability assessment (e.g. Münich et al., 2006; Borzi et al., 2009; Borfecchia et al., 2010; Ehrlich et al., 2013; Pittore and Wieland, 2013; Polli et al., 2010; Wieland et al., 2012) but also for different natural hazards (e.g., tsunami: Taubenböck, 2011; Mück et al., 2013), or for post-earthquake damage survey (e.g. Foulser-Piggott et al., 2012; Dell’Acqua et al., 2013). In this study, a seismic vulnerability assessment at urban scale is carried out in the high-seismic city of Avellino (Campania region, Southern Italy), which was struck strongly by the disastrous Irpinia earthquake of 23 November 1980. Building stock data from different sources are used, and results are compared within a multilevel approach. Data on building stock characteristics from different sources of information were collected within the SIMURAI (2010) research project: census data ([ISTAT, 2001](#)), data from an airborne Remote Sensing mission carried out over the Municipality, and data from a FIELD SURVEY. Such data are used, within a multilevel approach, in order to evaluate the influence of the detail level of input data on seismic vulnerability assessment at urban scale.

7.2 Seismic Hazard

In the present study, seismic hazard is evaluated according to the Italian National Technical Standards ([DM 14/1/2008](#)). According to this standard, the seismic hazard is defined in terms of the maximum horizontal expected acceleration in free field conditions on stiff soil with horizontal topographic surface, and in terms of the elastic acceleration response spectrum, with reference to pre-defined exceeding probability over the reference period. Site-dependent spectra are provided by ([INGV-DPC S1, 2007](#)) in correspondence to the points of a grid whose nodes are sufficiently close together (not more than 10 km away), and for different return periods TR, which fall into a target range between 30 and 2475 years. Stratigraphic effects are taken into account depending on the soil category of the site of interest, which is provided for Avellino city by a microzonation study.

7.3 Field Survey Data

Building stock data have been collected through a detailed FIELD SURVEY carried out by means of a survey form implemented in a tablet PC. In particular the survey was developed through specialized operators who compiled a survey form subdivided in different sections, with an increasing level of detail. The survey form includes the main parameters – among the ones that can be reasonably collected during a field survey – that may have a significant influence on building seismic capacity, addressing a particular attention to specific potential sources of seismic vulnerability, among which the most important are the structural typology, the age of construction (defining the codes and the rules used to build them), and the number of storeys (affecting the dynamic properties of buildings). Moreover, detailed geometric and morphologic data were collected, such as plan shape, interstorey height, bay length. Distribution of infill elements in RC buildings was also surveyed. In the following, main data resulting from the field survey are briefly presented.

On the whole, 1327 buildings were surveyed. Among these, 1058 were RC buildings and 265 were masonry buildings, see Figure 7-1a.

Steel and mixed buildings were present in negligible percentages (only 4 buildings out of 1327).

In Figure 7-1 the distributions of number of storeys and age of construction among the building population are reported. It is to be noted that in the period ranging from the '40-'50 up to the '80-'90 there was the greatest diffusion of the RC Buildings, at the turn of post-war economic development and reconstruction after the 1980 Irpinia earthquake. Moreover, pre- and post-81 buildings respectively represent about the 56 and 44% of the RC building population whose age of construction was determined, which represent the 80% of the total.

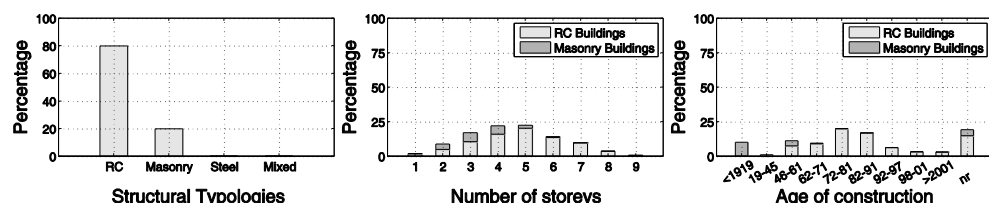


Figure 7-1: Structural typology (a), Number of storeys (b), and Age of Construction (c) of surveyed buildings.

Figure 7-2-Figure 7-5 show the spatial distribution (grouped per census cell) of the same parameters previously analyzed at urban scale. The attention is focused on the central area of the Municipality, which was subjected to the field survey. Distribution of structural typology per single building and within the single census cells are shown in Figure 7-2 and Figure 7-3, respectively.

It can be observed that masonry buildings are mainly placed in the central area of the city, from west to east, and in particular in the historical centre of the city. A large part of masonry building stock was constructed at the beginning of the 20th century or before, or early after World War II. The period characterized by the first significant growth of the RC building stock is around 60s and 80s, and it affected the northern and southern areas of the city. Then, after the disastrous 23rd November 1980 Irpinia earthquake that struck the area, an intense activity of reconstruction took place since the early 80s to the 90s.

It is to be note that the northern area of the city, constituted by RC buildings dating back to the period between post-World War II and Irpinia earthquake, was not significantly affected by the post-earthquake reconstruction process, in contrast to the central area where, close to masonry buildings, several post-1981 RC buildings are found, which were constructed in replacement of the most heavily damaged masonry buildings. A further urban expansion affecting the south-eastern and north-western areas, constituted almost entirely by RC building dating from after 1981, can be observed.

In 1981 Avellino was also classified for the first time as seismic in technical building code (DM 7/3/1981). This allows to make an important distinction between buildings dating from before 1981, which were designed for gravity loads only, and those dating from after 1981, designed according to seismic codes, although obsolete codes not accounting for capacity design rules.

Furthermore, in Figure 7-4 it can be observed that the central areas are mainly characterized by low-rise buildings unlike the areas affected by the two periods of greatest urban expansion –that is between the post-World War II period and the early '80s and from the '90s, respectively –which are populated by medium/high-rise buildings. In particular, a concentration of high-rise buildings can be found in Northern area, which was characterized by an intense urban activity in the years 60-80 with high buildability index.

Only after the 1980 earthquake several specific acts, decrees, zoning laws and ordinances were issued to regulate the (re-)construction activities. The first one was the Law n. 219/1981 (Legge n. 219 del 14/5/1981), that entrusted the urban planning to the damaged Municipalities, under the coordination of the Campania Region. Then, these laws led to a limitation in the height of buildings constructed during the intense urban expansion that took place in North-Western and South-Eastern areas in the 90's.

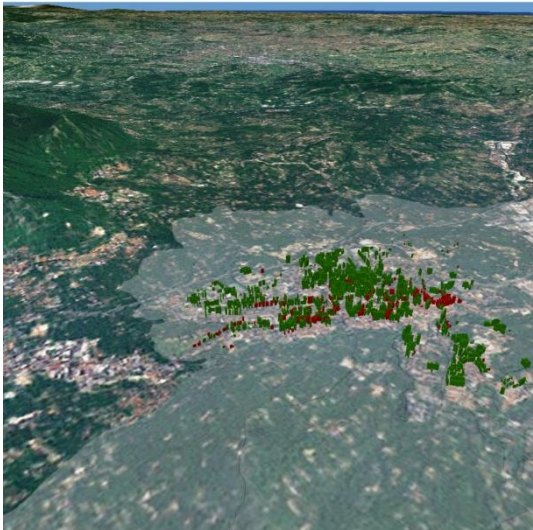


Figure 7-: Spatial distribution of building typologies.

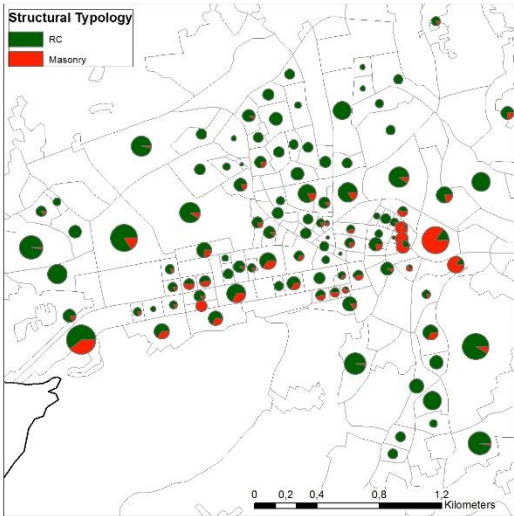


Figure 7-2: Spatial distribution at level of census cell of the building typologies.

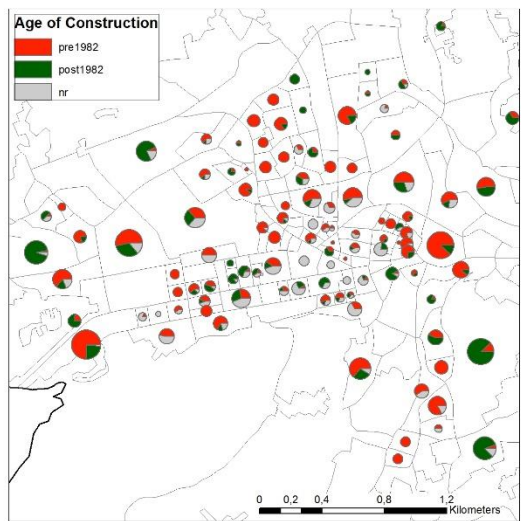


Figure 7-3: Spatial distribution at level of census cell of age of construction.

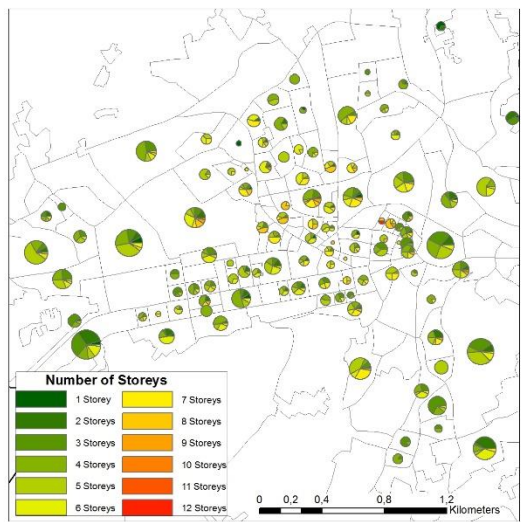


Figure 7-4: Spatial distribution at level of census cell of the Number of Storeys.

7.4 Remote Sensing Data

Remote Sensing (RS) datasets (aerial photos, satellite images, LIDAR, etc.), opportunely processed and elaborated, allow to map and identify landscape features, giving an effective effort to sustainable planning and management. Thus, RS techniques provide a wide range

of environmental information about landscape and its characteristics, especially in the case of studies concerning urbanized areas, offering significant advantages in terms of cost effectiveness and timeliness in the availability of information over larger areas. In this framework, RS techniques can be a valuable source of information about 3D geometry of buildings with the aim of supporting seismic vulnerability assessment of building stocks.

A specific methodology has been implemented and calibrated within the SIMURAI project by the research group of the “Earth Observations and Analyses” laboratory (UTMEA-TER) of the Italian National Agency for New Technologies, Energy and Sustainable Economic Development (ENEA) in order to extract 3D buildings parameters using RS data acquired from aerospatial platforms, in particular by means of active LIDAR (Light Detection And Ranging) technology, which allowed to assess the height and planimetric shape of buildings. A LIDAR airborne RS mission has been planned and carried out in 2007 over the entire municipality of Avellino, acquiring range point clouds data with a density of 4 points for square meter. The 3D geometric parameters of buildings were extensively obtained through a methodology integrating active LIDAR technology, aerophotogrammetry and GIS techniques, using the approach proposed by Borfecchia et al. (2010), as briefly described in the following.

The LIDAR data have been processed in order to extract the Digital Surface Model (DSM) and the Digital Terrain Model (DTM); then buildings have been extracted from non-ground points. Then, the next step has been the integration of RS and cartographic data, by means GIS techniques, in order to produce a complete and detailed 3D description of the built-up areas. To this end, the digital cartography at 1:2000 scale of the Municipality of Avellino has been used to overlay vector information about the buildings (especially, their footprint) with LIDAR data. Subsequently, combining digital cartography and height values coming from LIDAR, for each building geometric attributes and morphological features have been extracted in a semi-automatic way: area, perimeter, volume, total height of the building and ground altitude beneath itself. Finally, to store all the data acquired and the information

produced, a suitable GeoDatabase has been implemented and organized.

For further information about LIDAR data acquisition and processing the reader is referred to (Ricci et al., 2011), where the work carried out by the UTMEA-TER ENEA laboratory is described in detail.

Starting from the data concerning the heights of the buildings is possible to estimate for each of them the number of storeys by fixing the interstorey height (3.5m).

It is worth noting that the heights of the buildings, as detected through an appropriate survey form, are subsequently processed in order to provide a unitary value of height that can be used as an input value for the assessment of the vulnerability.

For example in the case of buildings with attic floor the input height is evaluated as the average value of the ridge-height and the eaves-height, while in the case of buildings without attic floor is essentially equal to the eaves-height. In addition, because of the vulnerability evaluation procedure presented in the following, building irregularity is considered through the use of the vulnerability modifier which allows for the change in the behavior with respect to regular buildings. Therefore the above-mentioned buildings are regularized and characterized by an average height. For these reasons, between the heights derived from the FIELD SURVEY and those derived from LIDAR there are some deviations, noticeable mostly in the central area (Figure 7-5), which sometimes may even lead to an error in the estimate of the number of storeys of the building. Clearly the deviations observed in the estimation of the number of storeys will lead to an erroneous estimate of the behavior of buildings and ultimately to an error in the estimation of expected damage, as it will be observed in the following. These deviations can be attributed to different factors including, (i) the different processing mode of the data of the above-quoted sources, especially for buildings irregular in height, over that in the case in which the ground morphology shows remarkable characteristics of complexity, (ii) the presence of pitched roofs, (iii) the presence of basement levels, (iv) an intrinsic error of LIDAR technology.

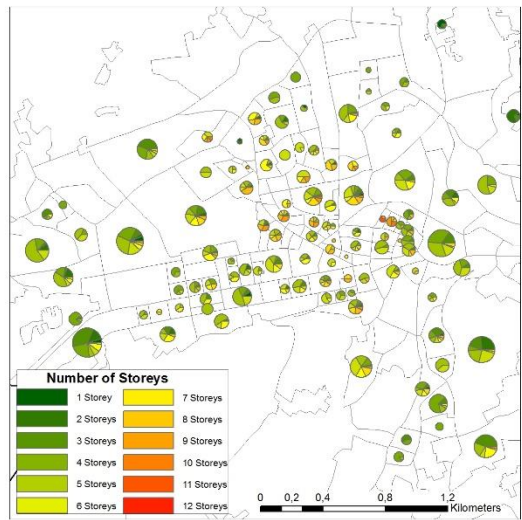


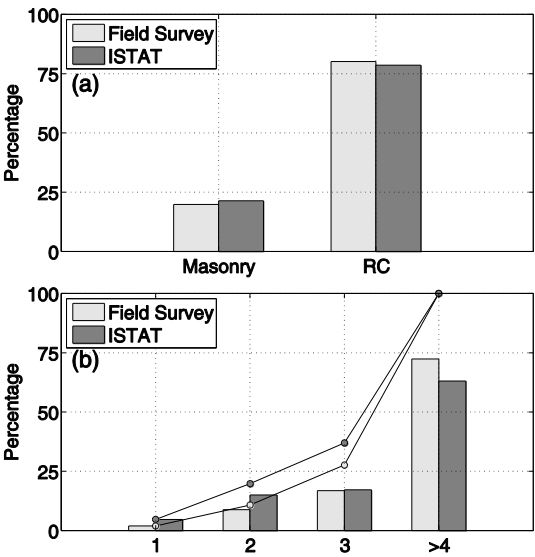
Figure 7-5: Spatial distribution at level of census cell of Number of Storeys according to LIDAR data.

7.5 Census Data

The Italian National Institute of Statistics (Istituto Nazionale di Statistica, ISTAT) survey is a nation-wide census that provides information on citizens, buildings and dwellings. The “14th general census of the population and dwellings” (14° Censimento generale della popolazione e delle abitazioni, ISTAT 2001) collected is used in this study. This census provides statistics for buildings, related to number of storeys (one-, two-, three- and \geq four)-storey buildings), Age of Construction (typically with a decennial-rate) and Structural Typology (masonry or RC buildings) for the spatial unit, that is the “census cell”. Nevertheless, due to confidentiality requirements these statistics are provided in an aggregate manner: as an example, it is not possible to get the number of RC buildings in a cell dating back to a specific age of construction and characterized by a specific number of storeys, but only to know how many RC buildings, how many buildings dating back to that age of construction and how many buildings with that number of storeys are present in that cell as a whole.

In the following the statistics for the 113 surveyed cells out of the 202 cells of Avellino from the ISTAT 2001 census are compared with the statistics obtained from the field survey carried out in the framework on the SIMURAI project. It is to be noted that a good matching can be observed with reference to the number of storeys and building typology (Figure 7-6a-b). More complex is the case of the age of construction, which was not surveyed in the 20% of cases (Figure 7-6c).

However, looking at the census track there is not always a good agreement as shown globally for the whole sample. Furthermore sometimes the total number of buildings detected in the two census results to be different. These deviations will result in errors in the estimate of damage to buildings, because the ISTAT data constitute the source of support for the LIDAR data, relatively to the parameters that cannot be derived in a direct manner. The LIDAR technology indeed allows the evaluation of the height and plan morphology of buildings, whereas it does not allow the estimation of parameters such as the age of construction and the structural typology, which will be obtained through a process of disaggregation, presented below, starting from the ISTAT data.



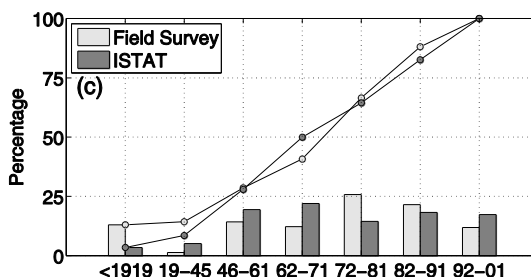


Figure 7-6: Comparison between the statistics obtained from the field survey carried out in the framework of the SIMURAI project and from the 14th general census (ISTAT): (a) building typology, (b) number of storeys, (c) age of construction.

7.6 Seismic Vulnerability Assessment Procedure

In this study, the seismic vulnerability assessment procedure proposed by Lagomarsino and Giovinazzi (2006) is adopted. Such study proposes two approaches, a “macroseismic” and a “mechanical” method. In both cases, the adopted building typological classification essentially corresponds to the European Macroseismic Scale EMS-98 proposal (Grünthal, 1998). Following the macroseismic approach, vulnerability and fragility curves (providing the expected (mean) damage grade and the probability of having each discrete damage grade under growing values of macroseismic intensity, respectively) are provided, derived from Damage Probability Matrices (DPMs) implicitly defined by the EMS-98. The mechanical approach is based on capacity spectrum method, employing bilinear SDOF capacity curves representative of each building class. Macroseismic and mechanical methods are compared, reciprocally calibrated and cross-validated.

The method is based on the assumption of a typological classification system essentially corresponding to that adopted by EMS-98, apart from the inclusion of sub-typologies: for masonry buildings, the type of horizontal structure is considered; moreover, for all building typologies three classes of height are considered.

The expected (mean) damage grade is provided by the following expression:

$$\mu_D = 2.5 \left[1 + \tanh \left(\frac{I + 6.25V - 13.1}{Q} \right) \right] \quad \text{Eq 7-1}$$

where I is the seismic input provided in terms of a macroseismic intensity, V and Q are the “Vulnerability” and the “Ductility” index, respectively, and μ_D ($0 < \mu_D < 5$) represent the mean damage value of the expected discrete damage distribution. V and Q are provided for each Building Typology and sub-Typology.

The probability of having the k -th discrete damage grade (p_k) is evaluated starting from the mean damage grade μ_D and assuming a binomial distribution for this probability:

$$\mu_D = \sum_{k=0}^5 p_k k \quad \text{Eq 7-2}$$

Hence the definition of parameters provides by the proposed classification system, such as the class of height, the type of the horizontal structure for masonry buildings, while for RC buildings the possibility that the structural concept is inspired whether or not to anti-seismic design criteria, if this is able to ensure requirements about the ductility and hysteretic capacity of the structures, as well as on the possible intensity of seismic actions employed for the design thereof, allows the identification of Building Type, and then the definition of the relative vulnerability curve. However, some of these parameters are not easily inferred if not through a detailed survey and then are very specific when compared to data from a quick and easy source of information such as census data or LIDAR data. The latter indeed provide information only on the structural typology of the buildings, as well as the number of storeys and age of construction. For this reason it is necessary, starting from the definition of Building Type given above, to identify the class of buildings compatible with the source of data with less informational level.

This operation for masonry buildings is carried out in two steps: (i) defining a correspondance between the vertical and horizontal structure and the vulnerability classes presented by EMS-98, (ii) exploiting the

relationship between the vulnerability class, that is the type of the horizontal and vertical structure, and the age of construction evaluated through a statistical study conducted on 50,000 buildings in the Irpinia earthquake of 1980 (Di Pasquale et al, 2005).

Thus for each building, once identified the number of floors and the age of construction, the vulnerability curve is obtained by weighting the vulnerability curves relative to the vulnerability class previously evaluated by means of the respective percentage of occurrence of each vulnerability class in the period considered.

As regards the RC buildings in order to establish a correlation between the age of construction and the behavior of buildings, from the data on changes in seismic classification that have occurred nationwide it is possible to identify the design criteria (in agreement or not with seismic codes) and eventually the extent of seismic actions employed for the design of buildings in the last century for each Municipality of the country.

In particular, for the Municipality of Avellino it results that the buildings dating back to before 1981 were designed only for vertical loads. Only after the disastrous earthquake of 1980 Avellino was classified for the first time as seismic in technical building code (DM 7/3/1981). Therefore, post-1981 RC buildings are assumed as belonging to the Building Typology designed according to a seismic code in zone II. Such buildings have been considered to belong to a low ductility class, due to the lack of capacity design principles in Italian technical standards prior to OPCM 3274 (20/3/2003).

In conclusion starting from Building Type defined through the identification of sub-typologies above presented, has been possible to define the behavior of a building from a few parameters inferred through a quick survey or even on the basis of census data, such as structural typology, number of storeys and age of construction typically divided into ten-year intervals (pre1919, 19-45, 46-61, 62-71, 72-81, 82-91, post1991). It should be noted that the authors identify three classes of height (Low-Rise, Mid-Rise, High-Rise) differently defined in terms of number of storeys for masonry ($_L = 1/2$, $_M = 3/5$, $_H = \geq 6$) and RC buildings ($_L = 1/3$, $_M = 4/7$, $_H = \geq 8$).

In Figure 7-7, as an example, it is shown the vulnerability curves for Masonry and RC buildings for the medium class of height, defined just ahead, on varying of the age of construction. It can be noted for RC buildings a sudden change of behavior for buildings constructed after the earthquake of 1980 due to change in the seismic classification of the Municipality.

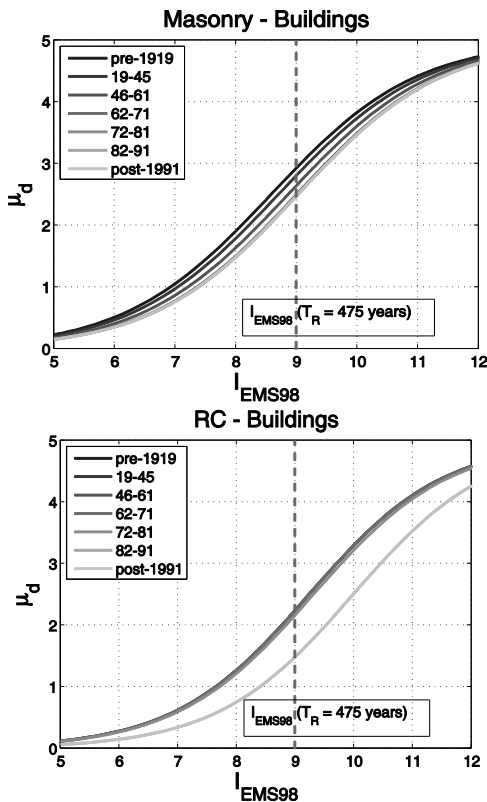


Figure 7-7: Vulnerability curves for different age of construction.

Similarly in Figure 7-8 are shown the vulnerability curves for masonry buildings dating back to before 1919 and those of RC buildings built after 1991 on varying of the class of height. From the figures it is possible to notice a significant change in the vulnerability curves for masonry buildings in the transition from one class of height to another and a very little change for RC buildings in the transition from the low to

the middle class of height, and no change in the transition from the middle to the high end, as shown in (Giovinazzi, 2005) where, according to EC8 prescriptions, building have to be designed with the aim to guarantee the same strength independently from their height.

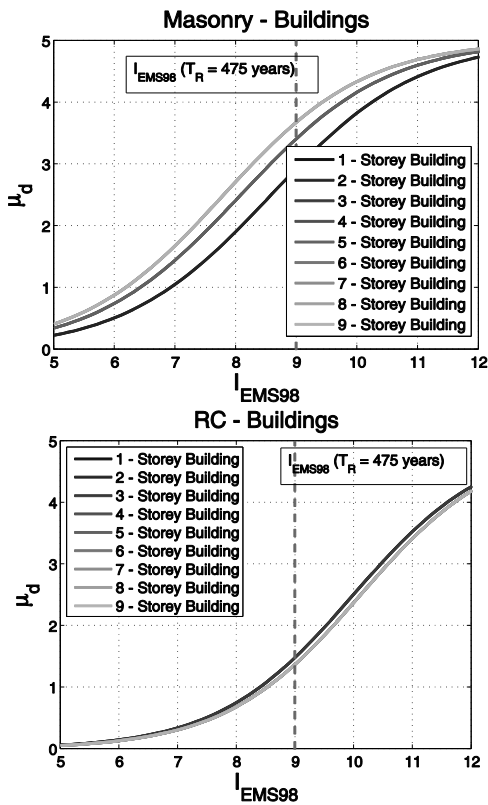


Figure 7-8: Vulnerability curves for different class of height.

Table 7-1: Differences in terms of vulnerability and ductility indexes ΔQ e ΔV for low-rise and high-rise buildings on respect to medium-rise ones (from (Giovanazzi,2005)).

	No Code		Low Ductility Class		Medium-High Ductility Class	
	ΔV	ΔQ	ΔV	ΔQ	ΔV	ΔQ
Low-Rise	-0.02	-	+0.02	-	-0.02	-0.3
High Rise	+0.04	-	-	-	+0.02	-

7.7 Methodology

The seismic vulnerability assessment methodology previously illustrated is applied assuming different data sources. For each building, the following input data are needed:

- Number of storeys;
- Plan Irregularity;
- Structural Typology;
- Age of Construction;
- Soil type;

FIELD SURVEY provides exhaustively data about global building dimensions, besides the age of construction and soil type. Based on the latter information, the Building Type is determined according to the previous Section. The information about Soil type is used to define a multiplier factor f_{PGA} of the PGA that generate a seismic action able to produce on a certain building category and a certain class of height, built on a certain soil, the same effect if it was built on stiff soil (Soil type A). According to I-PGA correlations to a PGA factor f_{PGA} an Intensity Increment ΔI corresponds and hence a Vulnerability Increment ΔV (Giovinazzi and Lagomarsino, 2004). According to the same work plan irregularity produces an increase in the Vulnerability Index equal to (+0.04).

Results of the seismic vulnerability assessment carried out according to the previously illustrated procedure can be reported in terms of mean damage value (μD), obtained with a macroseismic intensity value corresponding to a PGA value with a return period of 475 for the site of interest. The correlation between the macroseismic intensity I and PGA has been set in the form of:

$$a_g = c_1 c_2^{(I-5)} \quad \text{Eq 7-3}$$

where c_1 represents the PGA value corresponding to the reference intensity $I=5$ ($c_1=0.03$) and c_2 measures the rate of the PGA increase with intensity I ($c_2=1.6$).

Then, stratigraphic effects are taken into account through Intensity Increment ΔI depending on the soil category of the site of interest previously defined.

The procedure described in previous Section can be carried out assuming for the geometric building parameters the LIDAR data instead of the data from the FIELD SURVEY.

LIDAR data provide (based also on cartography) global dimensions of buildings, and hence Plan Irregularity in addition to the Number of storeys. The latter parameter is evaluated as the value providing the least scatter with an interstorey height equal to 3.5m. Hence, the available input data for the application of the seismic vulnerability assessment procedure are:

- Number of storeys;
- Plan Irregularity;
- Soil type.

The remaining parameters:

- Structural Typology;
- Age of Construction

can be evaluated by means of census data (ISTAT, 2001), which are provided aggregated for census cell (hypothesis “a”). The distribution of Age of Construction for both masonry and RC buildings for each census cell is evaluated, representing the probability that a generic building in that census cell belongs to a specified Structural Typology and Age of Construction. To this end, for each census cell a disaggregation process is carried out by minimizing the scatter from a reference distribution consisting of disaggregated data provided by ISTAT for the province of Avellino, which are assumed herein as a priori information about the correlation between Structural Typology and Age of Construction.

The main steps of the disaggregation procedure can be summarized as follows:

- Based on of the provincial distributions of the age of construction for RC and masonry buildings, $\overline{p_j^i}$, with $i=1:2$ means respectively which corresponds to $ST = \{RC; Masonry\}$ and

$j = 1:7$ which corresponds respectively to
 $AC = \{pre1919; 19-45; 46-61; 62-71; 72-81; 82-91; post1991\};$

- It requires that within each class, characterized by a specific age of construction, for the census track under consideration p_j , the percentage of occurrence of the first attempt of RC and masonry buildings, \tilde{p}_j^i , is consistent with the provincial data,

$$\tilde{p}_j^i = p_j \frac{p_j}{\sum_i p_j};$$

- Finally, it requires that such distribution is compatible with the percentage of RC and masonry buildings for the census track considered $p^i = \sum_j \tilde{p}_j^i$;
- Then the deviation vector between the distribution of the ages of construction from ISTAT data and that resulting from (iii) is evaluated $\Delta_j = p_j - \tilde{p}_j$;
- The deviation vector is then distributed among the different ages of construction by repeating iteratively steps (ii-iv) provided that $\sum_j \Delta_j = 0$.

Such disaggregation procedure provides the probability p_{ij} that a generic building within the census cell belongs to the i th Structural Typology and j th Age of Construction.

Therefore for each building known the number of storeys, the relative vulnerability curve is evaluated as a weighted average of the 14 vulnerability curves identified respectively by an age of construction between the 7 classes considered (pre1919, 19-45, classes 46-61, 62-71, 72-81, 82-91, post1991) and by a structural typology (RC or masonry), whose weights are constituted by the respective percentages of occurrence within each census track evaluated through the disaggregation procedure above presented. In order to evaluate the influence of disaggregation process of ISTAT data on estimated mean damage, three further hypotheses are considered:

Age of Construction is assumed to be provided by FIELD SURVEY, while Structural Typology is evaluated by means of Census data;

Structural Typology is assumed to be provided by FIELD SURVEY, while Age of Construction is evaluated by means of Census data;

both of them are assumed to be provided by FIELD SURVEY.

According to hypotheses “b” (or “c”), the same disaggregation process described above is carried out, but Age of Construction (or Structural Typology) is assumed to be provided by the FIELD SURVEY, and the Structural Typology (or Age of Construction) only is assumed as a random variable provided by census data through a disaggregation process. According to hypothesis “d”, both Structural Typology and Age of Construction are assumed to be provided by the FIELD SURVEY.

In the following, results from the application of the procedure based on LIDAR data on the same population of buildings will be compared with the results based on FIELD SURVEY data.

In the following the expected damage scenarios from at different scales, e.g. for the single building, for the single census track and the whole urbane scale are shown.

Indeed starting from the Building vulnerability curve, the mean damage value relative to a seismic event with a return period of 475 years relative to the centroid of the census track where the building is located is evaluated. The latter if does not fall in the nodes of the grid, presented in #2, is calculated as a weighted average of the values in the four vertices of the mesh of the grid containing the point, using as weights the inverse of the distance between the point in question and the four vertices, according to NTC2008 prescriptions.

Hence, the mean damage value obtained with different data sources (FIELD SURVEY or LIDAR) can be compared, evaluating the difference between the latter and the former; such difference can be considered the error resulting from an application of the procedure based on more poor data:

$$\text{err}_{\mu_D} = \frac{\mu_{D,LIDAR} - \mu_{D,Survey}}{\mu_{D,Survey}} \quad \text{Eq 7-4}$$

The latter is related with the error in the estimate of the Number of storeys as well as with the error in the disaggregation process of ISTAT data. In particular denoting by p_{ij} the probability that the building is constituted by i -th Structural Typology (ST) and j -th Age of Construction (AC), where $\sum_i \sum_j p_{ij} = 1$, if $\overline{p_{ij}}$ is the probability that the building belongs to the Structural Typology and the Age of Construction provided by the survey, $(1 - \overline{p_{ij}})$ represents the error made in the disaggregation process respect to the real value identified by the survey:

$$\text{err}_{\text{ST\&AC}} = 1 - \overline{p_{ij}} = 1 - P\left[ST_{\text{LIDAR}} = ST_{\text{Survey}} \ \& \ AC_{\text{LIDAR}} = AC_{\text{Survey}}\right] \quad \text{Eq 7-5}$$

Note that $\text{err}_{\text{ST\&AC}}$ depends both on possible error in census data compared with FIELD SURVEY data and on possible error in the disaggregation process of census data.

7.8 Analysis of results

General trends in expected mean damage based on FIELD SURVEY data are shown in Figure 7-9, illustrating μ_D as a function of the Class of height and of the Age of Construction of surveyed buildings. In the following, Mean and Median, represented respectively by a square and a rhombus dot, and 16th and 84th fractiles, represented by the lower and upper bound of the solid line, are reported for each distribution. An increase and a decrease in μ_D are observed, respectively, as expected according to the adopted seismic vulnerability assessment procedure (Lagomarsino and Giovinazzi, 2006). Moreover looking at the histogram of the mean damage value it can be observed that it is well approximated by a bimodal distribution, fundamentally distinguished by the different behavior of RC buildings dating back to before and after the Irpinia earthquake of 1980.

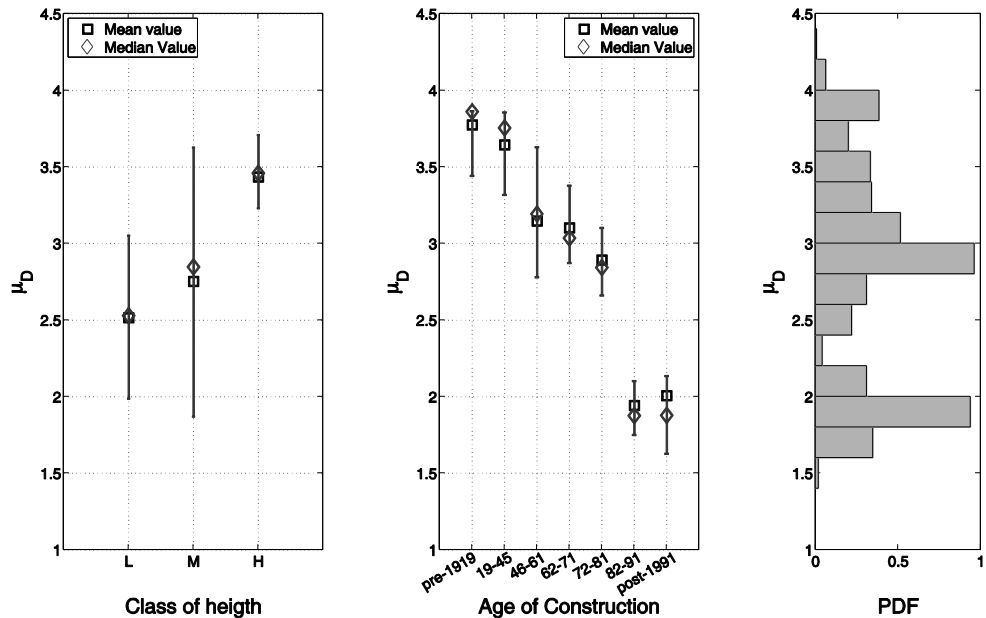


Figure 7-9: Expected mean damage based on FIELD SURVEY data as a function of the Number of storeys (a) and of the Age of Construction (b).

The error in the estimate of expected mean damage due to the use of LIDAR data (err_{μ_D}) depends on (i) the error in the determination of Structural Typology and the Age of Construction derived from the disaggregation of census data ($err_{ST\&AC}$) and (ii) the error in the estimate of the Number of storeys due essentially to differences in the way to process the data from the various data sources in addition to the possible approximation inherent in LIDAR technique. However one of the parameter defining the behavior of building in the present vulnerability assessment procedure is the class of height. As seen previously the LIDAR technology allows exclusively the evaluation of the height and plan morphology of buildings, while it does not allow the estimation of parameters such as the age of construction and the structural typology, which will be obtained through the process of disaggregation, presented above, starting from the ISTAT data. The definition of class of height, as presented by the Authors, requires the

knowledge of structural typology because the classes of height are differently populated for RC buildings rather than for masonry ones.

Nevertheless assuming that the number of storeys is stochastically independent from structural typology it is possible to evaluate the class of height from LIDAR as the weighted average of the class of height deriving from both structural typologies, whose weights are the percentages of occurrence of the structural typologies coming from ISTAT data for the census track. The difference between the class of height evaluated thereby and that coming out from FIELD SURVEY provides an estimate of the parameter that defines the error in the height of buildings. Hence, as expected, an increase in err_{μ_D} is observed if the height of the building is overestimated by LIDAR technique, and vice versa, see Figure 7-10b.

In Figure 7-10a the trend in err_{μ_D} with reference to the error in census data compared with FIELD SURVEY data and on possible error in the disaggregation process of census data ($err_{ST\&AC}$) is shown. As highlighted in the figure no clear trend in bias of the estimate of μ_D is shown, whereas a clear increase in dispersion can be observed.

Such trends depend on the influence of Structural Typology and Age of Construction parameters on the estimate of expected mean damage, according to the adopted seismic vulnerability assessment procedure.

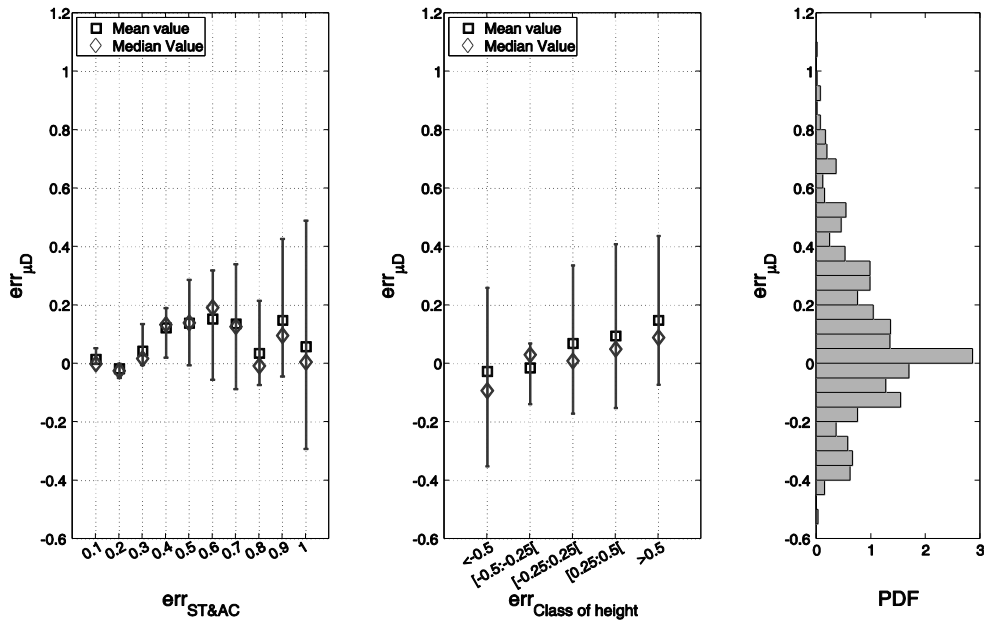


Figure 7-10: Error in the estimate of expected mean damage depending on the error in the determination of Structural Typology and Age of Construction derived from the disaggregation of census data (a) and on the error in the Class of height (b).

In order to investigate the influence of the use of hybrid data sources, LIDAR DATA are integrated not only with census data, but also with data from FIELD SURVEY.

According to hypotheses “c”, the same disaggregation process described above is carried out, but Structural Typology is assumed to be provided by the FIELD SURVEY, and Age of Construction only is assumed as a random variable provided by census data through the disaggregation process. The aim of such a procedure is to simulate an hybrid data sources, consisting of LIDAR data with regard to the height and plan morphology of buildings, and an easier, faster and less expensive to collect FIELD SURVEY exclusively for the knowledge of the structural typology, in addition to CENSUS DATA for what concerning the age of construction.

Hence for each building, known the structural typology, it is possible to identify the classes of height (Low-Rise, Mid-Rise, High-Rise) differently defined in terms of floor numbers for masonry ($_L = 1/2$, $_M =$

3/5, $_H = \geq 6$) and RC buildings ($_L = 1/3$, $_M = 4/7$, $_H = \geq 8$), and the relative error with regard to that derived from FIELD SURVEY (Figure 7-11). In particular, in 77% of cases there is a perfect coincidence in the evaluation of the class of height between LIDAR and FIELD SURVEY, while in 20% and 3% respectively of the cases we observe an overestimation and underestimation in the class of height from the LIDAR. The error just now presented is devoid of approximations resulting from the lack of knowledge of the structural typology, and therefore represents exclusively the error due to differences in the way to process the data from the various data sources in addition to the possible approximation inherent in LIDAR technique.

From the comparison with the data of Figure 7-10 an increase in the reliability of the results thanks to introduction of hybrid data sources above discussed can be observed.

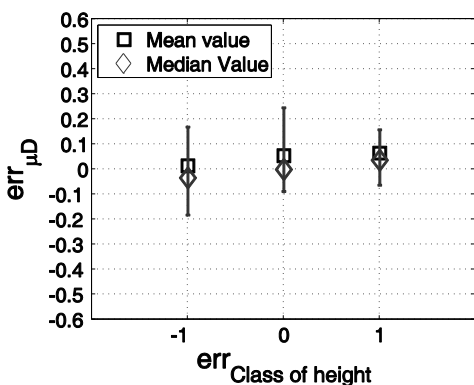


Figure 7-11: Error in the estimate of expected mean damage depending on the error in the determination of Class of height integrated by data on Structural Typology provided by FIELD SURVEY hypothesis “C”

Up to this point the results in terms of expected damage for single building of the whole dataset have been shown. In the following the results, previously presented at the level of single building, for each census track will be analyzed, considering an expected damage by averaging the damage of buildings present in the census track. Starting from the census distributions of age of construction and number of

storeys it is possible to evaluate a vulnerability curve representative of the behavior of the buildings present in the census track by weighting the curves for each classes characterized by a number of floors, a structural typology and an age of construction, on the basis of their percentage of occurrence over the census track, which corresponds to mediating the vulnerability curves obtained previously for each building present in the census track,. Accordingly it is possible to evaluate the expected damage scenario from a seismic event with a return period of 475 years for each census track.

Hence the relative error of the mean damage value due to the use of LIDAR data with respect to FIELD SURVEY ($err_{\mu_D}^{census_track}$), are to be charged to (i) the error in the determination of Structural Typology and the Age of Construction derived from the disaggregation of census data and (ii) on the difference between the distributions of the age of construction and structural typology coming from ISTAT data, used as sources of support for LIDAR data, compared to those from the FIELD SURVEY, (iii) the error in the estimate of the Class of height basically due to possible approximation inherent in LIDAR technique.

In the following the latter is investigated. The possible error in estimate of the Number of storeys due to LIDAR technique shown in #4 lead to an error in the estimate of expected mean damage only if the error in the number of storeys leads to an error in the estimation of the class of height.

As previously noted the LIDAR technology allows exclusively the evaluation of the height and plan morphology of buildings, while it does not allow the estimation of parameters such as the age of construction and the structural typology. Then to evaluate the class of height is therefore necessary to make some assumptions on the structural typology and the number of storeys as previously shown. Hence the difference between the class of height evaluated from LIDAR and that coming out from FIELD SURVEY provides an estimate of the parameter that defines the error in the class of height for the single buildings.

Considering the errors relative to all the buildings within one census track it can be estimated an average error, err_{CH} , similarly to what has been done for the error in terms of expected damage scenario at the

level of census track. As expected, an increase in $err_{\mu_D}^{census_track}$ is observed if the height of the building is overestimated by LIDAR technique, and vice versa.

Such trends also depend on the influence of Structural Typology and Age of Construction parameters on the estimate of expected mean damage, according to the adopted seismic vulnerability assessment procedure. Indeed it can be noted that in non-homogeneously sorted building databases the cross-correlation between different parameters that significantly affect seismic vulnerability can make it difficult to effectively highlight the influence of each single parameter.

Hence in order to evaluate the influence of disaggregation process of ISTAT data on estimated mean damage, the same source of error can be analyzed observing the results obtained according to hypotheses “c”, whereas the same disaggregation process described above is carried out, but Structural Typology is assumed to be provided by the FIELD SURVEY, and the Age of Construction only is assumed as a random variable provided by census data through the disaggregation process above described.

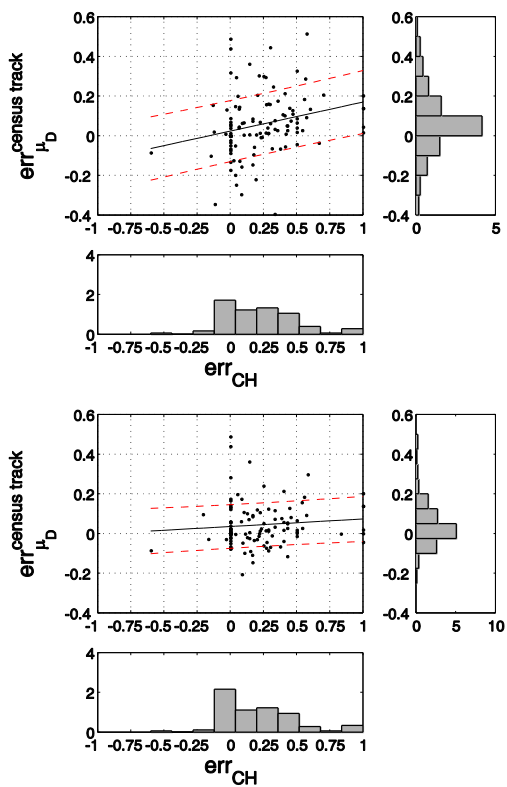
Results based on LIDAR data with Age of Construction and Structural Typology provided by disaggregation of census data (Figure 7-12a) show, on average, a slight overestimate in μ_D . An increase in the knowledge of Structural Typology (Figure 7-12b) leads to a slight reduction in the average value of μ_D , whereas no reduction in its dispersion can be noticed, in addition to a clear reduction in the estimated of mean value and dispersion of $err_{\mu_D}^{census_track}$.

Furthermore considering the case in which Both Age of Construction and Structural Typology are assumed to be provided by the FIELD SURVEY (hypotheses “d”), the additional information compared to the previous case is represented by the knowledge of the age of construction leading to a reduction of error in $err_{\mu_D}^{census_track}$ but not in terms of err_{CH} , because the latter depends only of the structural typology (Figure 7-12c).

In such a way any cross-correlation between different parameters that significantly affect seismic vulnerability are avoided and the

reliability of LIDAR data is investigated, removing the possible source of error arising from the disaggregation process, except for the differences in the way to process the data from the various data sources in addition to the possible approximation inherent in LIDAR technique.

Moreover as can be seen from the figure there is a progressive reduction of the regression line in the passage from hypothesis "a", to "c" and then to "d". this circumstance is related to the fact that the parameter class of height alone, produces slight variations in the vulnerability of the buildings, as shown in Figure 7-8, especially for buildings RC leading to a moderate dependence the two error functions.



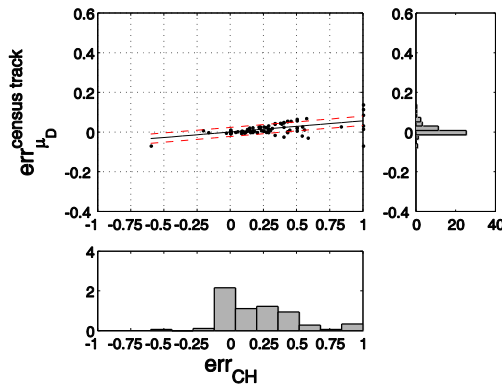


Figure 7-12: Error in the estimate of expected mean damage depending on the error in the determination of Class of Height based on hypothesis “a” (a), on hypothesis “c” (b) and . hypothesis “d” (c).

Previously the different sources of error affecting $err_{\mu_D}^{census_track}$ are listed, among which (i) the error in the determination of Structural Typology and the Age of Construction derived from the disaggregation of census data and (ii) on the difference between the distributions of the age of construction and structural typology coming from ISTAT data, used as sources of support for LIDAR data, compared to those from the FIELD SURVEY, (iii) the error in the estimate of the Class of height basically due to possible approximation inherent in LIDAR technique.

It would be interesting to investigate the relationship between the error $err_{\mu_D}^{census_track}$ and an error function that takes into account the approximation and the uncertainty arising from the disaggregation procedure, considering the differences in the distributions obtained after the disaggregation procedure with the distributions resulting from FIELD SURVEY.

However, the choice of this error function is a sensitive matter, such as employing a Mean Squared Error, any under- or overestimating of the respective frequencies within the investigated distribution would have the same sign, with the consequent loss of representativeness in terms of the expected scenario.

For this reason it has been introduced a dimensionless parameter representative of the distribution under investigation (eg, age of construction), p_j , consisting of a linear function between a maximum value in correspondence with the most recent age of construction and a minimum value in correspondence with the oldest one. The error function is somehow related to the sum of the product of the percentages of occurrence, p_j , with the value of the respective dimensionless parameter, evaluated in correspondence of the j -th age of construction, c_j , which corresponds to evaluate the weighted average of the dimensionless parameter where the weights are the percentages of occurrence of the investigated parameter (eg, age of construction).

The choice of the minimum and maximum value to use is congenial to the fact that the error function returns a unit value concurrently with the maximum error (all ancient buildings reported by ISTAT data against all recent buildings detected by the FIELD SURVEY and vice versa). For this purpose, the normalized parameter is defined by a maximum value equal to 0.5 and a minimum equal to -0.5. Ultimately the dimensionless parameter relative at the age of construction can be evaluated as:

$$c_j = \left(-0.5 + \frac{j - j_{\min}}{j_{\max} - j_{\min}} \right) p_j \quad \text{Eq 7-6}$$

Where $j = 1:7$ means respectively $AC = \{pre1919; 19-45; 46-61; 62-71; 72-81; 82-91; post1991\}$.

The error function would therefore be equal to the summation over all the ages of construction of the product of the dimensionless parameter, c_j , with the difference of percentage of occurrence obtained from the LIDAR data after the process of disaggregation, p_j , with ones coming from the FIELD SURVEY, \bar{p}_j :

$$err_{AC} = \sum_j (p_j - \bar{p}_j) c_j \quad \text{Eq 7-7}$$

It is to be noted that $err_{AC} > 0$ means an underestimation in percentage of Buildings dating back to $[pre1919; 1-45; 46-61]$ or an overestimation of percentage of Buildings dating back to $[72-81; 82-91; post1991]$ of LIDAR data with respect to that provided by FIELD SURVEY and hence an underestimation of damage predicted according to LIDAR data, see Figure 7-13. E.g. $err_{AC} = 1$ for a census track means, respectively, a 100% pre1919 Buildings and 0% post1991 Buildings for LIDAR data and a 0% pre1919 Buildings and 100% post1991 Buildings for FIELD SURVEY data.

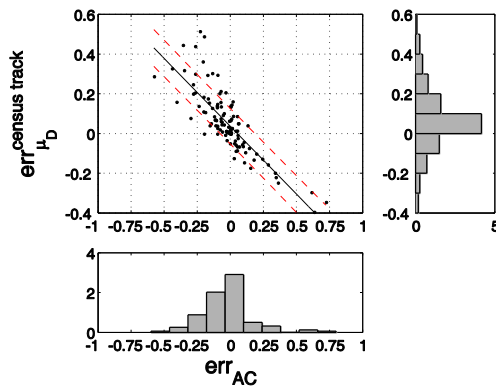


Figure 7-13: Error in the estimate of expected mean damage depending on the error in the determination of Age of Construction.

On the other end the dimensionless parameter for the structural typology, μ_D , is equal to 0.5 in correspondence of Masonry structural typology and -0.5 in correspondence of RC structural typology. The error function is somehow related to the sum of the product of the percentages of occurrence, p_i , with the value of the respective dimensionless parameter, evaluated in correspondence of the i -th structural typology, c_i , which corresponds to evaluate the weighted average of the dimensionless parameter where the weights are the percentages of occurrence of the investigated parameter (eg, structural typology).

The error function would therefore be equal to the summation over all the structural typologies of the product of the dimensionless parameter, c_i , with the difference of percentage of occurrence obtained from the ISTAT data, p_i , with ones coming from the FIELD SURVEY, \bar{p}_i :

$$err_{ST} = \sum_i (p_i - \bar{p}_i) c_i \quad i = 1:2 \quad \text{Eq 7-8}$$

Where $i = 1:2$ means respectively $ST = \{RC; Masonry\}$.

It is to be noted that $err_{ST} > 0$ means an underestimation in percentage of RC Buildings or an overestimation of percentage of Masonry Buildings of LIDAR data with respect to that provided by FIELD SURVEY and hence an overestimation of damage predicted according to LIDAR data, see Figure 7-14, e.g. $err_{ST} = 1$ for a census track means, respectively, a 100% RC Buildings and 0% Masonry Buildings for FIELD SURVEY data and a 0% RC Buildings and 100% Masonry Buildings for LIDAR data.

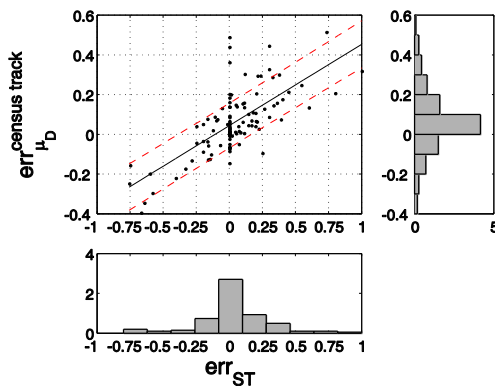


Figure 7-14: Error in the estimate of expected mean damage depending on the error in the determination of Structural Typology.

Finally, the spatial distribution of expected mean damage is reported in Figure 7-15-Figure 7-18. Data are aggregated for census cells for an easier understanding.

Figure 7-15 illustrates the “reference” expected mean damage based on FIELD SURVEY data. Briefly describing such distribution, we can observe higher values of μ_D in Central and Central-Northern areas, where masonry buildings and high-rise pre-1981 RC buildings are mainly located, respectively (see also Figure 7-3).

Figure 7-16 reports the spatial distribution of $err_{\mu_D}^{census_track}$ based on “pure” LIDAR data (hypothesis “a”), showing a slight general overestimate in expected mean damage. In particular more pronounced errors are observed in the in Central and Central-Northern areas, especially in the historic center of the town, located in the Central-Eastern area, where $err_{ST} < 0$ and $err_{AC} > 0$ (see census track 1-2-158) can be noted, which means that LIDAR data in conjunction with ISTAT data overestimate the percentage of more recent RC Building with respect to FIELD SURVEY data and hence lead to $err_{\mu_D}^{census_track} < 0$, that is an underestimation of predicted damage according to LIDAR data.

On the other hand in the Central-Northern and in Central-Western areas an $err_{ST} > 0$ and $err_{AC} < 0$ (see census track 97-107-205) can be noted, which means that LIDAR data in conjunction with ISTAT data overestimate the percentage of more ancient Masonry Building with respect to FIELD SURVEY data and hence lead to $err_{\mu_D}^{census_track} > 0$, that is an overestimation of predicted damage according to LIDAR data.

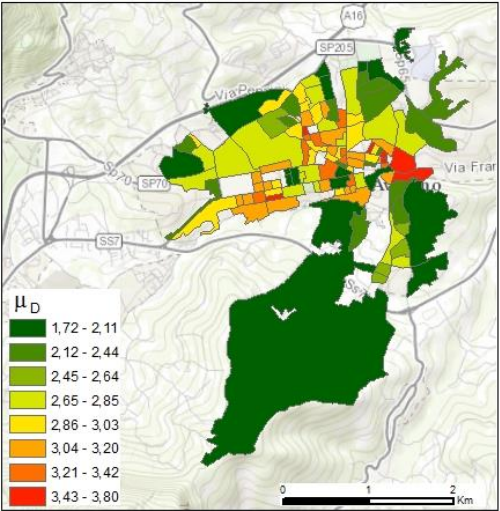


Figure 7-15: Spatial distribution of expected mean damage based on FIELD SURVEY data.

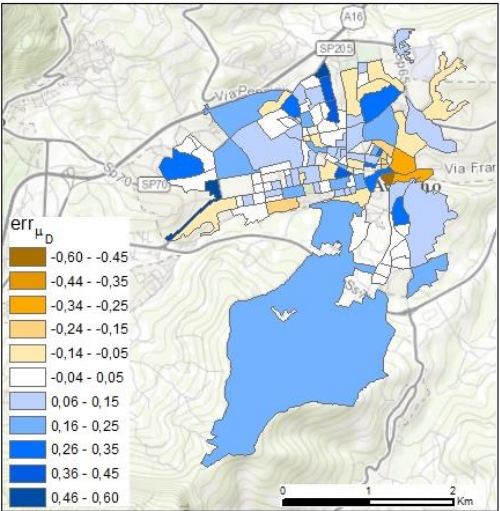


Figure 7-16: Spatial distribution of relative error in expected mean damage based on "pure" LIDAR.

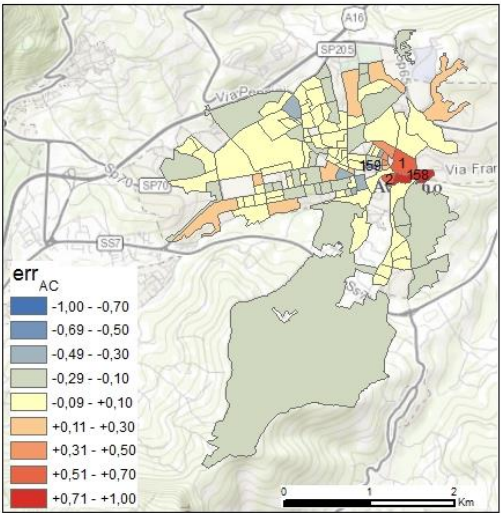


Figure 7-17: Spatial distribution of error in the determination of Age of Construction.

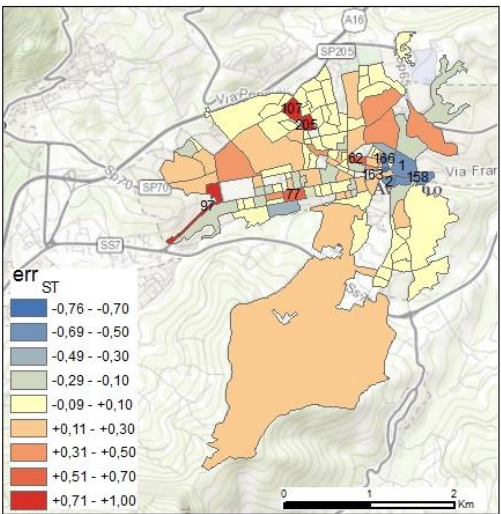


Figure 7-18: Spatial distribution of error in the determination of Structural Typology.

7.9 Summary of remarks

A good agreement between expected mean damage based on LIDAR data and on FIELD SURVEY data was generally observed. No significant bias in the former estimate – compared with the latter – was

shown. The sources of error in the estimate of expected mean damage based on LIDAR data were analyzed and discussed. Such error is mainly due to the unavoidable integration of LIDAR data with census data on Structural Typology and Age of Construction.

Clearly, the error in the output parameter (expected mean damage) observed when using LIDAR data depends on the limitations and/or the errors in the input data themselves, but it also depends on how such limitations and/or errors influence the output estimate through the adopted seismic vulnerability assessment procedure.

Indeed different input data are used, within a multilevel approach, in order to evaluate the influence of the detail level of input data on seismic vulnerability assessment at different scales, e.g. for the single building, for the single census track and the whole urbane scale. To this aim, data from the detailed field survey are assumed as a reference, and when using Remote Sensing data, due to the lack of information affecting such data source, some of the input parameters to the seismic vulnerability assessment procedure are assumed as random variables (e.g., the age of construction and structural typology). It has been shown that the reliability of the procedure improves with the increase of the scale of observation, leading to a more robust quantification of risk and vulnerability which is the aim of prevention, emergency and post emergency large scale assessment procedures.

The use of hybrid data sources is investigated, too, assuming that Remote Sensing are integrated not only with census data, but also with data from a (less detailed but easier, faster and less expensive to collect) field survey, in order to integrate the lack of information affecting Remote Sensing data.

Such observations may change when adopting a different seismic vulnerability assessment procedure or, better, when carrying out a seismic risk assessment in terms of Expected Loss.

The present study could be further developed in order to analyze the influence of the procedure followed for census data disaggregation. Moreover, developments in uncertainty estimation are foreseen in order to evaluate in a more quantitative and objective way the amount of the

error and the “acceptability” threshold – within a cost/benefit approach – for instance by means of confidence bounds for Expected Loss.

7.10 References

- Borfecchia, F., Pollino, M., De Cecco, L., Lugari, A., Martini, S., La Porta, L., Ristoratore, E., Pascale, C. (2010). "Active and passive remote sensing for supporting the evaluation of the urban seismic vulnerability." *Italian Journal of Remote Sensing*, 42 (3), 129-141.
- Borzi, B., Dell'Acqua, F., Faravelli, M., Gamba, P., Lisini, G., Onida, M., Polli, D. (2009). "Studio di vulnerabilità di una vasta area industriale mediante immagini telerilevate da satellite." *Progettazione Sismica*, No. 2/2009, pp. 105-117. ISSN 1973-7432. (in Italian)
- Decreto Ministeriale del 14/1/2008: "Approvazione delle nuove norme tecniche per le costruzioni." G.U. n. 29 del 4/2/2008. (in Italian)
- Decreto Ministeriale del 7/3/1981. "Dichiarazione di zone sismiche nelle regioni Basilicata, Campania e Puglia." (in Italian)
- Dell'Acqua, F., Lanese, I., Polli, D. (2013). "Integration of EO-based vulnerability estimation into EO-based seismic damage assessment: a case study on L'Aquila, Italy, 2009 earthquake." *Natural Hazards*, 68(1), 165-180.
- Ehrlich, D., Kemper, T., Blaes, X., Soille, P. (2013). "Extracting building stock information from optical satellite imagery for mapping earthquake exposure and its vulnerability." *Natural Hazards*, 68(1), 79-95.
- Foulser-Piggott, R., Spence, R., Saito, K., Brown, D.M., Eguchi, R. (2012). "The use of remote sensing for post-earthquake damage assessment: lessons from recent events, and future prospects." *Proceedings of the 15th World Conference on Earthquake Engineering*, Lisbon, Portugal, September 24-28. Paper No. 526.
- Giovinnazzi, S., Lagomarsino, S. (2004). "A macroseismic method for the vulnerability assessment of buildings." *Proceedings of the 13th World Conference on Earthquake Engineering*, Vancouver, Canada, August 1-6. Paper No. 896.

- Grünthal, G.. (1998). “Cahiers du Centre Européen de Géodynamique et de Séismologie: Volume 15 – European Macroseismic Scale 1998.” European Center for Geodynamics and Seismology, Luxembourg.
- INGV-DPC S1 (2007). “Progetto S1. Proseguimento della assistenza al DPC per il completamento e la gestione della mappa di pericolosità sismica prevista dall'Ordinanza PCM 3274 e progettazione di ulteriori sviluppi.” Istituto Nazionale di Geofisica e Vulcanologia – Dipartimento della Protezione Civile, <http://esse1.mi.ingv.it> (in Italian)
- ISTAT (2001). Italian National Institute of Statistics: Census Data 2001, <http://www.istat.it/it/archivio/44523>
- Lagomarsino, S., Giovinazzi, S. (2006). “Macroseismic and mechanical models for the vulnerability assessment of current buildings.” *Bulletin of Earthquake Engineering*, 4(4), 415-443.
- Medvedev, S.V. (1977). “Seismic Intensity Scale MSK-76.” Publication Institute of Geophysics of Poland, Academy of Sciences, Warsaw, Poland.
- Mück, M., Taubenböck, H., Post, J., Wegscheider, S., Strunz, G., Sumaryono, S., Ismail, F. A. (2013). “Assessing building vulnerability to earthquake and tsunami hazard using remotely sensed data.” *Natural Hazards*, 68(1), 97-114.
- Münich, J.C., Taubenböck, H., Stempniewski, L., Dech, S., Roth, A. (2006). “Remote sensing and engineering: an interdisciplinary approach to assess vulnerability in urban areas.” *Proceedings of the 1st European Conference on Earthquake Engineering and Seismology*, Geneva, Switzerland, September 3-8. Paper No. 1412.
- Ordinanza del Presidente del Consiglio dei Ministri n. 3274 del 20/3/2003. “Primi elementi in materia di criteri generali per la classificazione sismica del territorio nazionale e di normative tecniche per le costruzioni in zona sismica.” G.U. n. 105 dell'8/5/2003. (in Italian)

- Pittore, M., Wieland, M. (2013). "Toward a rapid probabilistic seismic vulnerability assessment using satellite and ground-based remote sensing." *Natural Hazards*, 68(1), 115-145.
- Polli, D., M., Dell'Acqua, F., Gamba, P. (2010). "Primi passi verso la valutazione della vulnerabilità sismica tramite strumenti di telerilevamento." *Progettazione Sismica*, No. 1/2010, pp. 79-92. ISSN 1973-7432. (in Italian)
- Ricci, P., Verderame, G.M., Manfredi, G., Pollino, M., Borfecchia, F., De Cecco, L., Martini, S., Pascale, C., Ristatore, E., James, V. (2011). "Seismic vulnerability assessment using field survey and Remote Sensing techniques." In: Murgante B., Gervasi O., Iglesias A., Tanian D., Apduhan B.O. (editors). *Computational Science and its Applications – ICCSA 2011*, Springer-Verlag Berlin Heidelberg, 2011. ISBN 978-3-642-21886-6. Volume 6783, Part II, pp. 109-124. doi:10.1007/978-3-642-21887-3_9
- SIMURAI Project (Strumenti Integrati per il MULTi Risk Assessment territoriale in ambienti urbani antropizzati, Integrated tools for large scale multi-risk assessment in urban anthropic environment), co-funded by the Italian Ministry of Research (MIUR)
- http://www.consorziotre.com/index.php?option=com_content&view=article&id=76&Itemid=62
- Taubenböck, H. (2011). "The vulnerability of a city – diagnosis from a bird's eye view." In: Mörner, N.A. (editor). *The tsunami threat - research and technology*, InTech, 2011. ISBN 978-953-307-552-5. doi:10.5772/14017
- Wieland, M., Pittore, M., Parolai, S., Zschau, J., Moldobekov, B., Begaliev, U. (2012). "Estimating building inventory for rapid seismic vulnerability assessment: Towards an integrated approach based on multi-source imaging." *Soil Dynamics and Earthquake Engineering*, 36, 80-83.

Chapter 8

Experimental Tests on GLD RC Frames with and without Infills

8.1 Introduction

Reinforced Concrete moment-resisting frame buildings, with interior and exterior infill panels partitions, are one of the most popular structural systems for multi-storey buildings. Actually, infill panels are known to strongly interact with the surrounding RC frame, and drastically alter the seismic behavior of the structure.

In previous sections, a seismic vulnerability assessment of infilled RC building is shown, which allows to take into account the influence of infill panel both in the definition of the non-linear static response of building and seismic capacity, relating displacement thresholds on the non-linear behavior of infill sub-assemblages, selected on mechanical basis and experimentally validated, to the description of damage reported in EMS98.

Hence, presence of infill elements leads, on a side, to an increase in lateral stiffness and strength of the building, and on the other side, to a premature brittle failure, due to local interaction with structural elements, thus limiting structural deformation capacity. Such remarks are supported by post-earthquake observed damage, in Mediterranean area, such as Turkey 1999 ([EERI, 2000](#)), L'Aquila 2009 ([Ricci et al., 2011](#)), Lorca 2011 ([De Luca et al., 2013](#)), and by numerical and experimental literature studies.

Indeed, RC elements in buildings designed for gravity loads only or according to obsolete seismic codes do not possess adequate seismic details (i.e., inadequate overlapping of longitudinal reinforcement, low transverse reinforcement ratio, ineffective anchorage of transverse reinforcement), potentially leading to a limitation in ductile deformation capacity of the elements (Bikinis and Fardis, 2010). Moreover, the absence of capacity design in shear for such elements can lead to a further decrease in deformation capacity due to a flexure-shear interaction failure (Elwood and Moehle, 2005). Beam-column joints also represent a critical issue; again, the lack of capacity design principles leads to a low shear strength of the joint, potentially leading to a shear failure that limits the deformation capacity of adjoining beams and/or columns (Park and Mosalam, 2013; Celik and Ellingwood, 2008).

Several experimental studies investigated the seismic behavior of RC frames with infills. Most of these studies focused the attention on the behavior of the panel, that is, the failure mode, the evolution of damage with increasing displacement demand, and, of course, the stiffness and strength contribution to the frame response (e.g., Liauw and Kwan, 1984; Stylianidis, 1985; Pires, 1990; Colangelo, 2003,2005; Calvi and Bolognini, 2001; Bergami, 2007). Other studies investigated the effects of interaction between panel and surrounding elements resulting in brittle failure mechanisms such as shear failure in RC columns (e.g., Mehrabi et al., 1996; Al-Chaar et al., 2002). However, modeling failure mode of panel and surrounding RC members depending on stiffness and strength characteristics of elements is a very challenging issue; some authors have made some attempt in this direction (e.g., Mehrabi et al., 1994) but further investigation is certainly needed. The specific issue of shear failure modeling in non-ductile RC frames due to local interaction with infill elements has been investigated with different approaches, from FEM-based micro-modeling to simplified lumped plasticity-based macro-modeling (e.g., D'Ayala et al., 2009; Celarec and Dolšek, 2012).

In this study, preliminary results of an experimental campaign on one-storey one-bay frames (scale 1:2) representative of the existing Italian building stock are presented. Frames are designed for gravity

loads only according to code provisions and with material properties representative of 1970s-90s. Frames are tested both with and without the presence of infills, in order to investigate the influence of such (non-structural) elements on global and local behavior of the frame.

Geometrical and mechanical characteristics of specimens are illustrated (i.e., geometry and reinforcement details of RC frames, geometry of infill panels, and mechanical properties of structural materials, typology of mortar and brick units). The design of test setup, aimed at avoiding any direct interaction between setup elements and beam-column joints in order to reproduce the actual behavior of the frame under seismic action, is discussed.

Experimental results show that the post-elastic behavior of specimens was controlled by brittle failure mechanisms. In Bare specimens expected base shear strength was attained, but post-elastic deformation capacity was limited by failure of beam-column joints after flexural yielding in beams. In Infilled specimen failure was due to shear failure at the top of the columns due to local interaction with infill panel.

8.2 Experimental Program

Test specimens

One -storey one-bay RC frames (scale 1:2) were tested. Specimens were designed in order to be representative of the bottom storey of a five-storey gravity load designed RC frame, according to Italian technical codes in force between 1970s and 1990s ([DM 30/05/1972](#); [DM 14/02/92](#)).

Geometry and reinforcement details are shown in Figure 8-1. Total bay length and storey height were equal to 2.30m and 1.60m, respectively. Corresponding clear dimensions were 2.10m and 1.35m. Transverse section dimensions of columns and beams were 20×20cm and 20×25cm, respectively. Deformed bars were used for longitudinal and transverse reinforcement, as usually adopted during the reference period.

In beams, longitudinal reinforcement was made of (3+3) 10mm diameter bars, corresponding to compression and tension reinforcement ratio equal to $\rho'=\rho=0.47\%$. 6mm diameter stirrups spaced at 15cm were

used as transverse reinforcement, corresponding to transverse reinforcement ratio equal to $\rho_{sw}=0.19\%$. Stirrup spacing complied with the lower limit provided by the adopted code.

In columns, eight 8mm bars were used as longitudinal reinforcement, uniformly distributed along the section perimeter, corresponding to a reinforcement ratio equal to $\rho=1.01\%$, very close to code prescriptions and design practice at the time. Transverse reinforcement was made of 6mm diameter stirrups spaced at 15cm, resulting in a transverse reinforcement ratio equal to $\rho_{sw}=0.19\%$. Stirrup spacing in columns was assumed based on usual design practice.

Longitudinal and transverse reinforcement were anchored with 90 degree hooks. The length of the hook was equal to ten times the bar diameter for stirrups. No transverse reinforcement was adopted in beam-column joints, consistent with code provisions. Column bases were fixed in a 40x60x390cm stiff foundation block.

Three specimens were tested, two with infill panels and one without. The former are identified as GB e GB2 (**G**=Gravity load designed; **B**=Bare frame); the latter as GI-80 (**G**=Gravity load designed; **I**=Infilled frame; 80=infill panel thickness, in mm).

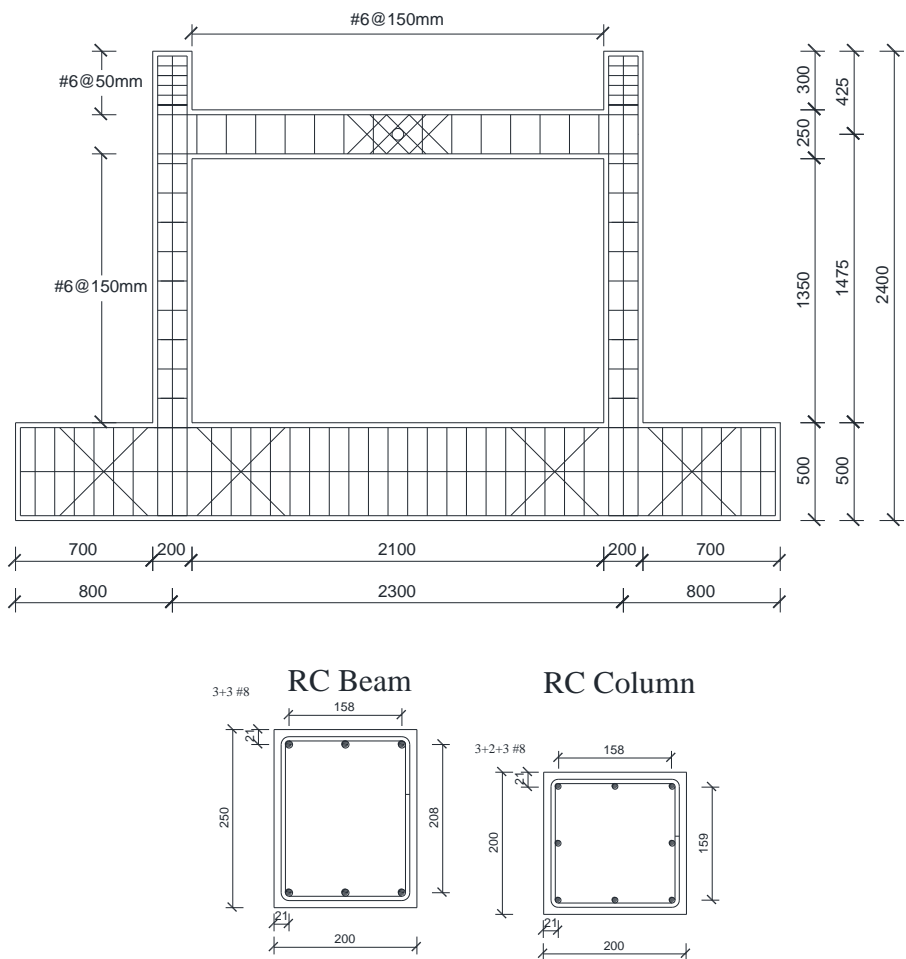


Figure 8-1: Geometry and reinforcement details of specimens

Material properties

Concrete compressive strength for each specimen was evaluated on three 15×15×15cm cubic samples of the casted concrete. Mean value of 28-day cylindrical strength is reported in Table 8-1.

Table 8-1: Properties of concrete

Specimen	Cylindrical compressive strength (f_c)
	[N/mm ²]
GB	21.6
GB2	25.4
GI-80	22.7

Commercial typology of reinforcing steel is B450C (NTC 2008), i.e., class C reinforcement with $f_{yk}=450$ N/mm² according to Annex C provisions of Eurocode 2 (EN 1992-1-1:2004 Annex C). Tensile tests were carried out on three samples for each bar diameter.

Table 8-2 reports mechanical properties, namely yield strength (f_y), ultimate strength (f_t) and hardening ratio (f_t/f_y). The yield stress is not dissimilar from ribbed steel bar “FeB44K” used in Italy during that period. (Verderame et al., 2012)

Table 8-2: Properties of reinforcing steel

Diameter	Yield strength (f_y)	Ultimate strength (f_t)	hardening ratio (f_t/f_y)
[mm]	[N/mm ²]	[N/mm ²]	[-]
6	507	572	1.13
8	586	648	1.11
10	490	572	1.17

Hollow clay bricks with cement mortar were used for infill material. Dimensions of brick units were 250×250×80(thickness) mm, with 8 holes per unit resulting in 68.2% void ratio. The category of the mortar was M15. Flexural and compressive strength of mortar were evaluated on three 40×40×160 mm samples, see Table 8-3.

Table 8-3: Properties of infill materials

Mortar	<i>Flexural strength</i>	[N/mm ²]	3.94
	<i>Compressive strength</i>	[N/mm ²]	14.03
Bricks	<i>Dimension</i>	[mm]	250×250×80
	<i>Void ratio</i>	[%]	68.2
Masonry wallette (three course)	<i>Dimension</i>	[mm]	770×770×80
	<i>Compressive strength (// to holes)</i>	[N/mm ²]	4.88
	<i>Compressive strength (⊥ to holes)</i>	[N/mm ²]	3.19
Masonry wallette (five course)	<i>Dimension</i>	[mm]	1285×1285×80
	<i>Shear strength</i>	[N/mm ²]	0.36

Mechanical properties of infill material were evaluated by means of wallette tests. Compression tests were carried out on three-course masonry prisms, perpendicular (see Figure 8-2a) and parallel (see Figure 8-2b) to the holes, and a diagonal shear test was carried out on a five-course masonry prism (see Figure 8-2c). Resulting strength values are reported in Table 8-3. Such values are quite similar to the values obtained by other Authors on masonry specimens with brick units and mortar quite similar to the present study ([e.g., Colangelo, 2001](#)).

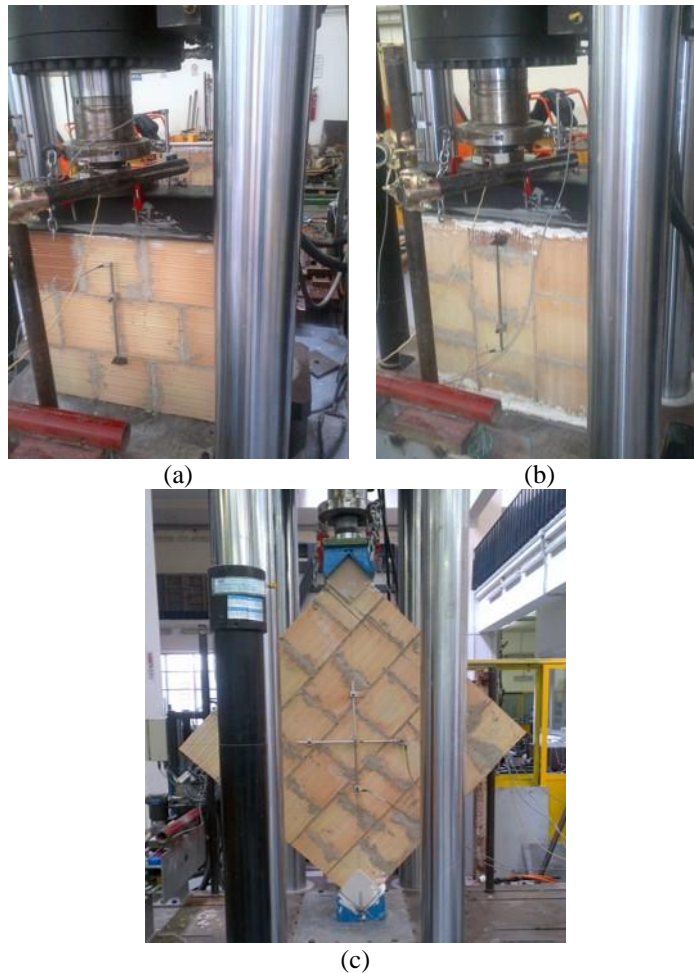


Figure 8-2: Compression tests on three-course masonry wallette specimens perpendicular (a) and parallel (b) to the holes, and diagonal shear test on five-course masonry wallette specimen (c)

Test setup

Figure 8-3 shows the test setup. The foundation block of the specimen was anchored to the strong floor by means of vertical post-tensioned steel rods connected to stiff steel profiles. The lateral load was applied by means of a hydraulic actuator (load capacity = 300 kN; stroke = ± 250 mm) in displacement control. The actuator was fixed to a steel reaction wall anchored to the strong floor. The vertical load on columns was applied by hydraulic jacks in load control.

Test setup was designed in order to avoid any direct interaction between setup elements and beam-column joints, in order to reproduce the actual behavior of the frame under seismic action. To this end, the actuator was connected to the midspan of the beam through steel profiles connected to a 60mm diameter steel rod passing through a transverse hole in the beam.

Displacement transducers (LVDTs) were used to measure crack width and deformations at different locations, namely at columns' and beam's ends (along external longitudinal reinforcement layers) and across joint panels, see Figure 8-4. Wire potentiometers were placed along infill panel diagonals in specimen GI-80. In specimen GB2 strain in longitudinal reinforcement was measured, too, by means of strain gauges.

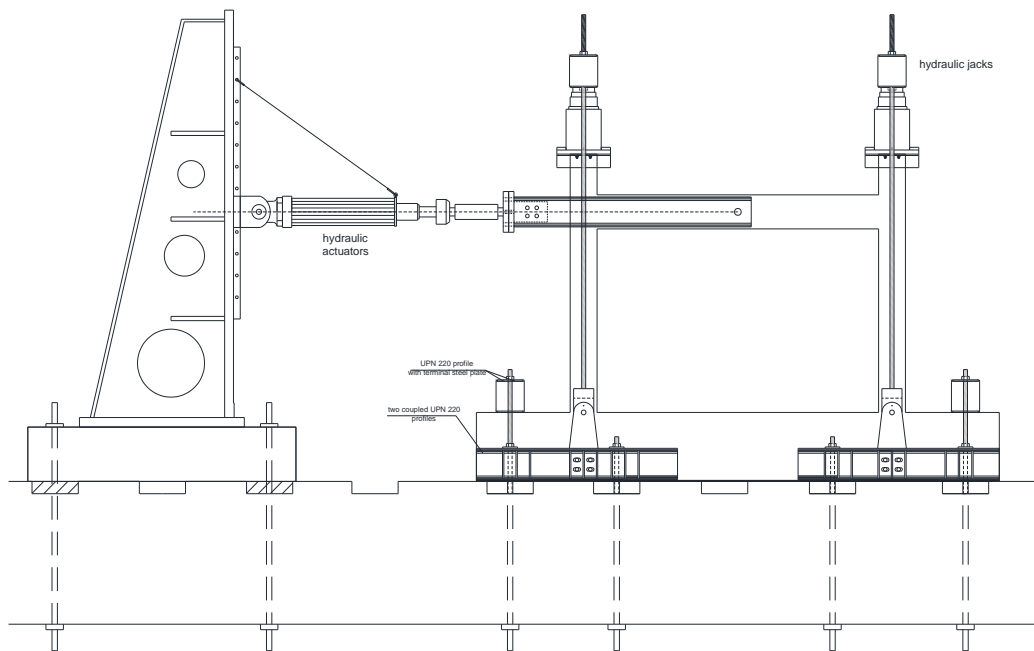


Figure 8-3: Test setup

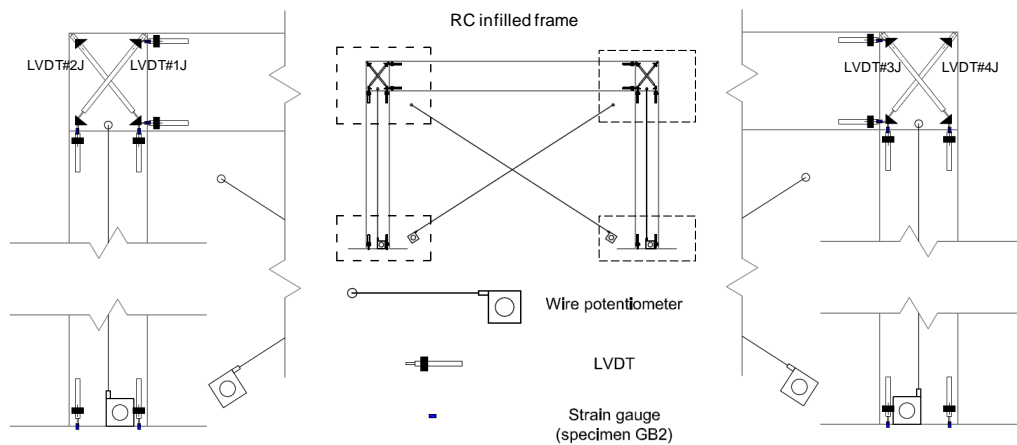


Figure 8-4: Instrumentation layout

8.3 Infilled Frame: Analysis of Experimental Results

General behavior: global response and observed damage

In this Section, lateral load-displacement response of tested specimen GI80 is illustrated (mainly referring to response envelope), and the evolution of observed damage with increasing imposed displacement is described. Figure 8-5 reports the lateral load-drift response of specimen GI-80.

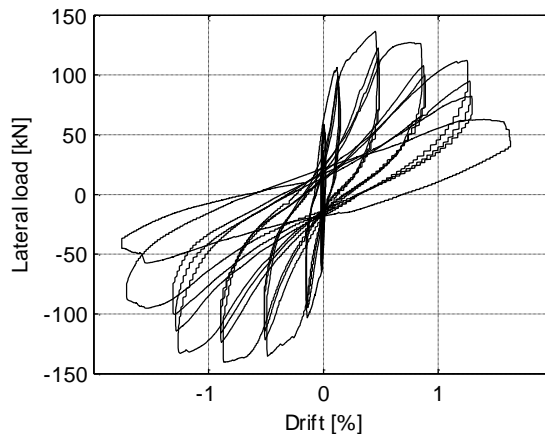


Figure 8-5: Lateral load-drift response of Infilled specimen GI-80

Specimen GI-80 exhibited an initial, uncracked stiffness of (196.5-239.0) kN/mm.

First appreciable decrease in stiffness was observed during cycle II (drift= $\pm 0.02\%$), with a lateral load about equal to 50% of the maximum; at the same drift first visible detachments between the panel and the surrounding frame were observed.

During cycle III (drift= $\pm 0.15\%$), minor but visible cracks occurred along mortar bed joints and brick units close to panel corners and along panel diagonal (Figure 8-6a); a further decrease in lateral stiffness was observed.

During cycle IV (drift= $\pm 0.50\%$), diagonal cracking in panel developed, and shear cracking initiated at the top of RC columns (Figure 8-6b); peak lateral load (136.6 kN) was attained in positive direction, and a substantial stiffness decrease was observed in negative direction.

Diagonal shear cracks in columns developed during cycle V (drift= $\pm 0.90\%$), and significant damage to individual brick units, at the centre of the panel, was observed (Figure 8-6c); peak lateral load (140.1 kN) was attained in negative direction, and lateral load started to decrease in positive direction.

During cycle VI (drift= $\pm 1.30\%$) individual brick units failed and severe widening of diagonal shear cracks took place (Figure 8-6d); severe intra-cycle drop of lateral strength was observed (Figure 8-5).

During cycle VII (drift= $\pm 1.70\%$), lateral load dropped at 46% and 68% of peak strength, in positive and negative direction respectively; test was terminated after opening of the stirrup at the top of the columns (Figure 8-6e), which led to the activation of a significant sliding along diagonal crack due to failure in restrain action on longitudinal reinforcement.

Table 8-4 reports a schematic description of damage evolution with increasing imposed drift in specimen GI-80.

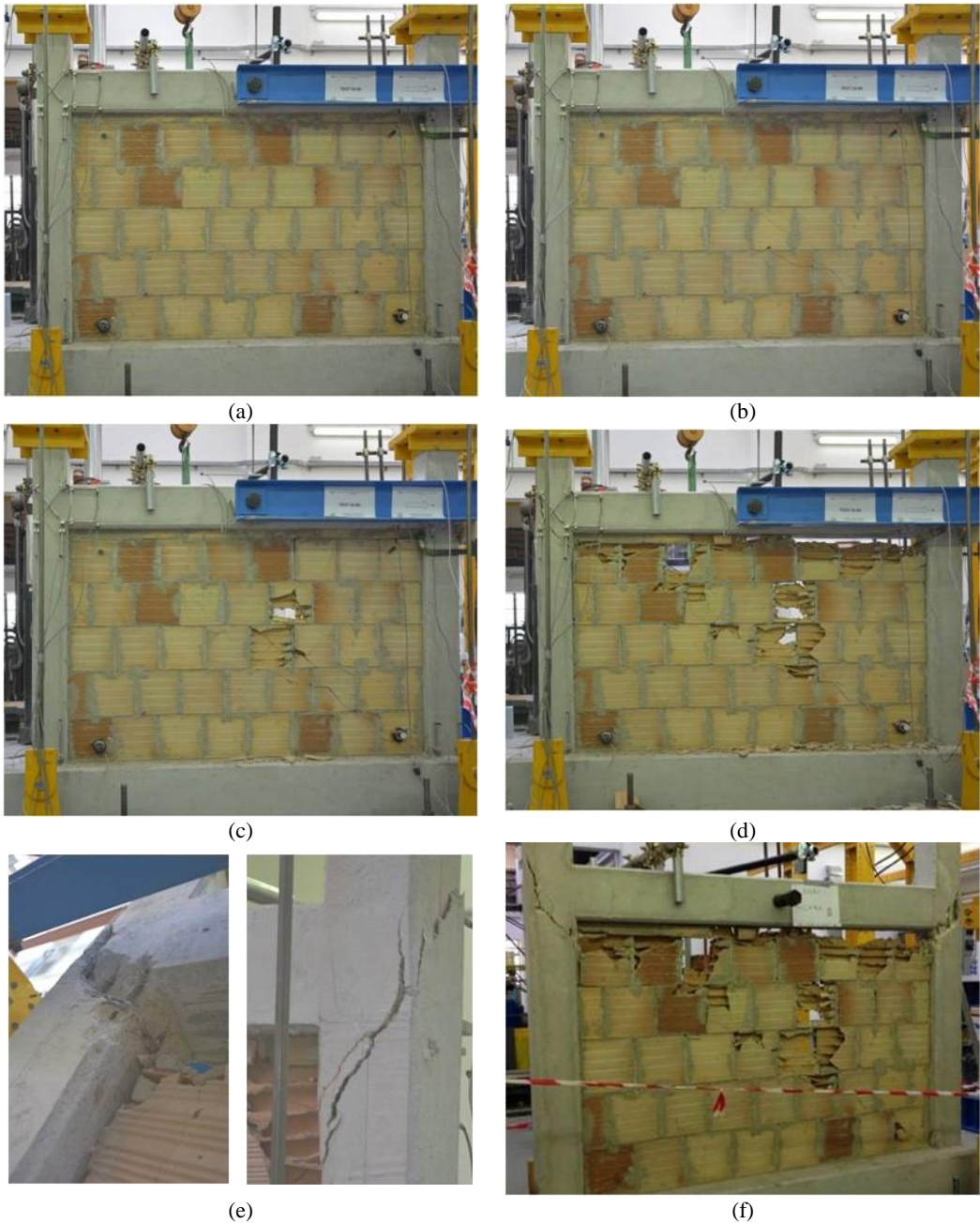


Figure 8-6: Damage to specimen GI-80

Table 8-4: Evolution of damage in Infilled specimen GI-80

Cycle	Drift [%]	Damage description
I	0.008	No damage
II	0.02	First visible detachments
III	0.15	Cracking initiates at panel corners and along diagonal (Figure 8-6a)
IV	0.50	Diagonal cracking develops; shear cracking initiates at RC column top (see Figure 8-6b)
V	0.90	Shear cracking at RC column top develops; significant damage to individual brick units (see Figure 8-6c)
VI	1.30	Failure of individual brick units (see Figure 8-6d)
VII	1.70	Stirrup opening in RC column and significant sliding along shear crack (see Figure 8-6e)

Local behavior

In this Section, most significant local measurement data, related to main damage and deformation mechanisms observed in Specimen GI-80, are reported and discussed.

Figure 8-7 shows the relationship axial strain of diagonal strut versus drift in infilled Specimen GI-80, as measured by wire potentiometer placed along opposite corners of the panel (see Figure 8-4). Positive slope of this relationship, during all the test, highlights that, also after shear damage of the column (shear cracking at the top of this element as reported in Table 8-4), imposed lateral displacement was applied to the panel, consistent with the observed increasing damage to the panel (see Table 8-4).

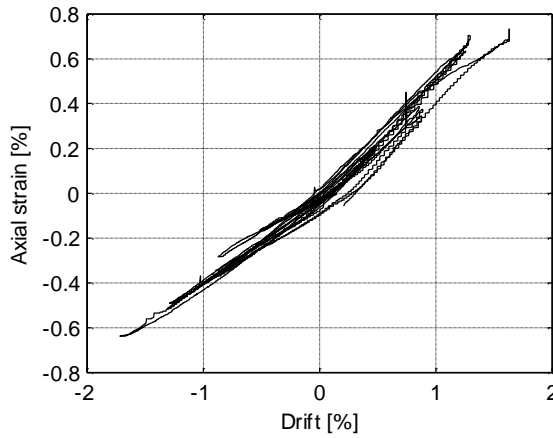


Figure 8-7: Axial strain of infill diagonal strut (elongation is taken as positive)

Figure 8-8 reports the lateral load-drift response of specimen GI-80. Figure 8-9a and Figure 8-10a show the lateral drift history. In Figure 8-9 and Figure 8-10 load Cycles are marked by means of vertical dashed lines. Figure 8-9b and Figure 8-10b show the lengthening of LVDTs placed across the diagonal shear cracks, for left and right column, respectively (see Figure 8-13).

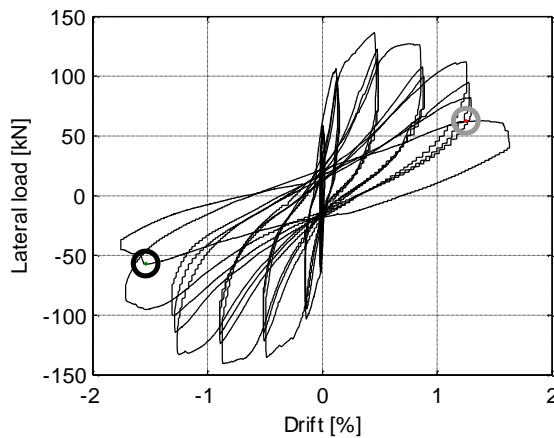


Figure 8-8: Lateral load-drift response of specimen GI-80. Load Cycles are marked by means of vertical dashed lines. Initiation of significant sliding along diagonal shear cracks and widening of these cracks is highlighted by means of a black and a grey circle for left and right column, respectively.

In particular, in Figure 8-9b and Figure 8-10b, first appreciable crack opening is observed in Cycle IV (drift=0.5%) as reported in Table 8-4, when the lateral load reaches for positive drift (or approaches for negative drift) the maximum resistance thus starting to degrade, as shown in Figure 8-8. During following cycles, softening in the response (Figure 8-8) is associated to progressive crack opening (Figure 8-9b and Figure 8-10b).

A sudden, further increase in such opening is observed at drift = -1.53% (Cycle VII, 2nd negative sub-cycle) and +1.26% (Cycle VII, 1st positive sub-cycle) for left and right column, respectively. In Figure 8-8 such “critical” steps, which can be considered as corresponding to the activation of shear failures, are highlighted by means of a black and a grey circle for left and right column, respectively. In fact, in the lateral load-drift response (see Figure 8-8), a sudden drop in lateral load (drift=-1.53%) and the initiation of a plateau behavior (drift=+1.26%) were observed, respectively; moreover, for left column at this step visible stirrup opening (see Figure 8-6e) was observed.

Figure 8-9c and Figure 8-10c show vertical displacements of the top of left and right column, respectively, as measured from the displacement of the hydraulic jacks used to apply the axial load. Note that a significant uplift of the top of the left column is observed – starting from Cycle IV – corresponding to maximum negative imposed displacements, that is, at the peak strain of the diagonal compressive strut between top left and bottom right corners of the panel. An uplift is observed corresponding to maximum positive imposed displacements, too, as a consequence of axial strain due to inelastic flexural behavior of columns. During Cycle VI, the amount of the latter becomes quite close to the former. A very similar, symmetrical behavior is observed for right column.

At “critical” drifts -1.53% and +1.26% sudden increases in vertical displacement of columns are observed, too. Such increases are observed during a sub-cycle, and they correspond to an abrupt change in the cyclic trend of vertical displacement observed previously. Such sudden increases in vertical displacement highlight the initiation of a significant sliding along diagonal shear cracks.

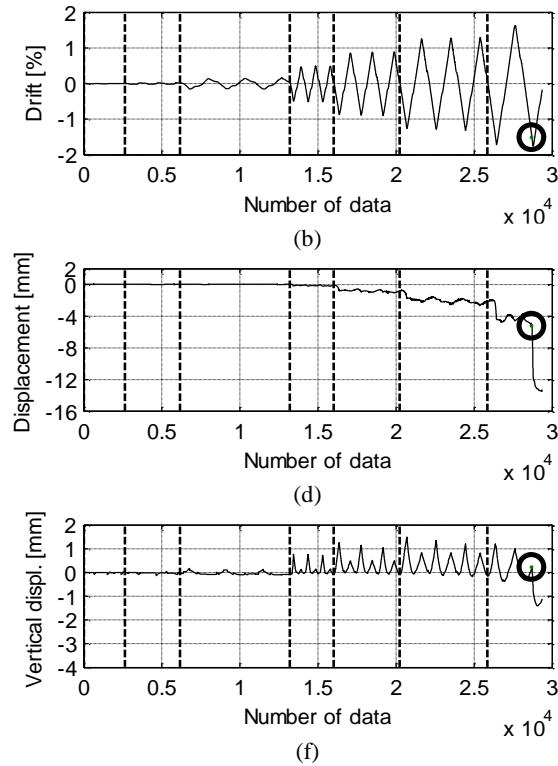


Figure 8-9: Lateral drift history (a), displacement of LVDTs across diagonal crack (b) in left joint, and vertical displacement of left (c) column of specimen GI-80. Load Cycles are marked by means of vertical dashed lines. Initiation of significant sliding along diagonal shear cracks and widening of these cracks is highlighted by means of a black and a grey circle for left and right column, respectively.

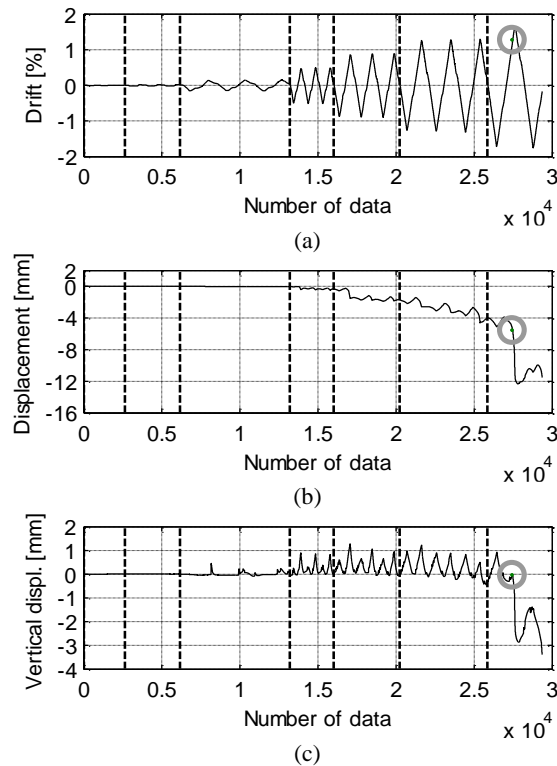


Figure 8-10: Lateral drift history (a), displacement of LVDTs across diagonal crack (b) in right joint, and vertical displacement of right (c) column of specimen GI-80. Load Cycles are marked by means of vertical dashed lines. Initiation of significant sliding along diagonal shear cracks and widening of these cracks is highlighted by means of a black and a grey circle for left and right column, respectively.

Figure 8-11 shows the relationship drift - base rotation of left column, the latter calculated as the difference between vertical displacements measured by LVDTs at the base section divided by their distance (see Figure 8-4).

As highlighted by the black circle, which corresponds to the "critical" step analyzed previously, after shear failure base rotation of left column suddenly starts to decrease. Note that shear failure took place during a sub-cycle corresponding to a drift=-1.53%, and after this step the global drift continued to increase up to the end of the sub-cycle (highlighted by the black square) corresponding to a drift=-1.70%, while base rotation was decreasing, for the first time during the test.

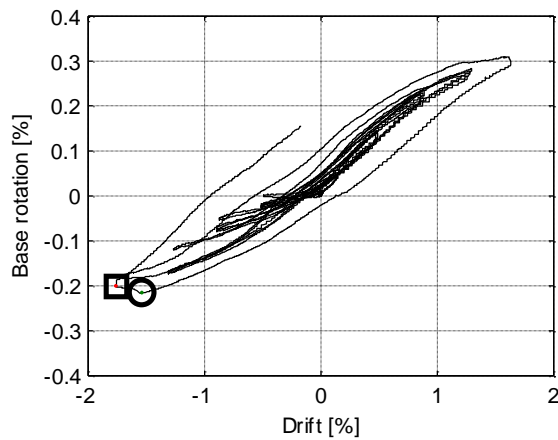


Figure 8-11: Lateral drift-base rotation relationship for left column of Specimen GI-80.

If base rotation is reported versus lateral load (see Figure 8-12b), no softening behavior is observed after shear failure; instead, an unloading behavior is observed (compare Figure 8-12a with Figure 8-12b).

It is likely to assume that, due to shear failure, a decrease in shear force took place in left column (resulting in the observed decrease in global lateral load), thus leading to a partial relaxing of the lower part of the column, as highlighted by the observed decrease in base rotation. These observations are based, of course, on the assumption that base rotation is monotonically proportional to shear force acting in the column; this is the case of no softening in flexural response of the lower part of the column.

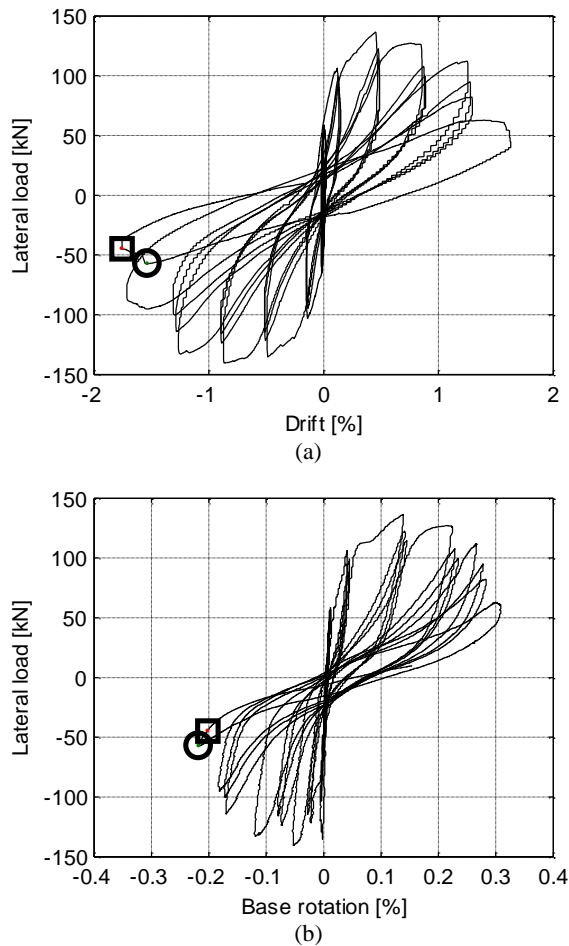


Figure 8-12: Global lateral load-drift (a) and global lateral load-base rotation for left column (b) relationships of Specimen GI-80.

Top displacement of the lower part of left column, on the left side of the diagonal crack (Δ_c), can be derived from the measurements of imposed lateral displacement of the beam (Δ_b) and of horizontal component of elongation of the LVDT placed across the crack (w_{bc}), the latter being the horizontal component of crack width (see Figure 8-13).

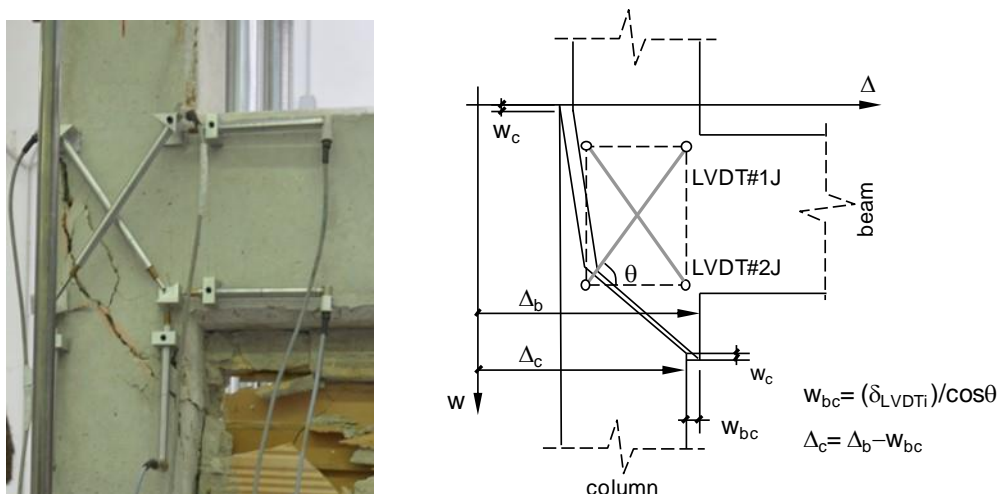


Figure 8-13: Instrumentation layout and derivation of displacement measures for left joint

Both of them are reported versus the global lateral displacement in Figure 8-14. As a further evidence of the damage mechanism described previously, a decrease in top displacement of the lower part of left column can be observed after shear failure and up to the end of the sub-cycle, opposite to imposed global displacement, for the first time during the test (see Figure 8-14a); the corresponding sudden increase in crack width is observed in Figure 8-14b. Note that at the end of the previous negative sub-cycle of Cycle VII the tangent of the relationship reported in Figure 8-14a approaches the horizontal, meaning that the increase in lateral displacement imposed to the frame does not lead to an increase in lateral displacement of the column, but only to an increase in crack width.

From a mechanical point of view, such condition corresponds to zero-stiffness of the shear hinge activated at the top of the column. Moreover, the accumulation of a residual crack width is demonstrated by left column displacements greater than displacements imposed to the frame for positive values (see Figure 8-14a) or, more directly, by crack width values increasing from one cycle to the other and remaining approximately constant within each cycle (see Figure 8-14b).

The same analysis is carried out for right column, see Figure 8-15. A very similar behavior is observed, compared to left column.

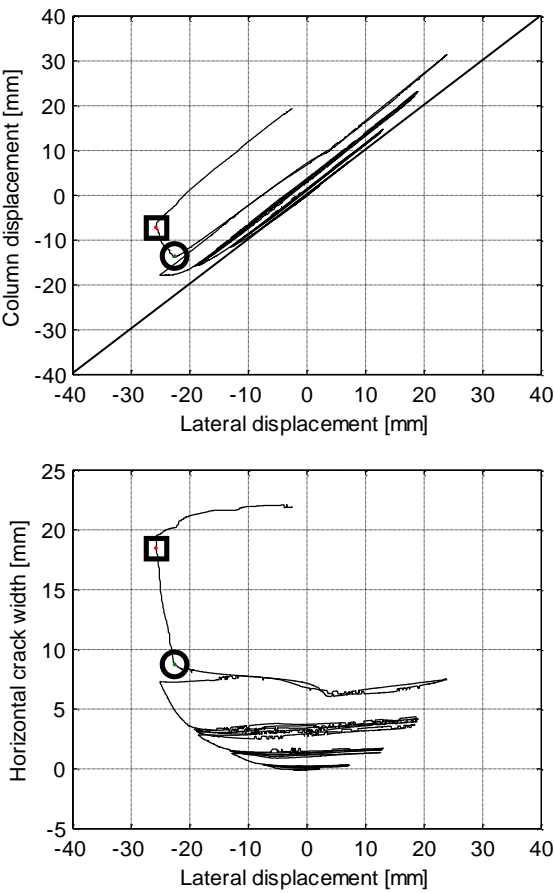


Figure 8-14: Left column displacement (a) and horizontal crack width (b) versus global lateral displacement for Specimen GI-80

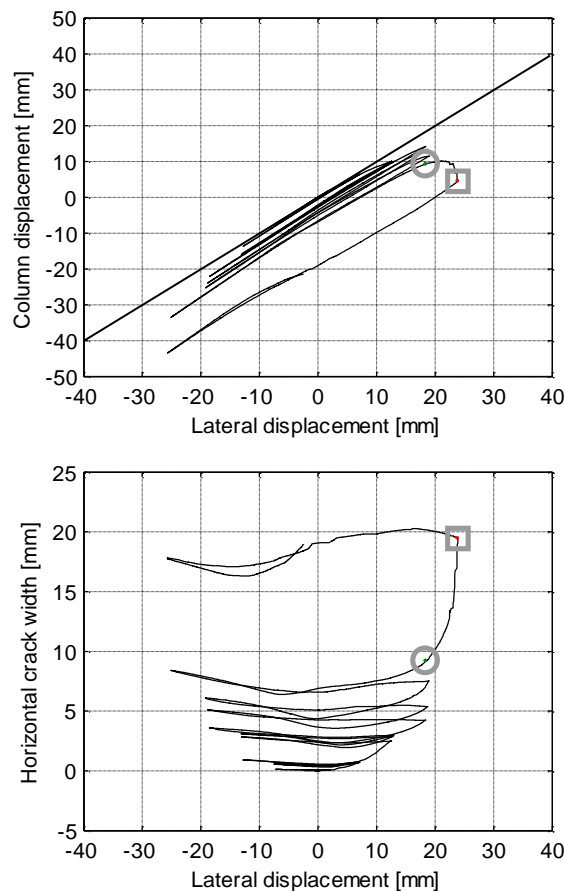


Figure 8-15: Right column displacement (a) and horizontal crack width (b) versus global lateral displacement for Specimen GI-80

8.4 Bare Frames: Analysis of Experimental Results

General behavior: global response and observed damage

Analogously, in this Section, lateral load-displacement response of tested specimens, GB and GB2, is illustrated and the evolution of observed damage with increasing imposed displacement is described.

Figure 8-18 shows lateral force –displacement relationship for GB and GB2 specimen, respectively. Specimens exhibited a similar behavior; post-elastic response of bare specimens, GB and GB2, was controlled by brittle failure of joints following flexural yielding of beams.

First appreciable decrease in lateral stiffness was observed during cycle II (drift= $\pm 0.30\%$) for a lateral load equal to 17 kN, with initial stiffness equal to 15.4 and 21.6 kN/mm for GB and GB2, respectively. First noticeable cracking was observed at beam ends during cycle II (drift= $\pm 0.70\%$), following first noticeable decrease in lateral stiffness.

During cycle III (drift= $\pm 1.10\%$), approaching beam yielding (as confirmed by local strain measurements, see Sections 8.4.1 and 8.4.2), hairline diagonal cracking developed in joint panels and flexural cracking in columns was visible; major decrease in lateral stiffness was observed.

During cycle IV (drift= $\pm 2.40\%$), flexural cracks at beam ends and at column base widened; at the same time, major diagonal cracking in joint panels was observed (Figure 8-16a Figure 8-17a); both specimens reached their peak lateral loads, in both directions, during this cycle (GB: +74.2/-76.2 kN; GB2: +80.5/-77.1 kN).

During next cycles, lateral load-displacement response showed severe softening (see Figure 8-18); widening of diagonal cracks in joints was observed, up to severe damage and concrete spalling in panel, see Figure 8-16b-c and Figure 8-17b, together with increase in flexural demand at the base of columns, resulting in concrete cover spalling and longitudinal bar buckling.

Test GB was terminated at cycle VII (drift= $\pm 5.10\%$), when significant shear sliding initiated along diagonal cracks in joints (see Figure 8-16d), as highlighted by vertical displacement in columns; during this cycle, lateral load dropped at 58% and 61% of peak strength, in positive and negative direction respectively.

Test GB2 was terminated at cycle VI (drift= $\pm 4.20\%$), when lateral load dropped at 70% and 81% of peak strength, in positive and negative direction respectively.

Table 8-5 reports a schematic description of damage evolution with increasing imposed drift in specimens GB and GB2.

Table 8-5: Evolution of damage in Bare specimens GB and GB2

Cycle	Drift [%]	Damage description	
		GB	GB2
I	0.30	No damage	No damage
II	0.70	Hairline flexural cracking in beams	Hairline flexural cracking in beams
III	1.10	Diagonal hairline cracking in joints	Diagonal hairline cracking in joints; Flexural cracking at column bottom
IV	2.40	Development of diagonal cracks in joints (\approx 1mm wide)	Development of diagonal cracks in joints (\approx 1mm wide); Flexural cracking at column top
V	3.30	Development of severe diagonal cracks in joints	Development of severe diagonal cracks in joints
VI	4.20	Buckling at column bottom	Spalling of concrete cover at column bottom
VII	5.10	Significant shear sliding along diagonal cracks in joints	/

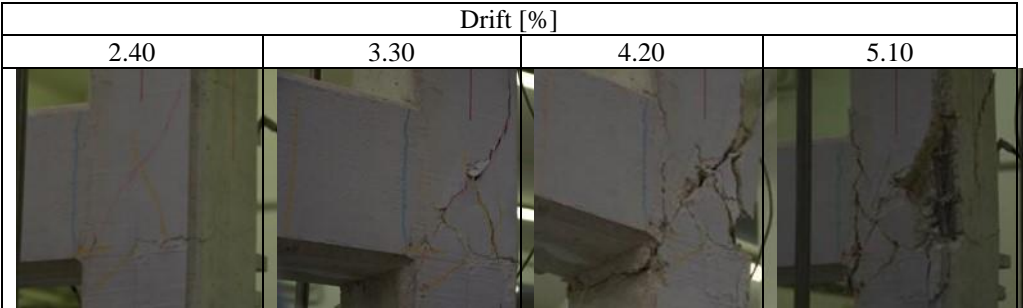


Figure 8-16: Damage to beam-column joint regions in specimens GB





Drift [%]			
2.40	3.30	4.20	5.10
			
(e)	(f)	(g)	

Figure 8-17: Damage to beam-column joint regions in specimens GB2

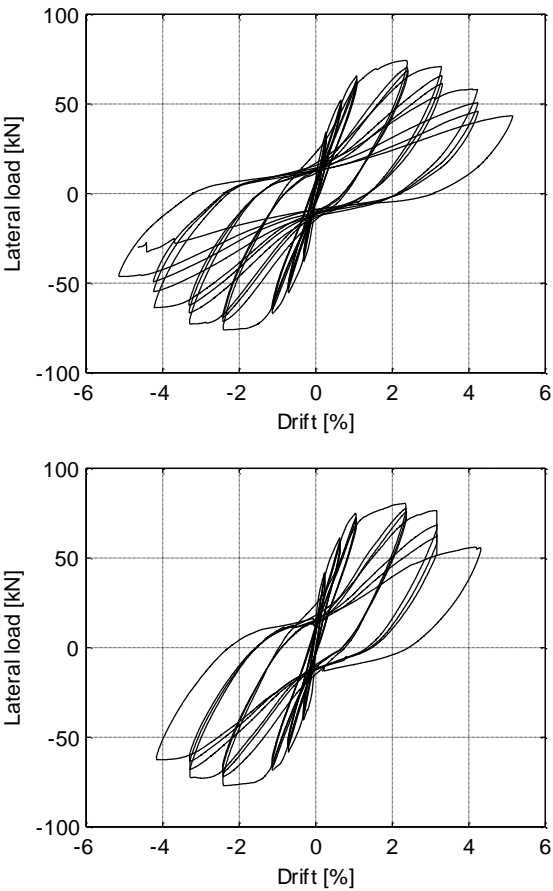


Figure 8-18: Lateral load-drift response of Bare specimens GB (a) and GB2 (b)

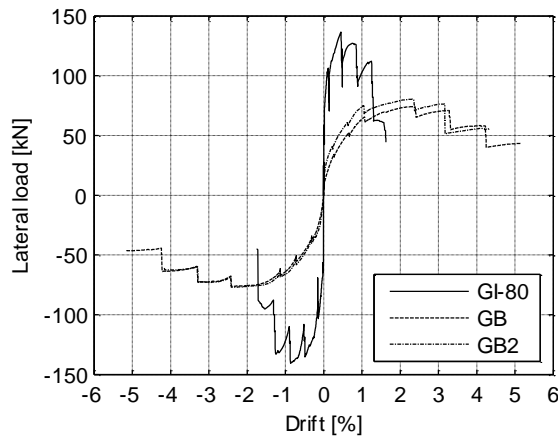


Figure 8-19: Envelopes of lateral load-drift responses

Finally, envelopes of lateral load-drift responses of the tested specimens (bare and infilled) are reported in Figure 8-19. The higher stiffness and strength of the infilled specimen GI-80 are clearly observed, as well as the severe softening behavior associated to the damage mechanism described above. The bare specimens GB and GB2 show a very similar envelope behavior, unless some minor inherent variability, especially for positive displacement values.

8.4.1 Local behavior of GB specimen

Most significant local measurement data, related to main damage and deformation mechanisms observed in Specimen, are reported and discussed.

Figure 8-20a reports the lateral load-drift response, lateral drift history (Figure 8-21a and Figure 8-22a), lengthening of LVDTs placed across the major diagonal joint cracks (Figure 8-21b and Figure 8-22b) – i.e. LVDT#1J for left joint and LVDT#3J for right joint, respectively, as reported in Figure 8-4– and vertical displacements of the top of columns (Figure 8-21c and Figure 8-22c) for specimen GB; edges of Cycles are marked by means of vertical dashed lines.

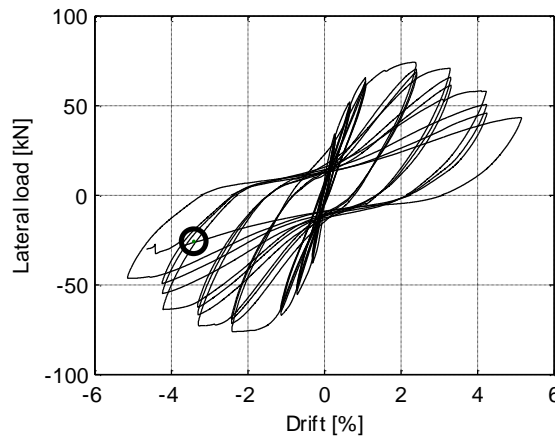


Figure 8-20: Lateral load-drift response of specimen GB. Load Cycles are marked by means of vertical dashed lines. Initiation of significant sliding along diagonal shear crack and widening of this crack for left joint is highlighted by means of a black circle

Again, a significant uplift of the top of both columns is observed – starting from Cycle IV – corresponding to maximum imposed displacements, as a consequence of axial strain due to inelastic flexural behavior of columns, see Figure 8-21c and Figure 8-22c.

Appreciable joint cracking is observed starting from Cycle IV, when the lateral load reaches the maximum resistance thus starting to degrade. During following cycles, softening in the response is associated to progressive crack opening. A sudden increase in crack width of left joint is observed at drift = -3.40% (Cycle VII, 2nd negative sub-cycle), see Figure 8-21b, together with a sudden increase in vertical displacement of the top of the column, see Figure 8-21c, highlighting the potential for an imminent joint axial failure. Such step is highlighted by means of a black circle. Upon this event, local drops in lateral load were observed, too (see Figure 8-20), and test was terminated.

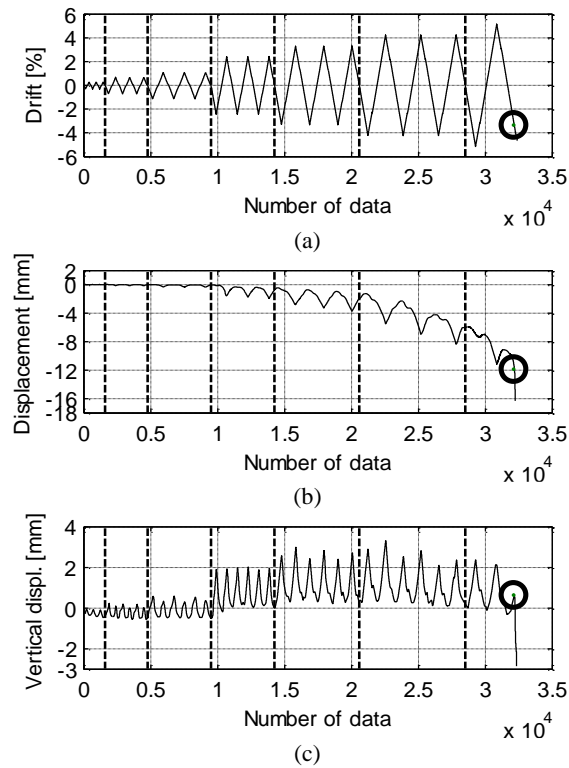


Figure 8-21: Lateral drift history (a), displacement of LVDTs across major diagonal crack (b) in left joint, and vertical displacement (c) of left column of specimen GB. Load Cycles are marked by means of vertical dashed lines. Initiation of significant sliding along diagonal shear crack and widening of this crack for left joint is highlighted by means of a black circle

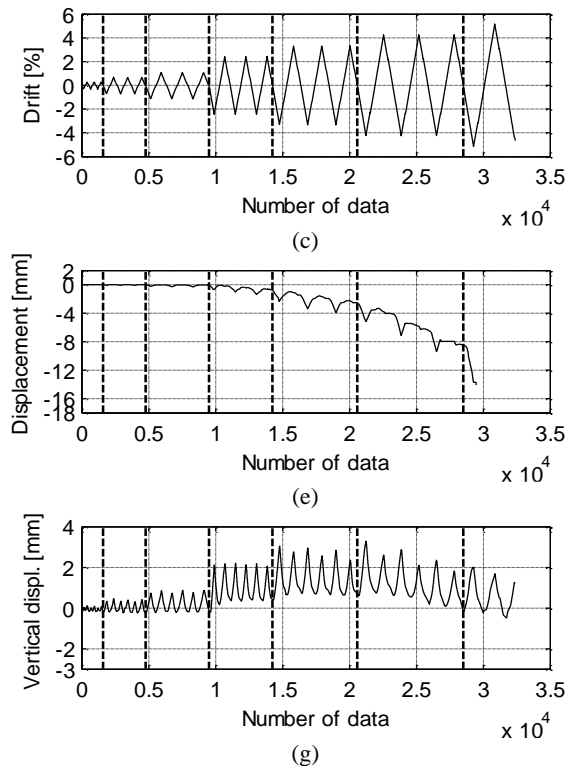


Figure 8-22: Lateral drift history (a), displacement of LVDTs across major diagonal crack (b) in right joint, and vertical displacement (c) of right column of specimen GB. Load Cycles are marked by means of vertical dashed lines. Initiation of significant sliding along diagonal shear crack and widening of this crack for left joint is highlighted by means of a black circle

Figure 8-23 reports the evolution of shear strain in left (a) and right (b) joint, evaluated from change of length measured by LVDTs placed across panel diagonals. A strongly asymmetric behavior can be observed. In both joints a major crack is observed along the diagonal between the internal joint panel corner and the opposite panel corner, thus leading to a panel deformation consistent with conventional “closing” displacements, which is taken as positive, see Figure 8-23 and Figure 8-24. Opening of these cracks was monitored by LVDTs placed along opposite diagonals (i.e., LVDT#1J for left joint and LVDT#3J for right joint, respectively, respectively, as mentioned above), which were reported in Figure 8-21b and Figure 8-22b. Shear strain of joints was evaluated from change of length measured by LVDTs placed across

both panel diagonals. Note that the representation of panel deformation referring to the scheme of shear strained body may poorly describe the actual behavior of the joint, especially under large inelastic deformations.

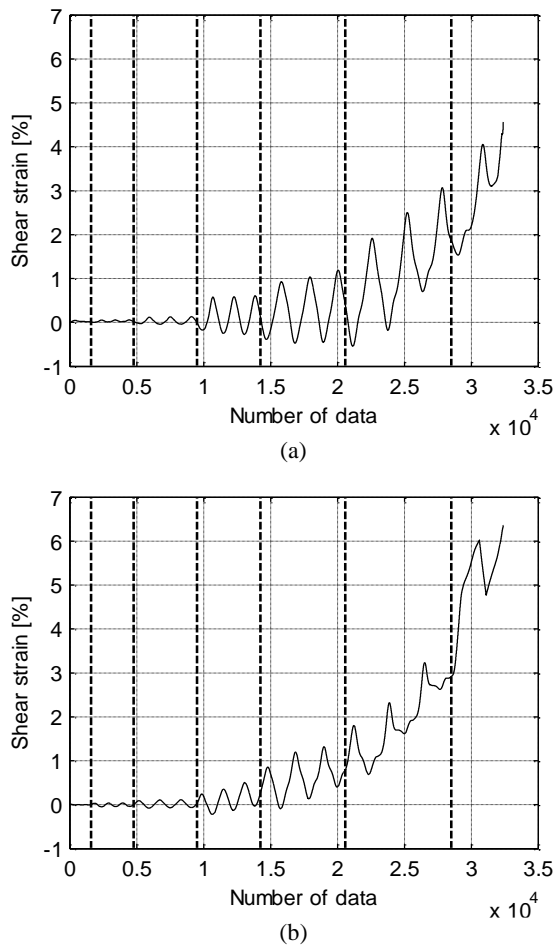


Figure 8-23: Shear strain of left (a) and right (b) joint in specimen GB

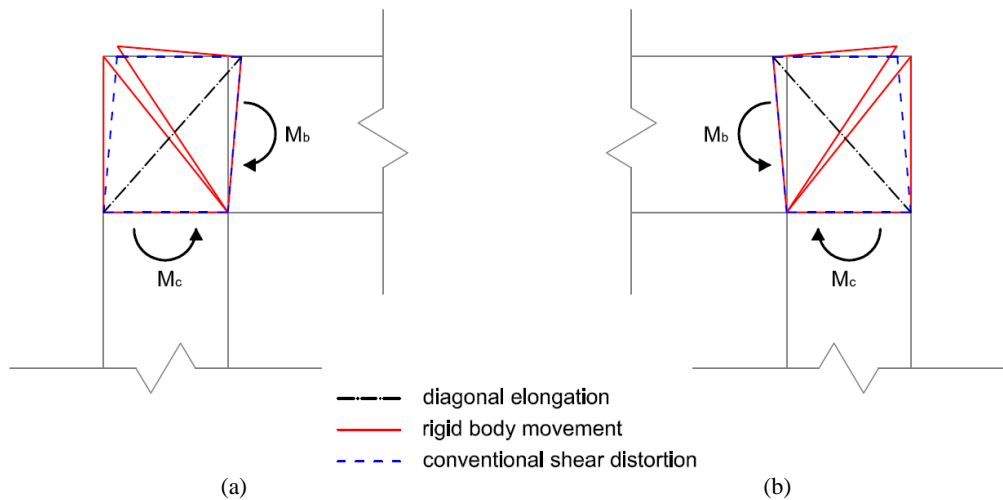


Figure 8-24: Major crack opening and corresponding equivalent shear deformation of joint panel for left (a) and right (b) joint

Figure 8-25 reports end rotation at the base of left column (a), end rotation at the top of left column (b), Figure 8-26 reports end rotation at the left end of beam (a), and shear strain of left joint (b) versus global lateral drift. Signs of these values are consistent with the schematic macroscopic representation of deformation mechanisms reported in Figure 8-27.

From Figure 8-26b it is evident that the joint shear strain accumulated under “closing” moments (i.e., for positive global drift values) was not recovered under “opening” moments, consistent with the major crack opening described above. Accordingly, under “opening” moments the major source of deformation in left joint sub-assembly was concentrated at beam-joint interface, that is, beam end rotation reported in Figure 8-26a. Under “closing” moments, on the contrary, beam end rotation approached zero even under large inelastic deformations, i.e. under major amplitude cycles. Similar trends are observed in the right side of the specimen, but these data are not reported in detail herein for the sake of brevity.

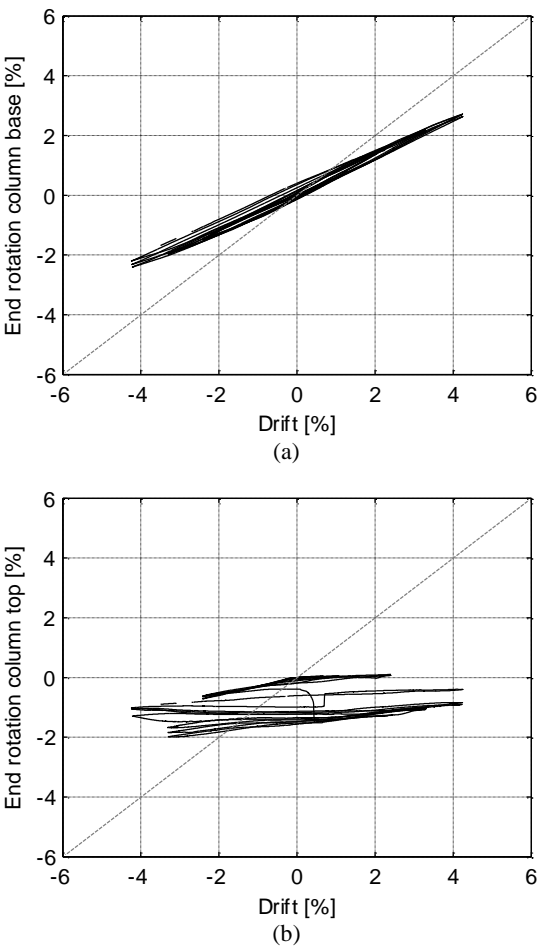


Figure 8-25: End rotation at the base of left column (a), end rotation at the top of left column (b) versus global lateral drift for Specimen GB

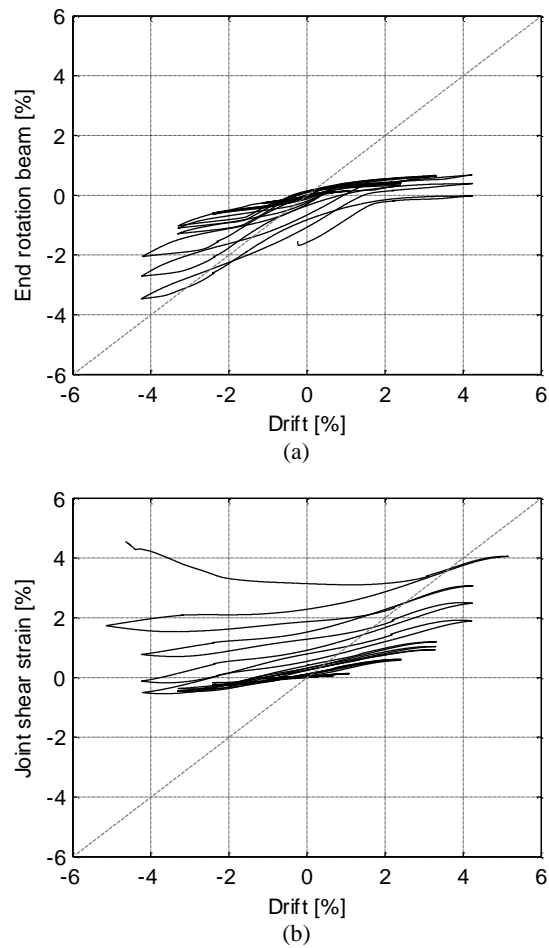


Figure 8-26: End rotation at the left end of beam (a), and shear strain of left joint (b) versus global lateral drift for Specimen GB

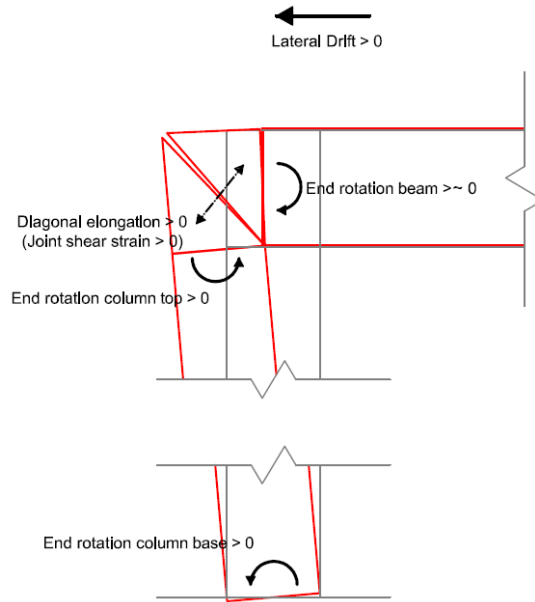


Figure 8-27: Schematic macroscopic representation of deformation mechanisms under positive imposed lateral displacement

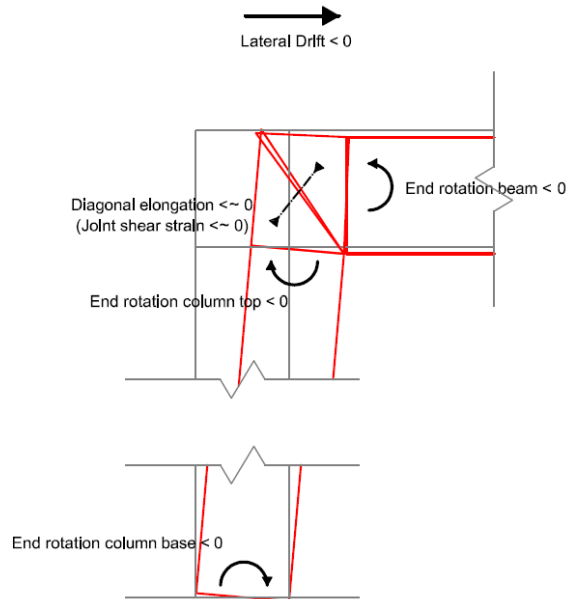


Figure 8-28: Schematic macroscopic representation of deformation mechanisms under negative imposed lateral displacement

Figure 8-29 reports photographic images of back view of left joint taken during cycle VI (drift= $\pm 4.20\%$) and cycle VII (drift= $\pm 5.10\%$), under maximum closing and opening imposing displacements. In the former case, a non-significant crack width at the end of beam is observed, whereas joint crack width reaches its maximum values (see Figure 8-26a and Figure 8-26b for positive drift). In the latter case, significant crack width at beam end is observed, together with a residual joint crack width (see Figure 8-26a and Figure 8-26b for negative drift).

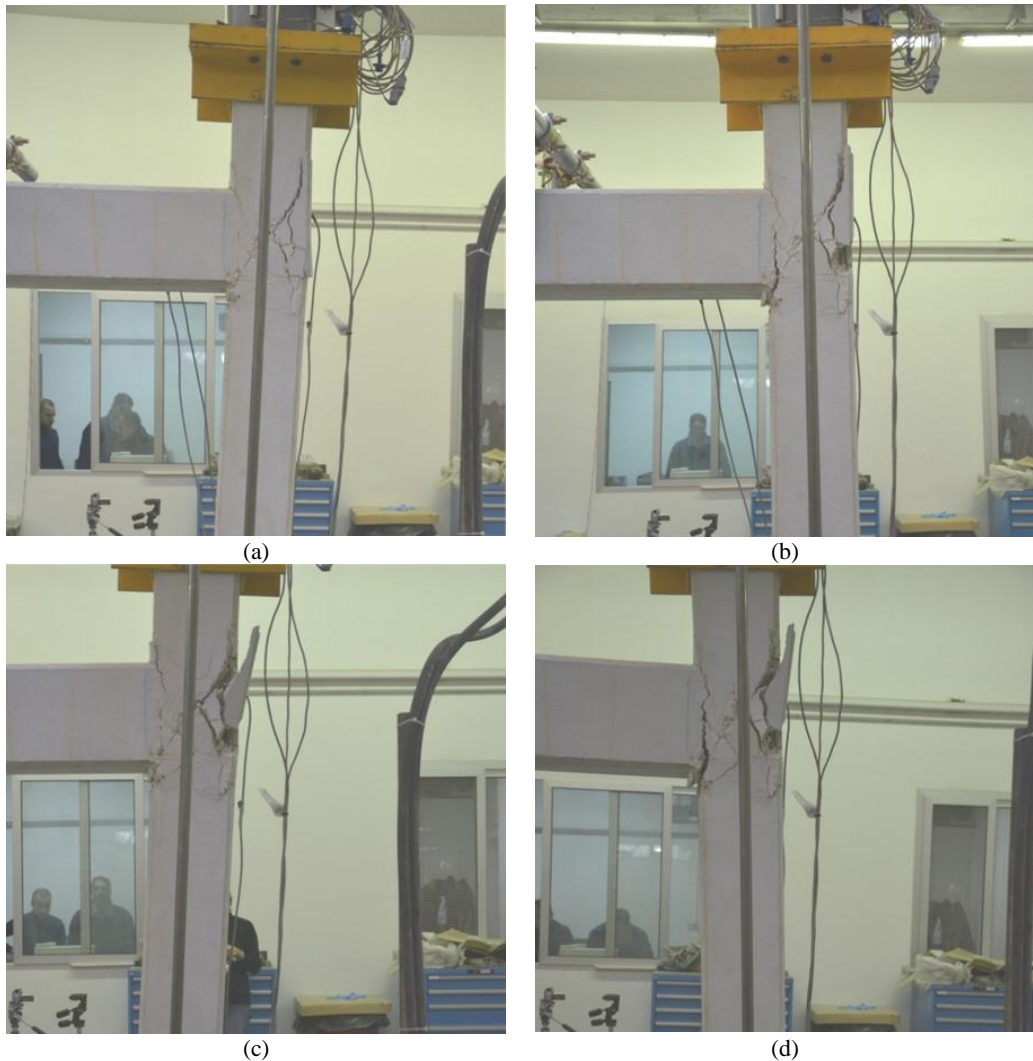


Figure 8-29: Photographic images of back view of left joint for closing (a,c) and opening (b,d) moments during cycle VI (drift= $\pm 4.20\%$) (a,b) and cycle VII (drift= $\pm 5.10\%$) (c,d)

Figure 8-30 reports the lateral load-drift response (a), lateral drift history (b-c), lengthening of LVDTs placed across the major diagonal joint cracks (d-e) – i.e. LVDT#1J for left joint and LVDT#3J for right joint, respectively – and vertical displacements of the top of columns (f-g) for specimen GB2; edges of Cycles are marked by means of vertical dashed lines.

8.4.2 Local behavior of GB2 specimen

Test GB2 was terminated one cycle earlier than GB, i.e. at cycle VI (drift= $\pm 4.20\%$).

Very similar trends in vertical displacement at the top of both columns, compared with test GB, are observed in Figure 8-31c and Figure 8-32c. Similarly, appreciable joint cracking is observed starting from Cycle IV, when the lateral load reaches the maximum resistance thus starting to degrade, and during following cycles softening in the response is associated to progressive crack opening, see Figure 8-31c (note the measure of major diagonal crack width in right joint was lost at the beginning of Cycle IV, due to technical problems to instrumentation).

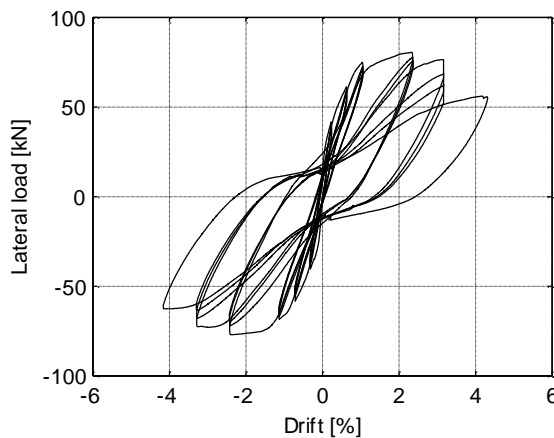


Figure 8-30: Lateral load-drift response of specimen GB2. Load Cycles are marked by means of vertical dashed lines

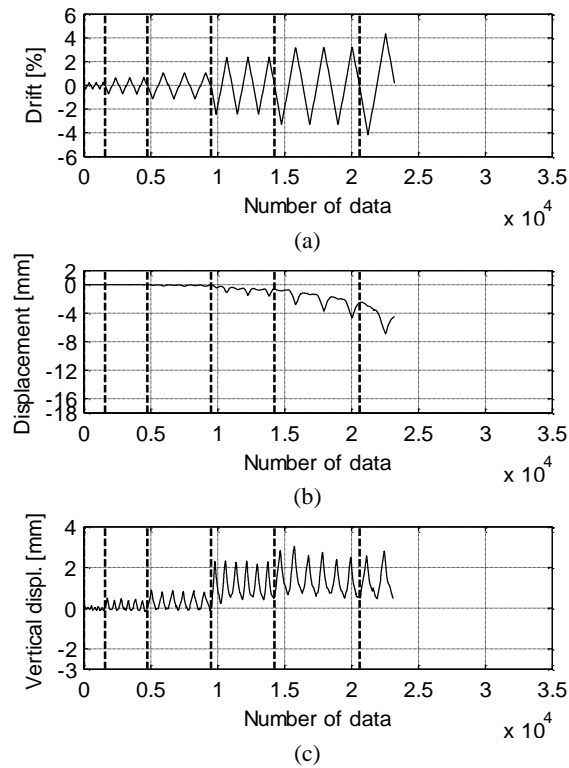


Figure 8-31: Lateral drift history (a), displacement of LVDTs across major diagonal crack in left (b) joint, and vertical displacement of left (c) column of specimen GB2. Load Cycles are marked by means of vertical dashed lines

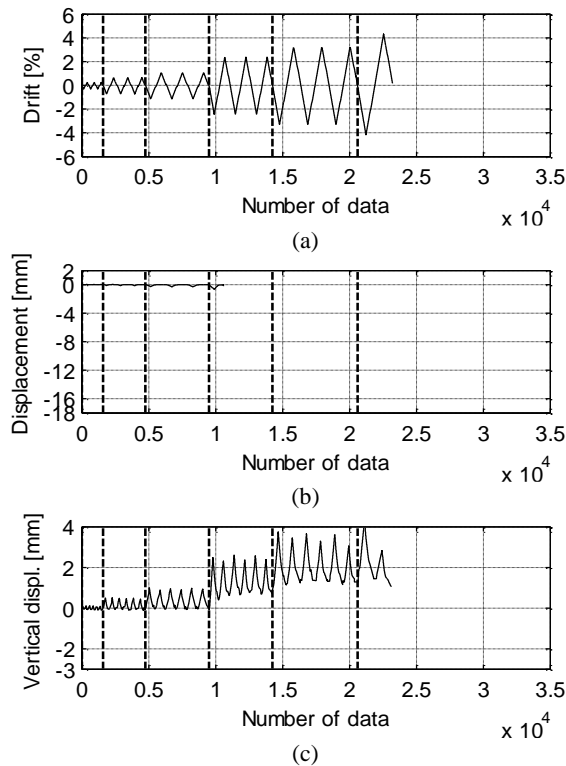
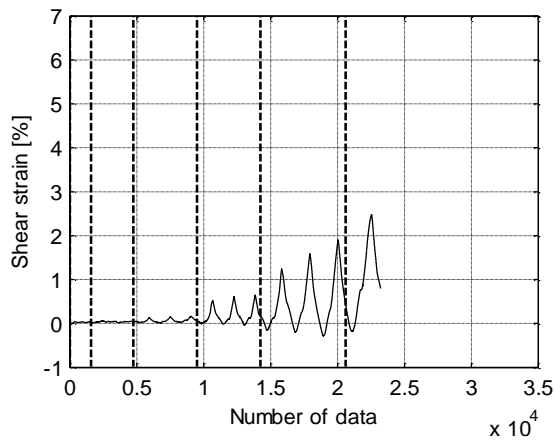
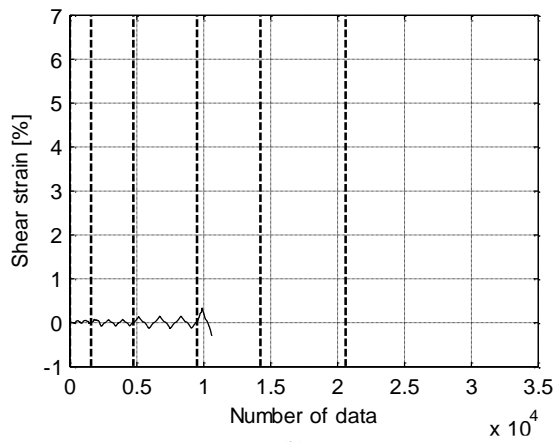


Figure 8-32: Lateral drift history (a), displacement of LVDTs across major diagonal crack in right (b) joint, and vertical displacement of right (c) column of specimen GB2. Load Cycles are marked by means of vertical dashed lines

Figure 8-33 reports the evolution of shear strain in left (a) and right (b) joint, evaluated from change of length measured by LVDTs placed across panel diagonals. Again, a strongly asymmetric behavior is observed (Figure 8-33a), with a major crack along the diagonal between the internal joint panel corner and the opposite panel corner, leading to a panel deformation consistent with conventional “closing” displacements.



(a)



(b)

Figure 8-33: Shear strain of left (a) and right (b) joint in specimen GB2

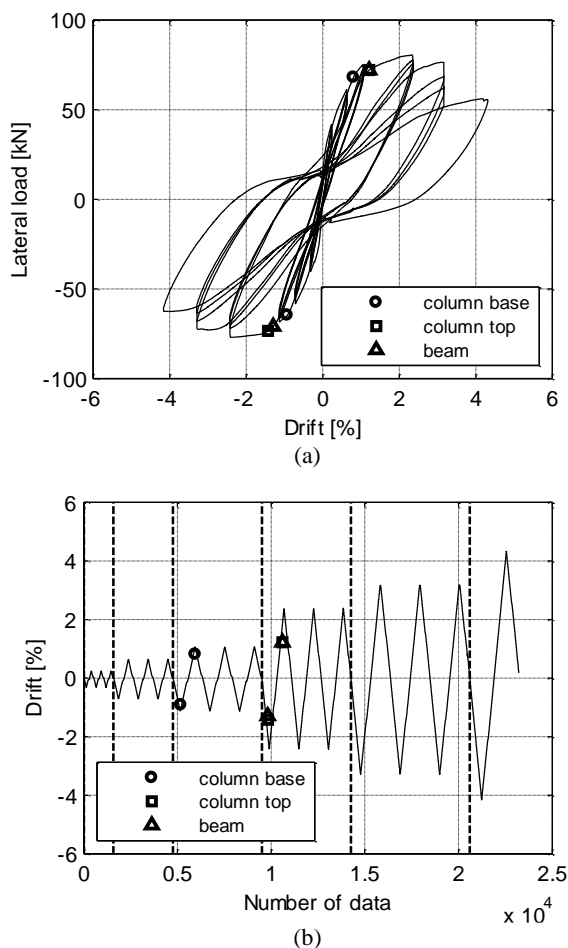


Figure 8-34: Yielding in longitudinal reinforcement according to strain gauges in left column of specimen GB2 in lateral load-drift response (a) and lateral drift history (b); yielding at left column base, left column top and beam left end are highlighted by means of a circle, a square and a triangle, respectively

Figure 8-34a and Figure 8-34b report the lateral load-drift and the drift history of test GB2 with the steps corresponding to yielding in longitudinal reinforcement at left column's bottom and top end sections and at beam's left end section.

Yielding in longitudinal reinforcement at the base of the column is observed at the end of the first sub-cycles of Cycle III, in both positive and negative directions, close to the significant reduction in lateral stiffness on the envelope of the response.

Then, yielding at the top of the column and at beam's end are observed very close to each other, during the first sub-cycles of Cycle IV, in both positive and negative directions, when the lateral load-drift response joins the envelope, prior to the attainment of the peak strength.

The fact that yielding at the top of the column and at beam's end are so close to each other is consistent with the expected flexural strength at first yielding of longitudinal reinforcement in these sections. As a matter of fact, yielding moments in column and beam – calculated with a fiber analysis using a linear model for the steel and the [Mander et al. \(1988\)](#) constitutive relationship for the concrete – are equal to 23.5 and 24.3 kNm, respectively; if reported at the intersection of the beam and column centerlines (assuming zero moment at the midspan of the clear length of the elements) they are equal to 27.8 and 26.6 kNm, respectively (see Table 8-6).

These observations are consistent with the damage observation reported in Table 8-5 (in particular, flexural cracking at column bottom in Cycle III and flexural cracking at column top in Cycle IV).

After first yielding was attained at the end sections of column and beam joining in left node, inelastic demand developed in beam, based on the observed damage evolution, thus supporting the hypothesis of a “BJ-failure”, that is, a failure of beam-column joint following flexural yielding in beam. The development of inelastic demand in beam rather than in column is also consistent with the expected flexural overstrength in these elements: maximum bending moment expected in column is greater than in beam, namely 27.1 versus 25.1 kNm (32.1 and 27.5 at the intersection of the beam and column centerlines), leading to a “strong column/weak beam” condition.

Table 8-6: Expected moment at first yielding and at maximum strength in beam and column (kNm)

	end section		centerline	
	M_y	M_{max}	M_y	M_{max}
	[kNm]	[kNm]	[kNm]	[kNm]
beam	24.3	25.1	26.6	27.5
column	23.5	27.1	27.8	32.1

8.5 Summary of remarks

The results of pseudo-static cyclic experimental tests on gravity load designed RC frames with and without masonry infill were shown. Tests were carried out on scale 1:2 specimens, designed according to older Italian technical code in order to be representative of existing RC buildings constructed between 1970s and 1990s.

Post-elastic behavior of specimens was controlled by brittle failure mechanisms. In Bare specimens, brittle failure mechanisms were observed in beam-column joints, with softening in global lateral force-displacement response associated to major diagonal cracking in joint panels, up to a sudden increase in vertical displacement of the top of the columns (observed in specimen GB), highlighting the potential for an imminent joint axial failure, that is, for the loss of vertical load carrying capacity.

In the Infilled specimen, as expected, the contribution of the infill panel led to significant global increase in stiffness and strength. Diagonal cracking developed in the panel since very low drift values (i.e., between 0.15 and 0.50%). A drop in lateral force associated to the development of severe diagonal cracking at the top of the columns was observed, followed by an abrupt increase in vertical displacement of the top of the columns highlighting – again – the potential for an imminent axial failure. The observation of the local behavior showed the evidence of a shear failure due to the local interaction between RC columns and infill panel.

The reported results can provide useful insights into the typical failure modes of substandard existing RC buildings. As a matter of fact, experimental investigation on brittle failure mechanisms and local interaction phenomena between structural and non-structural elements is of a primary importance in the study of the seismic response of this kind of buildings, due both to the limited availability of such data, and to the key role played by these phenomena, as demonstrated by recent post-earthquake damage observation.

8.6 References

- Al-Chaar G., Issa M., Sweeney S., 2002. Behavior of masonry-infilled nonductile reinforced concrete frames. *ASCE Journal of Structural Engineering*, 128(8), 1055-1063.
- Bergami A.V., 2007. Implementation and experimental verification of models for nonlinear analysis of masonry infilled r.c. frames. Ph.D. Thesis, Università degli Studi ROMA TRE, Rome, Italy.
- Biskinis D.E., Fardis M.N., 2010. Flexure-controlled ultimate deformations of members with continuous or lap-spliced bars. *Structural Concrete*, 11(3), 127-138.
- Calvi G.M., Bolognini D., 2001. Seismic response of reinforced concrete frames infilled with weakly reinforced masonry panels. *Journal of Earthquake Engineering*, 5(2), 153-185.
- Celarec D., Dolšek M., 2012. Practice-oriented probabilistic seismic performance assessment of infilled frames with consideration of shear failure of columns. *Earthquake Engineering and Structural Dynamics*, 42(9), 1339-1360.
- Celik O.C., Ellingwood B.R., 2008. Modeling beam-column joints in fragility assessment of GLD RC frames. *Journal of Earthquake Engineering*, 12(3), 357-381.
- Colangelo F., 2003. Experimental evaluation of member-by-member models and damage indices for infilled frames. *Journal of Earthquake Engineering*, 7(1), 25-50.
- Colangelo F., 2005. Pseudo-dynamic seismic response of reinforced concrete frames infilled with non-structural brick masonry. *Earthquake Engineering and Structural Dynamics*, 34(10), 1219-1241.
- D.M.14/02/1992. Norme tecniche per l'esecuzione delle opere in cemento armato normale e precompresso e per le strutture metalliche. Pubblicate sul Suppl. Ord. alla G.U. 18.3.1992, n. 65
- D.M.30/05/1972 Norme tecniche alle quali devono uniformarsi le costruzioni in conglomerato cementizio, normale e

- precompresso ed a struttura metallica. Pubblicate sul Suppl. Ord. alla G.U. 22.7.1972, n. 190
- D'Ayala D., Worth J., Riddle O., 2009. Realistic shear capacity assessment of infill frames: Comparison of two numerical procedures. *Engineering Structures*, 31(8), 1745-1761.
 - De Luca F., Verderame G.M., Gomez-Martinez F., Pérez-García A., 2013. The structural role played by masonry infills on RC building performances after the 2011 Lorca, Spain, earthquake. *Bulletin of Earthquake Engineering*, DOI 10.1007/s10518-013-9500-1.
 - EERI, 2000. 1999 Kocaeli, Turkey earthquake reconnaissance report. *Earthquake Spectra*, 16(S1), 237-279.
 - Elwood K.J., Moehle J.P., 2005. Drift capacity of Reinforced Concrete columns with light transverse reinforcement. *Earthquake Spectra*, 21(1), 71-89.
 - Liauw T.C., Kwan K.H., 1984. Nonlinear behaviour of non-integral infilled frames. *Computers and Structures*, 18(3), 551-560.
 - Mander J.B., Priestley M.J.N., Park R., 1988. Theoretical stress-strain model for confined concrete. *ASCE Journal of Structural Engineering*, 114(8), 1804-1826.
 - Mehrabi A.B., Shing P.B., Schuller M.P., Noland J.L., 1994. Performance of masonry infilled R/C frames under in-plane lateral loads. Report No. CU/SR-94/6. Department of Civil, Environmental, and Architectural Engineering, University of Colorado at Boulder, Boulder, CO, USA.
 - Mehrabi A.B., Shing P.B., Schuller M.P., Noland J.L., 1996. Experimental evaluation of masonry-infilled RC frames. *ASCE Journal of Structural Engineering*, 122(3), 228-237.
 - Park S., Mosalam K.M., 2013. Simulation of Reinforced Concrete frames with nonductile beam-column joints. *Earthquake Spectra*, 29(1), 233-257.
 - Pires F., 1990. Influencia das paredes de alvenaria no comportamento de estruturas reticuladas de betao armado

- subjectas a accoes horizontaes. Ph.D. Thesis, LNEC, Lisbon, Portugal. (in Portuguese)
- Ricci P., De Luca F., Verderame G.M., 2011. 6th April 2009 L'Aquila earthquake, Italy: reinforced concrete building performance. Bulletin of Earthquake Engineering, 9(1), 285-305.
 - Stylianidis K.C., 1985. Experimental investigation of the behaviour of the single-story infilled R.C. frames under cyclic quasi-static horizontal loading (parametric analysis). Ph.D. Thesis, University of Thessaloniki, Thessaloniki, Greece.
 - Verderame G.M., Ricci P., Esposito M., Manfredi G., 2012. STIL v1.0 – Software per la caratterizzazione delle proprietà meccaniche degli acciai da c.a. tra il 1950 e il 2000. ReLUIS, <http://www.reluis.it/>